PALACKÝ UNIVERSITY IN OLOMOUC

FACULTY OF SCIENCE

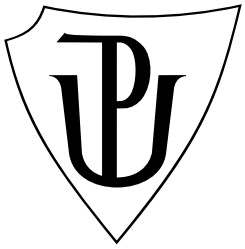

DOCTORAL THESIS

2017 **Mgr. Petr Hamal**

PALACKÝ UNIVERSITY IN OLOMOUC

FACULTY OF SCIENCE

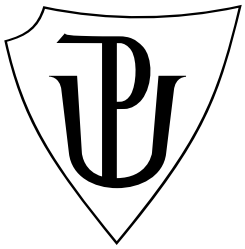

Mgr. Petr Hamal

Modelling and Simulation in High Energy Physics

Department of Experimental Physics
Joint Laboratory of Optics of Palacký University and the Institute of the Czech Academy of Sciences

Supervisor of the doctoral thesis: Mgr. Tomáš Sýkora Ph.D.

Study programme: Physics

Specialization: Applied physics

Olomouc 2017

Acknowledgement

First and foremost I would like to express my gratitude to my supervisor, Mgr. Tomáš Sýkora, Ph.D., for his leadership during my doctoral study starting with our co-operation in Software and Simulation group of the ALFA detector community and ending with the co-operation in the physical analysis of the exclusive pion production where his experiences, thoughts and guidance helped to make the analysis real.

I also owe my thank to prof. RNDr. Miroslav Hrabovský, DrSc. for accepting me as a Ph.D. student.

There would be no thesis without the support of doc. RNDr. Ondřej Haderka, Ph.D. Thank you!

I cannot forget to acknowledge my institutions - Palacký University in Olomouc and Institute of the Czech Academy of Sciences - which had supported my work.

I appreciated all members of the Particle physics group from Palacký University.

I would like to thank also ATLAS which gave me an opportunity to be a member of the respected and renowned international collaboration, to use its data and thus to contribute by my own analysis leading to the nice physical results.

I am grateful to Karl Heinz Hiller, the ALFA project leader who admitted me to the friendly ALFA community. My big thanks belongs to Hasko Stenzel for his excellent comments and indefatigable effort to put the logic of my analysis of the exclusive pion production in a perfect shape.

The last but not the least thank belongs to my beloved wife who encouraged me in difficult times.

I declare that I carried out this doctoral thesis independently under supervision of Mgr. Tomáš Sýkora, Ph.D., and only with the cited sources, literature and other professional sources.

In ..... date ..... signature of the author

Název práce: Modelování a simulace ve fyzice vysokých energií

Autor: Mgr. Petr Hamal

Studijní obor: Aplikovaná fyzika

Pracoviště: Společná laboratoř optiky Univerzity Palackého a Fyzikálního ústavu Akademie věd České republiky

Vedoucí práce: Mgr. Tomáš Sýkora, Ph.D., Matematicko-fyzikální fakulta, Univerzita Karlova

Abstrakt: Cílem předložené disertační práce je prezentovat schopnost autora aplikovat získané znalosti z oblasti modelování a simulace ve fyzice vysokých energií na příkladu fyzikální analýzy využívající experimentálně naměřených dat a následné porovnání získaných výsledků s teorií studovaného procesu. Práce je zaměřena na exluzivní proces produkce pionového páru $p + p \rightarrow p + p + \pi^+ + \pi^-$ v proton-protonových srážkách o těžišťové energii $\sqrt{s} = 7\,\mathrm{TeV}$ měřeného experimentem ATLAS na urychlovači LHC v CERNu. Tento proces je nejprve studován po teoretické stránce s využitím výsledků simulací uvedeného procesu. Celý softwarový rámec je pak následně aplikován i na experimentální data za účelem určení viditelného účinného průřezu exkluzivní produkce. Ke studiu procesu a jeho analýze jsou využity standardní softwarové nástroje z oblasti fyziky vysokých energií a analýzy dat jako jsou GEANT4, knihovny a nástroje ROOT, příslušné generátory studované produkce (GENEX, DIME) a softwarový rámec Athena standardně využívaný experimentem ATLAS.

Klíčová slova: Athena, ATLAS, CERN, difrakční fyzika, dopředné detektory, exkluzivní produkce, simulace, modelování, GENEX, DIME, ROOT, analýza

Title: Modelling and Simulation in High Energy Physics

Author: Petr Hamal

Field of study: Applied Physics

Department: Joint Laboratory of Optics of Palacký University and the Institute of the Czech Academy of Sciences

Supervisor: Mgr. Tomáš Sýkora, Ph.D., Faculty of Mathematics and Physics, Charles University

Abstract: The aim of this doctoral thesis is to present author's ability to apply the gained knowledge of modelling and simulation in high energy physics to the physical analysis of a given process using experimental data followed by a comparison of given results with a corresponding theory. The thesis is focused on the exclusive pion production $p + p \rightarrow p + p + \pi^+ + \pi^-$in proton-proton collisions measured by ATLAS experiment at centre-of-mass energy $\sqrt{s} = 7\,\mathrm{TeV}$. First of all this production is studied on a theoretical level using the results of the appropriate simulations. The obtained results are later applied on experimental data to estimate the cross-section of a given production. A common software tools are used to study the exclusive pion production, namely GEANT4, ROOT framework, generators of the given production like GENEX and DIME or the common tools used by ATLAS experiment known as Athena framework.

Keywords: Athena, ATLAS, CERN, diffractive physics, exclusive production, forward detectors, simulation, modelling, GENEX, DIME, ROOT, analysis

Contents

1. Preface

The main aim of the thesis "Modelling and Simulation in High Energy Physics" is to present author's ability to apply his knowledge of modelling and simulations in the analysis of the exclusive pion production data obtained by ATLAS (**A** **T**oroidal **L**HC **A**pparatu**S**) collaboration during proton-proton collisions at the LHC at centre-of-mass energy $\sqrt{s} = 7\,\text{TeV}$.

Gained knowledge of modelling and simulation came thanks to author's work for ALFA (**A**bsolute **L**uminosity **F**or **A**TLAS) community of the ATLAS in CERN (**C**onseil **E**uropéen pour la **R**echerche **N**ucléaire). The ALFA community which stands behind the detector of the same name - the ALFA detector [1] [1] gave the author an excellent opportunity to become its essential member and to fulfil oneself in the area of the modelling and simulation. The author worked with common tools and frameworks used in ATLAS collaboration including the GEANT4 framework [3] (serving for a simulation on a particle interaction with a mass), the Athena framework [4] (the main simulation, reconstruction and analysis framework of ATLAS collaboration) and ROOT Data Analysis Framework [5] (providing functionality for data analysis).

The author joint the ALFA community to work on the topics of the modelling and simulations which are essential for an understanding of the correct behaviour of the ALFA detectors. At the beginning the author contributed to the development of various software tools needed for simulations of the ALFA detectors within the ATLAS official framework - Athena. These steps included a development of the software tools used for a digitization, for a reconstruction and for a data preparation. This part of author's work made an unquestionable contribution not only to the ALFA community but also to the whole ATLAS collaboration. Author gave a plenary talk about the use of GUI for Athena developers.

Beside the modelling and simulation studies the author contributed to ALFA community by the analysis of data collected during several testing campaigns in CERN. The author contributed also to the ALFA community from his position as the Data Preparation convener (2012-2014).

The author contributed to two analysis of the total cross-section measurement in ATLAS using the ALFA detectors, [2] and [6].

Still, the exclusive pion production measured by ATLAS at $\sqrt{s} = 7\,\text{TeV}$ makes a principal topic of the author's doctoral thesis on which he presents the knowledge and the skills achieved during his doctoral study.

The exclusive pion production analysis goes behind the ALFA detector itself. It combines the knowledge of two detector systems of the ATLAS collaboration, the Inner detector as a part of the central ATLAS detector and the ALFA detector system as the part of the forward region of the ATLAS. This is also the first time when such analysis is done by ATLAS.

The introductory section Sect. 2 provides a physics motivation for a study of the exclusive pion production $p + p \to p + p + \pi^+ + \pi^-$and is followed by the Sect. 3 describing the basic mechanisms of the exclusive pion production. The Monte Carlo (MC) simulation section (Sect. 4) focusses on MC generators able to describe the studied process.

The next part of the thesis is devoted to the exclusive pion production analysis itself. The experimental set-up is described in Sect. 5, the particle kinematic reconstruction, data taking and the chain of the

[1] The main purpose is to determine the total cross-section of proton-proton collisions (i.e. [2])

selection criteria are described in Sects. 6 and 7. Following Sects. 8 and 9 are devoted to the overall corrections and the background estimation which are important for a correct interpretation of the analysis results. The results of the data analysis are described in Sect. 10 and are followed by a study of systematic uncertainty in Sect. 11. The summary of the results and the thesis itself are given in Sects. 13 and 14.

The additional studies, materials and other sources supporting the thesis (and especially the analysis) are given in Appendices.

2. Introduction

The significant amount of proton-proton collisions at the LHC is either elastic ($\approx$ 20%) or diffractive ($\approx$ 20% of the remaining in-elastics collisions, i.e. approximately 16%). In many of these collisions the transferred momentum is too small to make the perturbative QCD applicable, and instead of the QCD the alternative, Regge, theory has to be used. Naturally, if we believe in a universality of the QCD, there should be a "bridge" (mapping) between the Regge theory and the QCD and e.g. pomeron, the basic object in soft diffraction description, can be, in some kinematic region and in a good approximation, considered as a color-singlet state of two gluons.

The simplest process with the exchange of a pomeron is proton-proton (pp) elastic scattering. As the simplest example of a (inelastic) diffractive process can be considered the exclusive production of pion pairs $p + p \rightarrow p + p + \pi^+ + \pi^-$, in which pomeron-pomeron fusion (double pomeron exchange) can be tested, together with relevant corrections (proton-proton and pion-pion re-scattering).

Another, and probably very attractive, reason to study exclusive pion production is a search for glueballs - strongly interacting states with no valence quarks, which existence was predicted more than 40 years ago. Nevertheless, despite of some evidence based on the analysis of observed scalar meson decay modes, to which processes via pomeron fusion represent background, their existence was not established.

Finally, there is another potential motivation for measurement of exclusive pion production, as it can be used, at least theoretically, as an alternative for a forward detector position alignment and accelerator optics cross-check.

Data analysed in the present paper were taken during the special low luminosity LHC runs (with the dedicated $\beta^\star = 90$ m accelerator optics) at centre-of-mass-energy $\sqrt{s} = 7$ TeV in Autumn 2011. It is our aim to estimate the cross-section of exclusive pion pair production in pp collisions.

Pion pairs were detected by the ATLAS inner detector whereas the outgoing protons were measured by ALFA detector situated on both sides of ATLAS forward region ≈ 240 m from the ATLAS Interaction Point (IP).

The use of ALFA detectors makes this study different from any existing measurement done at higher (TeV) energies till now as outgoing protons were directly detected and a contamination of the measurement by proton remnants (if only the rapidity gap technique is used) is minimized.

The estimated visible $\pi^+\pi^-$ cross section measured by ALFA in work was estimated to 21 μb [7], under conditions that ALFA is 4 mm from the beam, the minimal pion energy is 100 MeV and minimal energy deposited in the calorimeter 4 GeV.

The analysis profits from the previous analysis *Measurement of the total cross section from elastic scattering in pp collisions at* $\sqrt{s}$ *=7 TeV with the ATLAS detector* [2] which was performed on the same dataset, with the same data taking conditions and the ALFA detector settings.

3. Pion pair production - theory

The exclusive production of a pion pair in pp collisions is one of the simplest processes intermediated by the strong interaction. Correspondingly, there is a long history of models describing the process including a discussion about applicability of the perturbative QCD, see e.g. [8].

There are several recent works ([9–13] and references therein) summarizing the state of art leading to two existing signal generators, GenEx [14] and DiMe [12], we use in the analysis. The models are relatively similar, but not identical, and provide different predictions. Each of the models uses several parameters which are not fixed by the underlying theory.

In what follows we briefly give a general description of the exclusive pion pair production and explain where free parameters of models origin.

The exclusive production of $\pi^+\pi^-$ pair in pp collisions can be described by the generic diagram in Fig. 1.

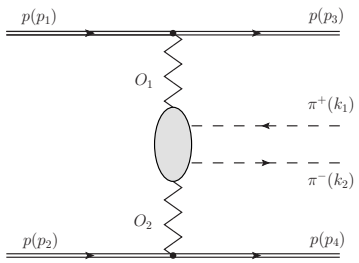

Figure 1: Generic diagram describing exclusive pion pair production in pp collisions.

The plot of reconstructed scattered protons Mandelstam variable t

$$t \approx {p_0}^2(1-\xi)\theta^2\,, \tag{1}$$

where θ is an angle between ATLAS z-axis and outgoing proton momentum 3-vector, ξ is a proton momentum loss during the interaction (Fig. 2) shows that the transferred momenta (from protons to central systems out of which pion pairs are created) are below 1 GeV. [2] This means that this part of the production mechanism cannot be described by the perturbative QCD. Instead Regge description is used.

Internal zigzag lines in Fig. 1 denote exchanges of objects O_1 and O_2, not necessarily of the same type, but having all hadronic charges equal to zero; $O_i \in \gamma, \mathbb{P}, \mathbb{O}, \mathbb{R}$, where γ stands for photon, $\mathbb{P}$ for pomeron, $\mathbb{O}$ for oderon, and $\mathbb{R}$ represents a set or reggeons: $f_{2\mathbb{R}}$, $a_{2\mathbb{R}}$, $\omega_{\mathbb{R}}$ and $\rho_{\mathbb{R}}$. In case when both pions are measured (i.e. they do not form a bound state), the C-parities of O_1 and O_2 have to be the same to get for pion system value equal to 1.

In the first approximation we can consider pion pair creation via diagrams in Fig. 3. and in Fig. 4.

The abbreviation `res` stands for any (energetically) possible resonant state.

[2] Not full story! We need to show that the same restriction is valid for t in $O_iO_j \to \pi^+\pi-$ process. But since the energy entering into this process is already restricted, the condition $t < 1\,\mathrm{GeV}^2$ is automatically satisfied.

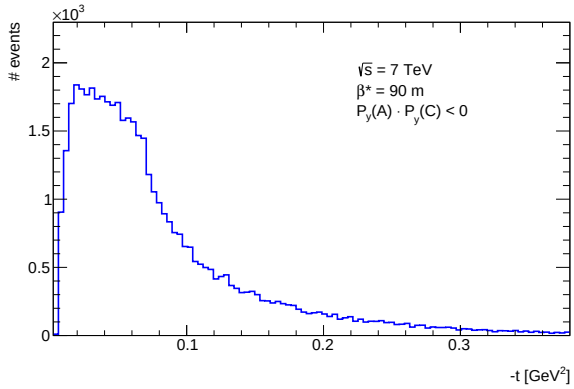

Figure 2: Outgoing proton t distribution in MC signal simulation (GenEx).

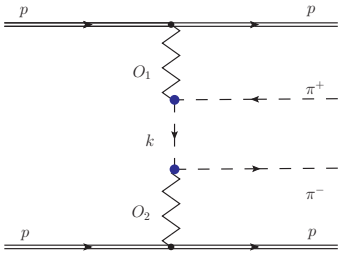

Figure 3: Schematic plot of central exclusive pion pair production in proton-proton collisions mediated by objects O_1 & O_2 and via the internal meson propagator.

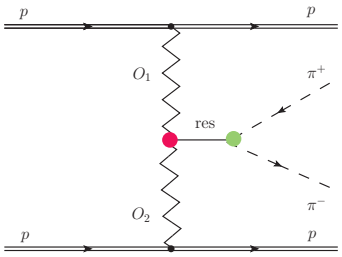

Figure 4: Schematic plot of central exclusive pion pair production in proton-proton collisions mediated by objects O_1 and O_2 and via a resonance `res`.

The full amplitude $\mathcal{M}$ for processes in Fig. 3 - so called continuum part - has contributions from different components of isospin:

$$|\mathcal{M}|^2 = |\mathcal{M}_{I=0}|^2 + |\mathcal{M}_{I=1}|^2 + |\mathcal{M}_{I=2}|^2, \tag{2}$$

but since we can write [10]

$$|\mathcal{M}_{I=0}|^2 \gg |\mathcal{M}_{I=1}|^2 \gg |\mathcal{M}_{I=2}|^2, \tag{3}$$

we can consider only the first term $M_{I=0}$. The $I = 0$ component dominance was discussed also in [12].

There are several contributions to the $M_{I=0}$ component which have to be taken in account, namely $\mathbb{P}$-$\mathbb{P}$, $\mathbb{P}$-$f_{2\mathbb{R}}$, $\mathbb{P}$-γ, $f_{2\mathbb{R}}$-γ and $f_{2\mathbb{R}} - f_{2\mathbb{R}}$ [9, 10] - meanwhile the other contributions can be neglected.

There is the second set of contributing diagrams, Fig. 4, where a pion pair originates from a resonance decay.

Finally, the interference terms between all amplitudes have to be taken in account. The relevance of the effect of interference was documented on the shift of the position of the peak ρ- resonance [15].

To calculate amplitudes of above mentioned diagrams we need to know/estimate vertex functions/form-factors (i.e. $p - O_i - p$, $\pi^+ - O_i - \pi^-$, $O_i - \texttt{res} - O_j$) [16].

3.1. Pion form factor and pion propagator reggeization

The pion form-factor is normalized on-shell, its value can be established from the reaction $p\pi \to p\pi$. There are several parametrization of off-shell pion form-factor, see eg. [10] (Eqs. 2.32, 2.29-31), [12] (Eqs. 4-5). For the mass of the central system $M_{\pi^+\pi^-}$ up to 1.5 GeV or $p_T(\pi)$ up to 1 GeV the difference between these parametrization is rather small although the final effect on the cross section is still of the order of hundreds percent [12] (Fig. 4). As the examples of off-shell form-factor parametrization we can take [12]:

$$F_M^{\rm exp}(t) = \exp\left(b_{\rm exp} t'\right) \tag{4}$$

$$F_M^{\rm or}(t) = \exp\left(-b_{\rm or}\sqrt{-t' + a_{\rm or}^2} + a_{\rm or} b_{\rm or}\right) \tag{5}$$

$$F_M^{\rm pow}(t) = \frac{1}{1 - t'/b_{\rm pow}} \tag{6}$$

where $t' = t - M^2$. It is clear that at the limit $t \to M^2$ the form-factors become equal to unity.

At the higher energies s, the standard pion propagator standing for an exchange of a pion of mass M, may be replaced by a full family of objects [10] (eq. 2.32):

$$\frac{1}{t - {m^2}_M} \to \beta_M(s)\frac{1}{t - {m^2}_M} + \beta_R(s)\mathcal{P}^{M^*}(t,s) \tag{7}$$

where

$$\mathcal{P}^{M^*}(t) = \frac{\pi\alpha'_{M^*}}{2\Gamma(\alpha_{M^*}(t)) + 1}\frac{1 + \exp(-i\pi\alpha_{M^*}(t))}{\sin\pi\alpha_{M^*}(t)}\left(\frac{s}{s_0}\right)^{\alpha_{M^*}} \tag{8}$$

is the reggeized propagator [10] (p. 144-145), Γ stands for Euler gamma function, the scale s_0 is selected to be 1 GeV^2 and α_{M^*} is the Regge trajectory with the slope $\alpha'_{M*} = \alpha'_\pi = 0.7\,\text{GeV}^{-2}$.

The functions $\beta_M(s)$ and $\beta_M(R)$ are introduced to interpolate between the meson and Regge exchange:

$$\beta_M(s) = \exp\left(-\left(s - 4m_{M*}^2\right)/\Lambda_{\rm off}^2\right), \quad \beta_R(s) = 1 - \beta_M(s) \tag{9}$$

and $\Lambda_{\rm off}$ is a free parameter of the model.

There are other possibilities to reggeize propagator (an option in DiMe, by default off)

$$\frac{1}{t - {m^2}_M} \to \frac{1}{t - {m^2}_M}\left(\frac{s}{s_0}\right)^{\alpha_{M^*}(t)} \tag{10}$$

where $\alpha_M(t) = \alpha_M(t) + \alpha'_M t$ is the Regge trajectory of the meson M, or

$$\frac{1}{t - m^2{}_M} \to \frac{1}{t - m^2{}_M} \exp(\alpha_M(t)\,|y_{M_3} - y_{M_4}|) \tag{11}$$

where y_{M_3} and y_{M_4} are rapidities of produced pions.

Clearly, at the present there is no other enough strong argument restricting the form of the pion off-shell form-factor or/and propagator.

3.2. Survival factor

The full picture of the exclusive pion pair production is more complicated as the diagrams containing protons pp re-scattering (Fig. 5), $\pi - \pi$ re-scattering (Fig. 6) and also re-scattering of pion(s) with proton (Fig. 7) have to taken into account.

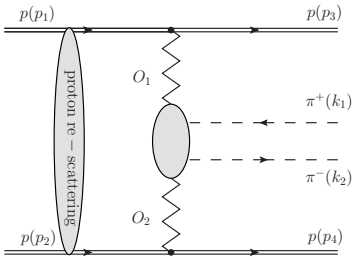

Figure 5: Schematic plot of a central exclusive pion pair production in proton-proton collisions, with proton re-scattering.

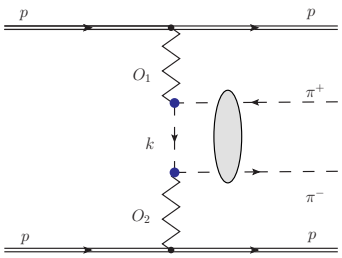

Figure 6: Schematic plot of a central exclusive pion pair production in proton-proton collisions with pion re-scattering.

The same same type of contributions we can expect also in a pion pair production via a resonance decay (Fig. 8).

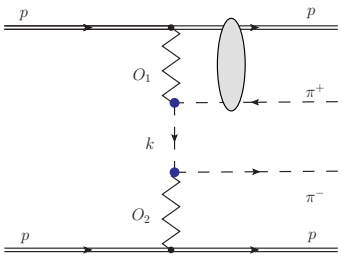

Figure 7: Schematic plot of a central exclusive pion pair production in proton-proton collisions with meson-proton re-scattering.

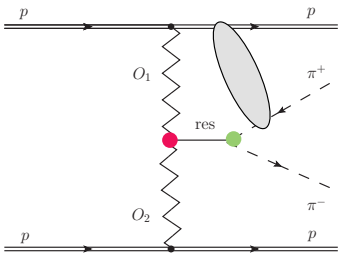

Figure 8: Schematic plot of a central exclusive pion pair production in proton-proton collisions with meson re-scattering and a pion pair production via a resonance decay.

3.3. Theory versus models

The effect of a proton-proton re-scattering (survival factor) is not implemented into the GenEx, the survival factor (= 0.22) was (independently on the interaction kinematics) introduced into the analysis by hand after the communication with GenEx authors. On the other hand DiMe has implemented a survival factor with the choice for 4 models describing it, including the Poisson suppression factor [12] originating from the requirement that no other particles may be produced in $\mathbb{PP} \to \pi\pi$ sub-process. DiMe considers only contributions from $\mathbb{P}/\mathbb{RP}/\mathbb{R}$ as relevant ones. Neither of the models has implemented contributions in which a pion pair originates from a resonance decay. As for off-shell form-factor, both models offer free parameters - Λ_{off} in case of GenEx, three sets of parameters for Eqs. 4 and 6. The same Λ_{off} parameter enters into the reggeization of the pion propagator in case of GenEx whether DIME parametrization is based on the Regge trajectory in Eqs. 10 and 11. In general, in case of small t it is not easy to distinguish GenEx and DIME generators, the differences come with higher t value or higher statistics.

4. Monte Carlo Simulation

Three different generators which are able to generate the exclusive pion production, together with the procedure how to generate and simulate such events, are described together with a description of the tools used in the Monte Carlo simulations. The main tool used in the simulations is the ATLAS offline software Athena [4]. The full simulation chain implemented in Athena consists of four steps: the event generation, the GEANT4 simulation, the digitization and the reconstruction step. A production of each step is controlled by the transformation jobs [17] which are a part of the ATLAS offline software. A result of the Monte Carlo simulation is stored in a file of ROOT [5] format called D3PD provided by the D3PD maker [18].

More about the ATLAS software computing can be found in [19–22].

4.1. Generators

The three generators are used for the Monte Carlo simulations in the analysis of the exclusive pion production, the GENEX generator [14], the di-meson (DiMe) generator [12] and the PYTHIA8 generator [23] with a central diffraction processes. None of the generators used in this analysis has been tuned for exclusive pion production at LHC energies.

4.1.1. GENEX

The GENEX [14] is a Monte Carlo event generator designed for the exclusive processes in proton-proton collisions focused on the exclusive production of meson pairs, $pp \to pM^+M^-p$, like $\pi^+\,\pi^-$ or $K^+\,K^-$. It is able to produce unweighted events within a relativistic phase space.

The GENEX, unlike other generators (e.g. EXHUME [24] or PYTHIA8 [23]) does not use parton structure functions of the colliding protons but rather Regge description. This makes it suitable for modelling soft processes. Thus it is possible to generate events with masses of a central system below 1 GeV (for the high energy collisions of units of tera-electron-volts).

There is only a non-resonant production - continuum - implemented in the GENEX generator version used in this analysis. Because of an absence of the absorption correction implementation in the model of the generator it was decided to implement it additionally on the cross-section result of the GENEX simulation. After a discussion with the GENEX author it was decided to set the value of the absorption correction factor to 0.22. But the absorption factor would be compared with a slightly different process of the exclusive diffractive production of $\pi^+\pi^-\pi^+\pi^-$ where such absorption factor is set to 0.21 [25].

GENEX parameters

The GENEX generator properties are described in [14]. The GENEX contains several event generation strategies. For the purpose of the exclusive pion production the event generator including the model presented in [11] and the parameters were change in following: the pions were generated with $|\eta| < 2.7$, centre-of-mass energy $tecm = 7\,000$ GeV and $\Lambda_{\text{off}} = 1$ with $eventGenerationStrategy = 2$.

A study of predictions sensitive to off-shell-pion form factor parameter Λ_{off} (Sect. 3) was also performed. The effect of three Λ_{off} values on the exclusive pion cross-section is shown in Fig. 9. It is seen that changing of the Λ_{off} parameter does not influence only the size of the exclusive pion cross-section but also the position of the distribution peak. The dependency is shown for both the elastic and the anti-elastic configurations.

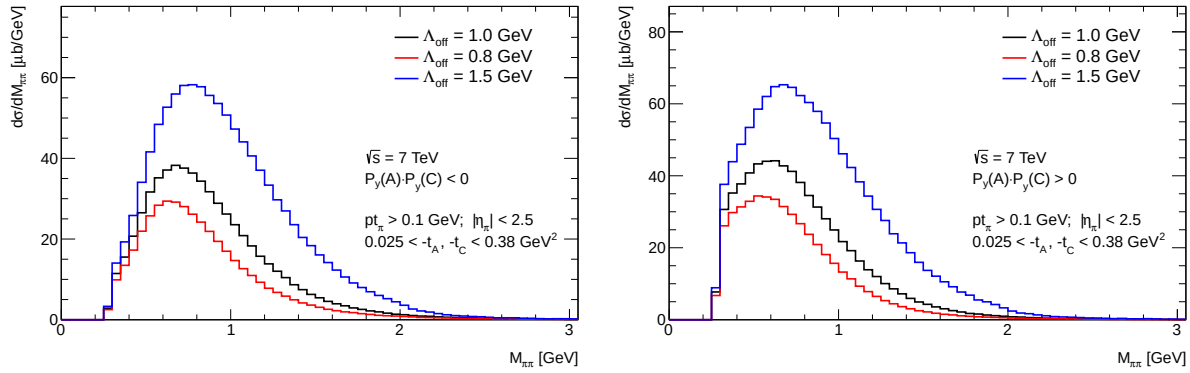

(a) (b)

Figure 9: A study of the off-shell-pion form factor parameter Λ_{off} implemented in GenEx. On (a) for the elastic proton configuration whereas on (b) for the anti-elastic proton configuration.

The GenEx generator is standing outside of the Athena, the ATLAS offline software. The GenEx generator allows to store the generated events in HepMC format [26] which is later transformed into the ATLAS collection by `HepMCReadFromFile` package such collection cn be used in the official simulation transformation job `AtlasG4_trf.py`.

4.1.2. Dime

There is, again, only a non-resonant production implemented in the DiMe generator (dimemcv1.06.f). This means that the DiMe generates the exclusive pion continuum without any resonant contribution. The absorption corrections are implemented in this model. There are also four parameters sets allowing to modify the survival factor (SF) and three options for off-shell pion form factor (FF). Only a simple study of form factor and survival factor was performed. The results are shown in Fig. 10. It is clear that a change of the survival factor or the form factor has an impact on the value of the cross-section, but the mean value of the peaks remain the same.

4.1.3. Central diffraction from Pythia8

The Pythia8 generator [23] is a set of tools for a generation of events in high energy collisions written in C++. It is mainly based on a parton level structure of the hadron-hadron collisions. The Pythia8 generator contains a wide range of processes including soft-QCD processes like the central diffraction (a.k.a. Double Pomeron Exchange - DPE). The model describing the central diffraction processes is limited. It is able to generate a central system with a minimum central system mass about 1 GeV. This

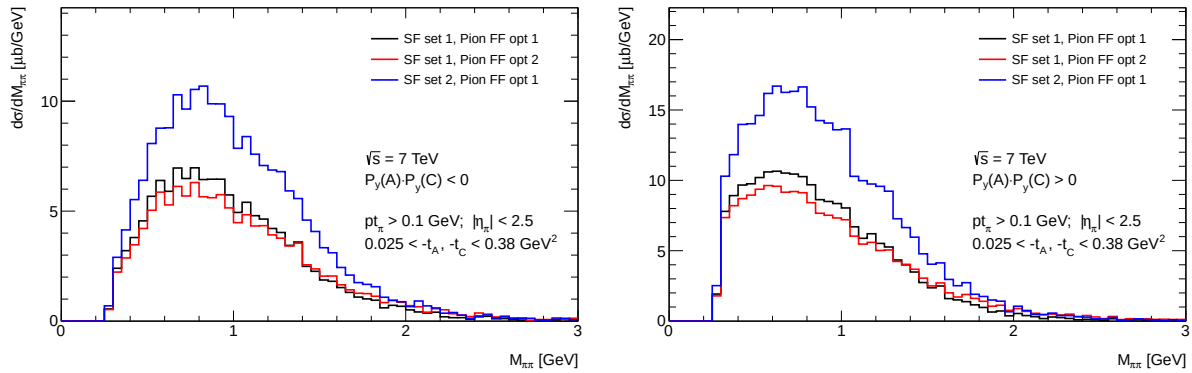

(a) (b)

Figure 10: A study of an impact of the survival factor (SF) sets and the off-shell-pion form factor (FF) options implemented in DiMe on the exclusive pion differential cross-section, on (a) for the elastic proton configuration whereas on (b) for the anti-elastic proton configuration.

is depicted on Fig. 11. Unfortunately the most of the exclusive pion-pair-system-mass value is below this limit.

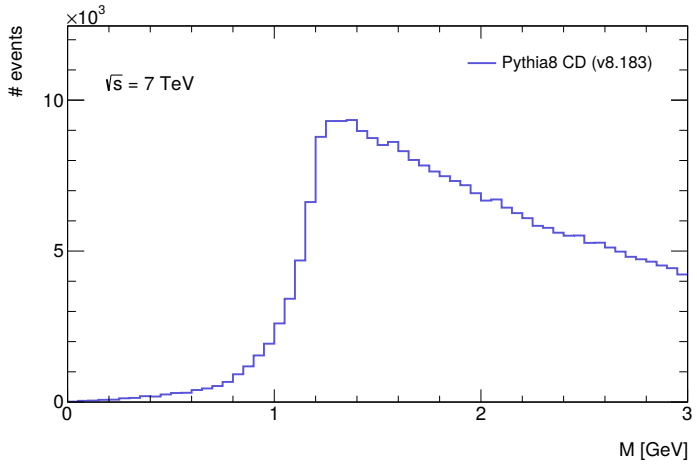

(a)

Figure 11: The central system mass limit implemented in Pythia8 (v8.183) central diffraction.

On other hand the Pythia8 can be used not only for the limited exclusive pion production analysis but also for the background studies of this exclusive process. In such case Pythia8 central diffraction simulation has to be normalised to data, see Sect. 9.

For the purpose of exclusive pion production analysis the central diffraction of the soft-QCD processes in Pythia8 are used. The central diffraction is switched on.

The Pythia8 generator is a part of the ATLAS offline software so the events are generated with the official transformation job `Generate_trf.py`.

4.2. Simulation set-up

The exclusive pion production is studied on data from the ATLAS run 191373 and the Monte Carlo simulation is set-up according to this run, Table 1. Proton beams are collided with a centre-of-mass energy at 7 TeV and transported with a nominal optics of a special high $\beta^{\star}$optics of 90 m [27]. The beam parameters are the same as in the analysis of the elastic scattering [28].

Table 1: Beam shape parameters used in Monte Carlo studies [28].

parameter	**value**	**unit**
$\sigma(v_x)$	182	µm
$\sigma(v_y)$	147	µm
$\sigma(p_x)$ beam 1	10.28	MeV
$\sigma(p_y)$ beam 1	8.95	MeV
$\sigma(p_x)$ beam 2	11.74	MeV
$\sigma(p_y)$ beam 2	9.00	MeV
$\sigma(\Delta E/E)$	1.13×10^{-4}	

There is a small difference in the beam crossing angle set-up between the data and the MC simulation. The beam crossing angle is set to zero in the MC simulation whereas in the data it was of a non-zero value [29]. This does not represent any problem as the nominal optics has zero beam crossing. The situation in data is different due to a usage of the effective optics. This optics is used to re-calibrate the magnet strength of Q1Q3 and the small residual crossing angle is compensate by a machine compensation system.

The ALFA detectors are in MC positioned $\approx$ 6 mm from the centre of the beam, for detail see Table 2 [28].

Table 2: The calibration values of the ALFA detectors positioning.

ALFA detector	**θ[rad]**	**x-offset [mm]**	**y-offset [mm]**
B7L1U	0.0050	0.337	5.981
B7L1L	0.0014	-0.356	-5.981
A7L1U	0.0039	0.630	6.255
A7L1L	0.0016	0.382	-6.173
A7R1U	0.0004	0.265	6.080
A7R1L	-0.0005	0.383	-6.303
B7R1U	0.0020	0.428	5.765
B7R1L	0.0013	0.494	-6.045

The interaction of the generated particles with detectors system as well as simulations of the physical processes is implemented in Athena simulation step [3]. The output is stored in Minimum Bias D3PD [30] which contains information from all detectors used in the analysis, namely from the Inner detector, from

[3] In the most of ATLAS offline software releases (a.k.a Athena releases), at least in Athena 17.X.Y.Z, if the ALFA detectors are switched on the central magnetic field is switched off.

the Minimum bias trigger system and from the ALFA detectors (and its D3PD part [31]). To be able to reconstruct the low p_t tracks ($p_t >= 0.1$ GeV) in the ATLAS Inner detector the `InDetFlags.doLowPt` is set to `True` value.

5. Experimental set-up

5.1. ATLAS Inner Detector

The ATLAS Inner detector (ID) [32] (Fig. 12) is nearest to the interaction point (IP) and contains three subsystems providing high-precision track reconstruction: a silicon pixel detector (innermost), a silicon microstrip detector, and a transition radiation tracker (outermost), which also helps to discriminate electrons from hadrons. The ID covers a range of $|\eta| < 2.5$. It is surrounded by a superconducting solenoid, which produces a 2 T axial field within the ID.

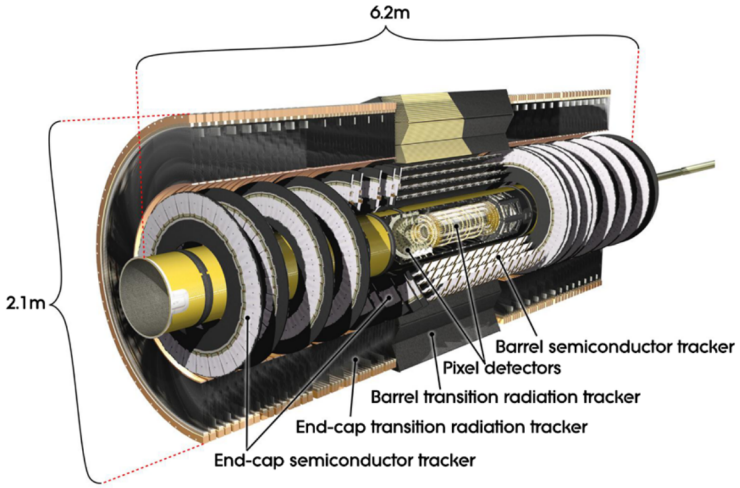

Figure 12: Cut-away image of the ATLAS Inner detector [33].

5.2. Minimum Bias Trigger Scintillators

The Minimum Bias Trigger Scintillators (MBTS) is one of the ATLAS Detector sub-components. It is placed ±3.6 m far from the ATLAS IP (on both ATLAS sides, A and C). It consists of 16 cells in two rings, the outer one and the inner one (Fig. 13). MBTS has the full ϕ space coverage in a transverse plane. The pseudo-rapidity acceptance of the outer ring is $2.08 < |\eta| < 2.78$, whereas the pseudo-rapidity acceptance the inner ring is $2.78 < |\eta| < 3.75$.

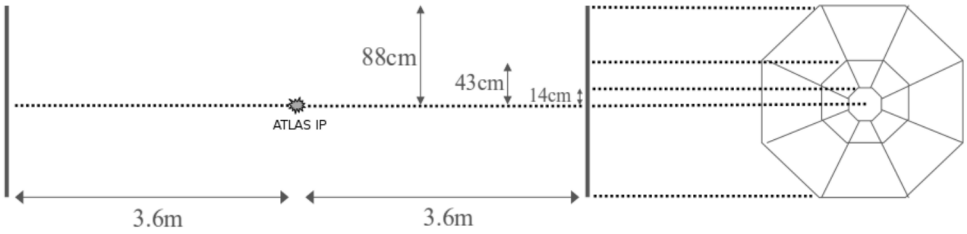

Figure 13: Minimum Bias Trigger Scintillators [34].

5.3. ALFA Detectors

The ALFA - **A**bsolute **L**uminosity **F**or **A**TLAS [1] - is a system of eight tracking detectors placed in so-called Roman Pots Fig. 15 vertically movable in four stations (Fig. 14) which are located in the outgoing beam lines of the ATLAS forward region ±240 m from the ATLAS Interaction Point (IP). The active part of the ALFA, depicted in Fig. 14, consists of a nearly edge-less scintillating fibres used for its two sub-components, the Main Detector (MD) and the Overlap Detector (OD). This system allows to detect the protons scattered under a very small angle outgoing from the IP.

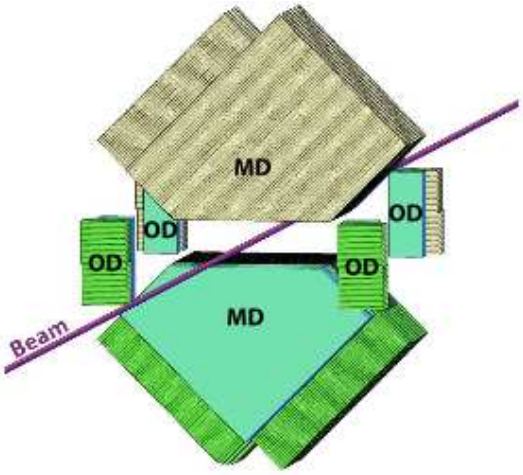

Figure 14: A schematic view of the main and the overlap detectors in two Roman pots of the station. The scintillating fibres are indicated by dashed lines while the triggers are indicated by plain objects [2].

The ALFA Roman Pots have thin (to minimize a creation of showers) steel windows of 0.2 mm and 0.5 mm thickness at the bottom and front/back sides. Two Roman Pots placed vertically create one ALFA station. On each ATLAS side two ALFA stations are placed. The distance between two consequent stations is approx. 4 m.

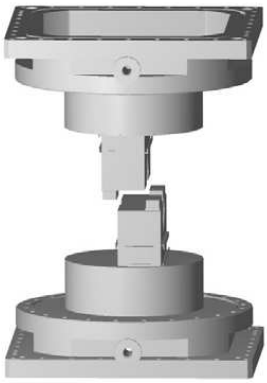

Figure 15: A schematic view of two Roman Pots in the ALFA station [2].

Both ALFA sub-components, MDs and ODs, are made of scintillating fibres. Their active area is defined with dedicated trigger counters. The MDs detect traversing protons coming from the proton-proton

interactions. A schematic view of the active detector area with trigger plates is shown in Fig. 14.

The MD consists of 10 titanium plates with two layers of fibres glued under +45° or −45°. Each Ti-layer contains 64 scintillating squared fibres of $0.5 \times 0.5\,\mathrm{mm}^2$. All 10 plates are staggered along a horizontal axis to increase a total spatial resolution. The theoretical resolution of a detector is $50\,\mu\mathrm{m}/\sqrt{12} = 14.4\,\mu\mathrm{m}$. In practice the resolution is slightly worse, typically between 25 µm and 35 µm, due to an imperfect staggering, inefficient fibre channels, a cross talk or a noise.

The MD is radiation hard up to 300 kRad (1 rad = 0.01 Gy) which is enough for low-μ runs data taking. The μ is stands for a mean value of number of interactions during a collision. For the low-μ runs the μ is below 1, for the standard LHC runs the $\langle\mu\rangle$ is usually in the range of $\langle\mu\rangle \in (20, 40)$. In case of run 191373 it was $\mu < 0.05$ [28].

The second part of the ALFA detector, so-called overlap detectors (ODs) are located on both sides of ALFA MD Figs. 15 and 16. The unit consists of 3 titanium plates of 30 vertically placed scintillating squared fibres of $0.5 \times 0.5\,\mathrm{mm}^2$. The titanium plates are staggered by 1/3 of the fibre size to increase OD resolution. The effective pitch of OD is 166 µm which results in a theoretical resolution of $166\,\mu\mathrm{m}/\sqrt{12} = 48\,\mu\mathrm{m}$. The overlap detectors measure only along the axis and they serve for a relative distance measurement between the upper and the lower detectors of the station.

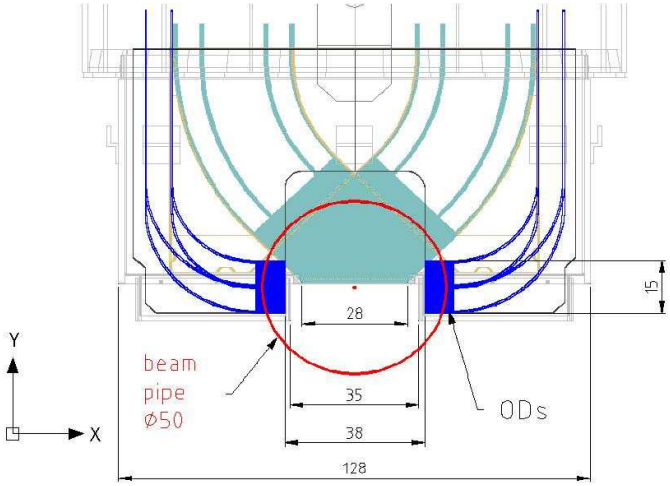

Figure 16: A front view of both, the main and overlap, detectors. The red circle and the red spot in the centre represent the beam pipe and the beam axis.

5.3.1. Naming scheme and numbering convention

The naming scheme of the data and Monte Carlo analysis is depicted in Fig. 17. ALFA stations are located on both ATLAS sides, A and C side. The ATLAS C-side covers the ALFA station A7R1 with two pots - the upper pot A7R1U (a.k.a. A5) and the lower pot A7R1L (a.k.a. A6) - located at about −237 m from the IP and the ALFA station B7R1 with two pots - the upper pot B7R1U (a.k.a. A7) and the lower pot B7R1L (a.k.a. A8) - located at about −241 m.

The ATLAS A-side covers the ALFA station A7L1 housing the upper pot A7L1U (a.k.a. A3) and the lower pot A7L1L (a.k.a. A4) located at about 237 m and the ALFA station B7L1 with two pots - the upper pot B7L1U (a.k.a A1) and the lower pot B7L1L (a.k.a. A2) - located at about 241 m.

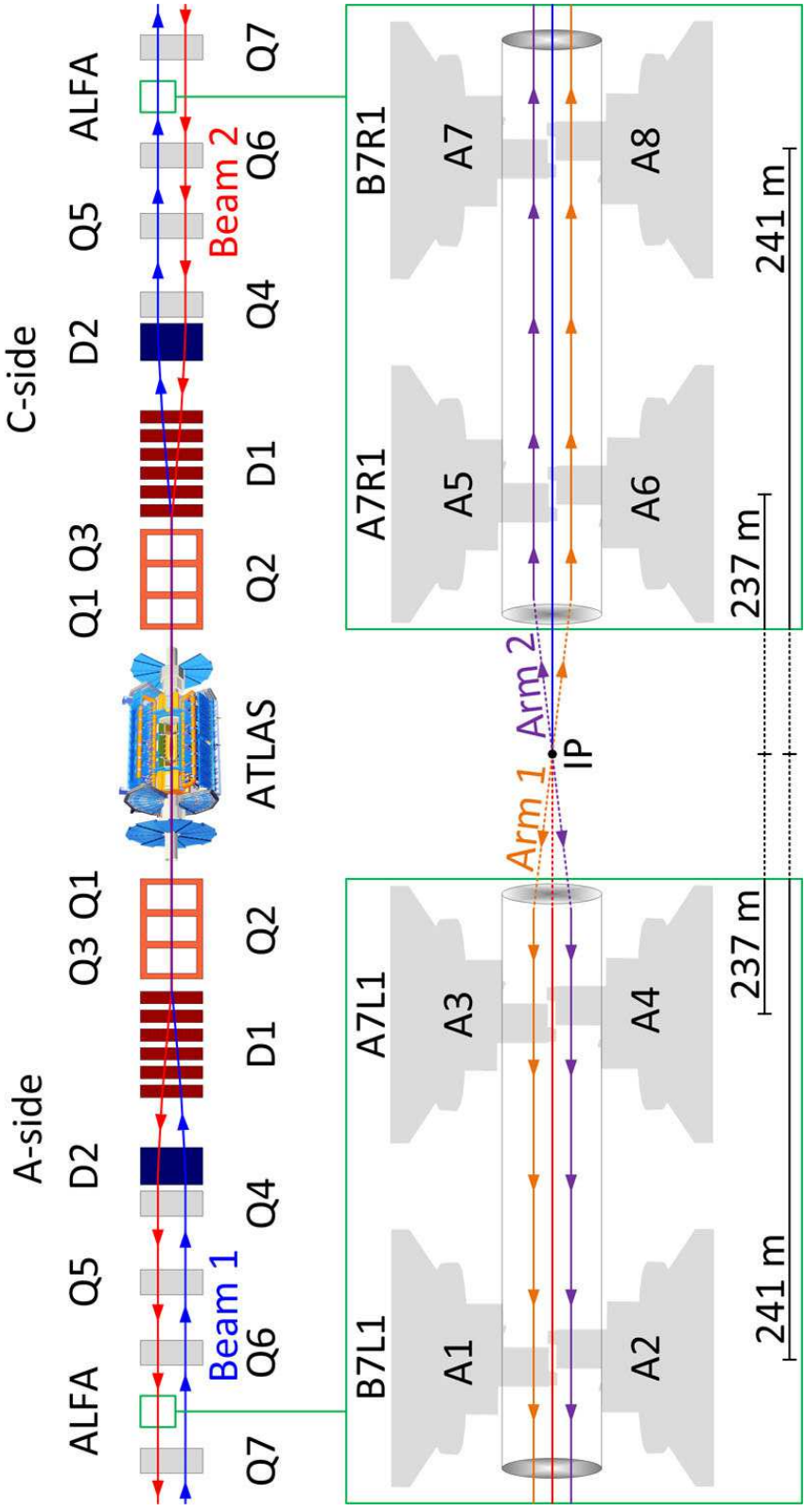

Figure 17: Schematic view of the ALFA set-up defining the naming and numbering conventions.

A distance between consequent ALFA stations in the ATLAS Run I era was approximately 4 m.

The ALFA stations on the ATLAS C-side are placed in the outgoing beam pipe of the beam 1 whereas the ALFA stations on the A-side are placed in the outgoing beam pipe of the beam 2.

Diffractive events are recorded in four possible combinations of the ALFA arms, in the Arm_1368 of the ALFA detectors A1+A3+A6+A8 (a.k.a. as Arm 1), in the Arm_2457 of the ALFA detectors A2+A4+A5+A7 (a.k.a. Arm 2), in the Arm_1357 of the ALFA detectors A1+A3+A5+A7 and in the Arm_2468 of the ALFA detectors A2+A4+A6+A8.

5.3.2. ALFA detector alignment

The proton position detected by the ALFA detector is reconstructed in a local coordinate system of the ALFA detector (Det CS) [28, 35]. The reconstructed position is transformed from the local coordinate system to the beam-based coordinate system (Beam CS) [28, 35] which was set as a common coordinate system of all ALFA detectors. The same coordinate system allows to compare the reconstructed positions among all ALFA detectors.

The analysis of the exclusive pion production uses the results of the ALFA detector alignment from that elastic scattering analysis [28] and are summarised in Table 3. These constants are stored in the COOL database [4] under the tag `FWDALFAposition_r191373_v2` in the folder `FWDALFAposition_calibration` of `COOLOFL_FWD/OFLP200` database and can be read by `AtlCoolConsole.py` utility which is a part of the ATLAS offline software release [19].

Table 3: The ALFA detector alignment constants [28].

ALFA	y offset [µm]	θ angle [mrad]	y offset [mm]
1	337.00	5.00	5.98
2	-356.00	1.40	-5.98
3	630.00	3.90	6.26
4	382.00	1.60	-6.17
5	265.00	0.40	6.08
6	383.00	-0.50	-6.30
7	428.00	2.00	5.76
8	494.00	-1.30	-6.05

5.4. Beam parameters and optics

[4] The COOL DB is the ATLAS database system serving for a sub-detector and a computing commissioning. Data are stored in the folders. Each folder can have several tags of different/updated values. The data are stored in the blocks (so-called interval of validity, IOV) with an associated start and end time between which they are valid.

5.4.1. Beam optics

The data were taken during the special ATLAS low luminosity run 191373 in Autumn 2011 using the special high $\beta^\star = 90\,\text{m}$ optics. In the ALFA elastic scattering analysis [28] the optics parameters were tuned to re-calibrate the magnet strength of Q1Q3 and the small residual crossing angle is compensate by a machine compensation system. The new set of optics parameters was called the effective optics.

5.4.2. Determination of the optics parameters

A nominal optics (a.k.a. designed optics) were determined for runs with a special high $\beta^\star = 90\,\text{m}$ optics. This optics is used in Monte Carlo simulation and it is a part of the ATLAS offline software and each Athena framework [4] releases. For the purpose of this analysis the nominal optics were read from the location

```
$ /cvmfs/atlas.cern.ch/repo/sw/software/x86_64-slc5-gcc43-opt/17.3.13/ \
AtlasSimulation/17.3.13/InstallArea/external/TwissFiles/TwissFiles/v003/ \
3.5TeV/0090.00m/nominal/v03
```

where nominal optics files are stored.

For the purpose of the data analysis the effective optics is used [28].

5.5. Trigger conditions

The ATLAS run 191373 was a dedicated run which served for the analysis of the elastically scattered protons which affected the trigger list. The trigger settings were not ideal the measurement of the exclusive pion production proceed such analysis.

On the HLT level the ALFA triggering was separated into two chains for both L2 and EF triggering, one called *ALFA_Phys_any* which contains only *L1_ALFA_ANY* item and one called *ALFA_Phys* which contains the rest of level 1 ALFA trigger items. The Table 4 summarises the level 1 ALFA trigger items with their trigger condition. A simple scheme of the ALFA triggering is depicted on Fig. 18. No algorithms were applied on the high level triggering for ALFA which means that a pass through of level 1 items was used. More about ALFA triggering scheme is described in [36].

Table 4: A list of level 1 ALFA trigger items used in the analysis and separated into two level 2 ALFA trigger chains of the ATLAS run 191373.

trigger item	**ALFA trigger condition**
L2_ALFA_Phys_any chain	
L1_ALFA_ANY	B7L1U || B7L1L || A7L1U || A7L1L || || A7R1U || A7R1L || B7R1U || B7R1L
L2_ALFA_Phys chain	
L1_ALFA_ELAST15	(B7L1U || A7L1U) && (A7R1L || B7R1L)
L1_ALFA_ELAST18	(B7L1L || A7L1L) && (A7R1U || B7R1U)

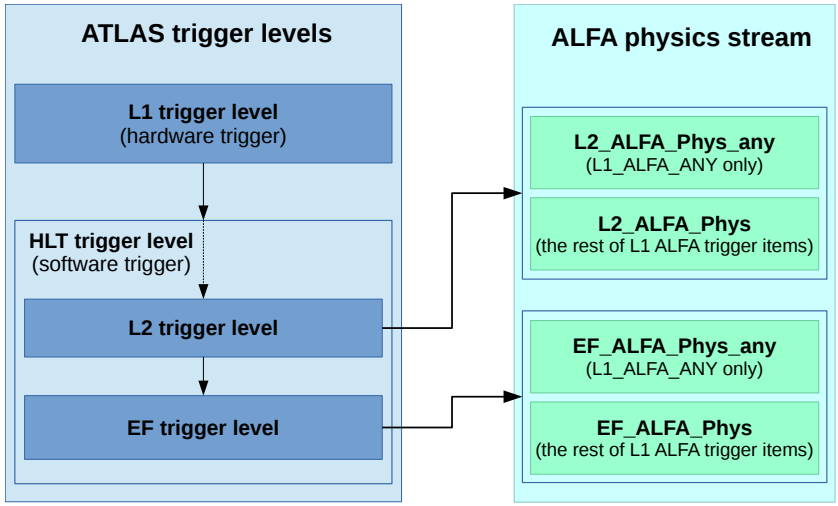

Figure 18: ALFA trigger level scheme.

5.5.1. Trigger pre-scales

The exclusive pion analysis was done on the ALFA Physics stream which contains HLT trigger level chains. The ALFA HLT trigger level contains two separated chains. In the exclusive pion analysis the level 2 trigger chains were used in the combination with level 1 ALFA trigger items. These two chains were pre-scaled with different pre-scale factors which are show in Table 5. The *L2_ALFA_Phys_any* chain was a pre-scaled by factor 15 whereas for the *L2_ALFA_Phys* chain no trigger pre-scale was applied (it was set to 1). The trigger pre-scales of the level 1 triggers used in the exclusive pion production analysis are summarised in the Table 6. It is seen that the level 1 trigger items used in the analysis were not pre-scaled.

Table 5: Pre-scale factors for ALFA triggering on level 2 in the ATLAS run 191373.

Channel name	**LB: 1 - 1 Key: 4612**	**LB: 2 - 263 Key: 4554**
L2_ALFA_Phys_any	100	15
L2_ALFA_Phys	1	1

Table 6: Pre-scale factors for ALFA triggering on level 1 in the ATLAS run 191373 used in the exclusive pion analysis.

Channel name	**LB: 0 - 263**
L1_ALFA_ANY	1
L1_ALFA_ELAST15	1
L1_ALFA_ELAST18	1

The exclusive pion analysis is split into two configurations based on the triggers. The first configuration so-called the **elastic** configuration is based on *L2_ALFA_Phys* HLT trigger chain in the combination with *L1_ALFA_ELAST15* and *L1_ALFA_ELAST18* level 1 triggers, whereas the second configuration so-called the **anti-elastic** configuration is based on *L2_ALFA_Phys_any* HLT trigger chain, see Table 7.

We decided to add an additional trigger selection based on the detector trigger information which is stored in the output file (a.k.a. D3PD file) after the data reconstruction process. The selection for the elastic configuration respects the trigger logic of the L1 elastic triggers, the selection for the anti-elastic configuration is defined in the similar way to the elastic configuration but for the detectors forming the anti-elastic arms.

Table 7: Trigger items and chains together with the overall trigger pre-scale for two exclusive pion analysis configurations.

Configuration	**L2 trigger chain**	**L1 trigger items**	**Overall pre-scale**
elastic	L2_ALFA_Phys	L1_ALFA_ELAST15 L1_ALFA_ELAST18	1
anti-elastic	L2_ALFA_Phys_any		15

During the analysis an inconsistency in the *L2_ALFA_Phys_any* trigger chain pre-scale between the value stored in COOL DB and written on the page [37] was observed. The *L2_ALFA_Phys_any* trigger chain pre-scale value in COOL DB is equal to 15 whereas *L2_ALFA_Phys_any* trigger chain pre-scale value on the page [37] is equal to 10. For clarify the situation the ALFA calibration stream and the ALFA physics stream were used. The calculation confirms the value of *L2_ALFA_Phys_any* trigger pre-scale calculated using appropriate rates from COOL DB. It was decide to use this re-calculated value for the *L2_ALFA_Phys_any* trigger chain. The Fig. 19 depicts the calculated *L2_ALFA_Phys_any* trigger chain pre-scale.

The efficiency of the ALFA triggers were studied during the ALFA analysis of elastically scattered protons [38]. It was shown that the trigger efficiency of the elastic configuration is $99.97 \pm 0.01\%$. The anti-elastic configuration - as it is defined for the exclusive pion analysis - was not studied in [38]. No dedicated

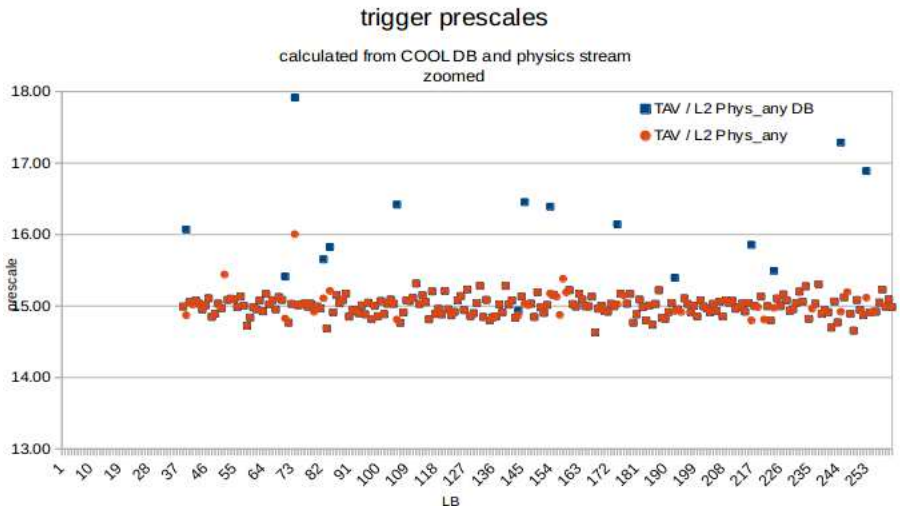

Figure 19: The L2_ALFA_Phys_any trigger chain pre-scales calculated using the rates from COOL DB (red distribution) and using a combination of a number of events from both the ALFA calibration and the ALFA physics streams. The value stored in [37] is 10.

triggers were included on a trigger list for ATLAS run 19373 used in our analysis. But the single-diffractive triggers (i.e. L1_ALFA_SDIFF5) were on the list and the efficiency was calculated for them in [38]. Thus we estimated the efficiency of the trigger describing the anti-elastic configuration by a simple combination of two single-diffractive triggers (one from each ALFA side). We selected a conservation approach and the worst average diffractive trigger efficiency $99.69 \pm 0.18\%$ decreased by its uncertainty and calculated the trigger efficiency of the anti-elastic configuration. We determined it to $99.02 \pm 0.25\%$.

6. Particle kinematic reconstruction

In the exclusive production we need to reconstruct kinematic parameters of two pions and two protons. The pion kinematic are provided by the Inner detector whereas the kinematics of the protons are reconstructed by the ALFA detector system.

6.1. Inner detector kinematic reconstruction

The Inner Detector (ID) is a system which is able to reconstruct a particle trajectory as well as its complete set of kinematics [39]. In the case of the exclusive pion production the ID reconstructs the pion kinematics with ≈10 MeV precision in both p_x and the p_y. The pion kinematics resolution for the GenEx Monte Carlo simulation of the exclusive pion production is shown in Fig. 20 where the red distribution corresponds to the negatively charged pions whereas the blue distribution corresponds to the positively charged pions.

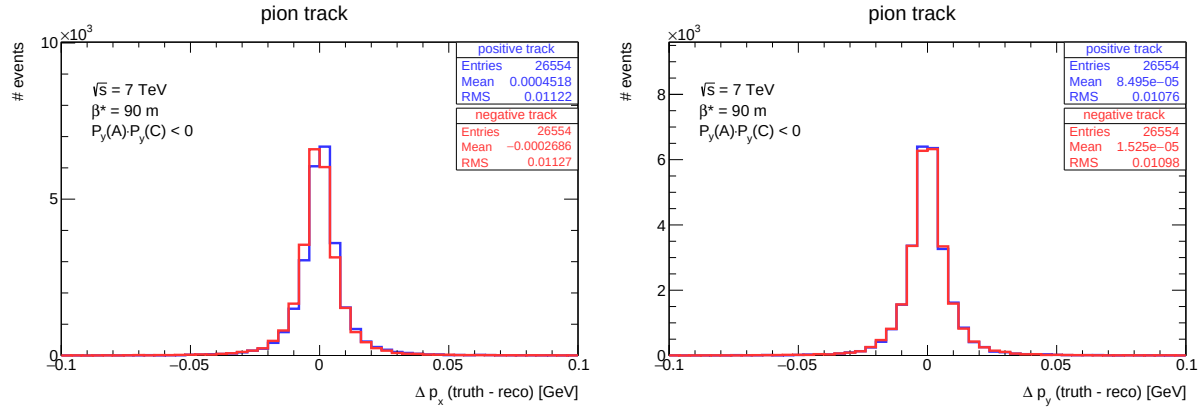

(a) (b)

Figure 20: The pion track kinematic reconstruction resolution (as a difference between the particle and detector level) for p_x in (a) and p_y in (b) reconstructed by the Inner detector in MC simulation. The red distribution is for negative pions whereas the blue distribution is for positive pions.

6.2. ALFA kinematic reconstruction

The ALFA detector is a tracking detector, see Sect. 5.3. We present two proton kinematics reconstruction algorithms, the so-called ALFA Reco algorithm [40] and the Lattice method algorithm [28].

6.2.1. ALFA Reco method

The ALFA Reco is an algorithm [40]) based on parametrization of the reverse mapping: $x, y, x', y' \rightarrow \Theta^*, \varphi^*, \xi$, where are proton's kinematics at the IP.

The ALFA Reco method requires a knowledge of the reconstructed diffractive proton position in two consequent ALFA detectors (see Fig. 21) and a beam spot position in the IP as the mandatory inputs.

The result of the proton kinematics and position reconstruction in the IP returns values for the following variables, p_x, p_y, E, v_x and v_y.

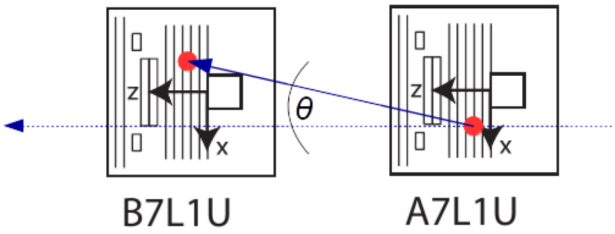

Figure 21: The local angle θ between two consequent ALFA detectors, here between B7L1U and A7L1U. The local angle is defined in both x and y coordinate.

6.2.2. Lattice method

The Lattice method is a method based on the knowledge of elastic protons transport equations from the ATLAS interaction point (IP) to the ALFA detectors and on the knowledge of the optics settings during the data taking. This method was used for the studies where the protons energy loss is zero like in the analysis of the elastically scattered protons [28]. But it can be shown - and in fact this analysis shows it - that the proton energy loss is very small and that such diffractive protons detected by the ALFA detector can be treated as elastic-like, and the Lattice method is useful in our analysis. It would be shown that the proton kinematics resolutions in p_x and p_y are comparable with the resolution with the kinematics of the tracks reconstructed in the Inner detector.

The proton trajectory equation for the transport of the elastically scattered protons can be described

$$\vec{z}(s) = \begin{pmatrix} u(s) \\ u'(s) \end{pmatrix} \tag{12}$$

$$\vec{z}^{\star} = T\vec{z} \tag{13}$$

$$\begin{pmatrix} u^{\star} \\ u^{\star\prime} \end{pmatrix} = \begin{pmatrix} T_{11}T_{12} \\ T_{21}T_{22} \end{pmatrix} \begin{pmatrix} u(s) \\ u'(s) \end{pmatrix} \tag{14}$$

where $u(s)$ represents a position in beam x or y coordinate system at a given position s whereas the $u(s)'$ represents the θ angle in a given position of s, and $T = M^{-1}$ is the inverse of transport matrix M described by the elements

$$\begin{aligned} M_{11} &= \sqrt{\frac{\beta}{\beta^{\star}}}(\cos\Psi + \alpha^{\star}\sin\Psi), & M_{12} &= \sqrt{\beta\beta^{\star}}(\sin\Psi), \\ M_{21} &= \frac{(\alpha^{\star} - \alpha)\cos\Psi - (1 - \alpha\alpha^{\star})\sin\Psi}{\sqrt{\beta\beta^{\star}}}, & M_{22} &= \sqrt{\frac{\beta^{\star}}{\beta}}(\cos\Psi - \alpha\sin\Psi), \end{aligned} \tag{15}$$

where β resp. $\beta^\star$ is optical function in a given position of s resp. in the interaction point of $s = 0\,\mathrm{m}$ and α is proportional to the β derivative. From a knowledge of the reconstructed proton position ($u(s)$) in ALFA detector and its local angle ($u'(s)$) we can calculate the proton position and its angle in the ATLAS IP using [28]

$$u^\star = T_{11} \cdot u + T_{12} \cdot u', \quad u^{\star\prime} = T_{21} \cdot u + T_{22} \cdot u'. \tag{16}$$

The lattice method allows to reconstruct the t-spectrum using both the reconstructed proton position (u) and the its local angle (u') as shown in Eq. 16. The t-spectrum is then

$$-t = u'^{\star 2} p^2, \tag{17}$$

where p is proton momentum in interaction point.

It will be shown later that the protons energy loss is of the order of units of GeV and therefore such approximation is justifiable [5].

6.2.3. ALFA Reco method performance plots

A set of control plots were made to see a precision of the proton kinematic reconstruction. The control plots are shown on Figs. 22–24. It is clear that the proton kinematic reconstruction provides suitable resolutions only for p_x and p_y. The resolution of the proton energy reconstruction it almost one order higher then the proton energy loss in the exclusive pion production.

The Fig. 22 shows the resolution of proton reconstructed kinematics using ALFA Reco algorithm, on Fig. 22a for the proton p_x and on Fig. 22b for the proton p_y.

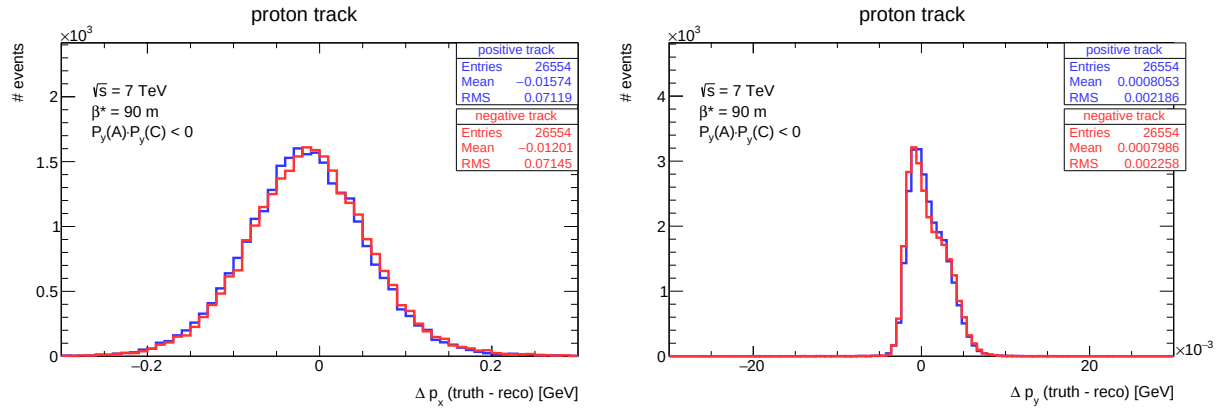

(a) (b)

Figure 22: The proton kinematics reconstruction resolution, in (a) for proton p_x and in (b) for p_y. The ALFA Reco algorithm is used for the proton kinematics reconstruction. The red distribution shows the proton with the positive z-direction whereas the blue distribution shows the proton with the negative z-direction.

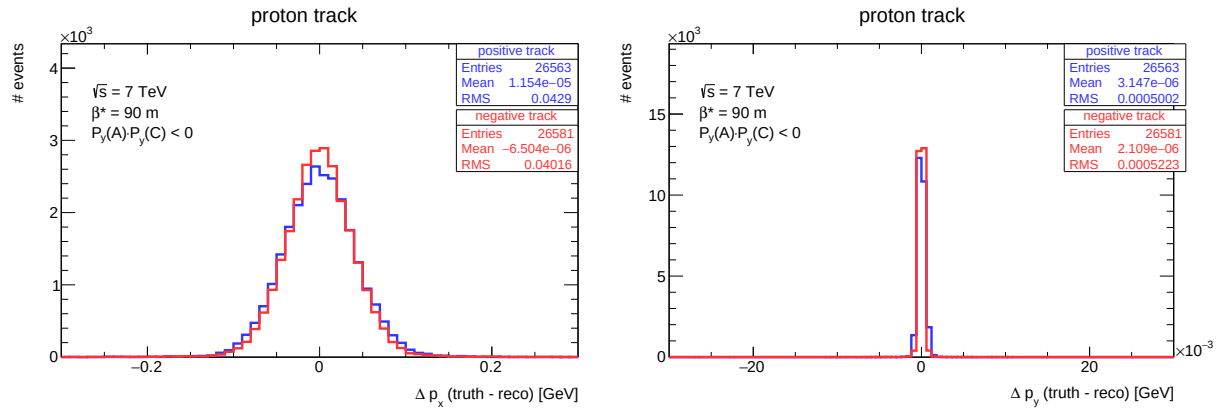

(a) (b)

Figure 23: The proton kinematics reconstruction resolution, in (a) for proton p_x and in (b) for p_y. The Lattice method algorithm is used for the proton kinematics reconstruction. The red distribution shows the proton coming in the positive z-direction whereas the blue distribution shows the proton moving in the negative z-direction.

The Fig. 23 shows a resolution of proton reconstructed kinematics using Lattice method algorithm, on Fig. 23a for the proton p_x and on Fig. 23b for the proton p_y.

Comparing Figs. 22 and 23 we can conclude that in case of the Lattice method algorithm a slightly better results are obtained for the proton p_x whereas for the resolution of proton p_y the resolution for both algorithms is more or less the same.

The proton energy resolution is shown on Fig. 24 where Fig. 24a shows that energy resolution for the Lattice method algorithm is not calculated and the Fig. 24b shows the energy resolution for the ALFA Reco algorithm. It is seen what was written earlier, in the case of the Lattice method there is no possibility to reconstruct proton energy whereas in the case of the ALFA Reco the resolution of the reconstructed proton energy is not enough precise for this exclusive pion production analysis.

We can conclude that the resolution of the pions kinematics is ≈10 MeV for both p_x and p_y whereas the resolution of the proton kinematics is ≈70 MeV for proton p_x, resp. ≈2 MeV for proton p_y in the case of the ALFA Reco method and ≈40 MeV for proton p_x, resp. ≈1 MeV for proton p_y in the case of Lattice method algorithm.

[5] The statement is supported by the results of Monte Carlo simulation. See Figs. 100 and 102 for the elastic configuration and Figs. 101 and 103 further in this note, in Sect. D.1, for a better clarification of the statement that the protons coming from the exclusive pion production look like the elastic ones in the ALFA detector.

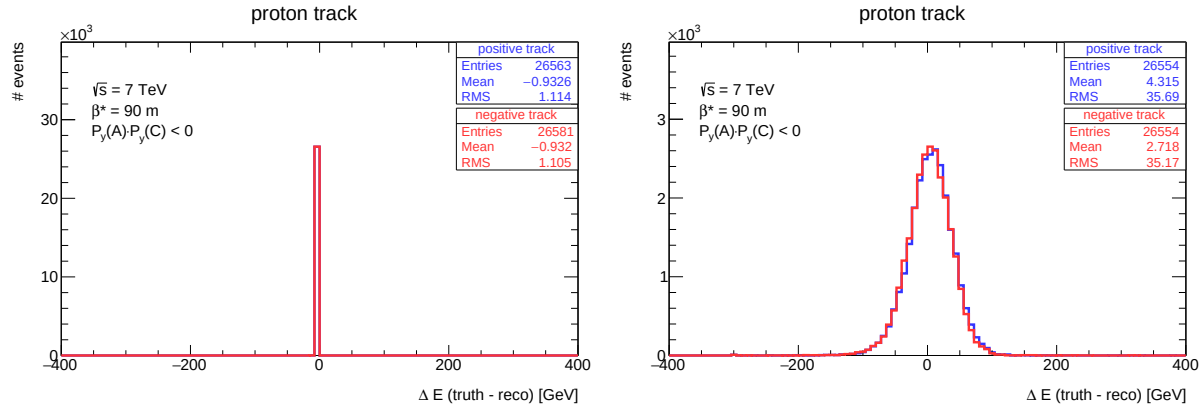

(a) (b)

Figure 24: The proton energy resolution, for (a) the Lattice method algorithm (by principle trivial) and in (b) for the ALFA Reco algorithm. The red distribution shows the proton moving in the positive z-direction whereas the blue distribution shows the proton going in opposite direction.

7. Data taking and event selection

This section describes the events selection techniques used in the exclusive pion pair production analysis. A cut flow of event selection was developed to select a signal from LHC data or Monte Carlo (MC) simulation. It is designed to cover both sample types the LHC data and the MC simulation, and it is based on event-by-event selection. The event selection is split into several modules. The most of the modules are common for both data and Monte Carlo simulation with the exception of the data quality and the trigger selection, later called as pre-selections which serve for data only. They are based on the run conditions like set of triggers and their pre-scales or luminosity-blocks dead time.

The common parts of the cut flow for both the data and MC simulation covers the track selection in both ATLAS Inner detector and the ALFA detectors, the vetoing on the signal from the Minimum Bias Trigger Scintillators, the background suppression based on the geometrical properties of the tracks reconstructed in ALFA detectors, and the cut on the kinematics of the exclusive system based on a momentum balance conservation law.

There is also a selection of the kinematic region in which the analysis is done and which is again the same for data and MC simulation samples.

7.1. Data taking a data quality pre-selection

The data for the ATLAS Run 191373 were taken in a period of Oct 20 2011 12:58:42 - 17:14:21 during a special high $\beta^\star = 90\,\text{m}$ during the LHC fill 2232. The collisions at ATLAS Interaction Point (IP1) were obtained for the RF bucket 1 (BCID 1) for both beams. The ATLAS run was filled with one nominal bunch of the intensity $7 \cdot 10^{10}$ protons and 12 pilot bunches of the intensity $1 \cdot 10^{10}$ protons as well as of one unpaired bunch of the intensity $7 \cdot 10^{10}$ protons. The optics setting designed for this data taking are described in [27, 41]. More information about the LHC fill 2232 is in [28].

The analysis of the exclusive pion production is done using the data of the ATLAS run 191373. This run contains 14 bunches where one bunch is nominal, one bunch is unpaired bunch and the rest of 12 bunches are the pilot bunches. For the purpose of this analysis the only nominal bunch with the intensity of $7 \cdot 10^{10}$ protons is used. The BCID of this bunch is equal to one. The 12 pilot bunches with a total intensity of $1 \cdot 10^{10}$ protons are not usable for the analysis due to a high background fraction.

The data contains 263 luminosity blocks in total. Not all luminosity blocks could be used, only these for the analysis with a life fraction higher than 95% and a duration time higher than 60 s were accepted [28]. The average life fraction of the selected luminosity blocks for the elastic configuration - defined by L1_ALFA_ELAST15 and L1_ALFA_ELAST18 triggers - is 99.73% whether the life fraction of the anti-elastic configuration - defined by L1_ALFA_ANY trigger - is 99.72%.

An important parameter for each data analysis is a knowledge of the luminosity. The principles of the luminosity measurements are well described in the ATLAS total cross-section measurement [2, 28]. The exclusive pion production analysis inherits the luminosity results from the [2, 28] due to the same data of the ATLAS run 191373 with the same sets of the good luminosity blocks as in the [2, 28]. The luminosity there was determined from LHC beam parameters using van der Meer scans [42].

The final result of the integrated luminosity for the ATLAS run 191373 including the statistical and the systematic errors is

$$L_{\text{int}}^{\text{run}} = 79.68 \pm 0.13^{(\text{stat})} \pm 1.87^{(\text{syst})}\,\mu\text{b}^{-1}. \tag{18}$$

For the luminosity blocks used in this exclusive pion production analysis, the integrated delivered luminosity including the statistical and the systematic errors is

$$L_{\text{int}} = 78.72 \pm 0.13^{(\text{stat})} \pm 1.85^{(\text{syst})}\,\mu\text{b}^{-1}. \tag{19}$$

The presented luminosity is applied on the results of the data analysis in the end of the event selection to obtain the exclusive pion cross-section.

7.2. Trigger pre-selection

The data of the ATLAS run 191373 were not taken with the triggers dedicated for a study like the exclusive pion production. Therefore the suitable events for the exclusive pion pair production are selected by choosing appropriate triggers.

It was decided to split the analysis into two configurations based on the ALFA triggers. The first configuration, called the elastic, is based on the `L2\_ALFA\_Phys` trigger chain and two elastic L1 trigger items, the `L1\_ALFA\_ELAST15` trigger item and the `L1\_ALFA\_ELAST18` trigger item. The second configuration, called the anti-elastic, is based on the `L2\_ALFA\_Phys\_any` trigger item. More about the trigger issue including the trigger pre-scales is described in Sect. 5.5.

7.3. Primary vertex selection

The primary vertex selection can be applied on the event selection to suppress the events that containing the reconstructed tracks from different interaction. The event passes the selection if an existence of the primary vertex with exactly two pion tracks with an opposite sign is visible.

7.4. ATLAS ID track selection

The four products are expected in the exclusive pion pair production, two protons going to the ATLAS forward region and two pions, π^+ and π^-, detected by the Inner detector (Sect. 5.1).

The ATLAS ID track selection serves for the event selection of a pion pair formed by π^+ and π^-. A common set of selections is applied on the tracks reconstructed in the ID. First, the condition on the existence of the reconstructed primary vertex is applied. If the primary vertex exists it has to contain exactly two reconstructed tracks with opposite signs to be processed to next both tracks have to pass a set of the track quality condition - defined bellow.

The ATLAS Inner detector tracks selection is executed after the quality pre-selection (Sect. 7.1) and the trigger pre-selection (Sect. 7.2).

Track quality condition

The track quality condition is a part of the standard ATLAS ID track selection, serves for a removing of the poor-quality tracks and was used in various ATLAS analyse, e.g. in the minimum bias analysis:

- **Pixel** - a number of hits in Pixel sub-detector, at least one hit is expected in a default configuration,
- **SCT** - a number of hits in SCT sub-detector depending on a track p_t, at least two hits for the track with $p_t > 100\,\text{MeV}$, four hits for the track with $p_t > 200\,\text{MeV}$ and six hits for the track with $p_t > 300\,\text{MeV}$ are expected in the default configuration,
- **B-layer** - an existence of b-layer hit, at least one b-layer hit is expected in the default configuration,
- **track pattern recognition** - a strategy for track finding. The "inside-out" strategy [39] of tracks finding is used in this analysis together with "low p_t" track reconstruction.

The track quality conditions may varied for a different set-up of the analysis, like the background studies.

7.5. ALFA track selection

The ALFA track was reconstructed with a standard track reconstruction criteria:

- fibre layers with more than ten hits are not used in a track reconstruction,
- at least three layers (out of ten) with hit activity are required,
- hit multiplicity of required layers has to be between one and three,
- at least three overlapping hit fibres (out of possible ten) in u and v coordinates has to be seen to reconstruct the track position.

The Fig. 25 shows an example of a hit pattern in layers forming one coordinate.

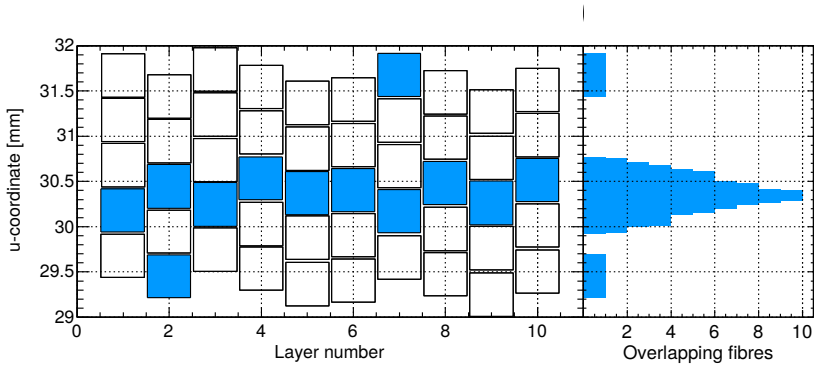

Figure 25: Hit pattern of a proton trajectory in the ten fibre layers comprising the u coordinate. The superposition of fibre hits attributed to a track is shown in the histogram. The position of maximum overlap is used to determine the track position [2].

The ALFA event selection is based on the combination of the reconstructed proton positions and its kinematics. The event is counted only if contains at least one fully reconstructed track (the position and the kinematics) on each ATLAS side.

The set of ALFA detectors topologies which are allowed for the exclusive pion production is shown in Fig. 26. The ALFA detector combinations are drawn in green colour. The ALFA arm configurations in Figs. 26a and 26b represent the elastic configuration on detector level whereas the ALFA arm configurations on Figs. 26c and 26d represent the anti-elastic configuration on the detector level. The naming scheme of depicted combinations is explained in detail in Sect. 5.3.1.

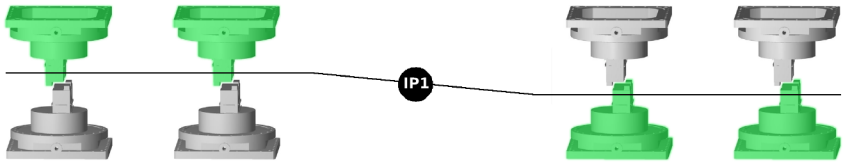

(a) ALFA arm 1

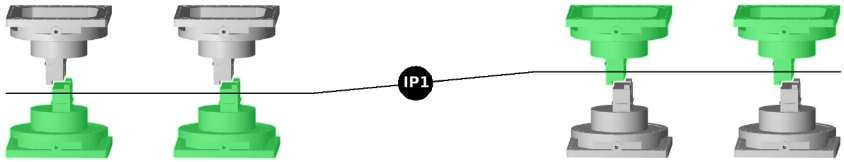

(b) ALFA arm 2

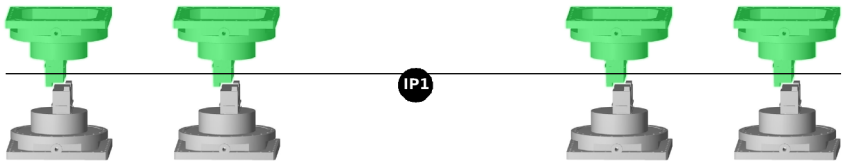

(c) ALFA arm 3

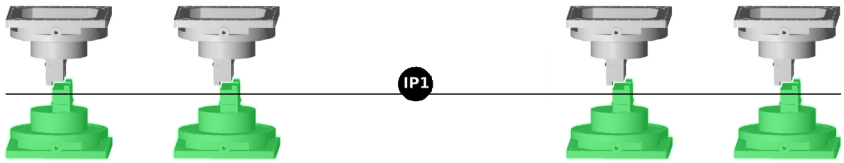

(d) ALFA arm 4

Figure 26: The ALFA detector combinations allowed for the exclusive pion production. Green ALFA detectors represent the detectors with a reconstructed tracks forming the ALFA arm. The ALFA arm 1 on (a) and the ALFA arm 2 on (b) represent the elastic configuration whereas the ALFA arm 3 on (c) and the ALFA arm 4 on (d) represent the anti-elastic configuration.

The ALFA reconstruction algorithm (a.k.a ALFA tracking algorithm) [28] is able to reconstruct more than one track in each ALFA detector. More reconstructed ALFA tracks can origin due to e.g. a beam halo, pile-up or showers. It can be hard to decide which track is the right one. Therefore it was decided to select only events with exactly one track. A potential loss of a signal is compensated by the corrections (see in Sect. 8).

The following selection was used:

- one ALFA clean track in detector - the ALFA detector contains exactly one reconstructed track,
- one ALFA clean track in an armlet - the both consequent ALFA detectors contain the ALFA detector clean track,

- one ALFA clean track in an arm - the ALFA arm formed by two ALFA armlets contains ALFA armlet clean tracks.

The ALFA event selection follows after the ATLAS ID track selection (Sect. 7.4). If the event passed both the ATLAS ID tracks selection and the ALFA event selection, it contains a potential exclusive system composed by two pions and two protons. In this point we can study the exclusive system on a set of control plots comparing data with a prediction of signal and background fractions. The signal fraction is predicted by the Monte Carlo simulation of the GenEx generator whereas the background fraction is predicted by the Monte Carlo simulation of the Pythia8 generator with the central diffractive processes. We assume that the dominant source of the background in our analysis comes from the central diffractive processes from which only a part mimicking a signal was detected. Our assumption is also supported by the running conditions - a very low pile-up which significantly reduces the coincidence of the types halo - single diffraction or halo - halo. The background is estimated at almost final event selection step - on selection using the system momentum balance is not applied. The signal and background distributions differ significantly from each other to be able to separate them. The best example represents the p_y momentum balance distribution of the exclusive system. Here the data distribution can be described by the MC GenEx simulation - on the side of the signal - and by the MC Pythia8 central diffraction simulation - on the side of the background. The agreement of the Pythia8 central diffraction simulation with the background is described in the section Sect. 9.

Both Monte Carlo signal fraction and background fraction are normalised to the data using the ROOT routine TFractionFitter. The routine returns the probability P_{mcSig} of the MC signal fraction and the probability P_{mcBckg} of the MC background fraction in data. These probabilities are then used to calculate the normalization factor F_{mcSig} of the MC signal fraction in Eq. 20 and the normalization factor F_{mcBckg} of the MC background fraction in Eq. 21. The fit itself is performed on the distribution describing the p_y momentum balance of the exclusive pion system just before the final selection cut based on momentum balance. The variable N_{data} in Eqs. 20 and 21 represents the integral of the p_y momentum balance of the data distribution whereas the variable N_{mcSig} represents the integral of the p_y momentum balance distribution for the MC simulation of the signal fraction and the vaiable N_{mcBckg} is the integral of the p_y momentum balance distribution for the MC simulation of the background fraction.

$$F_{\mathrm{mcSig}} = \frac{N_{\mathrm{data}} P_{\mathrm{mcSig}}}{N_{\mathrm{mcSig}}} \qquad (20) \qquad\qquad F_{\mathrm{mcBckg}} = \frac{N_{\mathrm{data}} P_{\mathrm{mcBckg}}}{N_{\mathrm{mcBckg}}} \qquad (21)$$

The result of the fit is shown in the Fig. 78 in Sect. 9 dedicated to the background study. To use the fit in the steps of event selection before the final one, it is necessary to renormalized it. The re-normalization process is described by the Eqs. 22 and 23 where $N^{'}_{\mathrm{data}}$ is the integral of the p_y momentum balance of the data distribution, $N^{'}_{\mathrm{mcSig}}$ is the integral of the p_y momentum balance of the MC signal distribution and $N^{'}_{\mathrm{mcBckg}}$ is the integral of the p_y momentum balance of the MC background distribution after the performance of the event selection.

$$F^{\mathrm{reNorm}}_{\mathrm{mcSig}} = F_{\mathrm{mcSig}} \cdot \frac{N_{\mathrm{data}} N^{'}_{\mathrm{mcSig}}}{N^{'}_{\mathrm{data}} N_{\mathrm{mcSig}}} \qquad (22) \qquad\qquad F^{\mathrm{reNorm}}_{\mathrm{mcBckg}} = F_{\mathrm{mcBckg}} \cdot \frac{N_{\mathrm{data}} N^{'}_{\mathrm{mcBckg}}}{N^{'}_{\mathrm{data}} N_{\mathrm{mcBckg}}} \qquad (23)$$

A set of control plots were made to compare the kinematics of the reconstructed protons in ALFA detectors with the kinematics of the tracks in the Inner detectors after applying of the ALFA tracks selection. It contains data together with the MC prediction of the signal and the background fractions. The MC fractions are normalized to the data using the fit technique described above, the MC signal fraction is scaled by $F^{\text{reNorm}}_{\text{mcSig}}$ factor and the MC background fraction is scaled by $F^{\text{reNorm}}_{\text{mcBckg}}$ factor. The control plots are shown in Fig. 27 where the ID track p_{x} resp. p_{y} distribution is shown in Fig. 27a resp. Fig. 27b, the proton p_{x} resp. p_{y} distribution is shown in Fig. 27c resp. Fig. 27d and the $\sum p_{\text{x}}$ resp. $\sum p_{\text{y}}$ system momentum balance distribution is shown in Fig. 27e resp. Fig. 27f. The data are represented by the black points whereas the Monte Carlo simulations are represented by the blue histogram for the GenEx simulation and by the red histogram for the Pythia8 central diffraction containing only the non-exclusive events.

A combination of the MC signal fraction and the MC background fraction described only by the Pythia8 central diffraction can hardly describe data after the ALFA event selection. Distributions show a non-negligible background fraction which is not included in the MC simulation. This is an expected result as at the beginning of the exclusive event selection chain there are also other background sources which are not included in the MC simulation. As will be shown later the dominant background for this exclusive pion production in data of the run 191373 comes from the central diffraction and this source of the background will be able to describe the background in data sufficiently well. The final result of the background study is summarised in Sect. 9, where also the final control plots comparing data with the MC signal fraction and the MC background fraction are presented in Sect. 7.10. Next, the distributions on the control plots above show that the background is very dominant in this step of the event selection. Therefore more event selections is needed.

The other control plots are shown in the Fig. 28. These are the kinematic distributions for the reconstructed track pairs - the pion pair candidates. The distribution compare both the data and the Monte Carlo simulations. The data are represented by the black points whereas the Monte Carlo simulations are represented by the blue histogram for the GenEx simulation and by the red histogram for the Pythia8 central diffraction containing only the non-exclusive events. The distribution of the track pair transverse momentum (Fig. 28e) and track pair mass (Fig. 28f) show a level of inconsistency which may point on an insufficient background prediction for this step of the event selection.

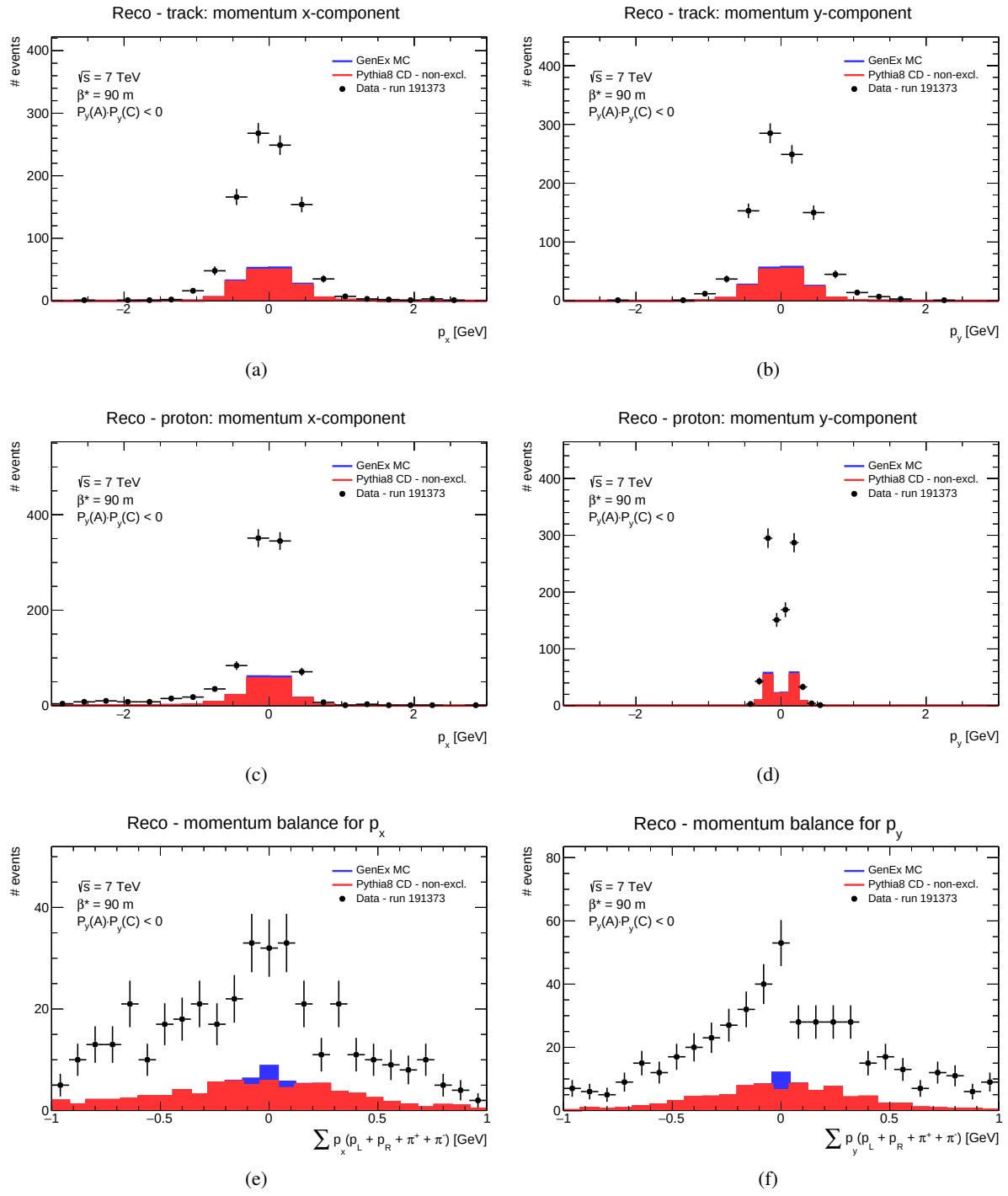

Figure 27: A set of control plots for the kinematic variables after the ALFA track selection, on (a) for the pion p_x distribution, on (b) for the pion p_y distribution, (c) for the proton p_x, on (d) for the proton p_y, on (e) for the momentum balance in p_x of the system formed by two protons and two tracks ($\pi^+\pi^-$) and on (f) for the momentum balance in p_y of the system formed by two protons and two tracks ($\pi^+\pi^-$). The data are represented by the black points whereas the Monte Carlo simulations are represented by the blue histogram for the GenEx simulation and by the red histogram for the Pythia8 central diffraction containing only the non-exclusive events. The MC histograms are stacked.

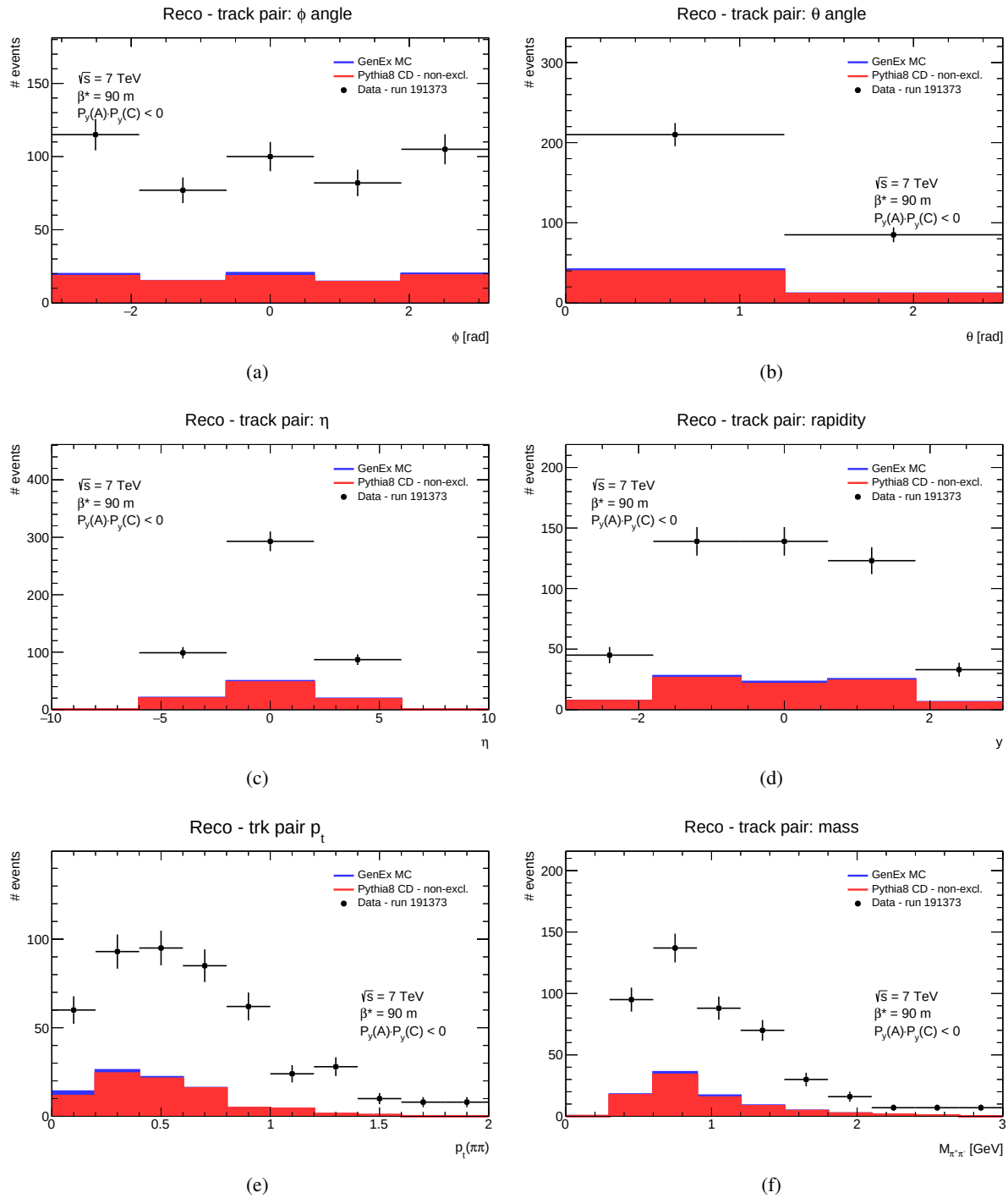

Figure 28: The reconstructed tracks pair kinematics distributions after the ALFA track selection, on (a) for the $\phi_{\pi^+\pi^-}$ distribution, on (b) for the $\theta_{\pi^+\pi^-}$ distribution, on (c) for the $\eta_{\pi^+\pi^-}$ distribution, on (d) for the rapidity $y_{\pi^+\pi^-}$ distribution, on (e) for the $pt_{\pi^+\pi^-}$ distribution and on for (f) and the $M_{\pi^+\pi^-}$ distribution. The data are represented by the black points whereas the Monte Carlo simulations are represented by the blue histogram for the GenEx simulation and by the red histogram for the Pythia8 central diffraction containing only the non-exclusive events. The MC histograms are stacked.

7.6. MBTS veto

The MBTS veto selection is designed to suppress the non-exclusive pion events using the information from the Minimum Bias Trigger system, described in Sect. 5.2. The Minimum Bias Trigger system consist of 16 cells uniformly separated into two rings, the inner one ant the outer one, with a different coverage of the η region, mentioned in Sect. 5.2.

The η region of the outer ring overlaps with the η region of the Inner detector (mentioned in Sect. 5.1) contrary to the inner ring which η region has no overlap with the η region of the Inner detector. Assuming that no track from the Inner detector hit the inner ring of the MBTS no activity should be seen in the MBTS inner ring in the case of the exclusive pion production. Taking in account imperfection of our assumption we will require that the number of the MBTS inner cells with a signal on both ATLAS sides A and C is lower than two, i.e. maximally one cell can give a signal,

- $(A_{\text{in}} + C_{\text{in}}) < 2$,

where A_{in} (resp. C_{in}) is the MBTS inner cell on side A (resp. C). The condition is less conservative then would be naively expected. It counts with the case that there is no real signal in MBTS nevertheless the amount of a noise in the cell causes a fake signal, i.e. by an electronic noise. For the purpose of the systematic uncertainty study, the default MBTS veto condition is modified to

- $(A_{\text{in}} + C_{\text{in}}) < 1$,

no signal from MBTS. The systematic uncertainty related with MBTS is in detail demonstrated in Sect. 11.3.

The MBTS veto is the dominant criterion in the background suppression as is shown in Fig. 29 where the background suppression is visible not only in tails of the $\sum p_{\text{y}}$ distribution but also within the signal peak around zero. Now the signal peak is well identifiable in the data distribution and the MC background simulation - represented by the Pythia8 central diffraction process - together with the MC signal fraction describes data distribution much better after the MBTS veto criterion.

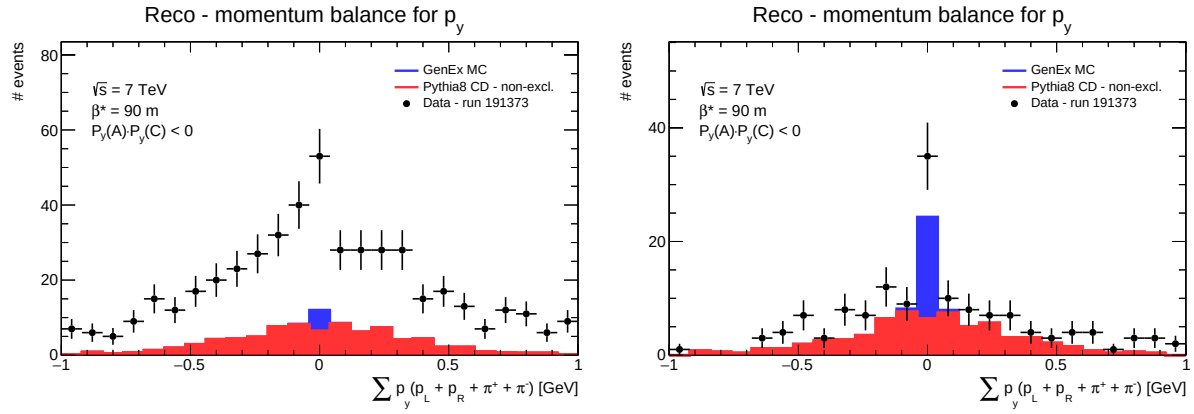

(a) (b)

Figure 29: The $\sum p_{\text{y}}$ of the exclusive pion production final state products (a) before and (b) after the MBTS veto is applied. The data are represented by the black points whereas the Monte Carlo simulations are represented by the blue histogram for the GenEx simulation and by the red histogram for the Pythia8 central diffraction containing only the non-exclusive events. The MC histograms are stacked.

The set of control plots was made also for this event selection step and it is shown in Fig. 30 where the ID track p_x resp. p_y distribution is shown in Fig. 30a resp. Fig. 30b, the proton p_x resp. p_y distribution is shown in Fig. 30c resp. Fig. 30d and the $\sum p_x$ resp. $\sum p_y$ system momentum balance distribution is shown in Fig. 30e resp. Fig. 30f. The data are represented by the black points whereas the Monte Carlo simulations are represented by the blue histogram for the GenEx simulation and by the red histogram for the Pythia8 central diffraction containing only the non-exclusive events. A central diffraction process from Pythia8 is able to describe the background fraction in data better then in previous event selection based - ALFA event selection in Sect. 7.5 - but still there is a non-negligible fraction of the background which is not described. The initial prediction of the background fraction in data by the Pythia8 central diffraction remains without any change.

The other control plots are shown in the Fig. 31, with the kinematic distributions for the reconstructed track pairs - the pion pair candidates. The distribution compare both the data and the Monte Carlo simulations. The data are represented by the black points whereas the Monte Carlo simulations are represented by the blue histogram for the GenEx simulation and by the red histogram for the Pythia8 central diffraction containing only the non-exclusive events. The distribution of the track pair transverse momentum (Fig. 31e) and track pair mass (Fig. 31f) show a level of inconsistency which may still point on an insufficient background prediction for this step of the event selection.

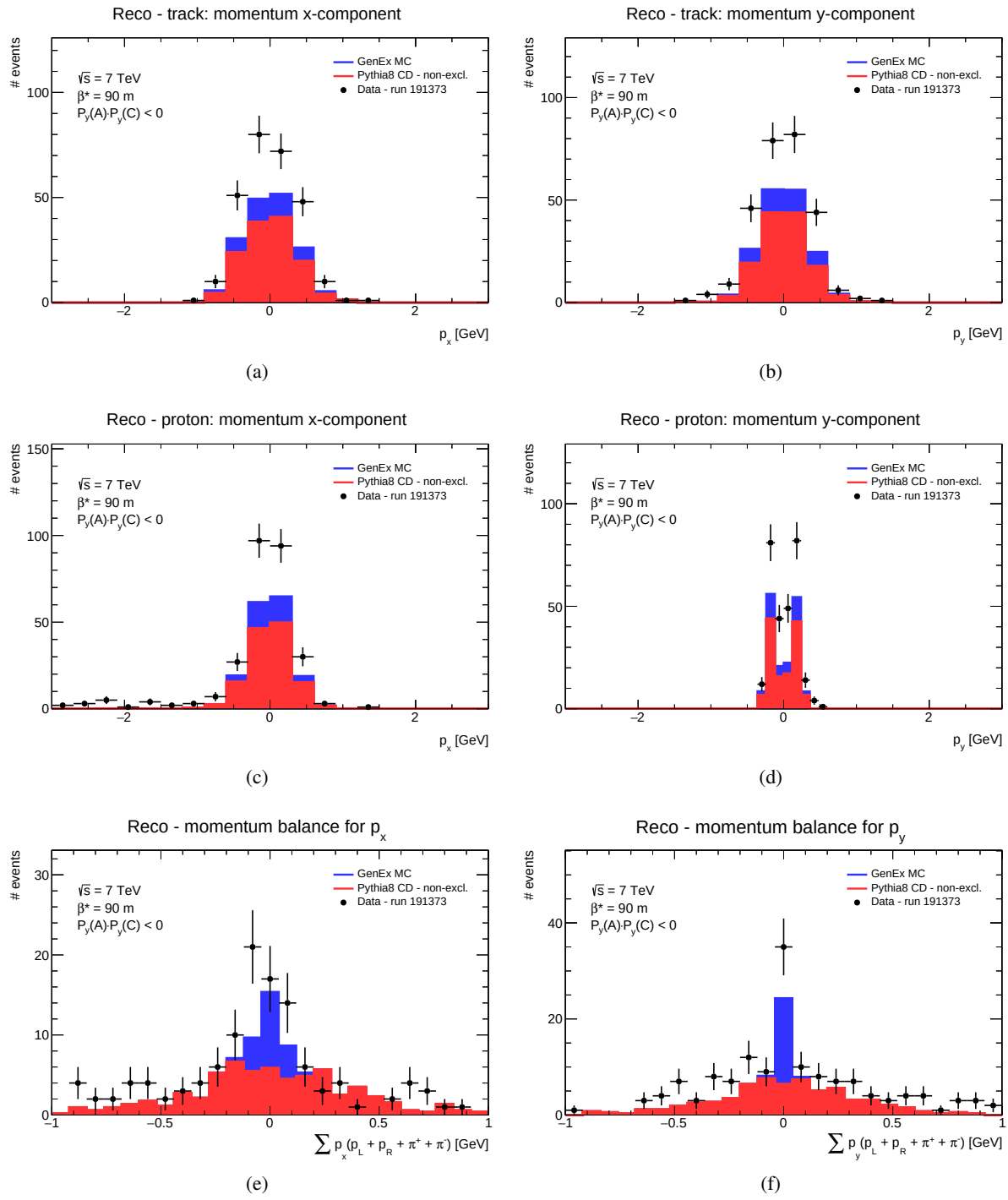

Figure 30: A set of control plots for the kinematic variables after the MBTS veto, on (a) for the pion p_x distribution, on (b) for the pion p_y distribution, on (c) for the proton p_x, on (d) for the proton p_y, on (e) for the momentum balance in p_x of the system formed by two protons and two tracks ($\pi^+\pi^-$) and on (f) for the momentum balance in p_y of the system formed by two protons and two tracks ($\pi^+\pi^-$). The data are represented by the black points whereas the Monte Carlo simulations are represented by the blue histogram for the GenEx simulation and by the red histogram for the Pythia8 central diffraction containing only the non-exclusive events. The MC histograms are stacked.

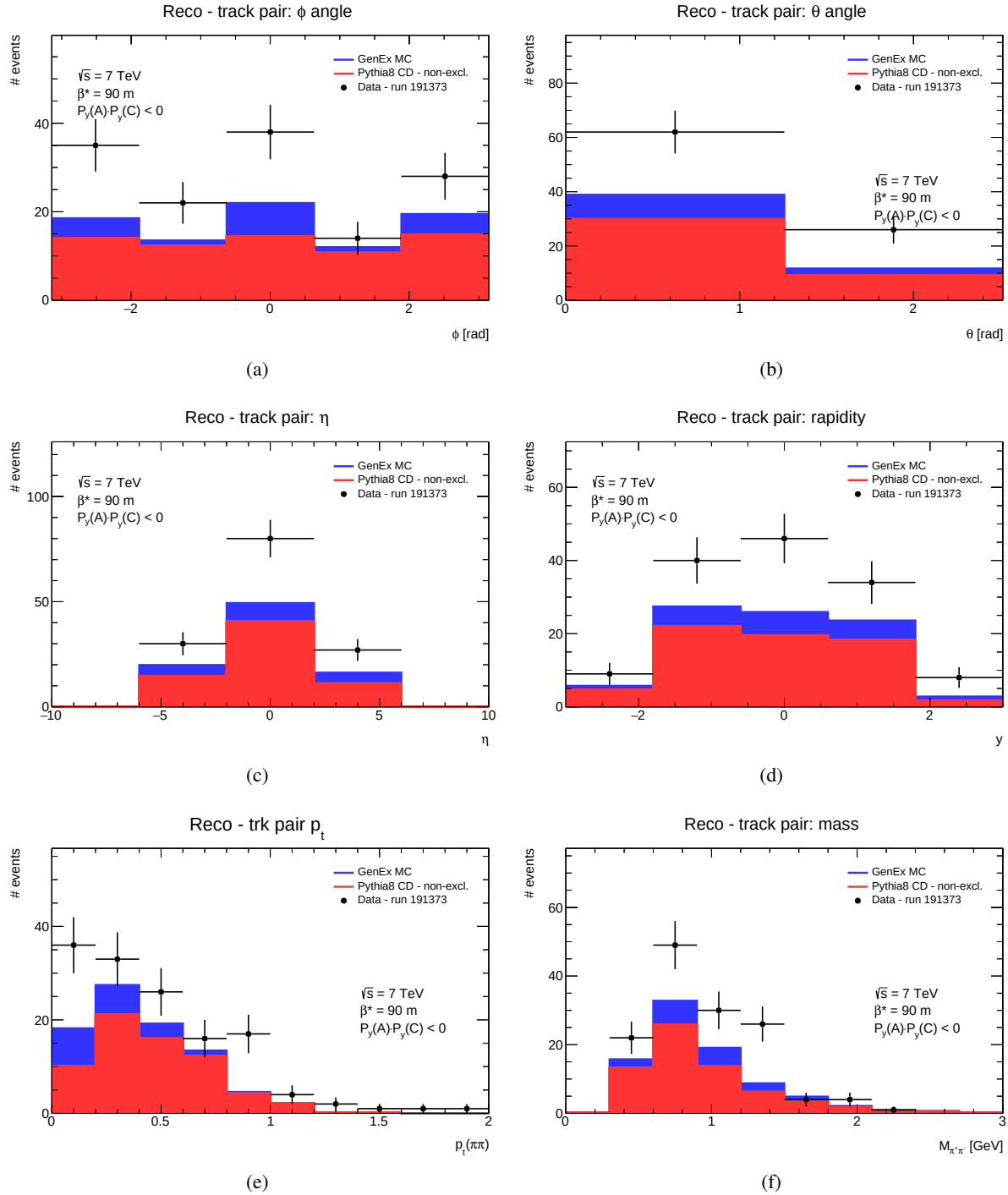

Figure 31: The reconstructed tracks pair kinematics distributions after the MBTS veto, on (a) for the $\phi_{\pi^+\pi^-}$ distribution, on (b) for the $\theta_{\pi^+\pi^-}$ distribution, on (c) for the $\eta_{\pi^+\pi^-}$ distribution, on (d) for the rapidity $y_{\pi^+\pi^-}$ distribution, on (e) for the $pt_{\pi^+\pi^-}$ distribution and on (f) for the $M_{\pi^+\pi^-}$ distribution. The data are represented by the black points whereas the Monte Carlo simulations are represented by the blue histogram for the GenEx simulation and by the red histogram for the Pythia8 central diffraction containing only the non-exclusive events. The MC histograms are stacked.

7.7. ALFA geometrical selection

For the ATLAS run 191373, the parallel-to-point optics in a vertical axis was used [28]. This means that a typical beam spot of the elastically scattered protons detected in ALFA detector is narrow in x-axis whereas in the y-axis its spread is limited by the ALFA geometrical acceptance. The typical shape of the elastic protons is shown in Fig. 32a.

The protons which originate from the exclusive pion production belong to a group of the diffractive protons with a non-zero energy losses. These energy losses cause a deflection in the x-axis. The bigger energy loss of the proton is the bigger deflection of the proton position in the x-axis is detected by the ALFA detector. This is nicely visible in Fig. 32c for the protons which lost quite a big amount of the energy - tens of GeV. In the case of the exclusive pion production pair there is no such visible shape because of the energy of the central system - formed by two pions - which is relatively small, up to few units of GeV. The beam spot of such protons reconstructed in the ALFA detector - and shown in Fig. 32b - looks similarly to the beam spot of the elastically scattered protons - shown in Fig. 32a.

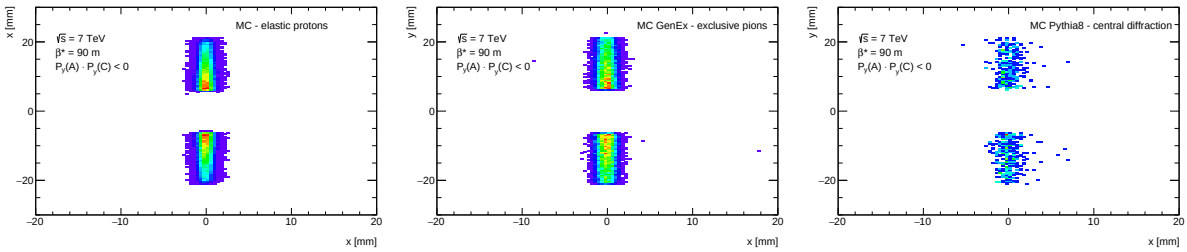

(a) (b) (c)

Figure 32: The plot (a) shows a typical shape of the elastically scattered protons reconstructed in ALFA detector whereas the plot (b) shows the typical shape of the protons coming from the exclusive production and the plot (c) shows a typical shape of the diffractive protons with bigger energy losses.

The ALFA geometrical selection is based on the knowledge that the beam shape of the protons of the exclusive production is comparable with the beam shape of the elastically scattered protons detected by the ALFA detector. Thus such shape can be described by the ellipse - defined as the x vs. θ_x correlation of the proton reconstructed position x and its local angle θ_x in x-axis - which will define a region of a potential exclusive signal. The proton local angle θ_x is defined between two consequent ALFA detectors as it is shown in Fig. 21. The main purpose of elliptical cut is to remove the background or fake protons and was derived in the analysis of the elastic scattering [28].

The reconstructed proton tracks in ALFA stations are shown in Fig. 33 - each of them is composed of two ALFA detectors, the upper on and the lower one, in the same z-position.

A combination of two consequent ALFA detectors allows to study a shape distribution based on a correlation between reconstructed proton position in ALFA detector and its local angle (Fig. 21). The study [2, 28] of the elastically scattered protons uses this correlation to remove the events with the inelastic protons which lies outside the ellipse, shown in Fig. 34a.

The same correlation is drawn for the Monte Carlo simulation of the GenEx generator. It shows that a shape of the correlation shown in Fig. 34b is comparable with the one from the study of the elastically

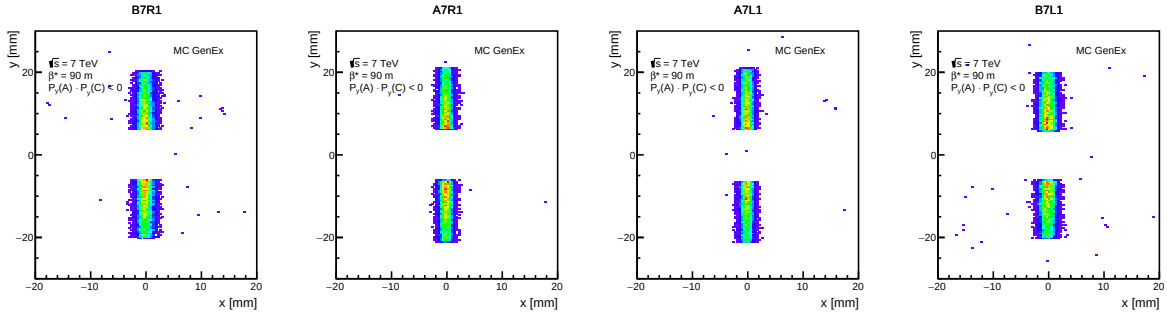

Figure 33: The map of the reconstructed protons in xy-plane of the ALFA stations B7R1, A7R1, A7L1 and B7L1 (from left to right). The MC GenEx simulation is used.

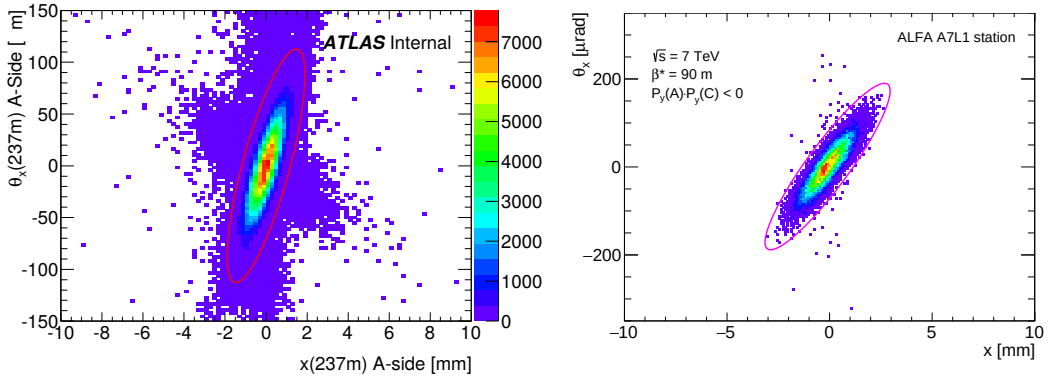

(a) (b)

Figure 34: A correlation between a proton reconstructed position and its local angle. An ellipse which selects elastic proton candidates is shown. Figure (a) was taken from [2, 28]. Figure (b) represents GenEx simulation of the exclusive pion production.

scattered protons [2, 28]. This means that the energy loss of the protons coming from the exclusive pion production is too low to distinguish them from the elastically scattered ones.

For the purpose of this study the new correlation between the local angle of the reconstructed proton and its position in x-axis was made and used for elliptical fit. The results of the fit are summarized in Table 8.

Table 8: A summary of the θ_x vs. x correlation used as the ALFA geometrical selection.

configuration	ALFA station	$\sigma(x)$ [µm]	$\sigma(\theta_x)$ [µrad]	angle [rad]
elastic	B7R1	53.84	0.38	1.5521
elastic	A7R1	57.56	0.36	1.5556
elastic	A7L1	53.88	0.37	1.5560
elastic	B7L1	52.30	0.38	1.5525
anti-elastic	B7R1	51.53	0.34	1.5518
anti-elastic	A7R1	65.64	0.32	1.5565
anti-elastic	A7L1	59.41	0.31	1.5565
anti-elastic	B7L1	49.05	0.31	1.5528

A set of control plots was performed also for this step of event selection and it is shown in Fig. 35 where the ID track p_x resp. p_y distribution is shown in Fig. 35a resp. Fig. 35b, the proton p_x resp. p_y distribution is shown in Fig. 35c resp. Fig. 35d and the $\sum p_x$ resp. $\sum p_y$ system momentum balance distribution is shown in Fig. 35e resp. Fig. 35f. The data are represented by the black points whereas the Monte Carlo simulations are represented by the blue histogram for the GenEx simulation and by the red histogram for the Pythia8 central diffraction containing only the non-exclusive events. The ALFA geometrical event selection removed the most of the background which is not described with the MC Pythia8 central diffraction process. The data are described quite well by the MC simulation containing the signal fraction represented by the GenEx simulation and containing the background fraction represented by the Pythia8 CD simulation.

Other plots are shown in the Fig. 36, the kinematic distributions for the reconstructed track pairs - the pion pair candidates. The distribution compare both the data and the Monte Carlo simulations. The data are represented by the black points whereas the Monte Carlo simulations are represented by the blue histogram for the GenEx simulation and by the red histogram for the Pythia8 central diffraction containing only the non-exclusive events. The distribution of the track pair transverse momentum (Fig. 31e) and track pair mass (Fig. 31f) show much better agreement between data and the MC simulation fractions then for the similar distribution represented in the previous selection step.

The next geometrical condition is applied on the lower edge of the ALFA detector. The condition serves to remove the reconstructed tracks bellow the ALFA edge which would come as fake tracks. Our study is based on the same data like in [28] therefore we adopt the detector edge study from that analysis together with edge positions of ALFA detector which are summarized in Table 9.

Table 9: ALFA detector edge position in respect to the beam centre [28].

detector / station	B7L1	A7L1	A7R1	B7R1
upper	5.981 ± 0.081	6.255 ± 0.077	6.080 ± 0.077	5.765 ± 0.073
lower	-5.981 ± 0.081	-6.173 ± 0.077	-6.303 ± 0.077	-6.045 ± 0.073

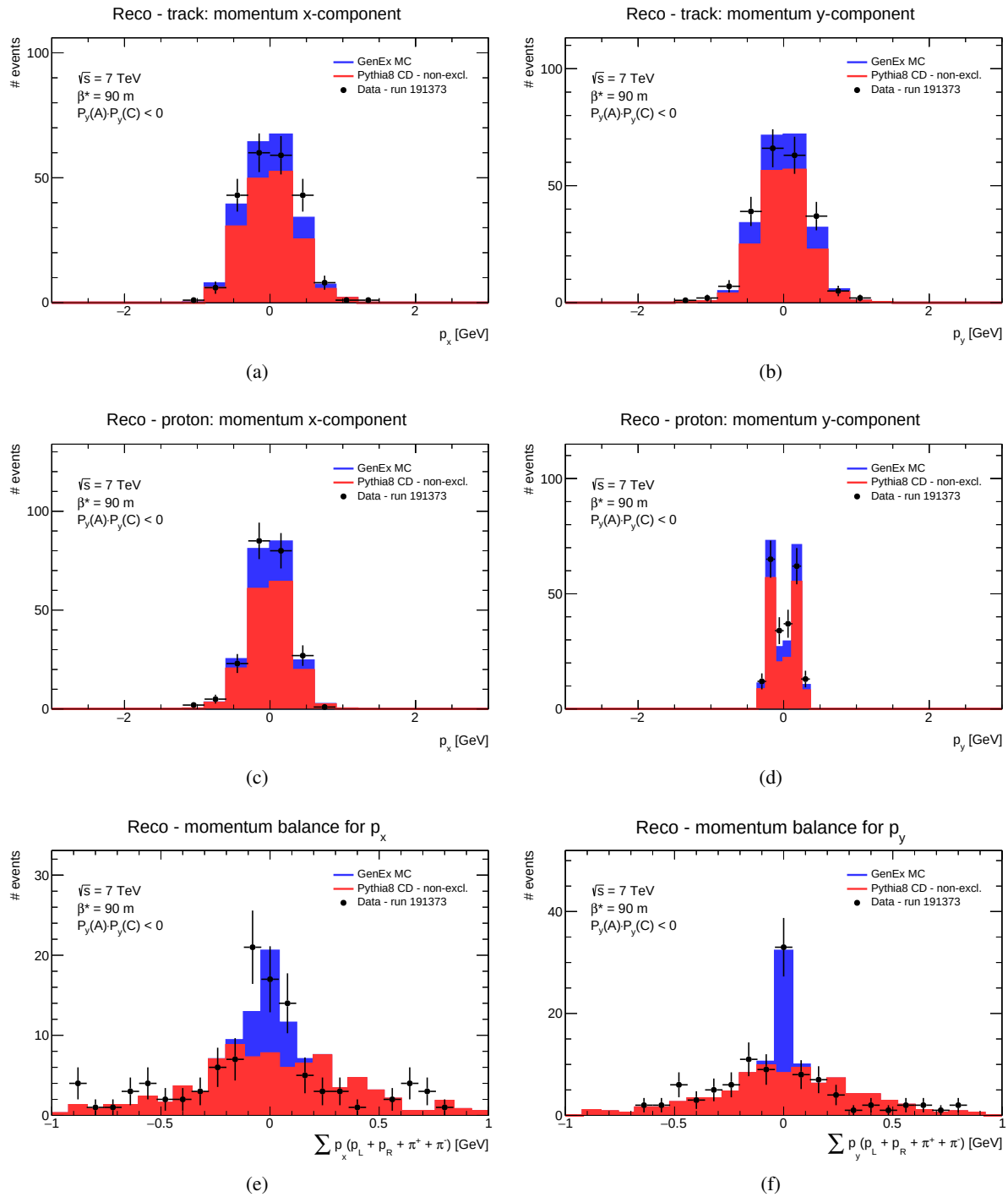

Figure 35: The set of control plots for the kinematic variables after the ALFA geometrical selection, (a) for the pion p_x distribution, (b) for the pion p_y distribution, (c) for the proton p_x, (d) for the proton p_y, (e) for the momentum balance in p_x of the system formed by two protons and two tracks ($\pi^+\pi^-$) and (f) for the momentum balance in p_y of the system formed by two protons and two tracks ($\pi^+\pi^-$). The data are represented by the black points whereas the Monte Carlo simulations are represented by the blue histogram for the GenEx simulation and by the red histogram for the Pythia8 central diffraction containing only the non-exclusive events. The MC histograms are stacked.

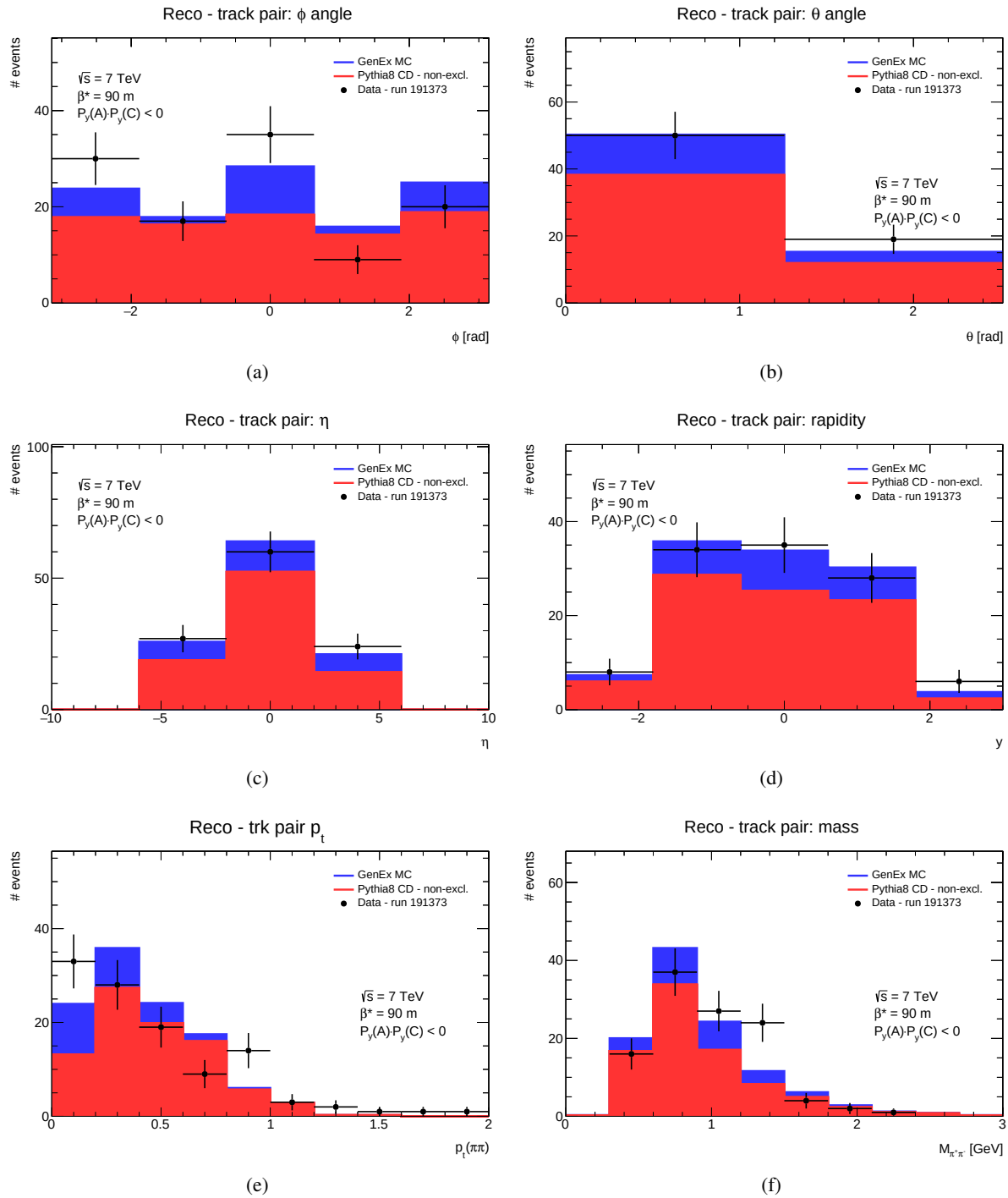

Figure 36: The reconstructed tracks pair kinematics distributions after the ALFA geometrical selection, (a) for the $\phi_{\pi^+\pi^-}$ distribution, (b) for the $\theta_{\pi^+\pi^-}$ distribution, (c) for the $\eta_{\pi^+\pi^-}$ distribution, (d) for the rapidity $y_{\pi^+\pi^-}$ distribution, (e) for the $pt_{\pi^+\pi^-}$ distribution and (f) for the $M_{\pi^+\pi^-}$ distribution. The data are represented by the black points whereas the Monte Carlo simulations are represented by the blue histogram for the GenEx simulation and by the red histogram for the Pythia8 central diffraction containing only the non-exclusive events. The MC histograms are stacked.

7.8. Kinematic selection

Till now no events selection have been focused on the complete kinematics. It is the system momentum balance which allows us to select the events very closed to an ideal exclusive sample. It would be ideal to use a full information about the system momentum balance. But as it was mentioned in Sect. 6 the proton kinematic reconstruction precision of the proton energy - together with its p_z - is insufficient for the purpose of our analysis. We can safely use only the p_x and p_y momentum components. This also means that after the kinematic event selection our sample can still contain the events which are not the exclusive ones. Following two equations describing the momentum balance of the exclusive system for p_x and p_y momentum component

$$p_x(p_A^{in}) + p_x(p_C^{in}) = p_x(p_A^{out}) + p_x(p_C^{out}) + p_x(\pi^+) + p_x(\pi^-), \tag{24}$$

$$p_y(p_A^{in}) + p_y(p_C^{in}) = p_y(p_A^{out}) + p_y(p_C^{out}) + p_y(\pi^+) + p_y(\pi^-), \tag{25}$$

where p_A^{in} and p_C^{in} are two protons incoming into the interaction and p_A^{out}, p_C^{out}, π^+ and π^- are two protons and two pions outgoing from the interaction.

The kinematic event selection is based on the momentum conservation. The kinematic selection is verified using the MC signal simulation with GenEx generator as the source of the exclusive pion processes and is shown in Fig. 37. This figure contains the momentum balance distributions of the system for the elastic configuration shown in Figs. 37a and 37b as well as for the anti-elastic configuration shown in Figs. 37c and 37d.

A knowledge of the kinematic properties of the studied products reconstructed by the ATLAS Inner detector and the ALFA detector is used. The kinematic properties are well reconstructed for the tracks reconstructed by the ATLAS Inner detector. A complete four-momentum of these tracks is well known. On the other side the situation for the tracks (protons) reconstructed in the ATLAS forward region by the ALFA detectors is more tricky. The ALFA detector is a tracking detector (Sect. 5.3) which is not able to reconstruct protons kinematics directly. Therefore the proton kinematics is reconstructed by algorithms which are using a proton back-tracking to the ATLAS interaction point. For the purpose of this analysis two algorithms were used. They are described in Sect. 6.2 dedicated to the ALFA kinematic reconstruction.

However, the procedure of proton kinematics reconstruction using the proton back-tracking to the ATLAS interaction point has a limitation due to the p_x and p_y resolutions. The Sect. 6.2 shows that the resolution of two components, p_x and p_y, of the proton four-momentum is only satisfied for this exclusive pion analysis. Therefore only these two components are used in the kinematic selection.

It is assumed here that the protons incoming into the interaction were head-to-head oriented, having the same energy and thus the part on the left side of the Eqs. 26 and 27 equals exactly to zero. If this would be true then the Eqs. 26 and 27 can be modified in following way

$$0 = p_x(p_A^{out}) + p_x(p_C^{out}) + p_x(\pi^+) + p_x(\pi^-), \tag{26}$$

$$0 = p_y(p_A^{out}) + p_y(p_C^{out}) + p_y(\pi^+) + p_y(\pi^-). \tag{27}$$

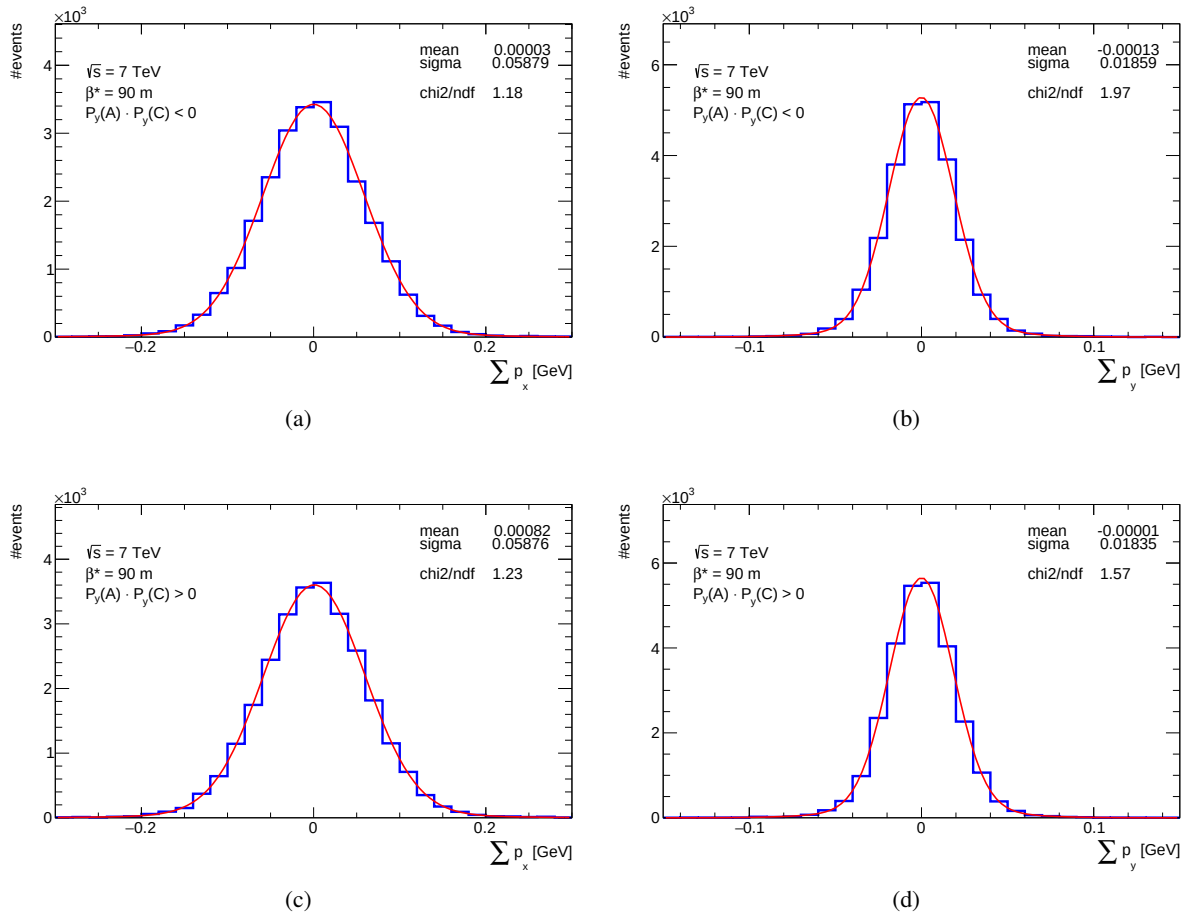

Figure 37: The sum of x-component on (a) and (c) and y-component on (b) and (d) of the exclusive pion production final state products momentum for the GenEx Monte Carlo signal simulation. The elastic-like configuration is shown in (a) and (b) whereas the anti-elastic combination is shown in (c) and (d).

which means that a peak around the zero value of the p_x or the p_y distribution of the system - visible in Fig. 37 - defines a region of the exclusive events.

The kinematic selection is tuned on the GenEx Monte Carlo simulation. A Gaussian fits are applied on both the $\sum p_x$ and $\sum p_y$ distributions to obtain their σ values, $\sigma(\sum p_x)$ and $\sigma(\sum p_y)$, as it is shown in Fig. 37. Then the $3.5\,\sigma$ value intervals are used in the kinematic event selection to define the signal region and to suppress the events outside that region to reduce a background fraction. The σ-values from both the Lattice method and the ALFA Reco method of the proton kinematic reconstruction are shown in Table 41 in Sect. D.1.

Here is how the kinematic selection is applied. First, the kinematic event selection is applied on p_y distribution of the system. If the event passes this selection then the kinematic events selection is applied on the p_x distribution of the system. The order of the kinematic event selections above is not important for the final result but it is helpful for a better understanding of the background evolution in the signal region. A better momentum resolution of the p_y distribution of the system plays a role to prefer p_y momentum distribution of the system before p_x momentum distribution of the system due to a better visibility of the

signal peak in the p_y distribution of the system.

A set of control plots was made also for kinematic event selection applied on the p_y momentum distribution of the full system. It is shown in Fig. 38 where the ID track p_x resp. p_y distribution is shown in Fig. 38a resp. Fig. 38b, the proton p_x resp. p_y distribution is shown in Fig. 38c resp. Fig. 38d and the $\sum p_x$ resp. $\sum p_y$ system momentum balance distribution is shown in Fig. 38e resp. Fig. 38f. The data are represented by the black points whereas the Monte Carlo simulations are represented by the blue histogram for the GenEx simulation and by the red histogram for the Pythia8 central diffraction containing only the non-exclusive events. All the distributions show a reasonably good agreement between the data and the MC simulation which consists of the signal fraction represented with GenEx generator and of the background fraction represented with Pythia8 central diffraction process, especially the distribution of the p_x momentum of the system.

Other plots are shown in the Fig. 39, the kinematic distributions for the reconstructed track pairs - the pion pair candidates - after the kinematic event selection applied on the p_y momentum distribution of the exclusive pion system. The distribution compare both the data and the Monte Carlo simulations. The data are represented by the black points whereas the Monte Carlo simulations are represented by the blue histogram for the GenEx simulation and by the red histogram for the Pythia8 central diffraction containing only the non-exclusive events. A trend describe data by the MC simulation of the signal and the background fractions is visible there.

The same kinematic event selection is also applied on the p_x momentum distribution. The result is shown in Fig. 40, where the Fig. 40a represents the p_x distribution of the tracks reconstructed in the Inner detector, the Fig. 40c represents the p_x distribution of the protons reconstructed in the ALFA detector, the Fig. 40b represents the p_y distribution of the tracks reconstructed in the Inner detector and the Fig. 40d represents the p_x distribution of the protons reconstructed in the ALFA detector. The p_x momentum distributions of the exclusive system is shown in Fig. 40e whereas the p_y momentum distributions of the exclusive system is shown in Fig. 40f. The data are represented by the black points whereas the Monte Carlo simulations are represented by the blue histogram for the GenEx simulation and by the red histogram for the Pythia8 central diffraction containing only the non-exclusive events. **A combination of the MC signal fraction represented by the GenEx MC simulation and with the MC background fraction represented by the Pythia8 central diffraction of non-exclusive events is able to describe the data distributions**. It is also seen that the background fraction inside the signal region is not negligible, it represents a fraction of about 20% of the events which passed the kinematic event selection.

Other control plots are shown in the Fig. 41, the kinematic distributions for the reconstructed track pairs - the pion pair candidates - after the kinematic event selection applied on the p_x momentum distribution of the exclusive pion system. The distribution compare both the data and the Monte Carlo simulations. The data are represented by the black points whereas the Monte Carlo simulations are represented by the blue histogram for the GenEx simulation and by the red histogram for the Pythia8 central diffraction containing only the non-exclusive events.

Originally the kinematic selections $\sum p_y$ and $\sum p_x$ were used separately. It gives an opportunity to study the momentum distribution $\sum p_x$ and $\sum p_y$ separately and thus to study an effect of the one event selection - applied on $\sum p_y$ distribution - to the second one - applied on $\sum p_x$ distribution. Of course one would merge both events selection to the one - based on the elliptical cut - which looks much more natural than the used selections as it is shown in Fig. 42. This approach was also studied and its results were included in the overall uncertainties of the exclusive pion cross-section measurement. A difference of the final cross-section values between these two approaches was found as very small and therefore it was decided

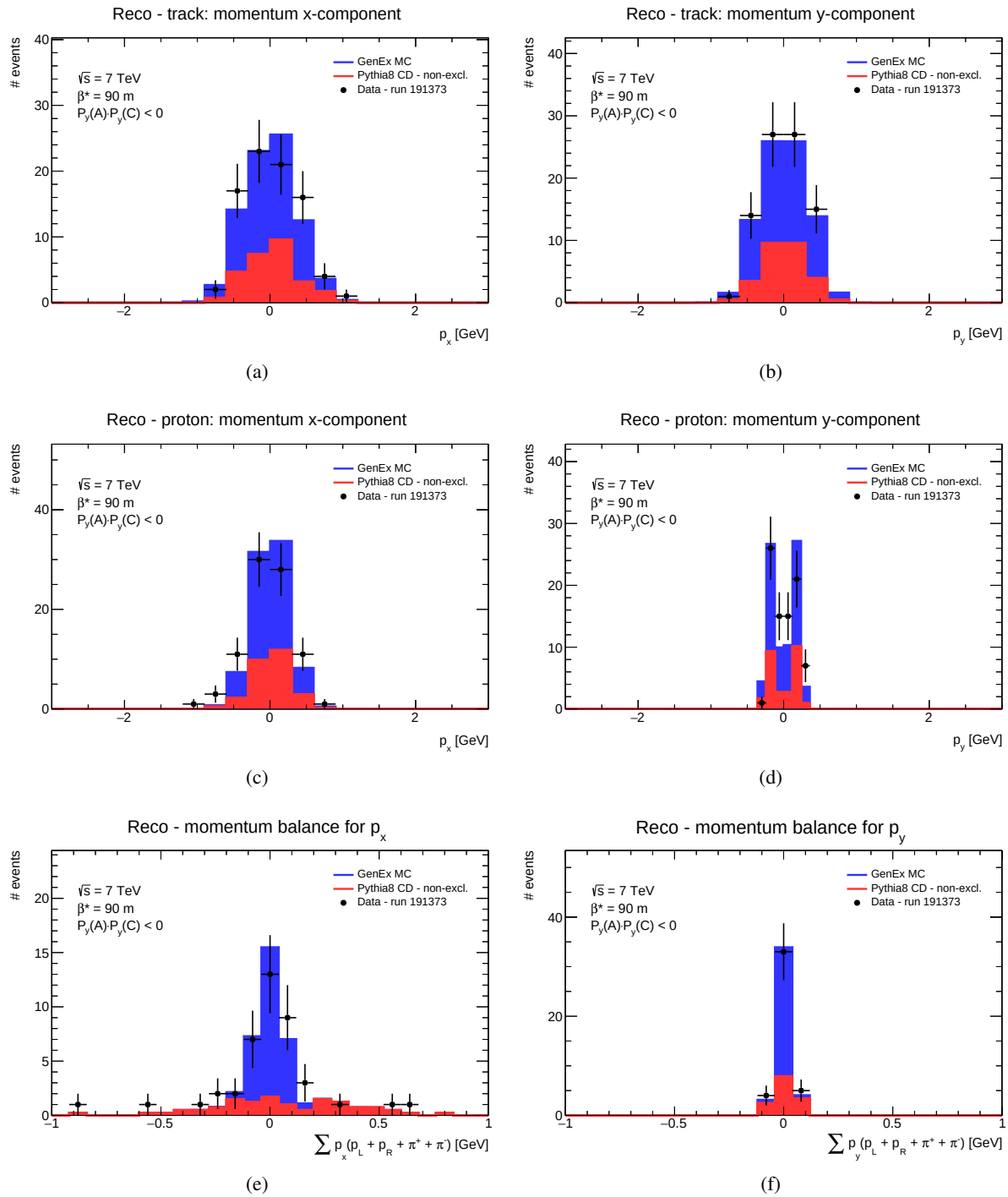

Figure 38: The set of control plots for the kinematic variables after the application of the kinematic event selection on $\sum p_y$ distribution, (a) for the pion p_x distribution, (b) for the pion p_y distribution, (c) for the proton p_x distribution, (d) for the proton p_y distribution, (e) for the p_x momentum balance of the system and (f) for the p_y momentum balance of the system. The data are represented by the black points whereas the Monte Carlo simulations are represented by the blue histogram for the GenEx simulation and by the red histogram for the Pythia8 central diffraction containing only the non-exclusive events. The MC histograms are stacked.

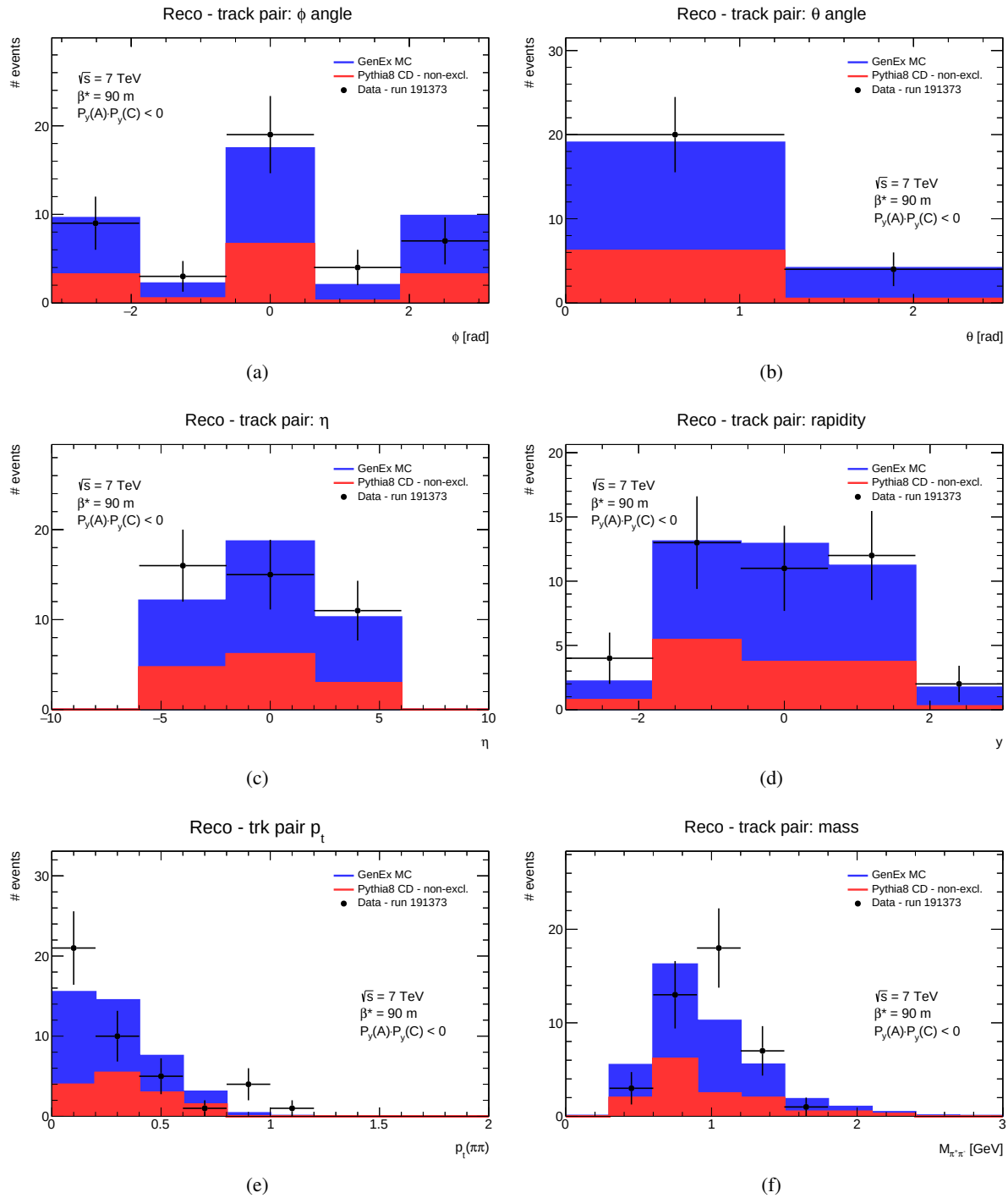

Figure 39: The reconstructed tracks pair kinematics distributions after the applying kinematic selection on $\sum p_y$ distribution, (a) for the $\phi_{\pi^+\pi^-}$ distribution, (b) for the $\theta_{\pi^+\pi^-}$ distribution, (c) for the $\eta_{\pi^+\pi^-}$ distribution, (d) for the rapidity $y_{\pi^+\pi^-}$ distribution, (e) for the $pt_{\pi^+\pi^-}$ distribution and (f) for the $M_{\pi^+\pi^-}$ distribution. The data are represented by the black points whereas the Monte Carlo simulations are represented by the blue histogram for the GenEx simulation and by the red histogram for the Pythia8 central diffraction containing only the non-exclusive events. The MC histograms are stacked.

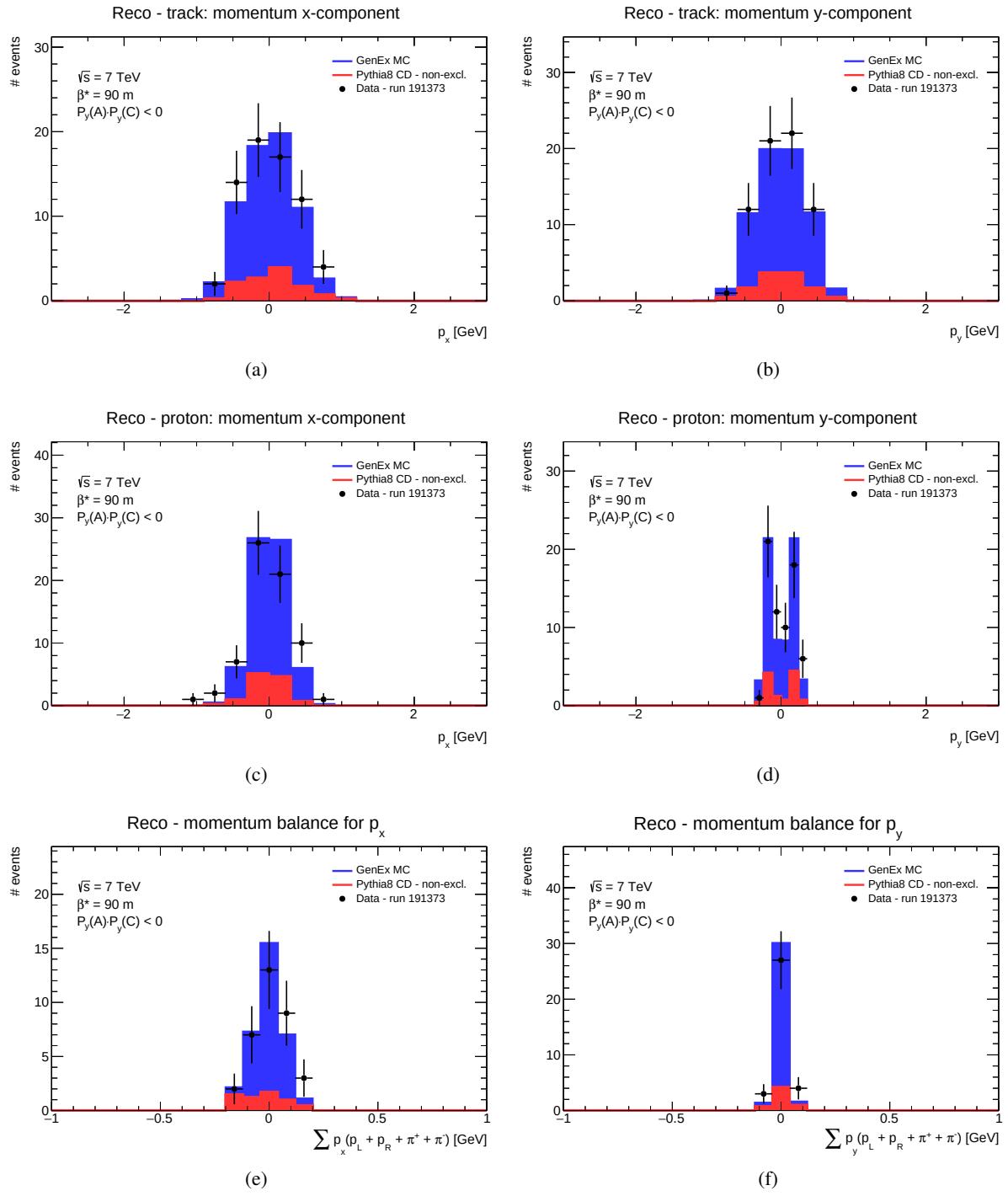

Figure 40: A set of control plots for the kinematic variables after the applying kinematic selection on $\sum p_x$ distribution, (a) for the pion p_x distribution, (b) for the pion p_y distribution, (c) for the proton p_x, (d) for the proton p_y, (e) for the momentum balance in p_x of the system formed by two protons and two pions ($\pi^+\pi^-$) and (f) for the momentum balance in p_y of the system formed by two protons and two pions ($\pi^+\pi^-$). The data are represented by the black points whereas the Monte Carlo simulations are represented by the blue histogram for the GenEx simulation and by the red histogram for the Pythia8 central diffraction containing only the non-exclusive events. The MC histograms are stacked.

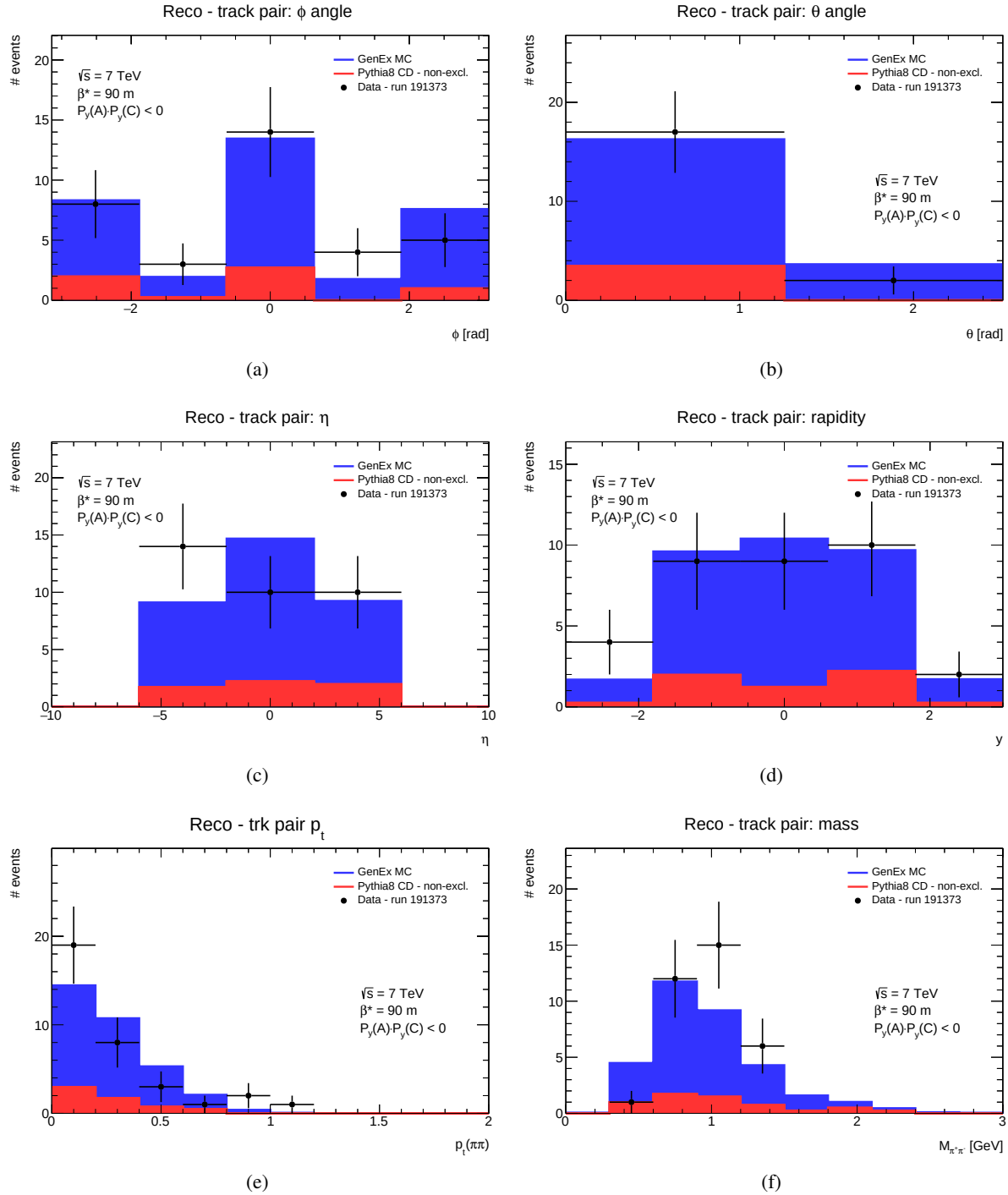

Figure 41: The reconstructed tracks pair kinematics distributions after the applying kinematic selection on $\sum p_x$ distribution, (a) for the $\phi_{\pi^+\pi^-}$ distribution, (b) for the $\theta_{\pi^+\pi^-}$ distribution, (c) for the $\eta_{\pi^+\pi^-}$ distribution, (d) for the rapidity $y_{\pi^+\pi^-}$ distribution, (e) for the $p_{T_{\pi^+\pi^-}}$ distribution and (f) for the $M_{\pi^+\pi^-}$ distribution. The data are represented by the black points whereas the Monte Carlo simulations are represented by the blue histogram for the GenEx simulation and by the red histogram for the Pythia8 central diffraction containing only the non-exclusive events. The MC histograms are stacked.

to keep the first way as the default one. A small difference of the results between these two approaches can be explained due to the small correlation between the $\sum p_x$ distribution and $\sum p_y$ distribution as is shown in Fig. 42 for the GenEx MC simulation.

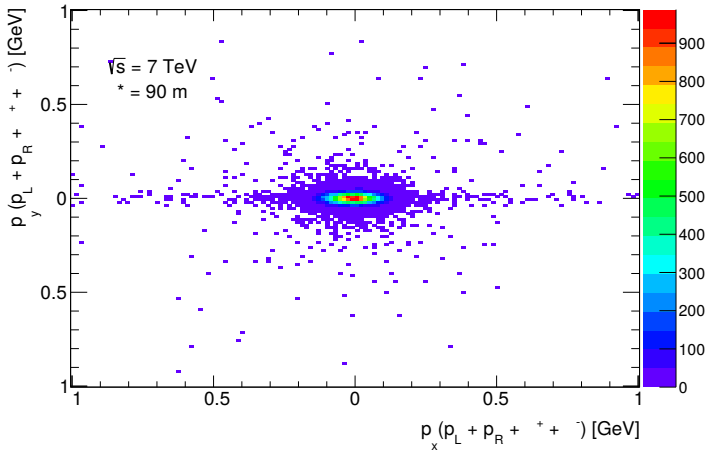

Figure 42: The correlation histogram between the $\sum p_x$ and the $\sum p_y$ distributions of the exclusive pion production. The GenEx Monte Carlo simulation is used.

7.9. Particle identification

It is assumed that the main fraction of the reconstructed tracks in the ID consists of the pions. But particles like kaons or protons would be also presented in the reconstructed tracks which then can contribute to the background of considered process and should be removed. A technique based on the knowledge of the particles ionization losses when passing through the ATLAS Pixel detector - which is a part of the ATLAS Inner detector - is able to probabilistically identify the particles. The Pixel detector is able to measure the average specific energy loss $\mathrm{d}E/\mathrm{d}x$ for the charged particles coming from proton-proton interactions at high energies [43]. The charged particle ionization loss $\mathrm{d}E/\mathrm{d}x$ is described by the Bethe-Bloch function, in simplified way $\mathrm{d}E/\mathrm{d}x \approx \beta\gamma$. This energy loss can be combined with the particle momentum, $p = mc\beta\gamma$. Then the particle is identified by calculating of its mass from a measurement of its momentum and its energy loss. The whole procedure is fully described in [43]. There is also shown that the specific ionization loss $\mathrm{d}E/\mathrm{d}x$ can be measured with a typical resolution of 10%. Therefore the particles like pions, kaons and protons are well identified in the low mass region up to ≈ 1.5 GeV and thus it is possible to use such identification for the purpose of our analysis to remove the events with non-pion particles. Based on the result obtained in [43], it was decided to use the range

$$0 \; < \; m_{\mathrm{trk}}(\mathrm{d}E/\mathrm{d}x) \; < \; 0.25\,\mathrm{GeV} \tag{28}$$

as a condition to recognise the pion tracks. The events containing the particles with a mass above 0.25 GeV are removed. The Fig. 43 shows a distribution of the particle masses calculated from ionization losses of the particles reconstructed in the ATLAS Pixel detector. The data - represented by the black points - are compared to the MC simulations of a signal fraction (GenEx) - the blue histogram - and of the background fraction (Pythia8 central diffraction with non-exclusive pion events) - the red histogram. The MC histograms are stacked.

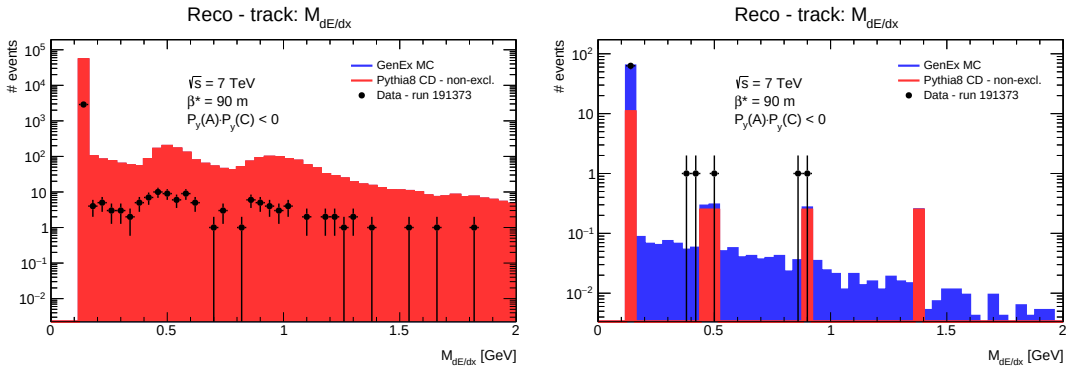

(a) (b)

Figure 43: The particle mass distribution $\mathrm{d}E/\mathrm{d}x$ given from the particle ionization loss, on (a) for the events after the ID track selection and on (b) before the particle identification selection. The data are represented by the black points whereas the Monte Carlo simulations are represented by the blue histogram for the GenEx simulation and by the red histogram for the Pythia8 central diffraction with non-exclusive events. The Monte Carlo simulation distributions are stacked.

The Eq. 28 defines the mass range for the particle tracks, similarly the mass ranges can be also defined for other particles as it is shown in Table 10. The values can be use for a better interpretation of peak visible in Fig. 43. The values in that table are based on the study done in [43].

Table 10: A conditions put on the track mass based on $\mathrm{d}E/\mathrm{d}x$ measurement.

clean particle candidate	**mass range GeV**
pion	$0.00 < m_{\mathrm{trk}}(\mathrm{d}E/\mathrm{d}x) < 0.25$
kaon	$0.25 < m_{\mathrm{trk}}(\mathrm{d}E/\mathrm{d}x) < 0.75$
proton	$0.75 < m_{\mathrm{trk}}(\mathrm{d}E/\mathrm{d}x) < 1.25$
deuteron	$1.25 < m_{\mathrm{trk}}(\mathrm{d}E/\mathrm{d}x)$

The set of the control plots was made for the particle identification selection. It is shown in Fig. 44, where the Fig. 44a represents the p_{x} distribution of the tracks reconstructed in the ID, the Fig. 44c represents the p_{x} distribution of the protons reconstructed in the ALFA detector, the Fig. 44b represents the p_{y} distribution of the track reconstructed in the ID and Fig. 44d represents the p_{y} distribution of the proton reconstructed in the ALFA detector. The data are represented by the black points whereas the Monte Carlo simulations are represented by the blue histogram for the GenEx simulation and by the red histogram for the Pythia8 central diffraction containing only the non-exclusive events. The distributions for the system momentum balance for the $\sum p_{\mathrm{x}}$ distribution is shown in Fig. 44e and the system momentum balance for the $\sum p_{\mathrm{y}}$ distribution shown in Fig. 44f. The particle identification selection improves a description of data distribution with a predicted MC simulation distribution which consist of two fractions, the signal fraction represented with the GenEx MC simulation and the background fraction represented with the Pythia8 central diffraction MC simulation.

The set of control plots on the Fig. 45 shows the kinematic distributions for the reconstructed track pairs after the particle identification selection is applied. The distributions compare both the data and the Monte Carlo simulations. The data are represented by the black points whereas the Monte Carlo simulations are

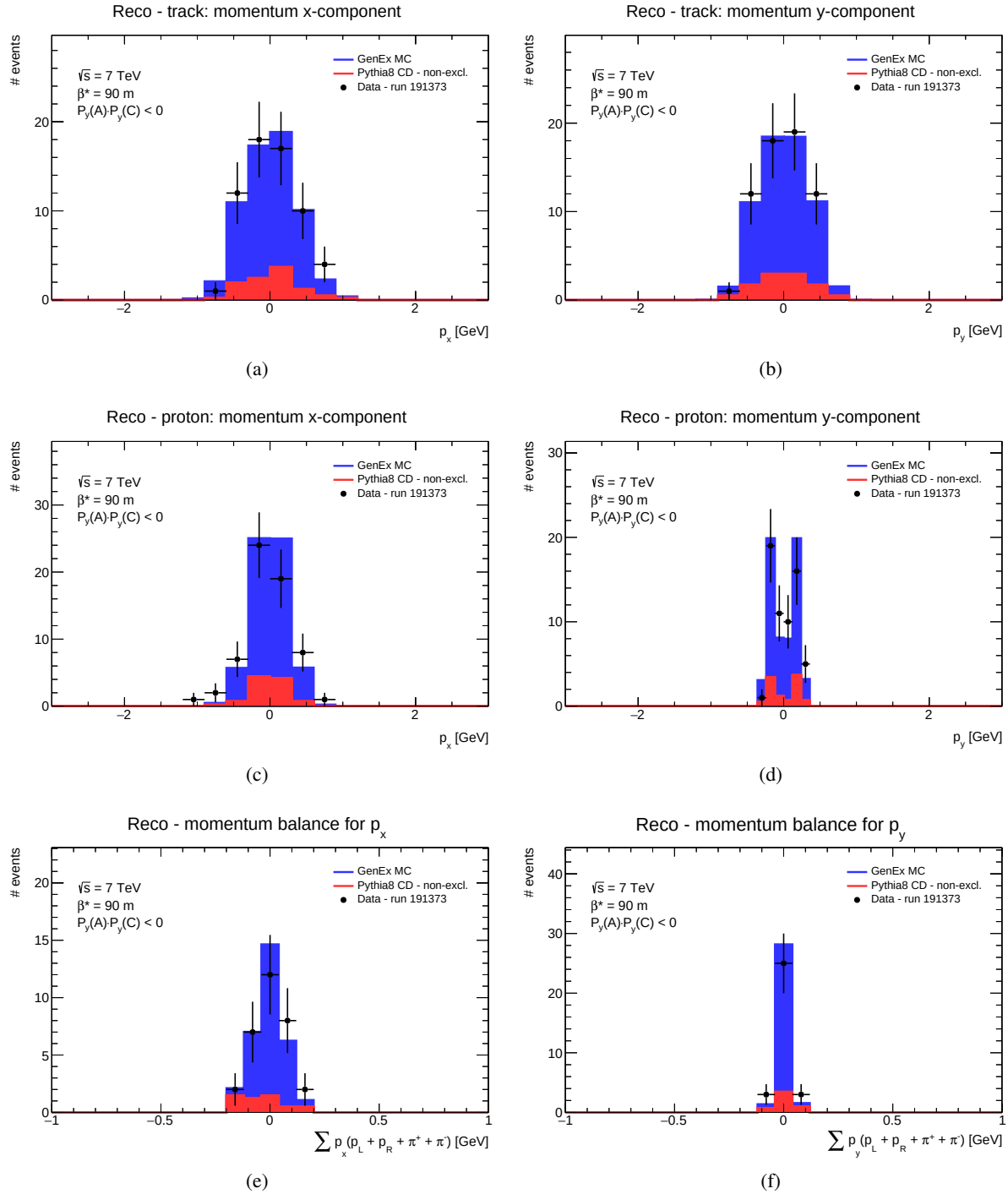

Figure 44: A set of control plots for the kinematic variables after the particle identification selection, (a) for the pion p_x distribution, (b) for the pion p_y distribution, (c) for the proton p_x, (d) for the proton p_y, (e) for the momentum balance in p_x of the exclusive system and (f) for the momentum balance in p_y of the exclusive system. The data are represented by the black points whereas the Monte Carlo simulations are represented by the blue histogram for the GenEx simulation and by the red histogram for the Pythia8 central diffraction containing only the non-exclusive events. The MC histograms are stacked.

represented by the blue histogram for the GenEx simulation and by the red histogram for the Pythia8 central diffraction containing only the non-exclusive events. These are the same set of control plots as for the previous event selections. The trend of moving the data distributions shapes of closer to the Monte Carlo simulations even if it is not well visible due to limited statistics.

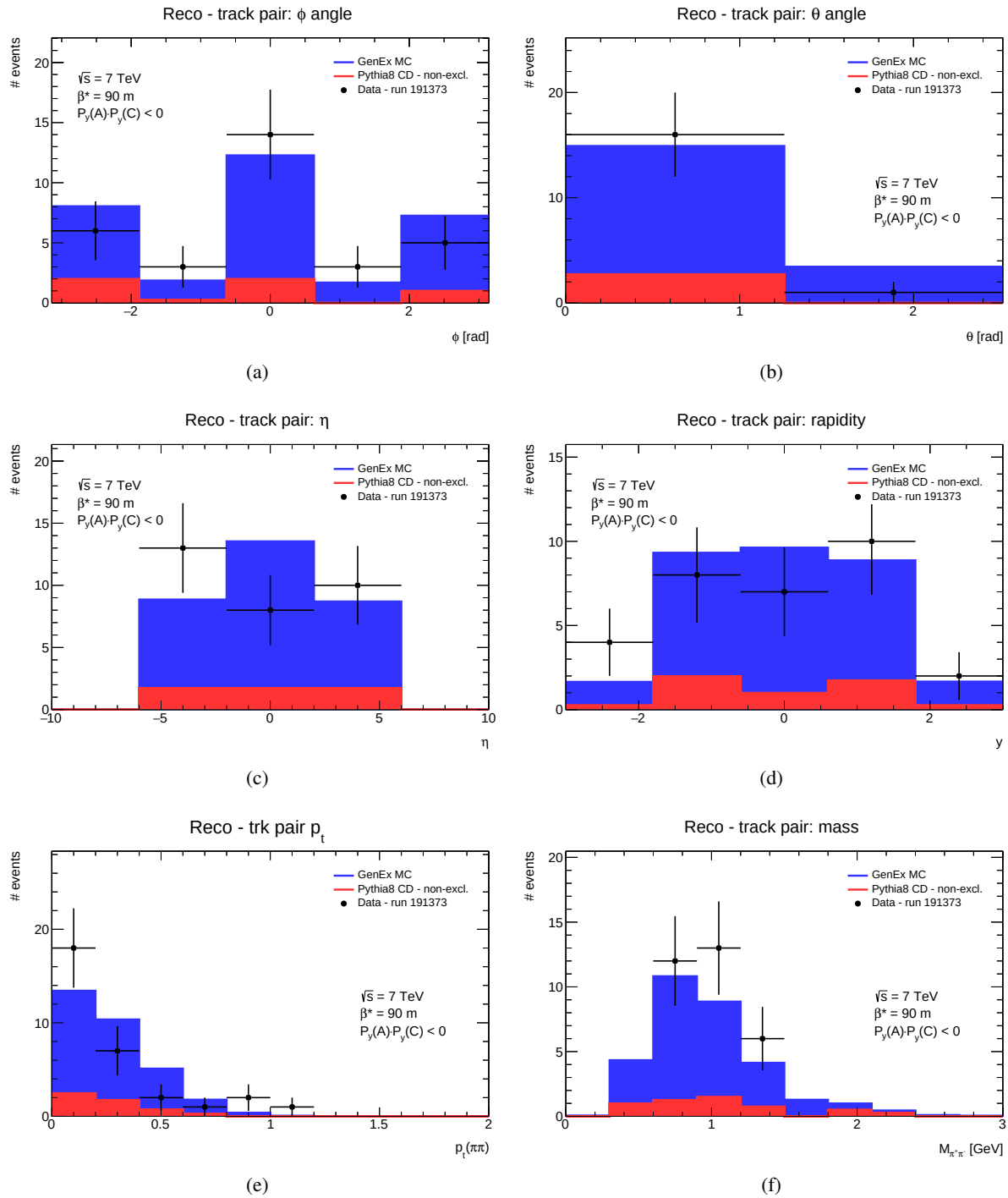

Figure 45: The reconstructed tracks pair kinematics distributions after the particle identification selection, (a) for the $\phi_{\pi^+\pi^-}$ distribution, (b) for the $\theta_{\pi^+\pi^-}$ distribution, (c) for the $\eta_{\pi^+\pi^-}$ distribution, (d) for the rapidity $y_{\pi^+\pi^-}$ distribution, (e) for the $p_{T_{\pi^+\pi^-}}$ distribution and (f) for the $M_{\pi^+\pi^-}$ distribution. The data are represented by the black points whereas the Monte Carlo simulations are represented by the blue histogram for the GenEx simulation and by the red histogram for the Pythia8 central diffraction containing only the non-exclusive events. The MC histograms are stacked.

7.10. Fiducial volume selection

A fiducial volume of the exclusive pion pair production process is considered here. The space is estimated knowing protons t-spectrum, pions η and p_{t} kinematic variables and pion system mass M with following additional conditions

$$0.0025 < t_A, t_C < 0.38\ \mathrm{GeV}^2 \qquad |\eta_\pi| < 2.5 \qquad pt_\pi > 0.1\ \mathrm{GeV} \qquad 2m_\pi < M_{\pi\pi} < 2.0\ \mathrm{GeV}, \tag{29}$$

where t_{A} and t_{C} are Mandelstam variables of protons on both A and C ATLAS sides (calculated using Eq. 17), η_π is the pseudo-rapidity of the pion track, p_{T_π} is the transverse momentum of the pion track, m_π is a charged pion mass and $M_{\pi\pi}$ is the invariant mass of the pion system.

The protons t-spectrum region constrained by the ALFA detector geometrical acceptance and also by the ALFA detectors position. The proton t-spectrum distribution of the GenEx Monte Carlo simulation was set up accordingly to the conditions of the ATLAS run 191373 described in Sect. 5.3.2. It is shown in Fig. 46. The histograms of the proton t-spectrum are shown in the range of proton t-value used in this event selection, so $0.0025 < t_A, t_C < 0.38\ \mathrm{GeV}^2$.

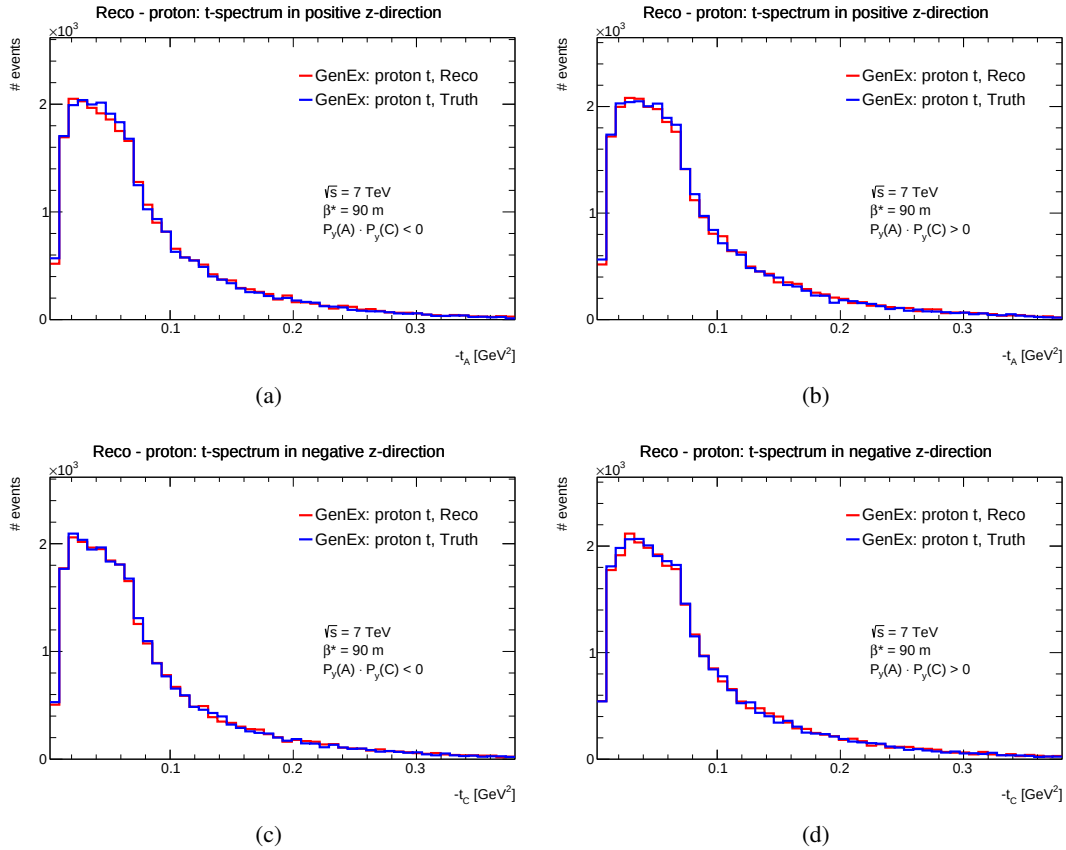

Figure 46: The proton t-spectrum distribution from the GenEx Monte Carlo simulation set up accordingly to the conditions during the ATLAS run 191373, (a, b) for the protons on the ATLAS side A and (c,d) for the protons on the ATLAS side C. The elastic configuration is on (a,c) and the anti-elastic configuration is on (b,d).

The fiducial volume selection is used in both Monte Carlo simulation analysis and the data analysis. The same space is also applied on the products of the GenEx Monte Carlo simulation (on particle level) for the purpose of correction calculation, Sect. 8. The fiducial volume selection represents the final event selection of our analysis.

A set of the control plots, using fiducial volume selection, compares several kinematic distribution of the protons reconstructed in ALFA detector and the tracks reconstructed in the ID between the data and the MC simulations in Fig. 47, where the Fig. 47a resp. Fig. 47b represents the p_x resp. the p_y distribution of the track reconstructed in the ID and the Fig. 47c resp. Fig. 47d represents the p_x resp. the p_y distribution of the proton reconstructed in the ALFA detector. The data are represented by the black points whereas the Monte Carlo simulations are represented by the blue histogram for the GenEx simulation and by the red histogram for the Pythia8 central diffraction containing only the non-exclusive events. The system momentum balance distributions are shown also in Fig. 47, where the $\sum p_x$ resp. $\sum p_y$ distribution is shown in Fig. 47e resp. in Fig. 47f.

A good agreement between the data and the MC simulations is visible. The MC simulation contain two fractions, the signal fraction represented by the GenEx and the background represented by the Pythia8 central diffraction process without exclusive pion events. The histograms show that a set of the event selections developed for this exclusive pion analysis at $\sqrt(s)$ =7 TeV works well and it is able to select the exclusive pion events. On other hand a selected set of events still contain a non negligible amount of a background, which is estimated is estimated by the Pythia8 MC simulation of the central diffractive events, Sect. 9.

The set of control plots shown in the Fig. 48 was made for the events which passed fiducial volume selection. This figure shows the kinematic distributions for the reconstructed track pairs. The distributions compare both the data and the Monte Carlo simulations. The data are represented by the black points whereas the Monte Carlo simulations are represented by the blue histograms for the GenEx simulation and by the red histograms for the Pythia8 central diffraction containing only the non-exclusive events. This set of the control plots is the same set of control plots made in the previous event selections progress of moving the data distributions closer to the distributions from the MC signal simulation represented by the GenEx generator. The agreement of the data with the MC simulations is not perfect - this can be caused by the generator settings (they were not tuned) used in MC simulation and/or the low data statistics.

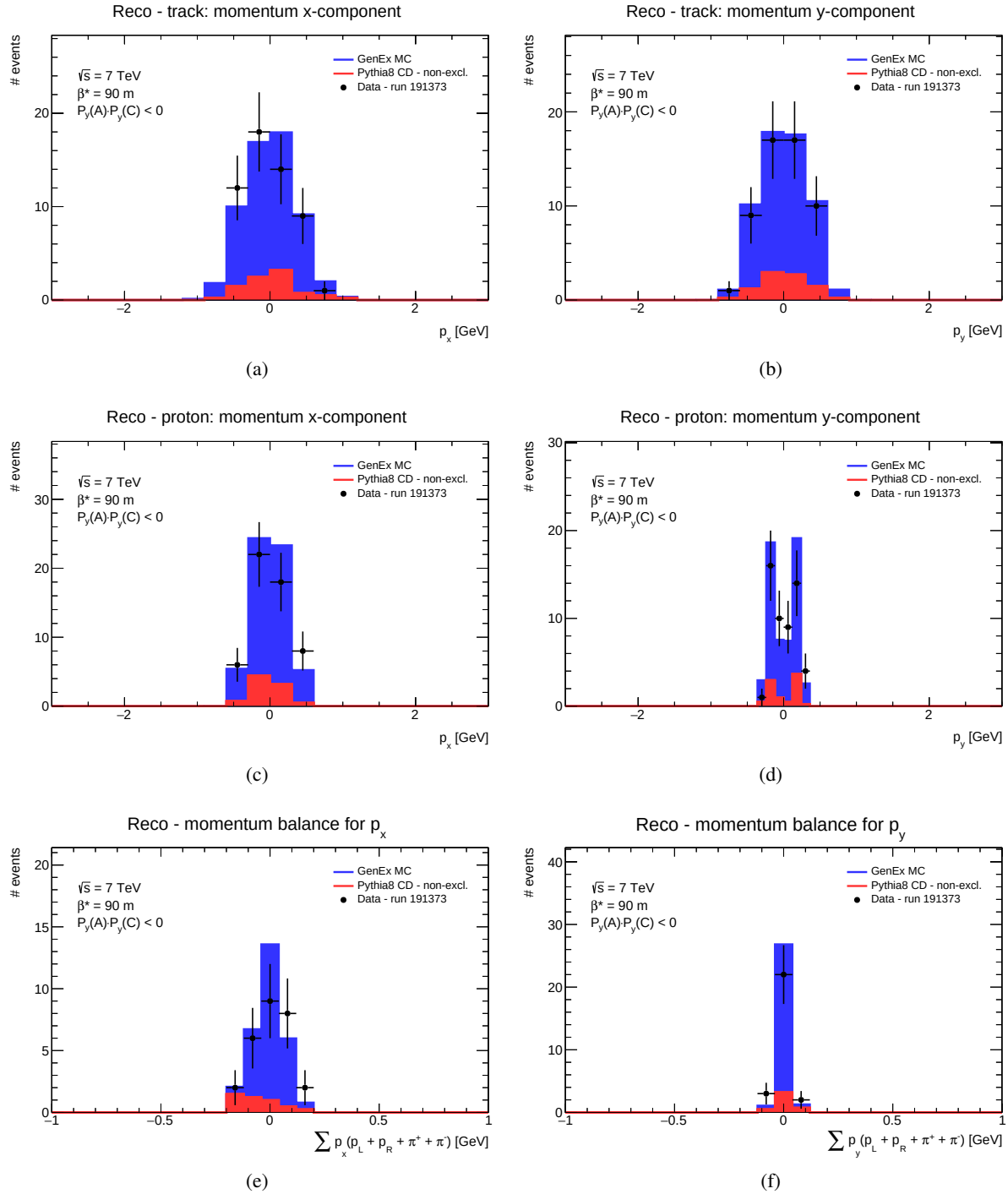

Figure 47: A set of control plots for the kinematic variables after analysis cut flow, (a) for the pion p_x distribution, (b) for the pion p_y distribution, (c) for the proton p_x, on (d) for the proton p_y, (e) for the momentum balance in p_x of the system formed by two protons and two tracks ($\pi^+\pi^-$) and (f) for the momentum balance in p_y of the system formed by two protons and two tracks ($\pi^+\pi^-$). The data are represented by the black points whereas the Monte Carlo simulations are represented by the blue histogram for the GenEx simulation and by the red histogram for the Pythia8 central diffraction containing only the non-exclusive events. The MC histograms are stacked.

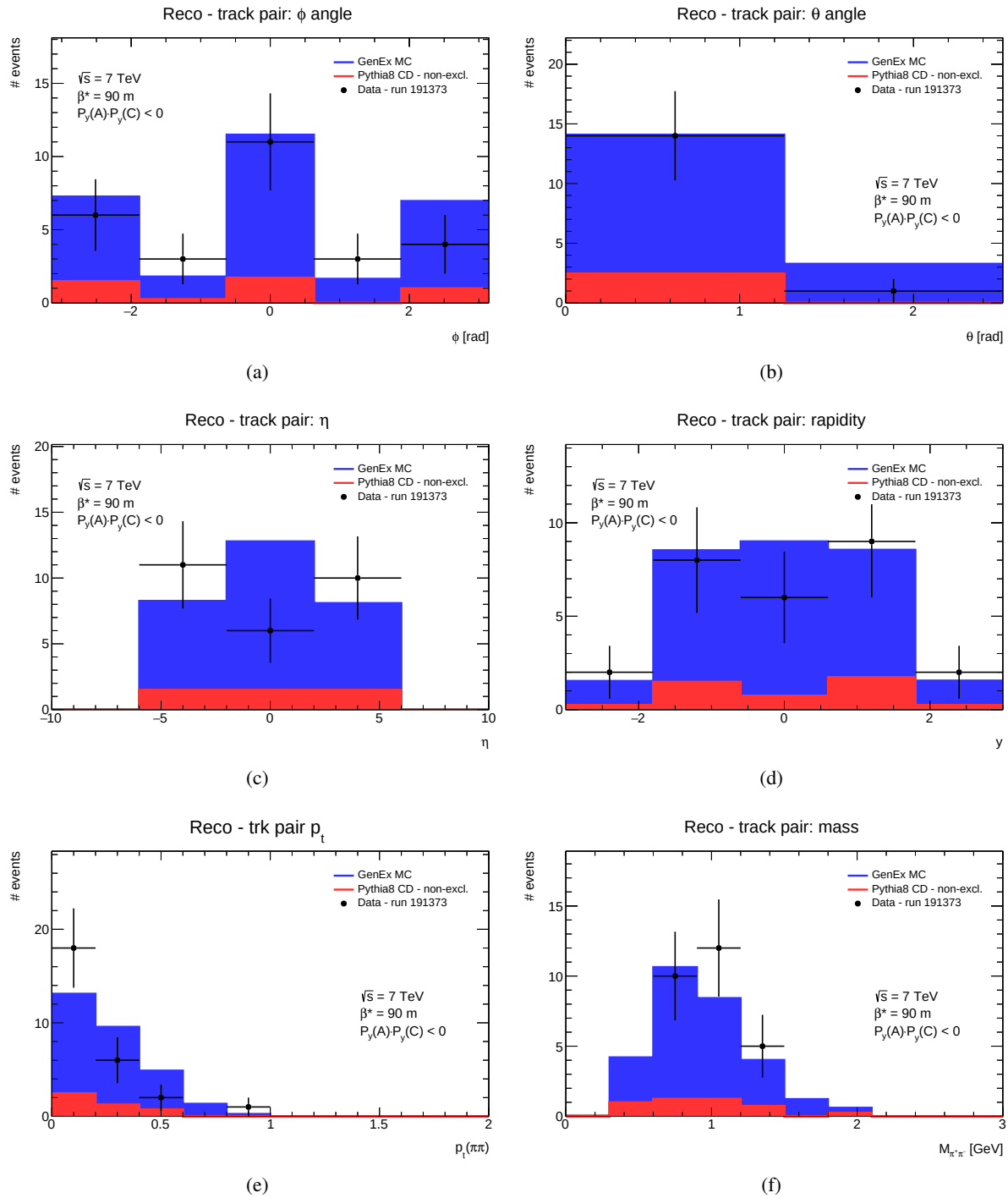

Figure 48: The reconstructed tracks pair kinematics distributions after the kinematic region selection, (a) for the $\phi_{\pi^+\pi^-}$ distribution, (b) for the $\theta_{\pi^+\pi^-}$ distribution, (c) for the $\eta_{\pi^+\pi^-}$ distribution, (d) for the rapidity $y_{\pi^+\pi^-}$ distribution (e) for the $p_{T_{\pi^+\pi^-}}$ distribution and (f) for the $M_{\pi^+\pi^-}$ distribution. The data are represented by the black points whereas the Monte Carlo simulations are represented by the blue histogram for the GenEx simulation and by the red histogram for the Pythia8 central diffraction containing only the non-exclusive events. The MC histograms are stacked.

7.11. Event selection summary

A set of the event selections was presented is previous sub-sections. We would like to briefly remind all that selections in this sub-section in following list:

- data quality pre-selection (applied only on data) in Sect. 7.1,
- trigger pre-selection, (applied only on data) in Sect. 7.2,
- primary vertex selection in Sect. 7.3,
- ATLAS ID track selection in Sect. 7.4,
- ALFA track selection in Sect. 7.5,
- MBTS veto in Sect. 7.6,
- ALFA geometrical selection in Sect. 7.7,
- kinematic selection in Sect. 7.8,
- particle identification in Sect. 7.9,
- fiducial volume selection in Sect. 7.10.

The purpose of the event selections is to select the events of the exclusive pion pair production and to remove as much background as it is possible.

8. Acceptance and unfolding

The acceptance and unfolding corrections play an important role on the road to the final results, as they influences the result of a measurement: geometrical acceptance of the detector systems, reconstruction efficiencies of used reconstruction algorithms, a trigger pre-scales used during the data taking, a restriction of kinematic region wherein the process is studied, a particle identification efficiency for a particle determination or the distributions shape corrections.

This section describes corrections we made and their effect on the exclusive pion production analysis. Due to the low statistics in data it was decided to calculate only one overall correction (single-bin correction) representing/covering all corrections mentioned above. The final number of the exclusive events - after the background subtraction - is corrected by this overall correction and the cross-section is obtained.

The exclusive pion analysis is divided into two configurations: the elastic and the anti-elastic ones. The overall corrections are calculated for both configurations, independently.

Although the overall correction is preferred solution - the default one, this section focusses on some of its components calculated bin-by-bin to see their impacts. The bin-based corrections are strongly limited by the low statistics. It was possible to made corrections in case of the elastic configuration. In the case of the anti-elastic configuration the final number of the exclusive pion pair events is less then 10 (in the selected phase-space) which complicates the bin-based correction calculation. From this reason the bin-based corrections are used just for the distributions shape corrections to compare the data with the Monte Carlo simulations.

All correction calculations were made using the GenEx Monte Carlo simulation (i.e. only signal). Both the particle and the detector levels[6] of the simulation and the analysis were performed for the same phase-space, defined in Sect. 7.10. The number of events passed that two levels is calculated. Then the overall correction factor is expressed as a ratio between the number of events $N^{\text{passed}}_{\text{detector\_level}}$ passed the analysis on the detector level and the number of events $N^{\text{passed}}_{\text{partical\_level}}$ passed the phase-space selection on the particle level,

$$f_{\text{corr}} = \frac{N^{\text{passed}}_{\text{detector\_level}}}{N^{\text{passed}}_{\text{partical\_level}}}. \tag{30}$$

A variable f_{corr} represents the overall correction which corrects the data final event selection to the cross-section value; the luminosity value is not a part of the overall correction. The Table 11 summarizes the values of f_{corr} for various case studies like the elastic/anti-elastic configurations, LatticeMethod/ALFAReco methods of the proton kinematics reconstruction or the GenEx/DiMe MC simulations. Values of f_{corr} are calculated for the case of the single tracks in an appropriate combination of the ALFA detectors like elastic/anti-elastic configuration, as described in Sect. 7.5.

[6] By the particle level in the Monte Carlo simulation the truth particle level is meant. By the detector level in the Monte Carlo simulation the reconstructed particle level is meant, and an information about a particle after the reconstruction is used.

Table 11: The overall correction values for several studies including elastic/anti-elastic configuration, different proton kinematic reconstruction algorithms or different MC signal simulations.

	GenEx				DiMe	
	elastic		anti-elastic		elastic	anti-elastic
	Lattice	**ALFA Reco**	**Lattice**	**ALFA Reco**	**Lattice**	**Lattice**
overall correction	0.0724611	0.0723752	0.0674902	0.0674795	0.0962788	0.0950474

The effect of one overall correction is demonstrated on several distributions. The plots show propagation of the corrections through the range of the pion-pair kinematic distributions started with pion-pair invariant mass shown in Fig. 49. At the beginning of the analysis, on the particle level, the histogram of the central system invariant mass is filled before any event selection (Sect. 7) expect the fiducial volume selection (Sect. 7.10) which is applied (see Fig. 49a). After the analysis cut flow (including all event selections from Sect. 7), the same histogram of the central system invariant mass made, but now for the detector level values like in Fig. 49b. Then the bin-based correction is calculated with a result shown in Fig. 49c. Such bin-based correction contains all the parts of the overall correction (described further in the section) like a geometrical acceptance, a reconstruction efficiency or distribution shape correction.

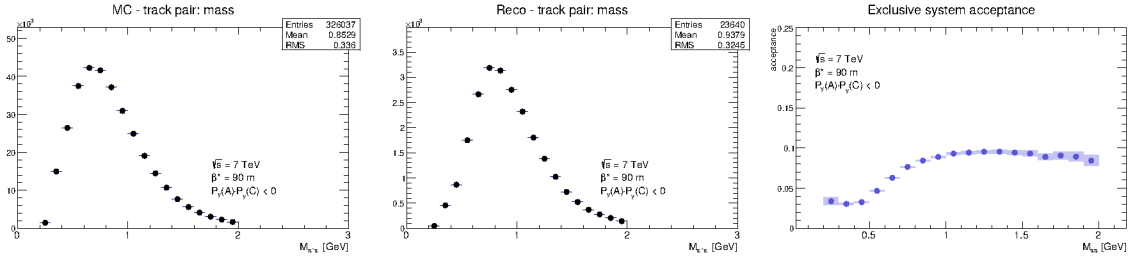

(a) (b) (c)

Figure 49: The central system invariant mass distribution on both (a) the particle and (b) the detector levels together with (c) its calculated bin-based correction for the elastic configuration. The GenEx Monte Carlo simulation was used.

The same procedure is also used in the bin-based correction calculation for the rest of the exclusive central system kinematic variables, namely $p_{\mathrm{T}(\pi\pi)}$ (Fig. 50a),$M_{\pi\pi}$ (Fig. 50b), $\phi_{\pi\pi}$ (Fig. 51a), $\theta_{\pi\pi}$ (Fig. 51b), $\eta_{\pi\pi}$ (Fig. 52a) and $y_{\pi\pi}$ (Fig. 52b). The bin-based corrections are shown for the both the elastic and the anti-elastic configurations.

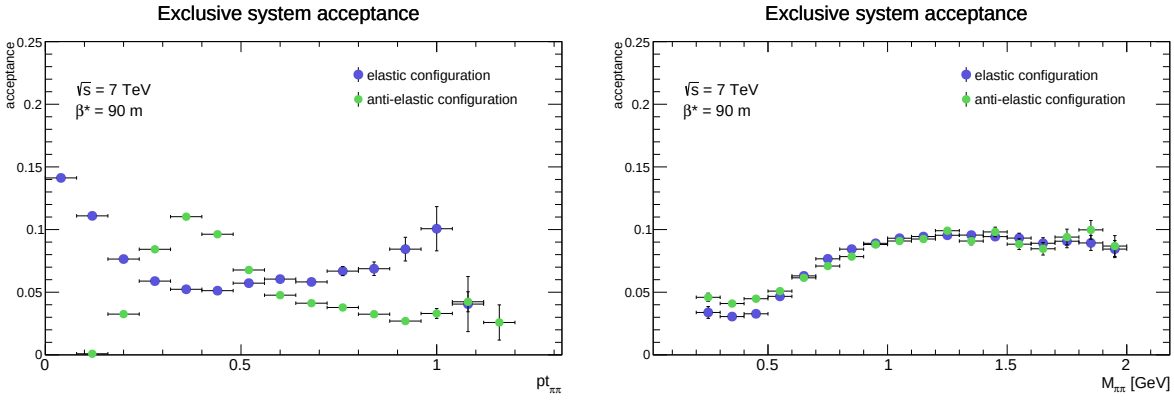

(a) (b)

Figure 50: The bin-based correction distributions (a) for the central system transverse momentum and (b) for the central system invariant mass. The GenEx Monte Carlo simulation was used.

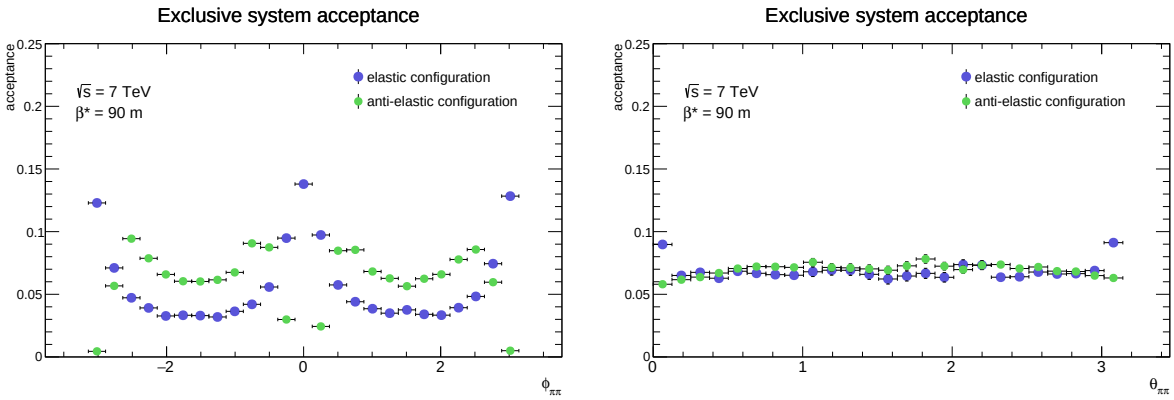

(a) (b)

Figure 51: The bin-based correction distributions (a) for the central system azimuthal angle ϕ and (b) for the central system polar angle θ. The GenEx Monte Carlo simulation was used.

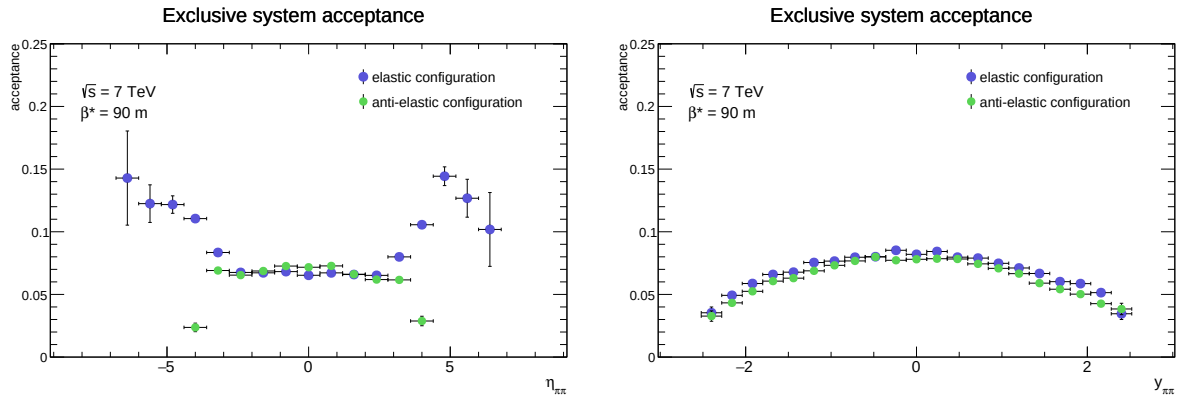

(a) (b)

Figure 52: The bin-based correction distributions (a) for the central system rapidity and (b) for the central system pseudo-rapidity. The GenEx Monte Carlo simulation was used.

8.1. Geometrical acceptance

Here we focus on the geometrical acceptances of both used detector systems, the Inner detector (ID) and the ALFA detector. For this purpose GenEx Monte Carlo simulation was used. Both systems are set up accordingly to the dedicated settings of the ATLAS run 191373.

The geometrical acceptance is calculated for each product of an exclusive pion pair production - protons and pions - separately as well as for the $\pi^+\pi^-$ central system.

The proton geometrical acceptance was calculated as a ratio between the number of events with the proton transported before the ALFA detector and the overall number of generated events containing proton. The acceptance is expressed as the proton geometrical acceptance and shown in Fig. 53 . The red dashed vertical lines define fiducial volume within which the protons are accepted for the exclusive pion pair production analysis. The ALFA geometrical acceptance is strongly dependent on the proton t-spectrum.

The pion geometrical acceptance was calculated as a ration between the number of events with pion transported before ID sub-detector and the overall number of events containing the pion. The pion geometrical acceptance is expressed as the function of the pion pseudo-rapidity $\eta(\pi^{\pm})$(Fig. 54). The ID geometrical acceptance depends slightly on a pion η value. Its value is close to the 100% around $\eta = 0$, then slightly decreases on the edge of the ID.

The pion geometrical acceptance is very high. When pions are combined into the pion pair, the geometrical acceptance of such system will slightly drop down as is shown in Figs. 55–57 where the pion-pair geometrical acceptance is calculated for $\phi_{\pi^+\pi^-}$, $\theta_{\pi^+\pi^-}$, $\eta_{\pi^+\pi^-}$, $y_{\pi^+\pi^-}$, $p_{\mathrm{T}_{\pi^+\pi^-}}$ and $M_{\pi^+\pi^-}$ distributions. The most of the pion-pair distributions evince the strong acceptance dependence on the pion-pair kinematics.

The separated pion-pair kinematics distributions for both the particle level and the detector level are shown in Figs. 58–60 to demonstrate a geometrical impact of the ID on the pion tracks. The distributions for both the particle level and the detector level are shown within the one histogram for $\phi_{\pi^+\pi^-}$ in Fig. 58a, for $\theta_{\pi^+\pi^-}$ distribution in Fig. 58b, for $\eta_{\pi^+\pi^-}$ distribution in Fig. 59a, for $y_{\pi^+\pi^-}$ distribution in Fig. 59b, for $pt_{\pi^+\pi^-}$ distribution in Fig. 60a and for $M_{\pi^+\pi^-}$ distribution in Fig. 60b.

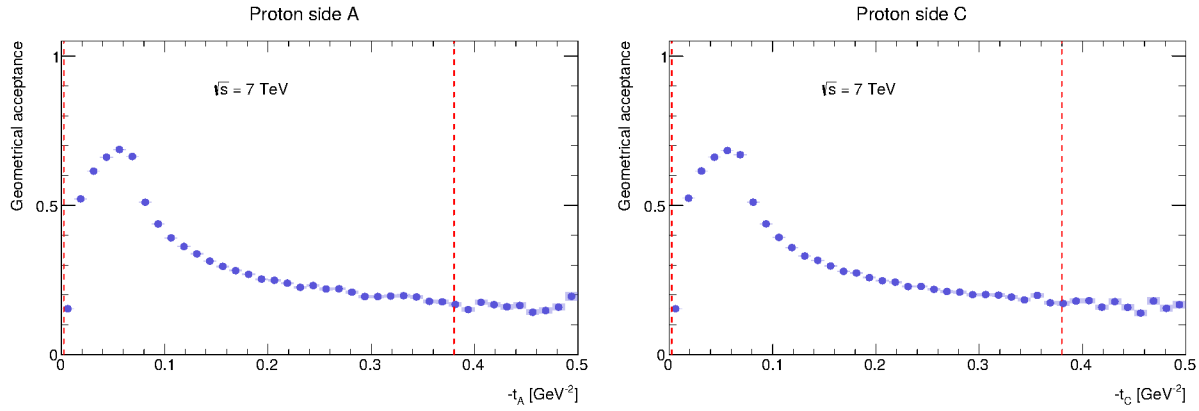

(a) (b)

Figure 53: The proton geometrical acceptance as a function of the t-spectrum distribution (a) for the proton on ATLAS side A and (b) for the proton on the ATLAS side C. The GenEx Monte Carlo simulation was used.

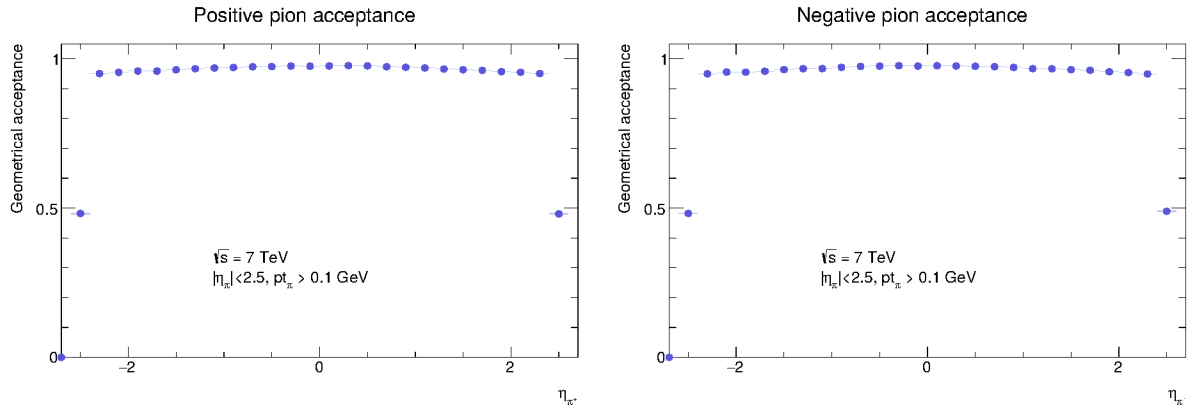

(a) (b)

Figure 54: The pion geometrical acceptance as a function of the pseudo-rapidity distribution (a) for the positive pion and (b) for the negative pion. The GenEx Monte Carlo simulation was used.

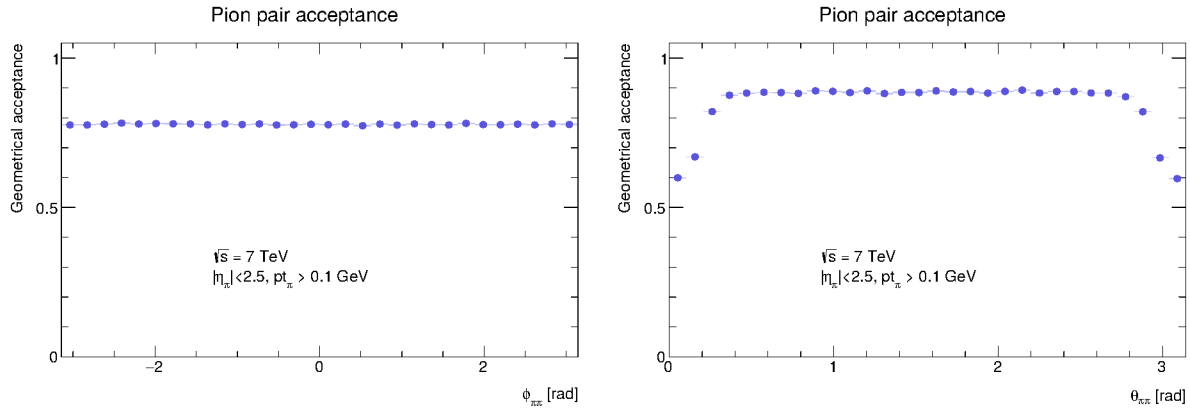

(a) (b)

Figure 55: The overall geometrical acceptance of the exclusive pion system as a function of the central system azimuthal $\phi_{\pi^+\pi^-}$ angle (a) and as the function of the central system polar $\theta_{\pi^+\pi^-}$ angle (b). The GenEx Monte Carlo simulation was used.

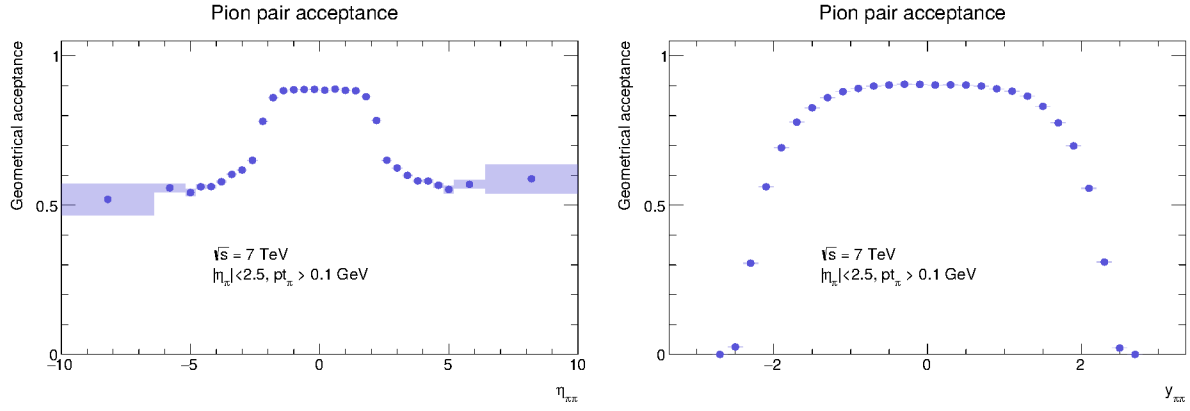

(a) (b)

Figure 56: The overall geometrical acceptance of the exclusive pion system as a function of the central system pseudo-rapidity $\eta_{\pi^+\pi^-}$ (a) and as the function of the central system rapidity $y_{\pi^+\pi^-}$ (b). The GenEx Monte Carlo simulation was used.

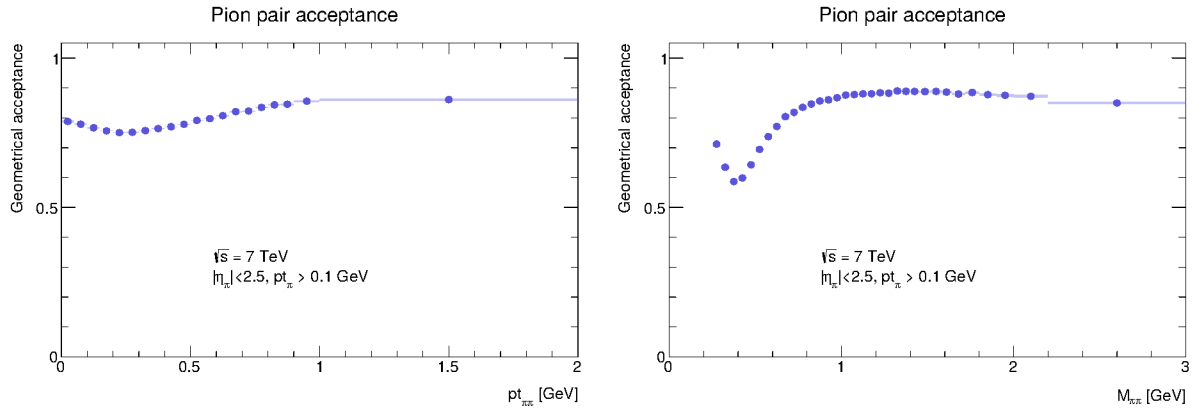

(a) (b)

Figure 57: The overall geometrical acceptance of the exclusive pion system as a function of the central system transverse momentum $pt_{\pi^+\pi^-}$ (a) and as the function of the central system invariant mass $M_{\pi^+\pi^-}$ (b). The GenEx Monte Carlo simulation was used.

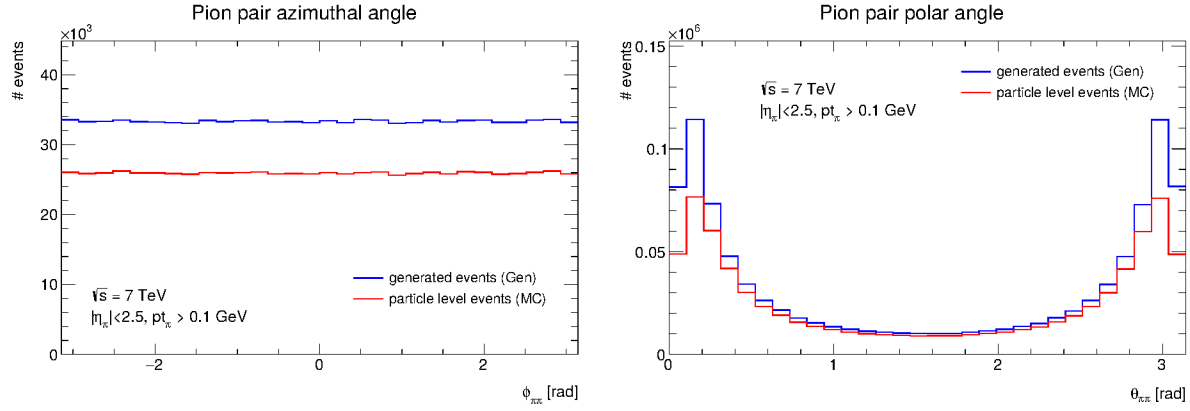

(a) (b)

Figure 58: The input distributions into the exclusive system geometrical acceptance calculation, the red distribution for the particle level and the blue distribution one for the detector level, (a) the central system azimuthal $\phi_{\pi^+\pi^-}$ angle and (b) the central system polar $\theta_{\pi^+\pi^-}$ are shown. The GenEx Monte Carlo simulation was used.

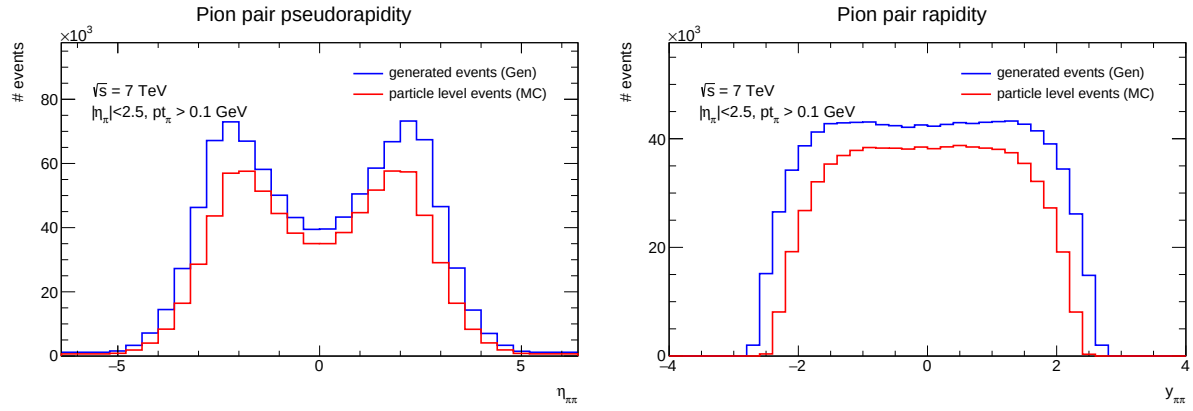

(a) (b)

Figure 59: The input distributions into the exclusive system geometrical acceptance calculation, the red distribution one for the particle level and the blue distribution one for the detector level, (a) the central system pseudo-rapidity $\eta_{\pi^+\pi^-}$ and (b) the central system pseudo-rapidity $\eta_{\pi^+\pi^-}$ are shown. The GenEx Monte Carlo simulation was used.

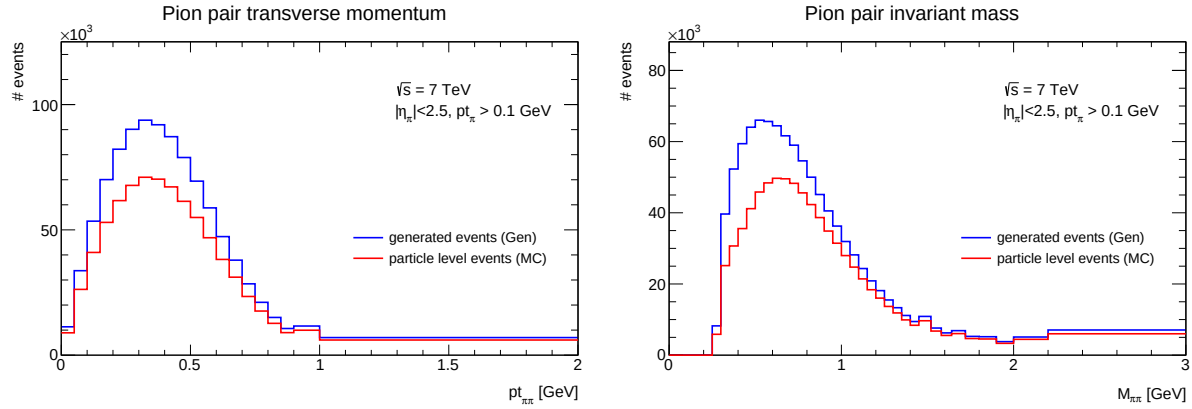

(a) (b)

Figure 60: The input distributions into the exclusive system geometrical acceptance calculation, the red distribution one for the particle level and the blue distribution one for the detector level, (a) the central system transverse momentum $pt_{\pi^+\pi^-}$ and (b) the central system invariant mass $M_{\pi^+\pi^-}$ are shown. The GenEx Monte Carlo simulation was used.

The geometrical acceptance of the exclusive pion system consists of the geometrical acceptances of each detector system, so from the geometrical acceptances of two ALFA detector systems, and from the pion-pair geometrical acceptance of the ID. Due to the detector systems combination the overall geometrical acceptance drop down to ≈ 0.2. The biggest impact on the result has the ALFA detector system which itself has quite low geometrical acceptance getting closer to 0.2. The exclusive pion system geometrical acceptance as a function of $\phi_{\pi^+\pi^-}$, $\eta_{\pi^+\pi^-}$, $y_{\pi^+\pi^-}$, $pt_{\pi^+\pi^-}$ and $M_{\pi^+\pi^-}$ is shown in Figs. 61 and 62. The geometrical acceptance is shown for the elastic configuration.

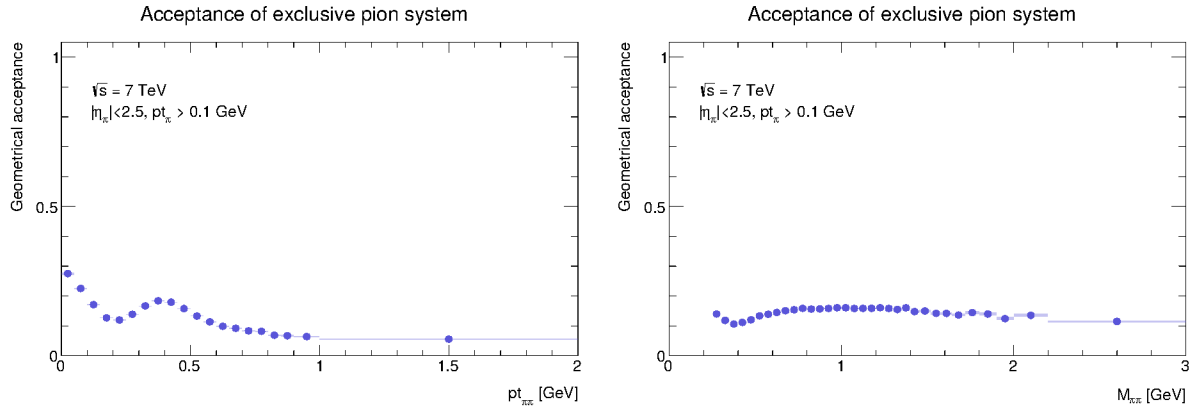

(a) (b)

Figure 61: Exclusive pion system geometrical acceptance (a) for the transverse momentum $p_{t_{\pi^+\pi^-}}$ and (b) for the invariant mass $M_{\pi^+\pi^-}$. The GenEx Monte Carlo simulation was used.

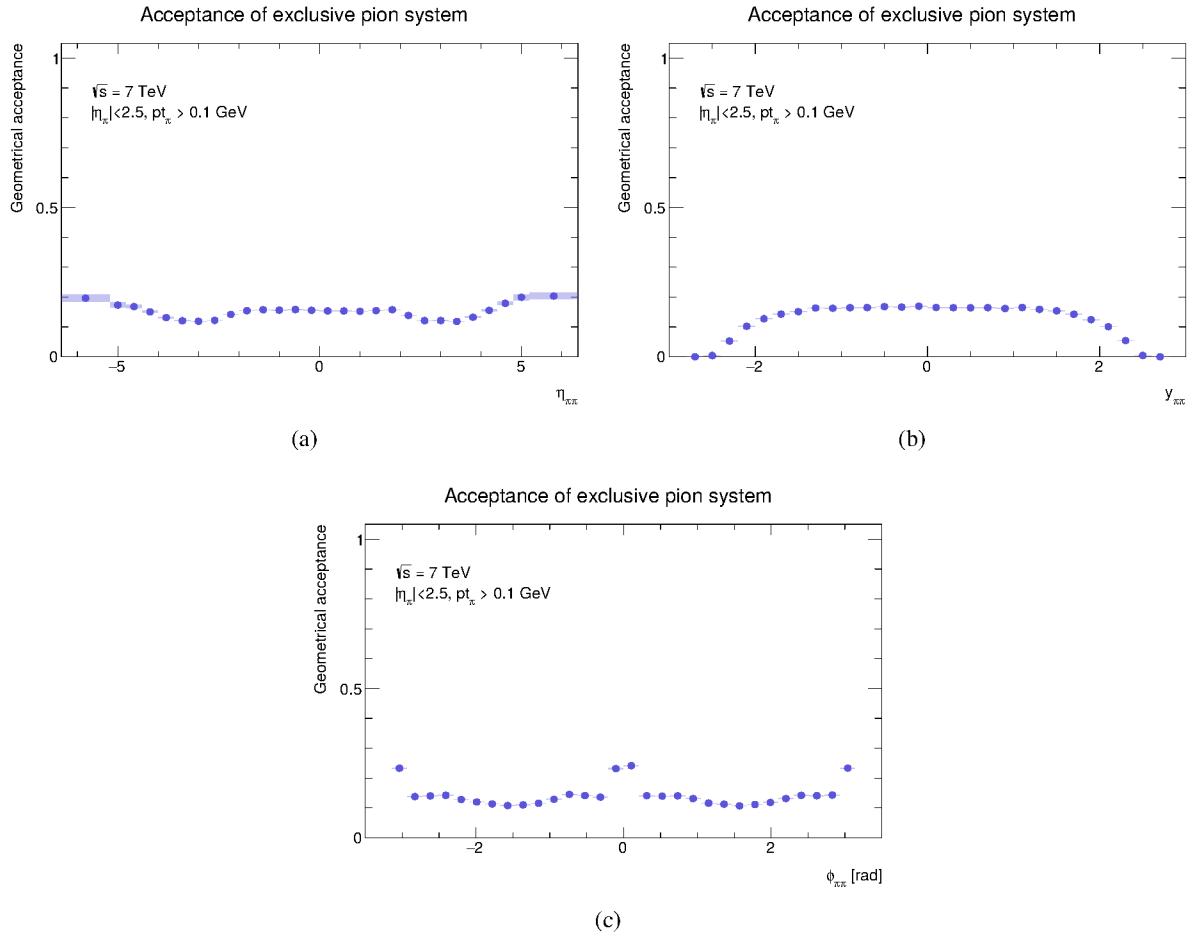

Figure 62: The exclusive pion system geometrical acceptance (a) for the pseudo-rapidity $\eta_{\pi^+\pi^-}$, (b) for rapidity $y_{\pi^+\pi^-}$ and (c) for the azimuthal angle $\phi_{\pi^+\pi^-}$. The GenEx Monte Carlo simulation was used.

8.2. Reconstruction efficiency

The reconstruction efficiency is the other part of the overall correction f_{corr} calculation. This section describes the reconstruction efficiency of both the ATLAS ID and the ALFA detectors. The efficiency informs how well a selected algorithm is able to deal with the information about the particle hits in the detector and based on them to reconstruct track(s). First, let us focus on the each product of the exclusive pion system separately and, only later on the whole exclusive pion pair system.

The reconstruction efficiency r_{eff} is calculated as the ratio between the number of events with the reconstructed track N_{reco} and the total number of events available for the track reconstruction process N_{tot}

$$r_{\text{eff}} = \frac{N_{\text{reco}}}{N_{\text{tot}}}. \tag{31}$$

This reconstruction efficiency calculation is the bin based and is done for the several kinematic variables. First, for the each product of the central exclusive system separately: for the proton on ATLAS side A, for the proton on ATLAS side C, for the π^+ and for the π^-. Second, for the ID represented by the pion

pair $\pi^+\pi^-$, and third, for the whole exclusive system represented by the central system kinematics of the exclusive pion production.

A set of control plots was done for $\phi_{\pi^+\pi^-}$, $\theta_{\pi^+\pi^-}$, $\eta_{\pi^+\pi^-}$, $y_{\pi^+\pi^-}$, $pt_{\pi^+\pi^-}$ and $M_{\pi^+\pi^-}$.

8.2.1. ALFA detector reconstruction efficiency

The response of the ALFA detectors implementation (simulation) to the signal may differ from the response of the detectors installed in the LHC tunnel, e.g. due to the implementation of a signal-noise production mechanisms or a missing implementation of electronic channel cross-talk. Also data samples (simulation vs real data) are different due to a missing model of a beam background or pile-up modelling (existing but not used) within simulation.

We define a detector efficiency as an effectiveness of the detector (and corresponding algorithm) finding objects of interest O_{in} which have passed through the detector.

Having a clean source of O_{in}, then it is the ratio

$$\epsilon_{\text{det}} = \frac{N_{\text{found}}}{N_{\text{all}}}, \tag{32}$$

where N_{found} is a number of objects O_{in} detector found and N_{all} is the total number of objects which passed the detector.

The efficiency of ALFA trigger tiles (Fig. 63) to register any kind of signal - clean signal, pile-up signal, signal and background - is close to 100%, without a possibility to distinguish kind of signal.

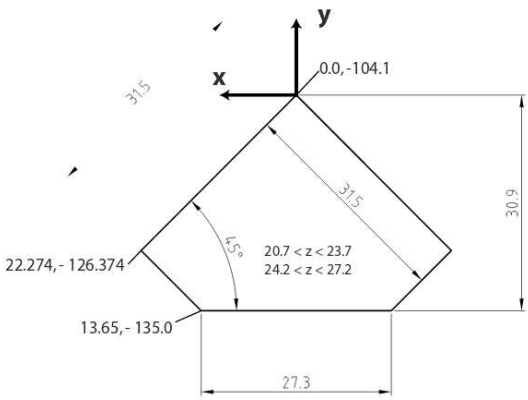

Figure 63: ALFA trigger plate schematics.

In case of pion pair exclusive production we are looking for protons passing the ALFA detector (system) and having two pions (opposite sign) tracks in central detectors - the statistics for such selection of O_{in} in data is, for $\sqrt{s} = 7\,\text{TeV}$, very low (Table 21 in Sect. 10), especially in case of anti-elastic topology (Sect. 5.5.1) and the Eq. 32 cannot be effectively used.

But, to determine the detector efficiency to reconstruct forward protons, it is not necessary to use only the signal sample. Any process/sample containing forward protons can be used if forward proton distributions have the same kinematic domains.

In case of elastic topology signal protons energy losses in exclusive processes are very close to 0, and protons from elastic collisions can be used (separately or together with signal protons).

The situation is slightly different in case of anti-elastic topology. Knowing detector efficiencies for each ALFA detector and assuming that their measurements are independent, the efficiencies of anti-elastic arms could be calculated as their corresponding products. On the other hand the outer detectors are affected by showers caused by the inner ones and their efficiencies are affected.

From this reason it is better to consider the efficiencies of the full armlets. These were found in elastic analysis but contains relatively big errors ($\sim 17\%$). There is still a way to use elastic analysis, assuming that both armlets is each elastic arm have the same efficiency, and together they give the efficiency of full arm i.e.

$$\epsilon_{\text{elastic arm}} = \epsilon^2_{\text{elastic armlet}}, \tag{33}$$

This would bring an additional error in the analysis but it is heavily dominated by a statistical error anyway. Note that all detectors in each elastic arm are oriented in the same way, i.e. the trigger tiles are in front of the fibre planes for topology 0257 and after them in case of the topology 1346.

Using the described approach we get following detector efficiencies (no errors included here) in Table 12:

Table 12: ALFA topology efficiencies.

topology	**efficiency**
0257	0.897
1346	0.880
0246	0.888
1357	0.888

We are going to give another derivation of topology efficiencies now. Before this we remark that the efficiencies of both elastics topologies obtained in the elastic analysis are in agreement with the definition expressed by the Eq. 32 if N_{tot} is the number of elastic events and N_{found} is number of events with at least 1 track reconstructed in all detectors. Also, no t (=angular) dependency of detector efficiency was found and the number of events when detectors triggered but no track was reconstructed in any of them in a given topology was estimated.

We select a data stream ALFA physics and then for elastic topology triggers L1_ELAST15 and L1_ELAST18 (forming L2_ALFA_Phys chain), for anti-elastic topology L1_ALFA_ANY (forming L2_ALFA_Phys_any chain).

In case of the elastic topology at least one of the station on both sides fired. We expect that data sample contains majority of events originating in elastic collisions, with (much) smaller fragments of exclusive processes (including our signal) and (as we are not checking status of the ATLAS inner detector) also combinations e.g. of elastic (EL) event with single diffractive (SD) one, of 2 single SD events, SD event + beam halo (BH), BH + BH. Since the value of pileup was very low (~ 0.003) we do not expect that the fraction EL+SD and SD+SD has a significance. In case of elastic topology we do not expect also a significant fraction of events when protons entering to the first station are accompanied by showers. The

showers can however develop during the interaction of particles with detectors. Finally, there can be also a fraction of event made of pure showers developed till detectors from the ATLAS IP.

In case of the anti-elastic topology, on top of any exclusive signal, the sample contains combinations of SD + BH and BH + BH which amount should be comparable with their contribution to the elastic topology.

Independently of topology we use the cut which should efficiently differentiate between a one particle and multi-particle states entering into the detectors - our goal is to to filter out multi-particle states (EL with showers, EL+SD, SD+SD, showers) and in this way to equalize MC and real data samples. In what follows we call this condition *UV*-selection, as it is used both in simulations and real data analyses. More detailed information about *UV*-selection will be given in the paragraph **UV-selection details** bellow in this text.

Using the definition of the detector efficiency, the Eq. 32 in such situation, we get

$$\epsilon_{\text{topology}} = \frac{N_{>0}}{N_{\text{UV}}} \times \left.\frac{N_{UV}}{N_{\text{accept}}}\right|_{\text{MC}}, \tag{34}$$

where $N_{>0}$ is the number of events with more than 1 track reconstructed in each of the detectors in a given topology, N_{UV} is number of events which passed the *UV*-selection and N_{accept} is the number of signal events in acceptance of the given topology. It is *UV*-selection which should filter out multi-particle states, both in MC (here it will be only showers in outer stations) and data.

ALFA trigger and UV-selection

Due to an unfinished implementation of the ALFA trigger planes into the ALFA detectors simulation model (the detector trigger planes are implemented but not their readout) we use *truth* information to calculate whether protons are in detector acceptances. MC simulation uses Forward Transport algorithm [ref] to transport protons in front of inner ALFA detectors, then a full Geant4 simulation starts. Positions of protons, just before entering detectors, are calculated (ignoring multi-scattering effect), and the detector acceptances are given by the shape of trigger scintillation counters.

The Table 13 summarizes the efficiency of the *UV*-selection for separate detectors in MC (the middle column)

Table 13: ALFA detector efficiencies for MC simulation (GenEx) of the reconstruction and the *UV*-selection.

detector	**trk/trigg**	**trigg/acc**	**trk/acc**
B7L1U	0.994 ± 0.003	0.958 ± 0.003	0.952 ± 0.003
B7L1L	0.995 ± 0.003	0.950 ± 0.003	0.946 ± 0.003
A7L1U	0.997 ± 0.003	0.986 ± 0.003	0.982 ± 0.003
A7L1L	0.989 ± 0.003	0.978 ± 0.003	0.968 ± 0.003
A7R1U	0.995 ± 0.003	0.978 ± 0.003	0.973 ± 0.003
A7R1L	0.994 ± 0.003	0.986 ± 0.003	0.980 ± 0.003
B7R1U	0.995 ± 0.003	0.948 ± 0.003	0.943 ± 0.003
B7R1L	0.996 ± 0.003	0.958 ± 0.003	0.954 ± 0.003

and the Table 14 summarizes it for data.

Table 14: ALFA detector efficiencies for data of the reconstruction and the *UV*-selection.

detector	**trk/trigg**	**trigg/acc**	**trk/acc**
B7L1U	0.974 ± 0.002	0.820 ± 0.001	0.799 ± 0.001
B7L1L	0.981 ± 0.002	0.795 ± 0.001	0.780 ± 0.001
A7L1U	0.969 ± 0.002	0.860 ± 0.001	0.833 ± 0.001
A7L1L	0.976 ± 0.002	0.872 ± 0.002	0.851 ± 0.002
A7R1U	0.984 ± 0.002	0.876 ± 0.002	0.862 ± 0.002
A7R1L	0.984 ± 0.002	0.867 ± 0.002	0.853 ± 0.002
B7R1U	0.978 ± 0.002	0.812 ± 0.001	0.794 ± 0.001
B7R1L	0.991 ± 0.002	0.793 ± 0.001	0.786 ± 0.001

The number of reconstructed tracks **trk** (number of reconstructed tracks > 0) is calculated using the sample restricted by the *UV*-selection, noted as **trigg**. The number of all accepted events is labelled as **acc**.

The first column shows a detector efficiency to reconstruct any track based on the selected (by *UV*-selection) sample. Note the relatively good agreement between MC and data (difference ≤ 2.2%) and also that reconstruction efficiencies between inner and outer stations are also close (difference ≤ 0.5% for MC, ≤ 1.7%) to each other, as we expected - the *UV*-selection equalized samples for each detector, despite showers in the outer stations.

The Table 15 summarizes the efficiency of *UV*-selection in MC for full arms (0,1 - elastic, 2,3 - anti-elastic):

Table 15: ALFA full arm efficiencies for the MC simulation (GenEx).

arm	**accepted**	**triggered**	**ratio**
0	57187 ± 239	51785 ± 228	0.906 ± 0.006
1	55451 ± 235	49075 ± 222	0.885 ± 0.006
2	65269 ± 255	58426 ± 242	0.895 ± 0.005
3	64135 ± 253	57397 ± 240	0.895 ± 0.005
arm	**triggered**	**reconstructed**	**ratio**
0	51785 ± 228	51292 ± 226	0.990 ± 0.006
1	49075 ± 222	48524 ± 220	0.989 ± 0.006
2	58426 ± 242	57859 ± 241	0.990 ± 0.005
3	57397 ± 240	56887 ± 239	0.991 ± 0.005

and Table 16 summarizes the same for data.

Table 16: ALFA full arm efficiencies for data.

arm	accepted	triggered	ratio
0	588102 ± 767	448041 ± 669	0.762 ± 0.002
1	555692 ± 745	418473 ± 647	0.753 ± 0.002
2	1879 ± 43	961 ± 31	0.511 ± 0.020
3	1421 ± 38	651 ± 26	0.458 ± 0.022
arm	**triggered**	**reconstructed**	**ratio**
0	448041 ± 669	443928 ± 666	0.991 ± 0.002
1	418473 ± 647	413667 ± 643	0.989 ± 0.002
2	961 ± 31	864 ± 29	0.899 ± 0.042
3	651 ± 26	619 ± 25	0.951 ± 0.053

The differences of *UV*-efficiencies between MC and data are significant, especially for anti-elastic topology, but understandable - in data the number of accepted events is given by a ALFA trigger, which reacts on each input, including showers. In Monte Carlo the input is, especially for inner detectors, based on a single particle.

The final detector efficiency in data is then, accordingly to Eq. 34, summarized in Table 17.

Table 17: ALFA topology efficiencies in data.

ALFA topology	efficiency
0257	0.897 ± 0.006
1346	0.875 ± 0.006
0246	0.805 ± 0.038
1357	0.851 ± 0.048

We correct data using the information based on MC since we assume that response of the detector and its implementation in MC are close to each other, viz following paragraph.

UV-selection details

UV-selection is based on the event fibre multiplicities - in the first (w.r.t. the ATLAS IP) four *U* and *V* detector layers with, - at least two of four *U* and (simultaneously) *V* layers having more than one hit and, - maximally three hits in any of the layers.

The first two conditions originate from the estimate of one fibre efficiency, our requirement on the *UV*-selection efficiency - Table 13 - and shower probability suppression.

The third condition on the maximum number of hits in layer comes from the fact that for a signal we require one signal fibre with maximally two cross-talk fibres surrounding the signal, the situation we observed during beam tests of the ALFA detectors.

Application of the *UV*-selection to full topologies is based on logical AND - each of the detector has to satisfy the *UV*-selection conditions.

8.2.2. Inner detector reconstruction efficiency

The ID reconstruction efficiency is calculated in the similar way as for the protons. Also here the ratio between the number of the reconstructed tracks and their total number is used. The track reconstruction efficiency of the ID is shown in Figs. 64 and 65 as the function of the track transverse momentum p_t (Fig. 64a), the track azimuthal angle ϕ (64b), (the track pseudo-rapidity η (Fig. 65a) and the track rapidity y (Fig. 65b). The track reconstruction efficiency strongly depends on the track characteristic.

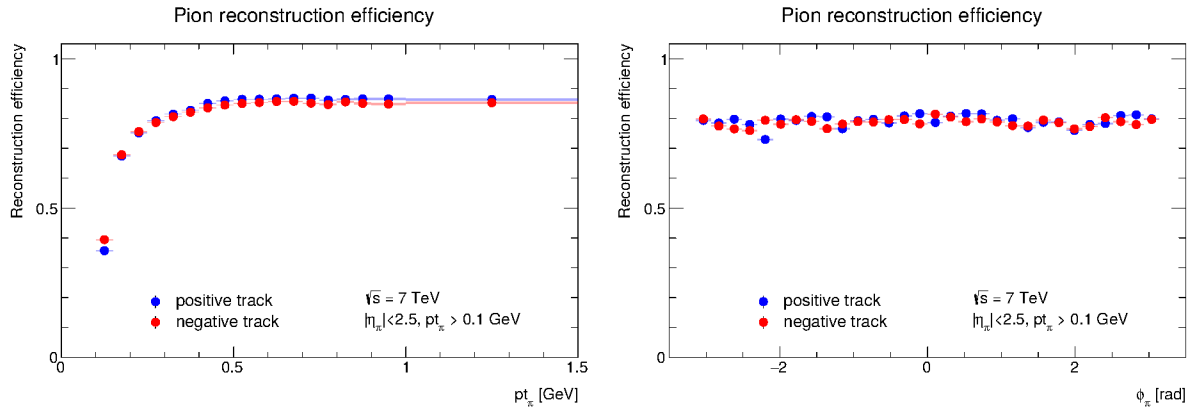

(a) (b)

Figure 64: The ID reconstruction efficiency (a) as the function of the track transverse momentum p_t and (b) as the function of the track azimuthal angle ϕ. The blue points represent the positive track whereas the red points represent the negative track. The GenEx Monte Carlo simulation was used.

The two-pion system reconstruction efficiency is calculated as the function of the two-pion system transverse momentum $p_{T_{\pi\pi}}$ shown in Fig. 66a, as the function of the two-pion system invariant mass $M_{\pi\pi}$ (Fig. 66b), the two-pion system pseudo-rapidity $\eta_{\pi\pi}$ (Fig. 67a), the two-pion system rapidity $y_{\pi\pi}$ (Fig. 67b) and the two-pion system azimuthal angle $\phi_{\pi\pi}$ (Fig. 67c). The average two-pion system reconstruction efficiency is $\approx 65\%$.

The overall reconstruction efficiency

Separate reconstruction efficiencies are combined together to describe the overall effect on the whole exclusive system. Figs. 68 and 69 show the reconstruction efficiency of this exclusive system. It is seen that the average value is slightly 50%.

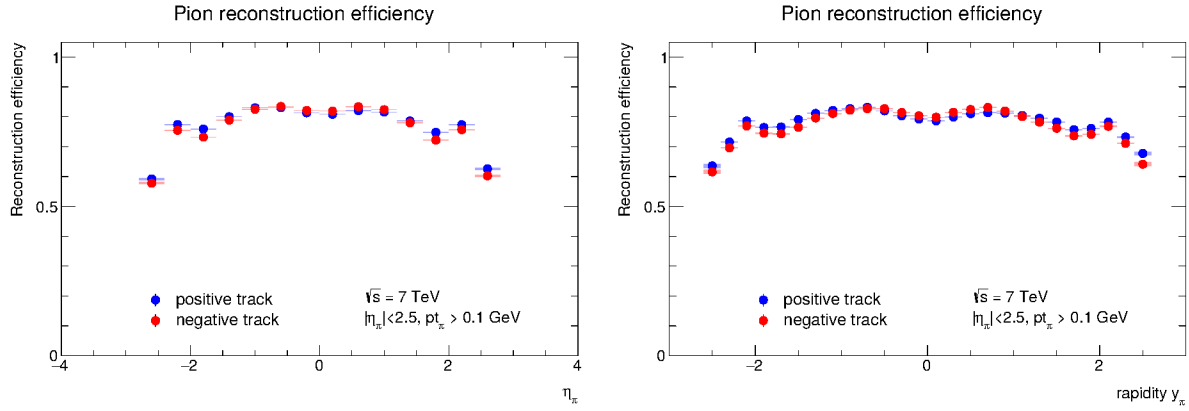

(a) (b)

Figure 65: The ID reconstruction efficiency on (a) as the function of the track pseudo-rapidity η and on (b) as the function of the track rapidity y. The blue points represent the positive track whereas the red points represent the negative track. The GenEx Monte Carlo simulation was used.

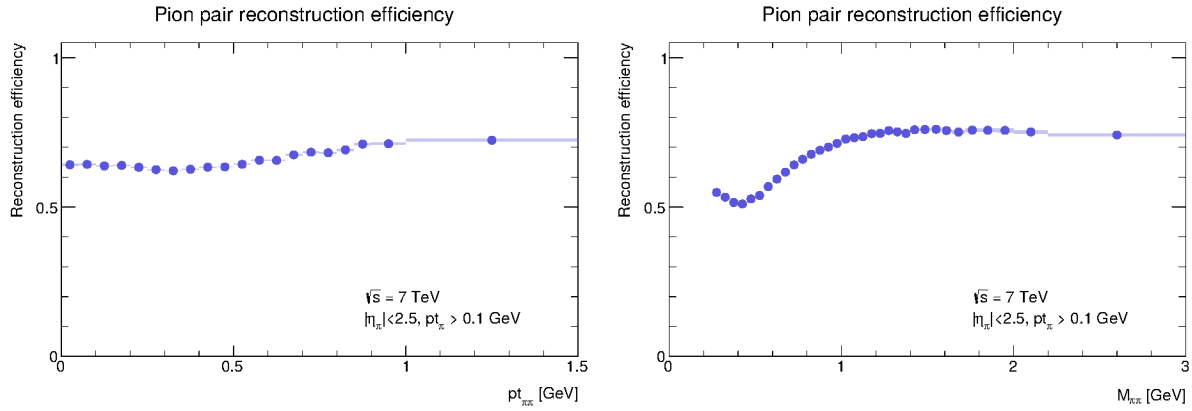

(a) (b)

Figure 66: The ID reconstruction efficiency (a) as the function of the two-pion system transverse momentum $pt_{\pi\pi}$ and (b) as the function of the two-pion system invariant mass $M_{\pi\pi}$. The GenEx Monte Carlo simulation was used.

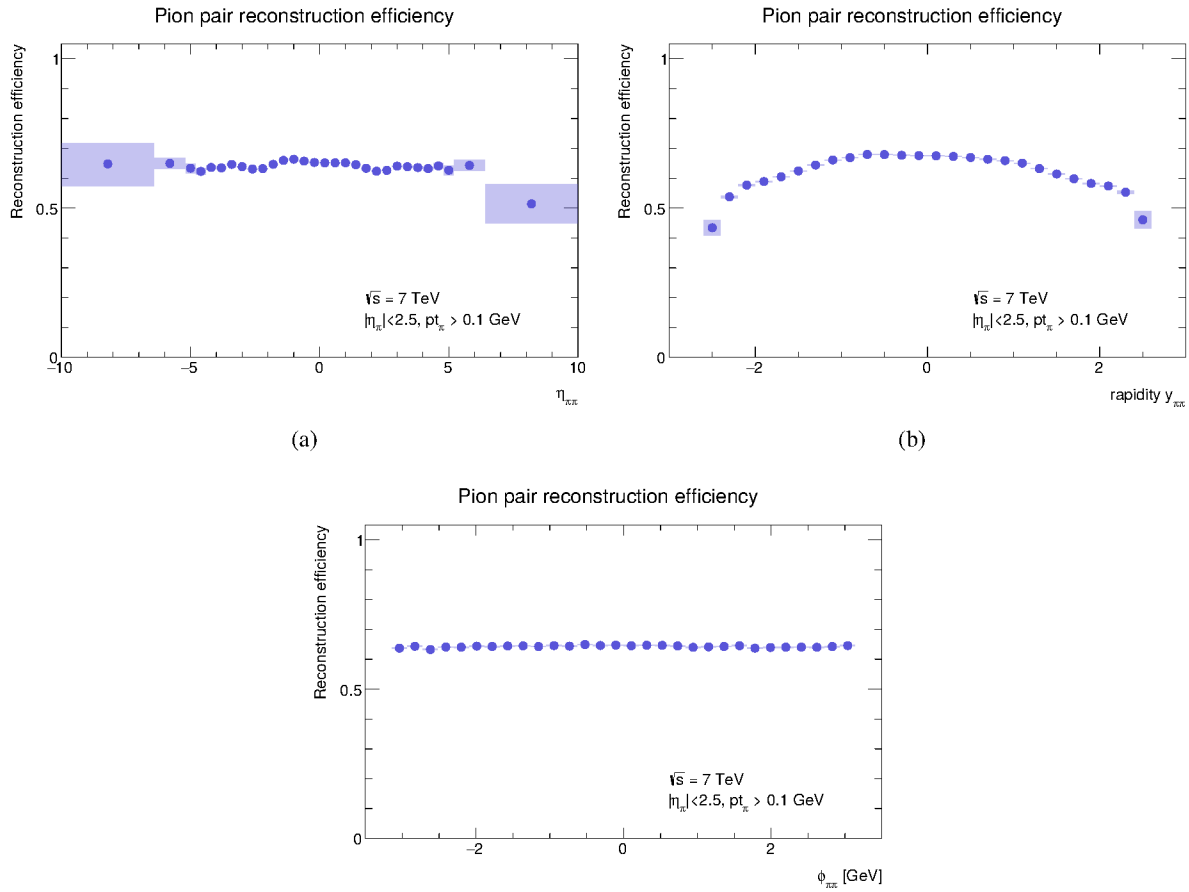

Figure 67: The ID reconstruction efficiency (a) as the function of the two-pion system pseudo-rapidity $\eta_{\pi\pi}$, (b) as the function of the two-pion system rapidity $y_{\pi\pi}$ and (c) as the function of the two-pion system azimuthal angle $\phi_{\pi\pi}$. The GenEx Monte Carlo simulation was used.

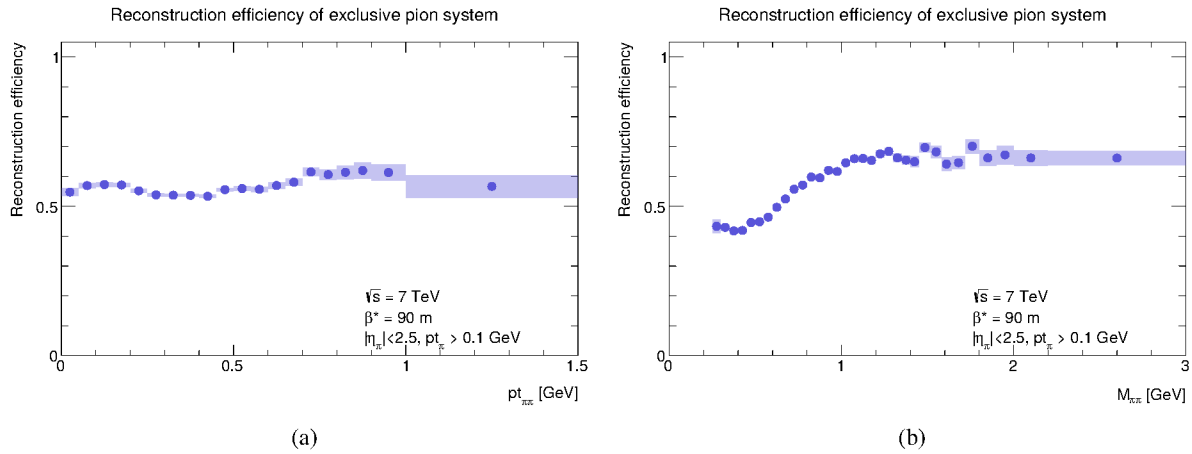

Figure 68: The overall system reconstruction efficiency as the function of (a) the transverse momentum $pt_{\pi^+\pi^-}$ and (b) the invariant mass $M_{\pi^+\pi^-}$.

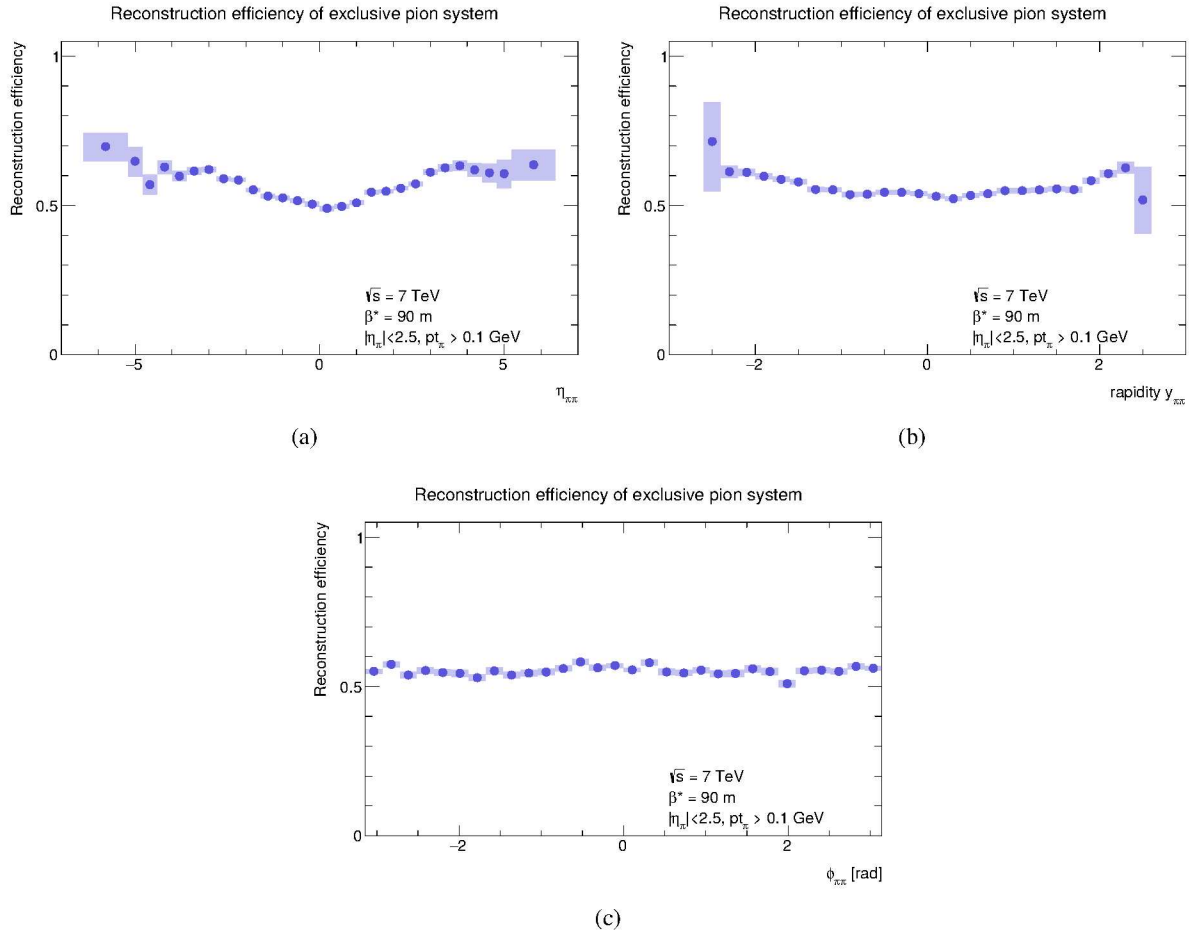

Figure 69: The overall system reconstruction efficiency as the function of (a) the pseudo-rapidity $\eta_{\pi^+\pi^-}$, (b) the rapidity $y_{\pi^+\pi^-}$ and (c) the azimuthal angle $\phi_{\pi^+\pi^-}$.

8.3. Fiducial volume

The exclusive pion analysis is calculated within a specific fiducial volume which is defined in the Sect. 7.10, applied on both the data and the MC simulation to keep them equally. The fiducial volume correction factor calculation was performed using the GenEx Monte Carlo simulation of the exclusive pion production.

The Fig. 70 shows the effect of the fiducial volume selection for the pion-pair invariant mass distribution. The events were generated by the GenEx generator. Both distributions - the distribution of a generated fiducial volume and the distribution of the selected fiducial volume - are drawn on the particle level - before any simulation of physical processes and interactions.

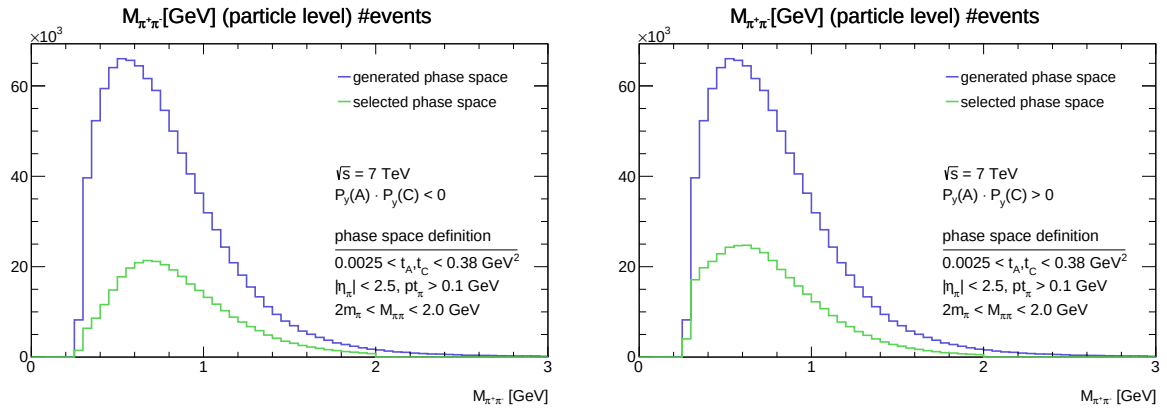

(a) (b)

Figure 70: The effect of the fiducial volume selection for the pion pair mass distribution on the particle level (a) for the elastic configuration and (b) for the anti-elastic configuration. The GenEx generator is used.

8.4. Particle identification

The particle identification correction serves to correct the final results on the imperfections of the particle identification. To find it the GenEx Monte Carlo simulation was used. A control plot describing particle identification efficiency is shown in Fig. 71 as the function of the pion pseudo-rapidity $\eta(\pi^{\pm})$. The calculation is based on the ratio between the number of events $N^{\text{pid}}_{\text{passed}}$ passed the particle identification selection and the number of events $N^{\text{pid}}_{\text{tot}}$ before this selection

$$r^{\text{pid}}_{\text{eff}} = \frac{N^{\text{pid}}_{\text{passed}}}{N^{\text{pid}}_{\text{tot}}}. \tag{35}$$

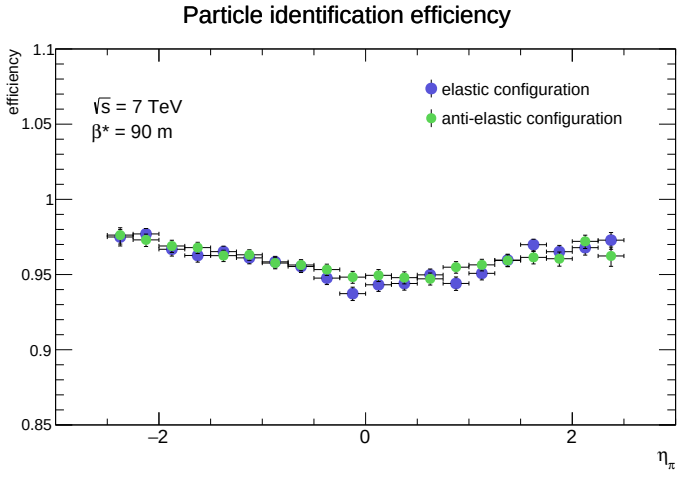

(a)

Figure 71: The particle identification efficiency as a function of the pion pseudo-rapidity $\eta(\pi^{\pm})$. The GenEx Monte Carlo simulation was used.

8.5. Unfolding

The unfolding correction presented in this sub-section has only an informative purpose due to the fact that the real unfolding is included in the overall correction.

The unfolding correction serves for the distributions shape corrections. It is based on a comparison of the distribution shape on the particle level with the distribution shape on the detector level. A simple example of the migration matrix as an input to the unfolding calculation based on the GenEx MC simulation is presented and shown in Figs. 72 and 73 - which compares the pions distributions on the particle level with the pions distributions on the detector level. The migration matrix is determined after the analysis cut flow.

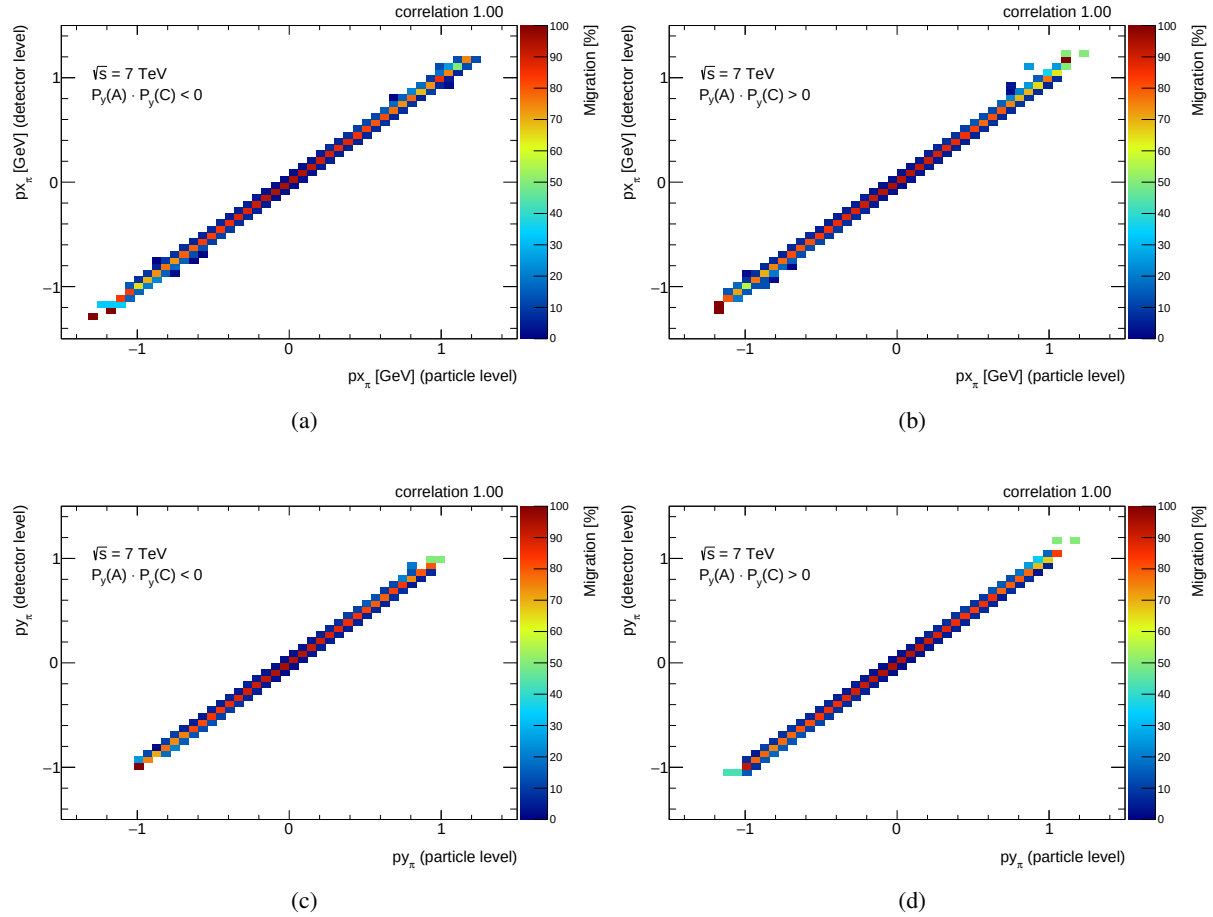

Figure 72: The migration matrix plot. The GenEx Monte Carlo simulation was used.

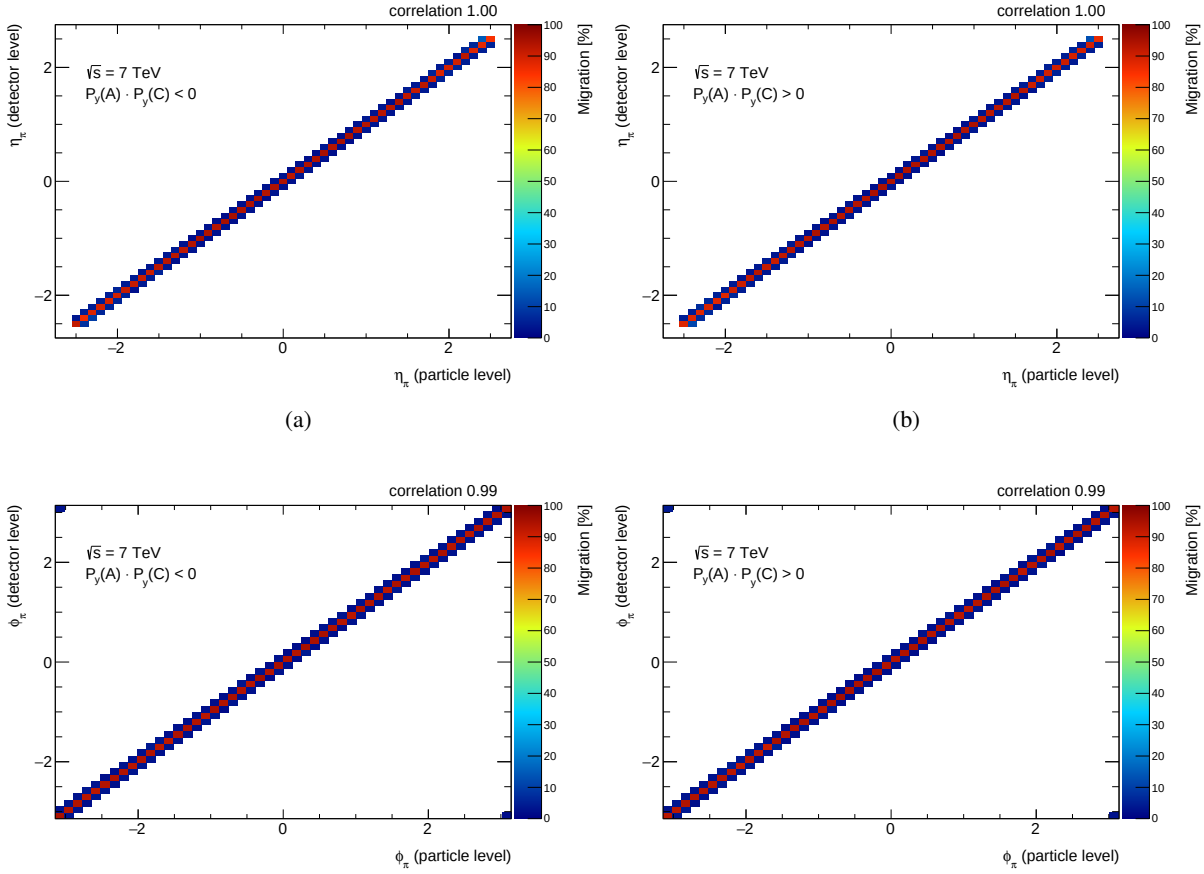

Figure 73: The migration matrix plot. The GenEx Monte Carlo simulation was used.

9. Background

Background in data has several components. To remove background first the condition on MBTS is applied. This condition removes a significant amount of the background. In mainly case of the exclusive $\pi^+\pi^-$ production it is assumed that remaining fraction of the background comes from the central diffraction processes. One of the reasons supporting this expectation is that the exclusive pion production is studied on a special low mu run ($\mu = 0.035$), so almost no pile-up is expected and we can practically neglect the coincidences of SD + beam halo, or SD + SD or beam halo + beam halo in combination with the previous reason.

The Pythia8 simulation with processes of the central diffraction is used to estimate the level of background and its subtraction. Although the Pythia8 central diffraction (a.k.a DPE - Double Pomeron Exchange) does not fully describe the exclusive $\pi^+\pi^-$ production phase space due to the lower threshold of a generated central mass in Pythia8 which is 1 GeV. So the main fraction of the exclusive $\pi^+\pi^-$ production can lie under this threshold. Nevertheless, it is still possible to estimate the background fraction. The exclusive pion pair events were removed from the Pythia8 MC simulation on particle level[7] and thus only the central diffraction events without them are used in the background subtraction. The full analysis chain is applied on such MC sample. A number of events N_{bckg} which passed the analysis chain are counted as the background events. This number is later used to subtract them from the number of the events N_{data} which passed the analysis chain for data. After the background events subtraction defined by Eq. 36 the rest of the events N_{sig} from the data is counted as the exclusive events. Finally the overall corrections are applied on the signal events to calculate the cross-section of the exclusive pion production:

$$N_{\text{sig}} = N_{\text{data}} - N_{\text{bckg}}. \tag{36}$$

Still, the situation is more complex. A normalisation of MC sample to data has to be made. There are two ways of the background normalisation, using opposite-sign or same-sign events. The ideal behind is simple: let us consider several kind of processes, $p+p \to p+p+\pi^+ +\pi^-$, $p+p \to p+p+\pi^+ +\pi^- +\pi^+ +\pi^-$ which can be studied using the same-sign events and $p + p \to p + p + \pi^+ + \pi^- + \pi^0$ which contributes into opposite-sign events.

In total four methods for normalization of MC to data are considered. The normalisation process is performed before the $\sum p_y$ kinematic selection (but after the condition on MBTS, particle identification and fiducial volume selection). The signal region is defined by $3.5\,\sigma(\sum p_{\text{y}})$ cut, see Fig. 74.

The first method of the normalisation uses same-sign events in both data and Pythia8 CD non-excl sample outside the signal region. A number of events in data $N_{\text{bckg}}^{\text{data-ls}}$, resp. in Pythia8 CD non-excl. sample $N_{\text{bckg}}^{\text{Pythia8CD-ls}}$, outside a signal region is determined. Then the normalisation factor $r_{\text{bckg}}^{\text{same-sign-osr}}$ calculation is defined as

$$r_{\text{bckg}}^{\text{same-sign-osr}} = \frac{N_{\text{bckg}}^{\text{data}}}{N_{\text{bckg}}^{\text{Pythia8CD}}}. \tag{37}$$

[7] The removing of the events on particle level means to remove MC truth (or generated) events from the sample before any sample analysis

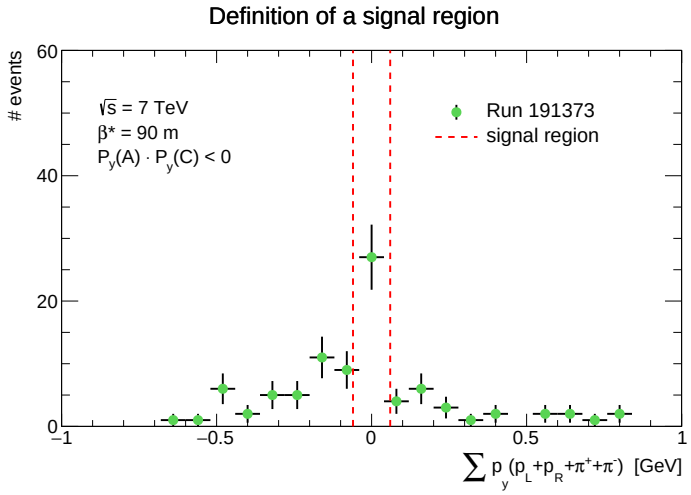

Figure 74: A definition of a signal region for a $3.5\,\sigma(\sum p_y)$ cut interval.

The second method of the normalisation uses same-sign events in both data and PYTHIA8 CD non-excl sample in the full kinematic range (so it covers signal and outside-a-signal regions). A number of events in data $N_{\text{bckg}}^{\text{data}}$, resp. in PYTHIA8 CD non-excl. sample $N_{\text{bckg}}^{\text{Pythia8CD}}$, in a given region. The normalisation factor $r_{\text{bckg}}^{\text{same-sign}}$ is defined as

$$r_{\text{bckg}}^{\text{same-sign}} = \frac{N_{\text{bckg}}^{\text{data}}}{N_{\text{bckg}}^{\text{Pythia8CD}}}. \tag{38}$$

The third method of the normalisation uses opposite-sign events in both data and PYTHIA8 CD non-excl sample outside the signal region. A number of events in data $N_{\text{bckg}}^{\text{data-os}}$, resp. in PYTHIA8 CD non-excl. sample $N_{\text{bckg}}^{\text{Pythia8CD-os}}$, in a given region. The normalisation factor $r_{\text{bckg}}^{\text{oppo-sign-osr}}$ is defined as

$$r_{\text{bckg}}^{\text{oppo-sign-osr}} = \frac{N_{\text{bckg}}^{\text{data-os}}}{N_{\text{bckg}}^{\text{Pythia8CD-os}}}. \tag{39}$$

The Table 18 summarises calculated factors of the four PYTHIA8 central diffraction non-exclusive simulation normalisations. The results are comparable within their statistical errors. From this comparison one would suggest to use any of these methods to use it for a background subtraction in data.

Table 18: The factors for the PYTHIA8 CD non-excl. sample normalisation on data for three studied cases.

type of normalisation		**ratio**
same-sign events outside the signal region	$r_{\text{bckg}}^{\text{same-sign-osr}}$	$0.2500 \pm 0.0625^{(\text{stat})}$
same-sign events in the full region	$r_{\text{bckg}}^{\text{same-sign}}$	$0.2366 \pm 0.0561^{(\text{stat})}$
opposite-sign events outside the signal region	$r_{\text{bckg}}^{\text{oppo-sign-osr}}$	$0.2509 \pm 0.0338^{(\text{stat})}$
opposite-sign events in the full region	$r_{\text{bckg}}^{\text{oppo-sign}}$	$0.2613 \pm 0.0779^{(\text{stat})}$

The calculated factor for the method using the opposite-sign events outside the signal region was used and the normalized distributions of the PYTHIA8 central diffraction simulation with non-exclusive pion events were compared with the data distributions, see Fig. 75a for the opposite-sign events outside the signal region and the Fig. 75b for the same-sign events outside the signal region. PYTHIA8 describes the data outside of the signal region within the statistical uncertainty, the result is influenced by the low data statistics.

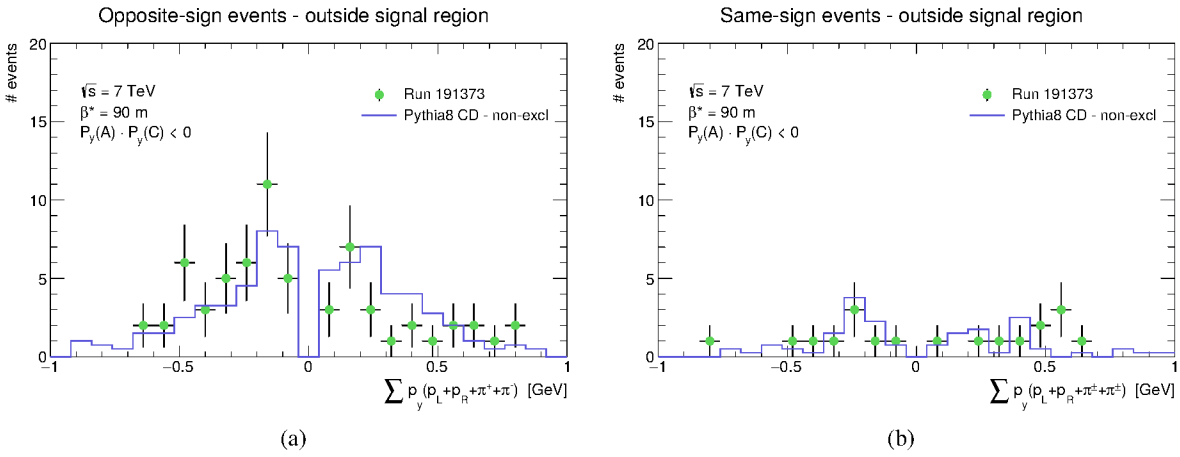

(a) (b)

Figure 75: The comparison of the normalised PYTHIA8 CD non-excl. sample distribution outside of the signal region with the same distribution in data, (a) for the opposite-sign events and (b) for the same-sign events.

The same comparison was done also for the region including a signal region, again for the method based on the opposite-sign events normalization. The results are shown in Fig. 76, for the opposite-sign events on Fig. 76a as well as for the same-sign events on Fig. 76b.

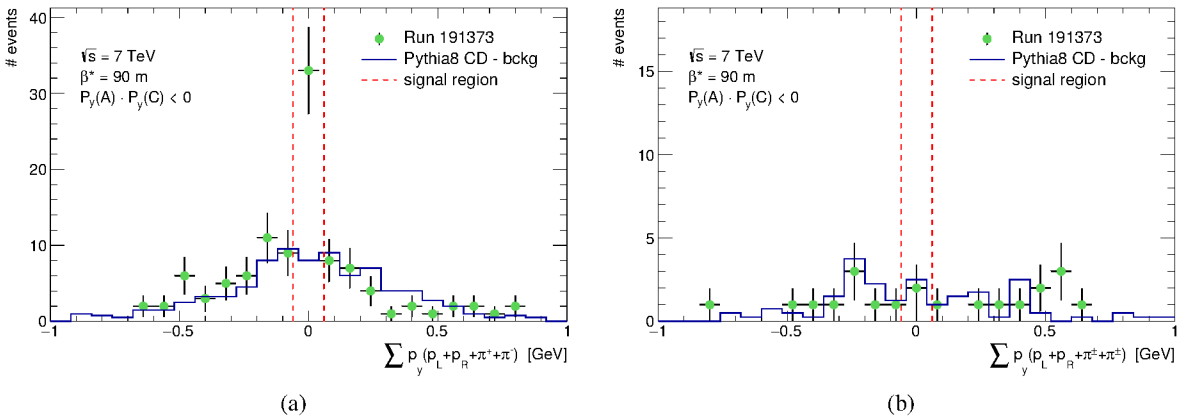

(a) (b)

Figure 76: A comparison of the normalised PYTHIA8 central diffraction simulation with non-exclusive pion distribution for the opposite-sign events in the full region with the same distribution in data, (a) for the normalisation using opposite-sign events and (b) for the normalisation using same-sign events.

As two background normalization methods use only the events outside the signal region, a closure test was performed to check the signal contamination in that region. The aim was to avoid a potential contamination

of the exclusive pion pair events from the PYTHIA8 central diffraction outside of the exclusive pion signal, and thus to avoid a biased background normalization.

First, the sample of the events with the opposite-sign pion pairs was studied. The fraction of the exclusive events outside of the signal region is negligible in comparison with the fraction of the non-exclusive pion events, Fig. 77a. Expected behaviour within the signal region is shown in the Fig. 77b where a high fraction of non-exclusive pion fraction contaminates the signal itself.

Second, the sample of the events with the same-sign pion pairs which passed the exclusive pion selection cut was studied. In this case no non-exclusive event as well as no exclusive events survive the selection therefore at least it can be said that our PYTHIA8 simulation does not include any exclusive pion events masked as the same-sign pion pairs which would contribute to the background estimation.

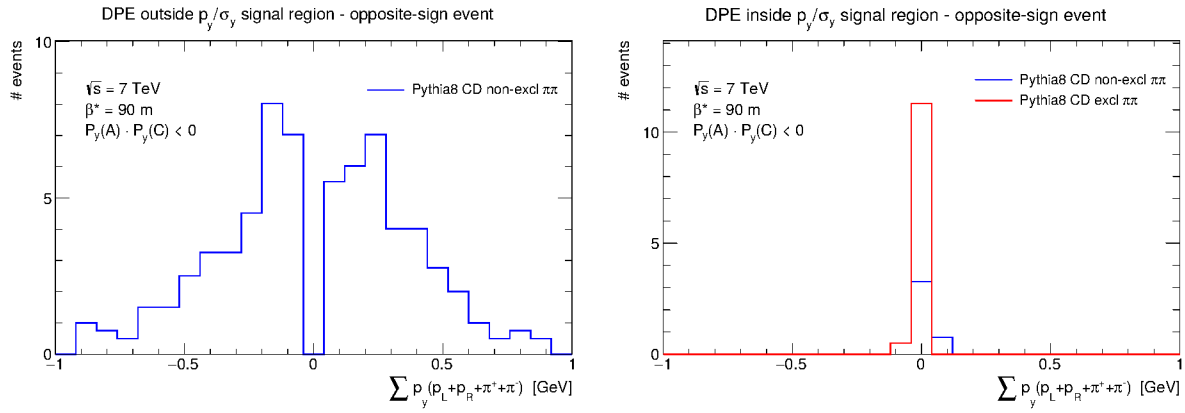

(a) (b)

Figure 77: A comparison of the exclusive pion process to the non-exclusive pion processes from the PYTHIA8 central diffraction MC simulation, (a) for the events outside the exclusive region and (b) for the events inside the exclusive region.

The fourth method of the background estimation study the opposite-sign events coming out of the opposite-sign method outside the signal region. The full region is used and it counts not only with a background but also with a signal fraction. It is based on the fit of data distribution with the signal fraction (MC GENEX simulation) and with the background fraction (PYTHIA8 simulation of the central diffraction stripped off exclusive pion pair events). A class from the ROOT framework called "TFractionFitter" is used to perform the fit. The fit returns an estimated probability of the signal and the background fraction of MC simulation in data distribution. The probability is used for calculation of the normalization factor of the background fraction using Eq. 40:

$$r_{\text{bckg}}^{\text{fit}} = \frac{I^{\text{data}} P(\text{bckg})}{I^{\text{Pythia8CD}}}, \tag{40}$$

where I^{data} is an integral of the data distribution, $I^{\text{Pythia8CD}}$ is an integral of the MC PYTHIA8 non-exclusive distribution and $P(\text{bckg})$ is the estimated probability of the background fraction in data distribution.

Finally the background fraction is scaled and the number of events which represents the background fraction in data is obtained. A visualised fit of the data distribution is shown in Fig. 78a whereas the data

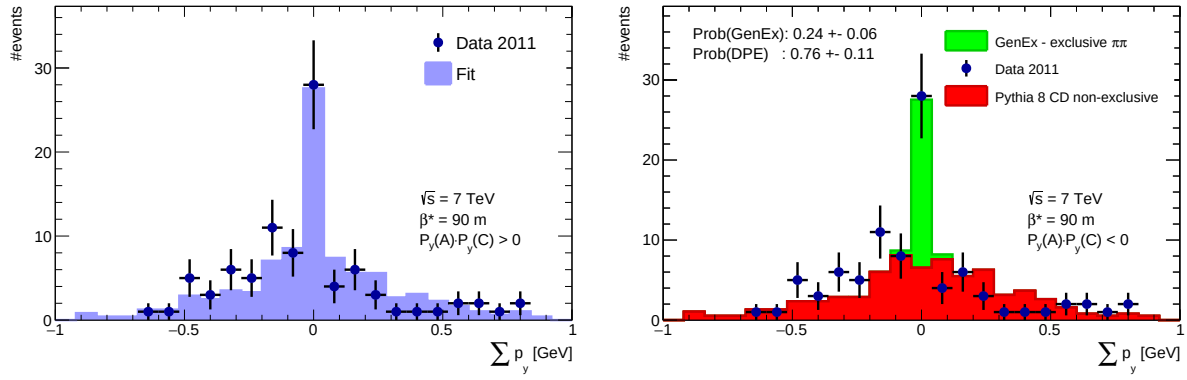

(a) (b)

Figure 78: Data distribution fit by MC simulation, using GenEx as a signal fraction and Pythia8 central diffraction without exclusive pion process as the background fraction, (a) for the overall fit and (b) with MC fractions. The MC histograms are stacked.

distribution together with MC signal (GenEx) and MC background (Pythia8 CD non-excl.) is shown in Fig. 78b.

A closure test of the background subtraction was performed for the background subtraction based on the result from ROOT class "TFractionFitter" for a various signal regions. The size of the signal region of p_y/σ_{p_y} was changed from 0.5 to 8.0 where the p_x/σ_{p_x} was fixed to 3.5 which is a default value of the kinematic selection, see Sect. 7.8. The test was performed for data from elastic configuration. The background and the signal fractions in each p_y/σ_{p_y} signal region were normalized with the same normalization factor.

The result of the closure test of the background subtraction is shown in Fig. 79. The figure compares the data before the background subtraction (the green points) with the MC simulation prediction (the black points) - the sum of the signal and the background fractions. A good agreement was achieved. The same behaviour is observed also in case of comparison of data distribution after the background subtraction (the cyan points) - which should contain only a signal - and the MC simulation with the signal fraction (the blue points). The cross-section of the exclusive pion production after the background subtraction for the elastic configuration from 2.5 to 8.0 of p_y/σ_{p_y} value alternates about the expected value given by the GenEx MC simulation.

It suggests that our assumption about background compensation was correct and applicable on our study. The behaviour of the data distribution after the background subtraction for the signal intervals defined from 0.5 to 2.0 of p_y/σ_{p_y} can be explained in at least two ways. The first is the effect of the ALFA detector resolution implemented in the MC simulation which does not fully describe the resolution seen in the data. The second one may be an effect of a very low statistics of the exclusive pion events in data.

The signal regions from 0.5 to 3.5 of p_y/σ_{p_y} are drawn to see the number of events propagation, together with the table of data events (before the background subtraction) together with numbers of accepted events. The table shows also the effect of the ALFA detector resolution implemented in the MC simulation which causes events migrations between the p_y/σ_{p_y} intervals. This is a problem of a very low signal intervals.

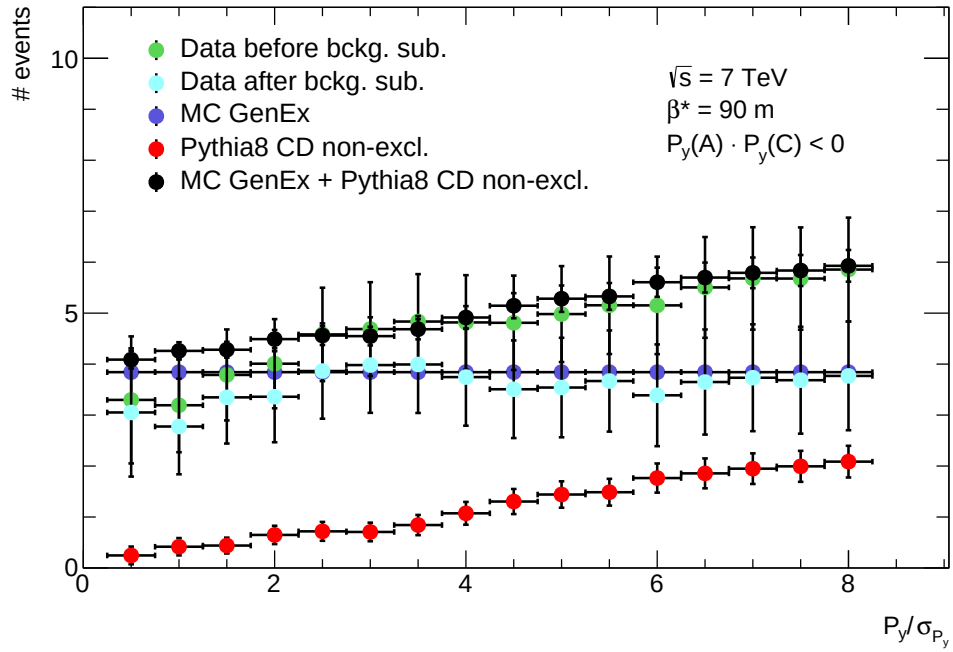

Figure 79: An effect of the background subtraction in data for various p_y/σ_{p_y} signal regions. A normalization from ROOT TFractionFitter is used for the signal and the background in each p_y/σ_{p_y}.

Around the default $3.5 p_y/\sigma_{p_y}$ signal interval, the situation is stable and therefore the effect described above does not have such big impact on the final analysis result.

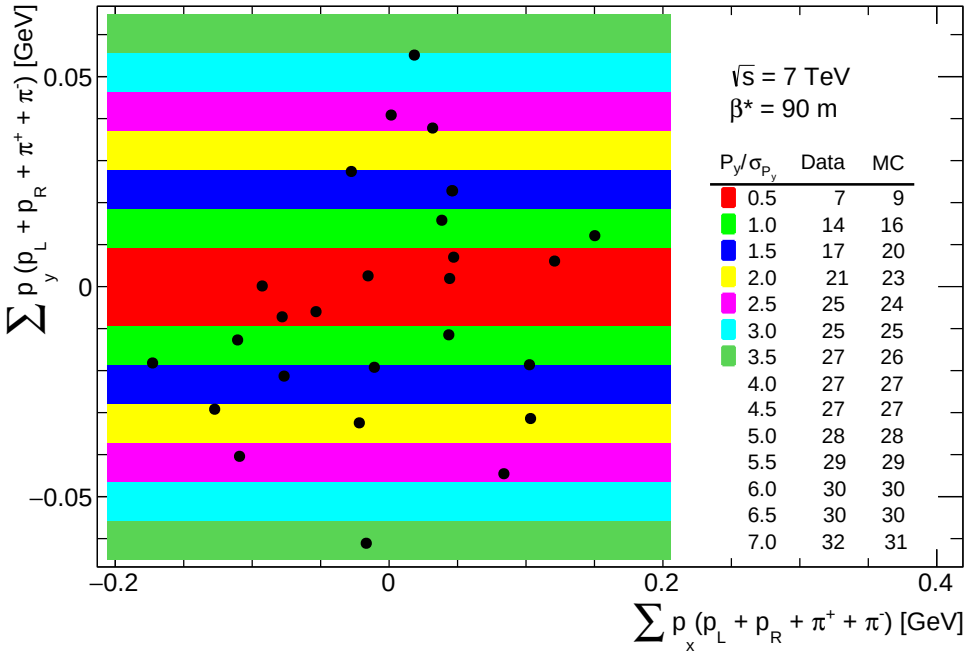

Figure 80: The event distribution of data for various signal region intervals, from 0.5σ to 3.5σ interval, before background subtraction. The table shows the comparison of real data number of events with the number expected from MC ones, in the selected p_y/σ_{p_y} interval.

An effect of narrow and independent cuts p_x/p_y may not be convincing. The elliptical kinematic cut taking in account $p_x p_y$ shows better behaviour then the previous narrow kinematic cut. In the elliptical cut the signal region for both the p_y and p_x distributions of the exclusive system elastic is defined with the same $p_{x,y}/\sigma_{p_{x,y}}$ value whereas the previous kinematic cut was fixed in p_x to $3.5\, p_{x,y}/\sigma_{p_{x,y}}$. The closure test for the elliptical cut was performed with the recalculated settings of the all event selection as well as for the recalculated corrections, for all considered $p_{x,y}/\sigma_{p_{x,y}}$ signal regions. The results are summarized in Fig. 81 where the closure test for various signal regions is shown in Fig. 81a and the events propagation in the kinematic region is shown in Fig. 81b.

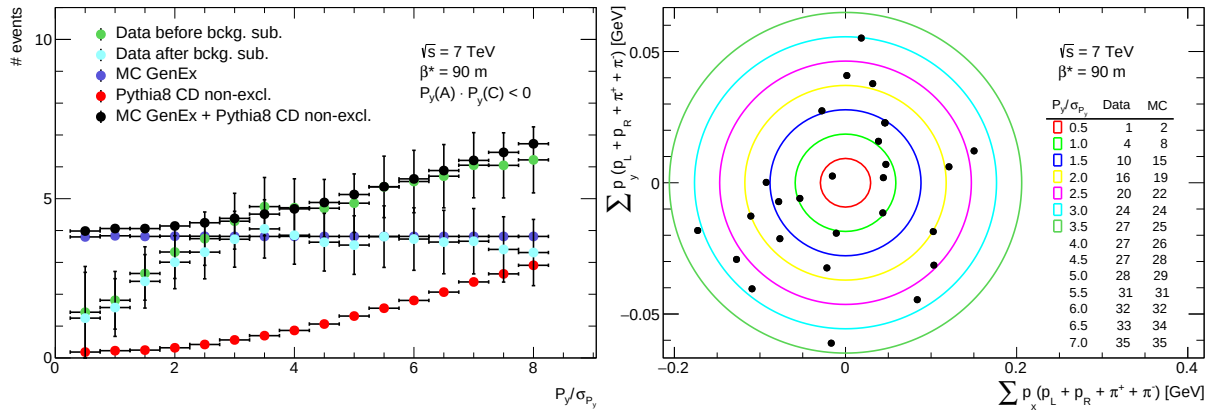

(a) (b)

Figure 81: (a) An effect of the background subtraction in data for various p_y/σ_{p_y} signal regions. A normalization from ROOT TFractionFitter is used for the signal and the background in each p_y/σ_{p_y}. (b) The event distribution of data for various signal region intervals, from 0.5σ to 3.5σ interval, before background subtraction. A simple table shows the real number of events with the expected ones for a selected p_y/σ_{p_y} interval.

The background study results are summarised in Table 19.

Table 19: An estimated fraction of a background in data

	Data		**Background**	
type of normalisation	**elastic**	**anti-elastic**	**elastic**	**anti-elastic**
same-sign events outside the signal region	27	3	4.5	0.4
same-sign events in the full region	27	3	4.3	0.4
opposite-sign events outside the signal region	27	3	4.5	0.3
TFractionFitter	27	3	4.7	0.3

There is another test to compare four methods, based on a variation of a size of the signal region by changing a value of p_y/σ_{p_y}. The p_y kinematic selection is defined in Sect. 7.8. The test was done only for the elastic configuration, as for the anti-elastic configuration the statistics is too low. A default value of the p_y/σ_{p_y} for the analysis is 3.5. The size of the signal region of p_y/σ_{p_y} was changed from 0.5 to 8.0.

For each value of p_y/σ_{p_y} the new overall correction factor was calculated. The result of this test is shown in the Fig. 82. In the ideal situation when sample contains just signal, one expect a flat distribution independently of the p_y/σ_{p_y} value. But the data before the background subtraction (represented by the

green points in Fig. 82) are characterised by the increasing value of the cross-section. The background in the selected sample increases with an increase of the p_y/σ_{p_y} value. After applying the background subtraction it is expected that such corrected data distribution would be almost flat. Within the statistical uncertainty all the background subtraction methods return similar results. This behaviour is supported by another closure test in Fig. 79 where a good agreement between the data after the background subtraction and the MC signal, represented by the GenEx, is visible. We can see that all methods estimate practically the same amount of the background and therefore they are almost identical.

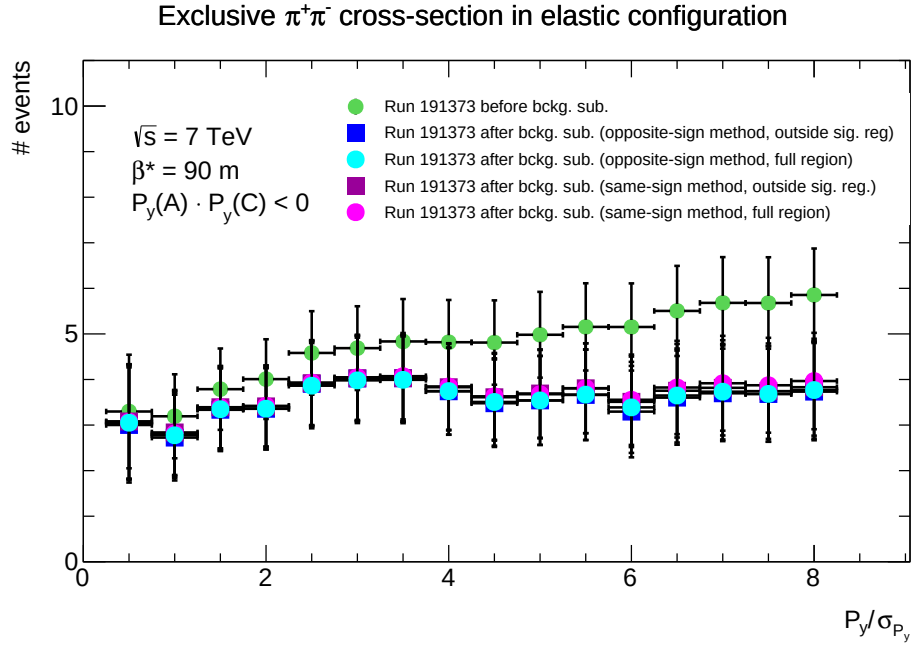

Figure 82: A background subtraction evolution as the function of p_y/σ_{p_y} ratio signal region for the elastic configuration of data and the Pythia8 CD non-exclusive sample. The blue graph represents data before background subtraction. The last three graphs represent the data after background subtraction, in cyan graph for a background normalisation using same-sign events in full region, in green graph for a background normalisation using same-sign events outside the signal region and in magenta graph for a background normalisation using opposite-sign events outside the signal region.

9.1. Accidental coincidences

The other source of the background may come from the accidental coincidences of tagged protons in the ALFA detectors and tagged pions in the Inner detector which do not origin in the same pp interaction, i.e. the protons come from the halo events. The idea of the background from these accidentals is supported by the distribution of the MBTS inner cells with a signal, shown on Fig. 83. We expect that the activity in the inner cells of the MBTS is very low (i.e. up to 2 cells with signal) for the exclusive pion process and low for other diffractive processes (i.e. up to 6) which are used as the other background source (described above in this section).

The rest of the distribution (approx. above 6 cells with signal) is not well described with mentioned processes. It was found that this fraction of the distribution can be described by the accidental coincidences

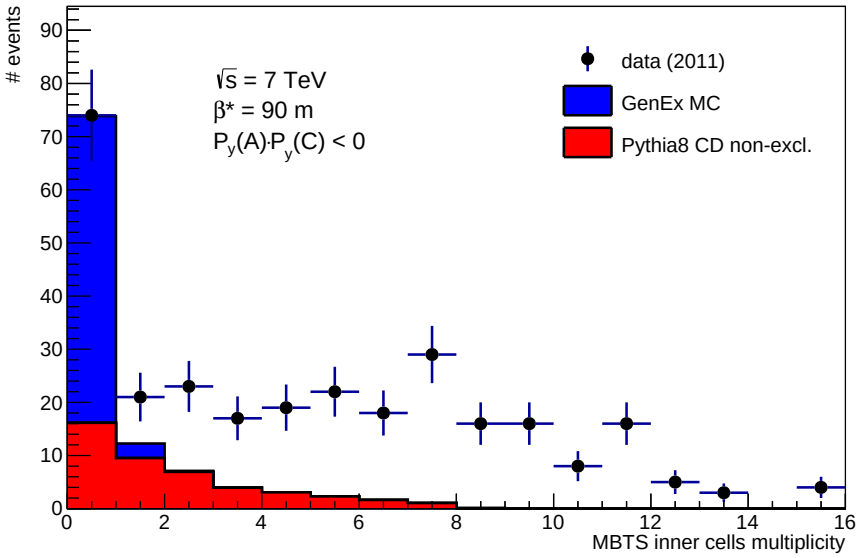

Figure 83: The multiplicity of the MBTS inner cells comparing data with MC signal simulation (GenEx) and MC background simulation (Pythia8 CD) after the analysis selection cut flow, except the kinematic selection.

of events related only to the activity in the ALFA detectors and the events related only to the Inner detector. So two independent sets of events were prepared.

The first set of events was related to the activity in the ALFA detectors. We applied the cuts on data pre-selection from Sects. 7.1 and 7.2 and the cuts on ALFA track selection from Sect. 7.5. We did veto on the number of reconstructed tracks in Inner detector and veto on MBTS activity in the inner cells.

The second set of events was related to only for the activity in the Inner detector. We selected the events with the same RF bucket 1 (BCID 1) like in the first set of events and also selected events with a random trigger on level 1 (L1_RD0_FILLED). We did a veto on any activity in ALFA detectors nor on trigger level neither on track reconstruction level and did not vetoing on MBTS activity. The tracks from the inner detector were selected using the cuts described in Sects. 7.3 and 7.4.

We took these two sets of events and randomly merged the events from the first set with the events from the second set to obtain the events mimicking the exclusive pion event. Then the rest of the standard analysis selection criteria were applied defined in Sect. 7, expect the kinematic selection described in Sect. 7.8. First we looked on a multiplicity of MBTS inner cells to know whether the accidental events describing the fraction of higher multiplicities seen in data. The accidental events were normalized to data in the range of the multiplicity from 6 to 16. The Fig. 84 shows the results. The events from the accidental coincidences describe the fraction of high multiplicities. It is also seen that there is some fraction in very low multiplicities which could show on a potential source of the background. So we continued and applied the kinematic selection on that events. And the result is that in our case of the data for the exclusive pion analysis coming from the 7 TeV ATLAS run no event passed the last selection. This result thus show that no contamination from the accidental coincidences was found in the events after the analysis event selection.

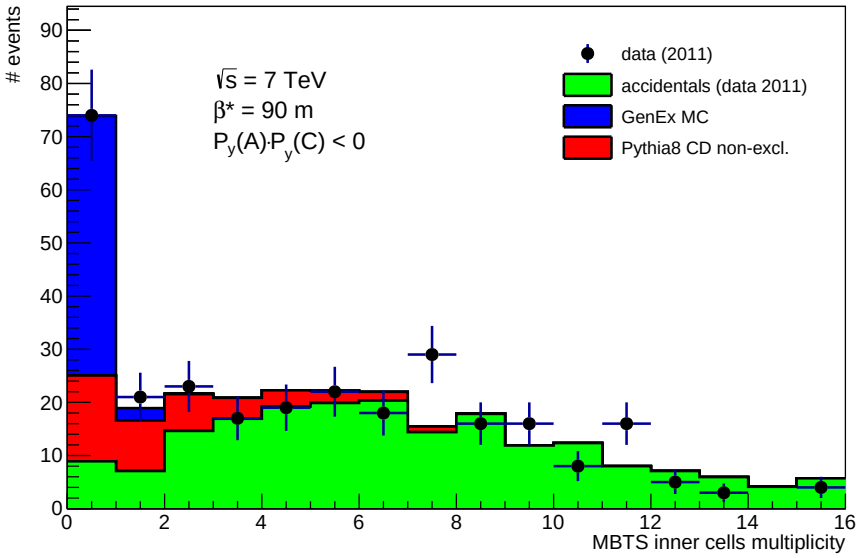

Figure 84: The multiplicity of the MBTS inner cells comparing data with accidental coincidences, MC signal simulation (GenEx) and MC background simulation (Pythia8 CD) after the analysis selection cut flow, except the kinematic selection.

9.2. Background summary

According to the results of a background study we can say that in our case of the exclusive pion analysis at 7 TeV the background fraction is well described by the central diffractive processes - simulated by the Pythia8- and especially by the method of the opposite-sign normalization using the TFractionFitter from ROOT framework. We disprove that accidental events would contribute to the background (primary as the main source) of this analysis.

10. Data analysis

Let us summarise the effect of pre-selection steps on the number of events. The corresponding statistics is written in the Table 20 and covers both the elastic and the anti-elastic configurations.

Table 20: The data cut flow statistics for both the elastic and the anti-elastic configurations.

Run 191373	**Number of events**	
	Elastic configuration	**Anti-elastic configuration**
Total number of events	6620953	
BCID	1898901	
Trigger pre-selection	1155523	413096
Good lumi-blocks	1106855	397683

The next two event selections are based on the number of expected exclusive products. The condition of two good tracks with the opposite sign is applied on data from the ATLAS ID whereas the condition of two reconstructed protons each on one ATLAS side is applied on information from the ALFA detectors. These condition are described in detail in Sects. 7.4 and 7.5. The next event selection focuses on the background events. For this purpose the information from the MBTS is used. How the MBTS event selection works is described in Sect. 7.6. The next set of the event selection criteria is based on the geometrical and kinematic properties of the exclusive system. These selections are described in Sects. 7.7–7.8. They are tuned accordingly by the results from the GenEx Monte Carlo simulation.

The complete data cut flow is summarised in Table 21, the table includes statistics for both the ALFA Reco and Lattice method proton kinematics reconstruction (Sect. 6.2). It also compares the two configurations, the elastic and the anti-elastic ones. Only few events survived the chain, for the elastic configuration there are 27 events whereas for the anti-elastic configuration are only 3 events when lattice method was used. High statistical error is expected due to the low statistics. The analysis is split into two configurations, as for the anti-elastic configuration the trigger pre-scale is 15 (so quite high).

Table 21: The data cut flow statistics for both proton kinematics reconstruction cases, the ALFA Reco method and the Lattice method.

GenEx	configuration			
	elastic		anti-elastic	
	Lattice method	ALFA Reco method	Lattice method	ALFA Reco method
Data Quality & Trigger pre-selection	1106855		397683	
ID selection	1505		1099	
ALFA track selection	485	484	11	11
MBTS veto	138	137	5	5
ALFA geometry selection	112	112	5	5
Kinematic cut $\sum p_y$	42	42	3	3
Kinematic cut $\sum p_x$	34	39	3	3
Particle identification ($M_{dE/dx}$)	31	36	3	3
Kinematic region cut	27	31	3	3

Although the statistics is quite low, an estimation on a visible cross-section of the exclusive pion production at $\sqrt{s} = 7$ TeV was calculated. The results of the exclusive pion cross-section are written further in the text in Sect. 10.4. Before the final results let us focus on some shape distribution comparison and momentum balance distributions.

10.1. Shape distribution comparison

The aim of this section is to show an agreement between the basic distributions made of the data and the Monte Carlo simulations. The overall corrections which is described in Sect. 8 and is used to correct the final distributions is based on that agreement. In case of big differences and without their clear understanding the overall correction calculation would not be used.

Ten distributions in total were used, the p_x and p_y of the reconstructed tracks, the p_x and p_y of the reconstructed protons and the $\phi_{\pi^+\pi^-}$, $\theta_{\pi^+\pi^-}$, $\eta_{\pi^+\pi^-}$, $y_{\pi^+\pi^-}$, $p_{t(\pi^+\pi^-)}$ and $M_{\pi^+\pi^-}$ of the reconstructed central system formed by two reconstructed tracks with an opposite sign. The comparison among data and GenEx Monte Carlo simulation was made.

In the case of the anti-elastic configuration there are only few events. It does not make a sense to plot any bin-by-bin distributions for such low statistics. Therefore only distributions for the elastic configuration are considered, although also for this configuration a limitation in the number of bins of the distributions is visible.

A set of control distributions is shown in Figs. 85–89. These distributions are filled by the events collected before the kinematics event selection to avoid a bias by the artificial cuts. Within the statistical errors in data the shape distributions are comparable between data and the GenEx MC simulation.

The distributions in Fig. 85 compare the tracks kinematics of p_x and p_y reconstructed by the ATLAS ID. The black point of represents the data whereas the blue histogram represents the GenEx MC simulation.

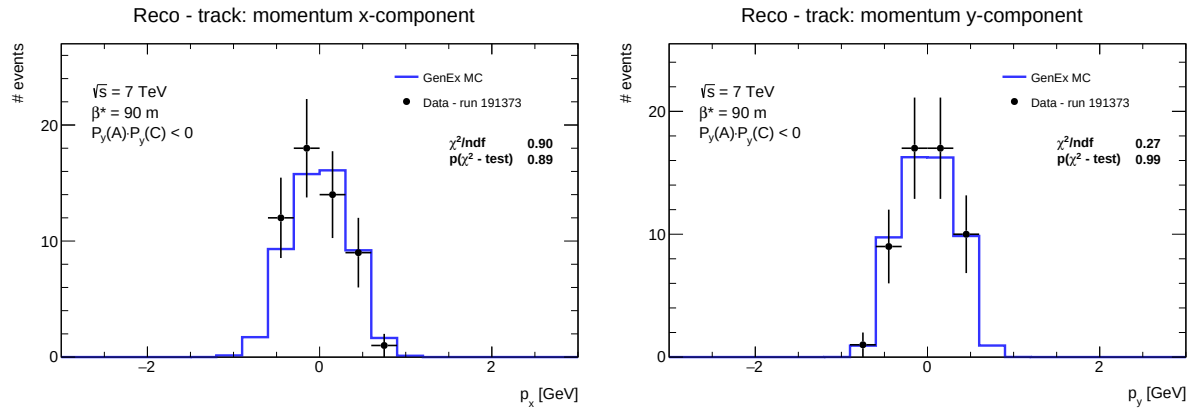

(a) (b)

Figure 85: Distributions of (a) p_x and (b) p_y momentum components of the track reconstructed in the ATLAS ID. Both the data and the GenEx Monte Carlo simulations are drawn.

The distributions in Fig. 86 compare the proton kinematics of p_x and p_y reconstructed by the ALFA detectors using the Lattice method algorithm. A visible space around zero in the proton p_y distribution comes from the geometrical acceptance of the ALFA detectors in the vertical axis; ALFA detector were positioned about 6 mm from the centre of the beam. There is also a difference in the binning between the p_x and p_y distributions. The finer binning in the case of the p_y distribution is caused by a better resolution for this kinematics variable. The black points represent the data whereas the blue histogram represents the GenEx MC simulation.

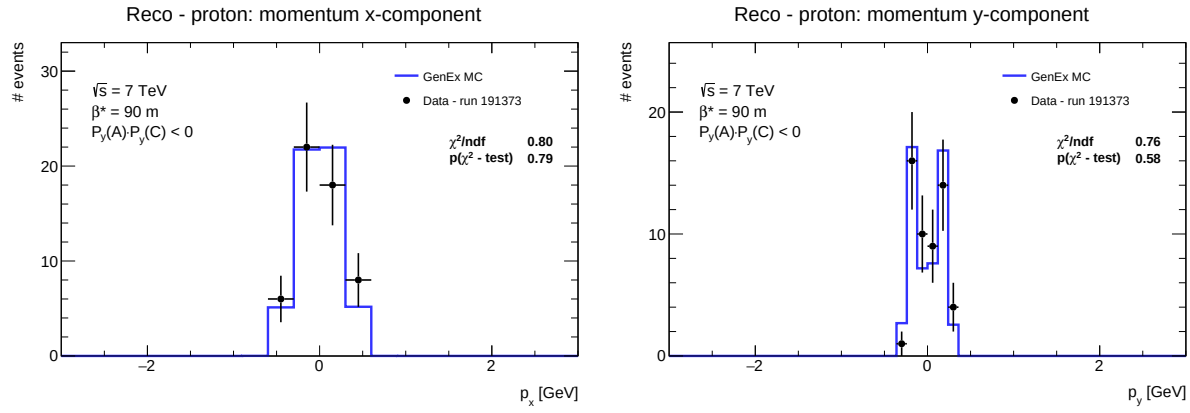

(a) (b)

Figure 86: Distribution of (a) p_x and (b) p_y components of the proton reconstructed in the ALFA detectors. Both the data and the GenEx Monte Carlo simulations are shown.

The distributions in Fig. 87 compare the central system azimuth angle $\phi_{\pi^+\pi^-}$ and the polar angle $\theta_{\pi^+\pi^-}$. The black points represent the data whereas the blue histogram represents the GenEx MC simulation.

The distributions in Fig. 88 compare the central system pseudo-rapidity $\eta_{\pi^+\pi^-}$ and the rapidity $y_{\pi^+\pi^-}$. The centrality of the exclusive system is well visible. The black point of represents the data whereas the blue histogram represents the GenEx MC simulation.

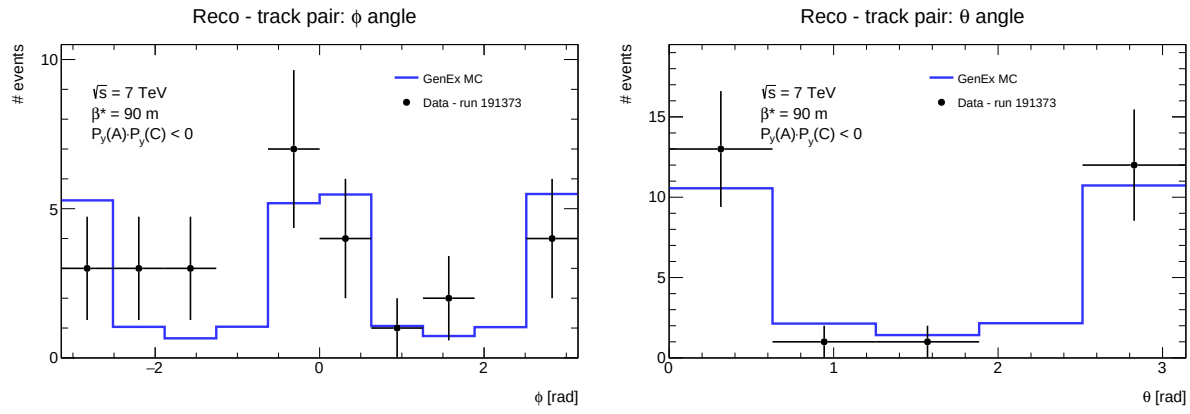

(a) (b)

Figure 87: Distribution of (a) $\phi_{\pi^+\pi^-}$ and (b) $\theta_{\pi^+\pi^-}$ of the track pair reconstructed in the ATLAS ID. Both the data and the GenEx Monte Carlo simulations are shown.

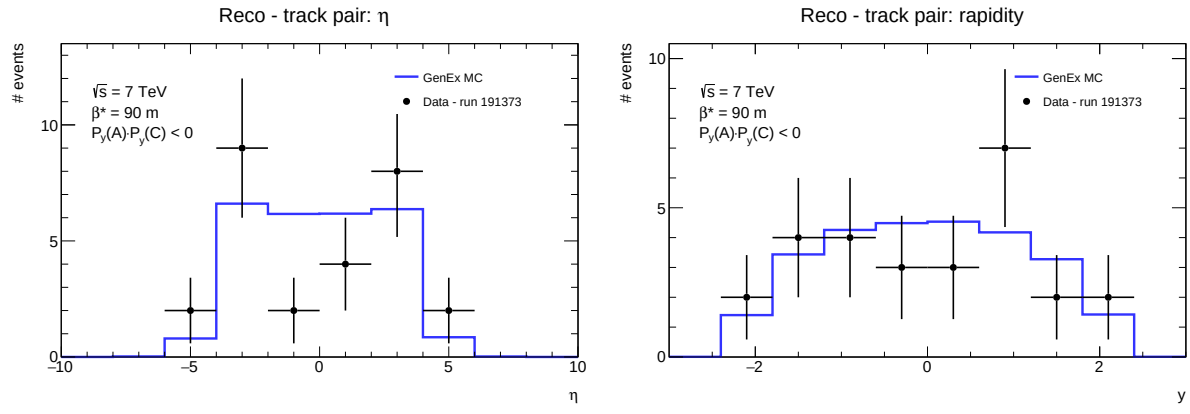

(a) (b)

Figure 88: Distribution of (a) $\eta_{\pi^+\pi^-}$ and (b) $y_{\pi^+\pi^-}$ of the track pair reconstructed in the ATLAS ID. Both the data and the GenEx Monte Carlo simulations are shown.

The distributions in Fig. 89 compare the central system transverse momentum $p_{T_{\pi^+\pi^-}}$ and the invariant mass $\theta_{\pi^+\pi^-}$. The mass of central system is bellow 2 GeV. The black points represent the data whereas the blue histogram represents the GenEx MC simulation.

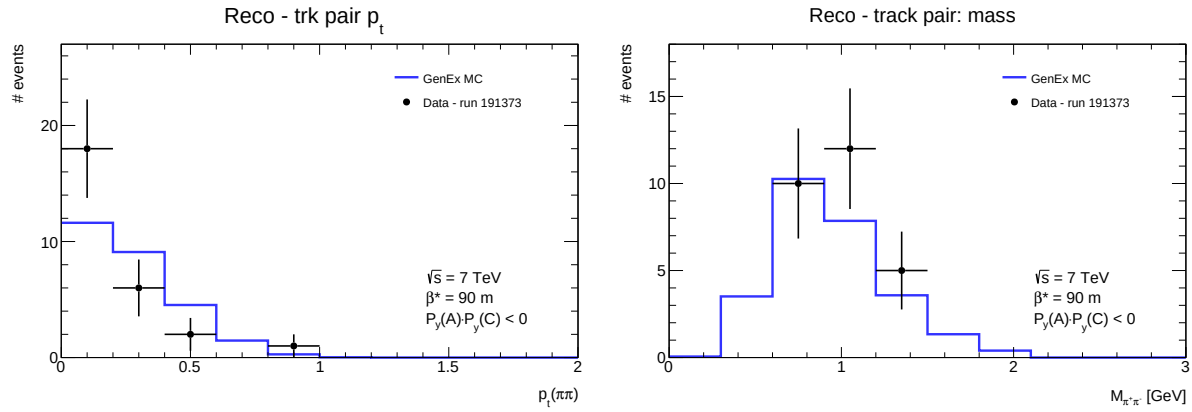

(a) (b)

Figure 89: Distribution of (a) $p_{t(\pi^+\pi^-)}$ and (b) $M_{\pi^+\pi^-}$ of the track pair reconstructed in the ATLAS ID. Both the data and the GenEx Monte Carlo simulations are shown.

10.2. Exclusive pion momentum balance distributions

The shape of the momentum balance of the exclusive pion system is considered were only the x and y components of the products momentum are used due to an insufficient proton kinematic reconstruction in the p_z and the E momentum components as was explained in Sect. 6.2. Due to the low statistics in the case of the anti-elastic configuration, only the distributions for the elastic configuration of the analysis are considered here.

The $\sum p_x$ and $\sum p_y$ distributions are shown in Fig. 90. The black points represent the data whereas the blue histogram represents the GenEx MS simulation and the red histogram represents the Pythia8 MC simulation. The distributions contain events before the kinematics selections on $\sum p_y$ and $\sum p_x$ to see their full ranges. In the case of the GenEx MC simulation (only signal) a clear peak around the zero value is well visible and tells that the system is balanced and we can define the signal region, see Fig. 74. In the case of data the peak is accompanied tails on both sides outside the signal region. We assume that the tails in data outside the signal region contain only the non-exclusive events. To understand the tails in data one can look on the Pythia8 Monte Carlo simulation of the central diffraction processes which are a dominant background processes for the exclusive pion production. A comparison of the data with the Pythia8 Monte Carlo simulation shows a quite good agreement of the distributions shape in both the central peak and the tails. This agreement is used also in the background subtraction process.

The shape comparison of the p_x and the p_y momentum components is shown in Fig. 91 also for the events which passed the full analysis cut flow. Within the statistical uncertainties the data based distributions are comparable with the MC ones.

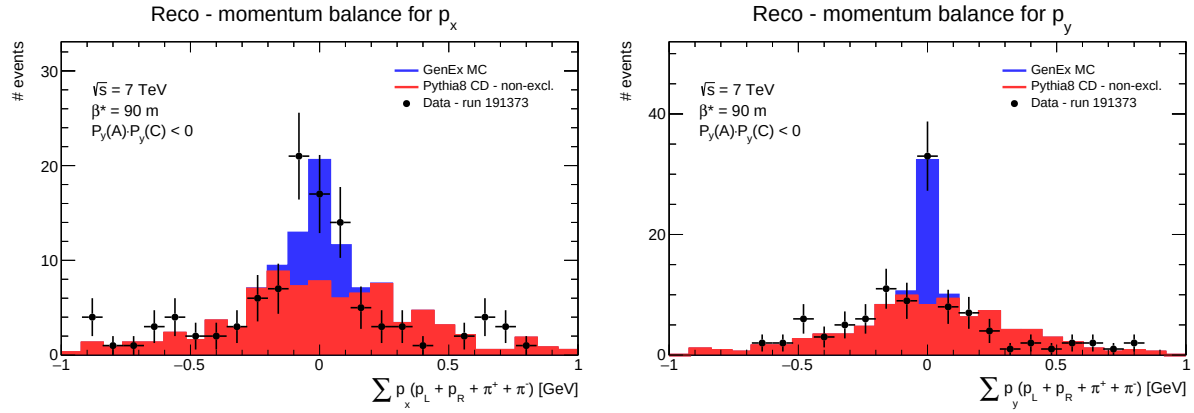

(a) (b)

Figure 90: The momentum balance distributions for the p_x and p_x components of the exclusive central system. The blue histograms represent the GenEx MC simulation, the red histograms represent the Pythia8 central diffraction MC simulation and the black distribution shows data. The event selection before the momentum balance cut is applied.

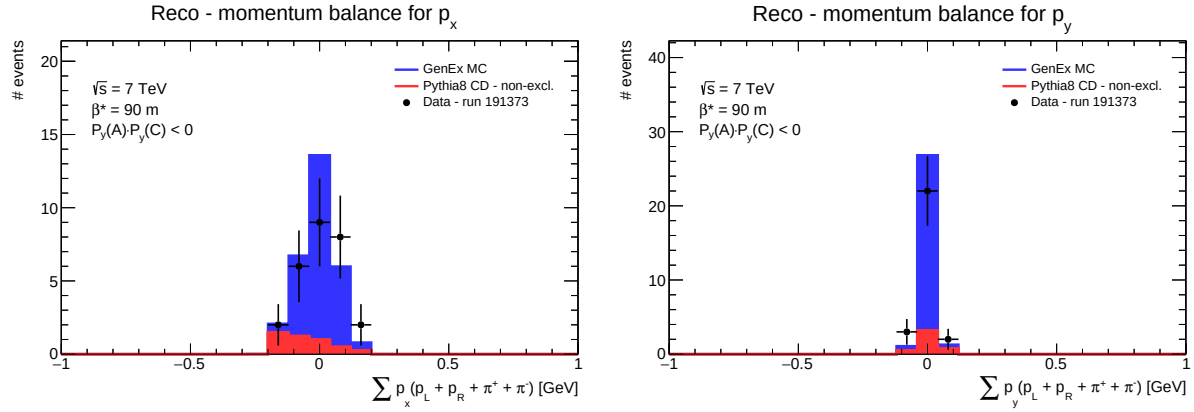

(a) (b)

Figure 91: Momentum balance distributions for the p_x and p_x components of the exclusive central system. The blue histograms represents the GenEx MC simulation, the red histograms represents the Pythia8 central diffraction MC simulation and the black distribution shows data. The distributions are shown after the full analysis cut flow was applied.

10.3. Exclusive pion cross-section distributions

in this section we focus on the distributions after analysis cut flow - but before the background subtraction. Due to the very low statistics in anti-elastic configuration, only the distributions for the analysis of the elastic-configuration are discussed. Bin-by-bin correction was used to correct the number of events in the distribution to obtain the differential cross-section distributions. The calculation of the overall correction factor f_{corr}(Sect. 8) was based on the GenEx MC simulation. The distributions are made on both the particle level and the detector level of the GenEx MC simulation were used in the bin-by-bin corrections where the correction itself is a ratio between the number of the events on detector level and the number of the events on the particle level in a given bin. Such results were used in the data distribution corrections. The differential cross-section distribution of the exclusive pion production are shown in Figs. 92–94, one by one for the $\phi_{\pi^+\pi^-}$, $\eta_{\pi^+\pi^-}$, $y_{\pi^+\pi^-}$, $p_{t(\pi^+\pi^-)}$ and $M_{\pi^+\pi^-}$ distributions.

The Fig. 92a shows the differential cross-section as a function of the central system azimuth angle $\phi_{\pi^+\pi^-}$ whereas the Fig. 92a shows the same quantity as a function of the central system polar angle $\theta_{\pi^+\pi^-}$ of the exclusive pion production.

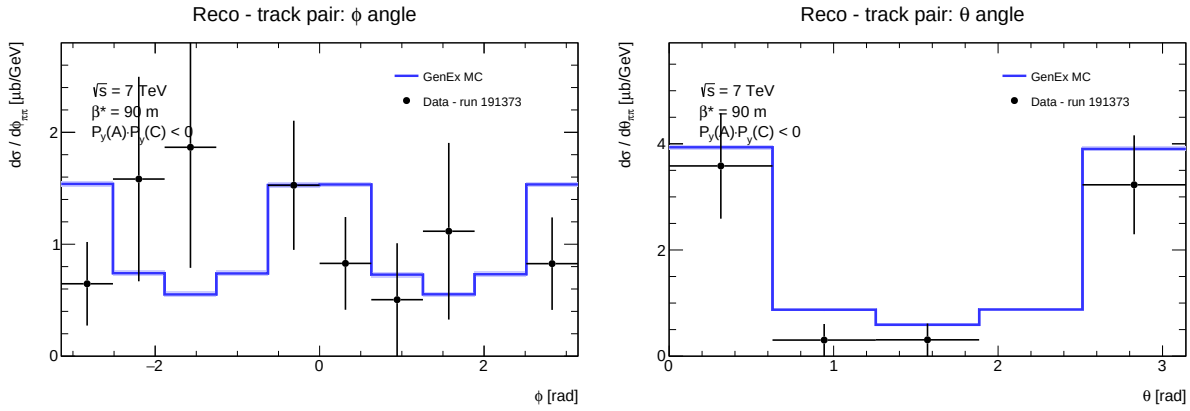

(a) (b)

Figure 92: A differential cross-section distribution as a function of (a) the central system azimuth angle $\phi_{\pi^+\pi^-}$ and (b) the central system polar angle $\theta_{\pi^+\pi^-}$. The data are represented by the black points whereas the GenEx MC simulation is represented by the blue histogram.

The Fig. 93a shows the central system pseudo-rapidity $\eta_{\pi^+\pi^-}$ distribution whereas the Fig. 93b describes the central system rapidity $y_{\pi^+\pi^-}$ distribution.

The Fig. 94a shows the central system transverse momentum $p_{\text{T}_{\pi^+\pi^-}}$ distribution whereas the Fig. 94b describes the central system invariant mass $M_{\pi^+\pi^-}$ distribution of the exclusive pion production. Comparing the data with the Monte Carlo simulation we see not good agreement of $p_{\text{T}_{\pi^+\pi^-}}$ values, but the data evince higher statistics. On the other hand the $M_{\pi^+\pi^-}$ distribution does not indicate any differences between the data and the Monte Carlo simulation. Due to the low statistic in data, there are no visible resonances. The distributions of the GenEx MC simulation also do not contain any resonances, but this is expected behaviour because this model does not include them.

The cross-section for the elastic configuration was calculated for each distribution of the differential cross-section and the results are summarised in table Table 22. The results are compared with the cross-section calculated using the single-bin correction which is a default correction method in this exclusive

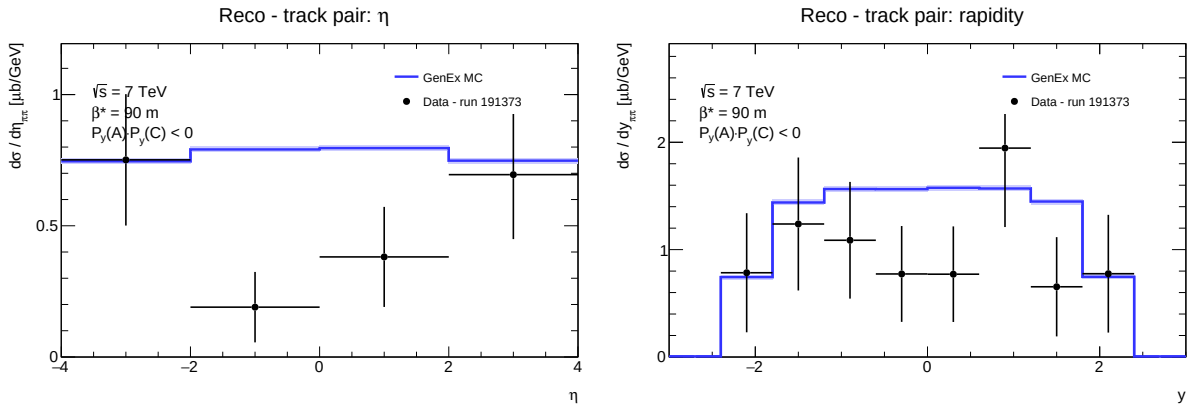

(a) (b)

Figure 93: A differential cross-section distribution as a function of (a) the central system pseudo-rapidity $\eta_{\pi^+\pi^-}$ and (b) the central system rapidity $y_{\pi^+\pi^-}$. The data are represented by the black points whereas the GenEx MC simulation is represented by the blue histogram.

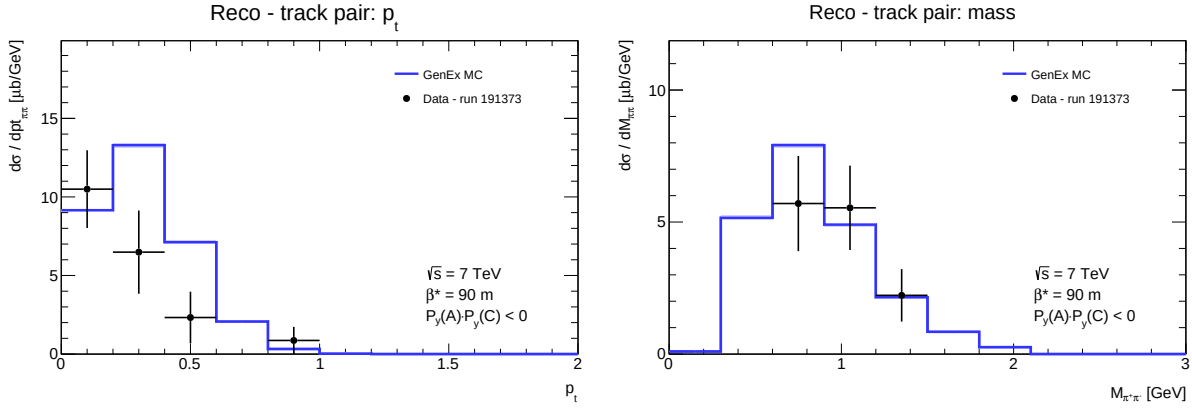

(a) (b)

Figure 94: A differential cross-section distribution as the function of (a) the central system transverse momentum $pt_{\pi^+\pi^-}$ and (b) the central system invariant mass $M_{\pi^+\pi^-}$. The data are represented by the black points whereas the GenEx MC simulation is represented by the blue histogram.

pion analysis. Quite big fluctuations between the cross-sections calculated integration of the differential cross-sections is visible.

Differences can be caused by low data statistics followed with by event fluctuations. The effect of the fluctuation can be suppressed with the cross-section calculation using the single-bin correction. This is also a reason why the single-bin correction is used as the default method for exclusive pion cross-section calculation. Note that the calculation based of the differential cross-section is performed only for the elastic configuration where the statistics allow to do such calculation even if very limited. In the case of the anti-elastic configuration the only way is to calculate the integrated cross-section using the single-bin corrections.

Table 22: The integrated exclusive pion cross-section at $\sqrt{s} = 7$ TeV calculated in two ways, using single-bin calculation and integrating the differential cross-section. Before background subtraction.

cross-section	**Elastic configuration**					
	single bin calculation	$\phi_{\pi^+\pi^-}$	$\eta_{\pi^+\pi^-}$	$y_{\pi^+\pi^-}$	$pt_{\pi^+\pi^-}$	$M_{\pi^+\pi^-}$
σ [μb]	4.73 ± 0.91	5.59 ± 1.21	4.45 ± 0.87	4.82 ± 0.94	4.04 ± 0.81	4.04 ± 0.78

10.4. Exclusive pion cross-section after background subtraction

As discussed in previous sections we assume that the main source of the background in the exclusive pion production comes from the central diffractive processes. Pythia8 with the central diffraction (Pythia8 CD) was used for the background estimation. The background subtraction process is described in Sect. 9 where it is shown that the central diffractive processes without the exclusive pion pair production[8] in Pythia8 reasonably describe the shape outside the signal region in data, Fig. 78, as well as the amount of the background for various $p_{\mathrm{y}}/\sigma_{p_{\mathrm{y}}}$ intervals, Fig. 82.

A numerical impact of the background subtraction methods on the exclusive pion cross-section is summarised in Table 23. Based on the results of a background study from Sect. 9, we use as the default method for the background subtraction the opposite-sign events in the whole kinematic region.

Table 23: Exclusive pion cross-section after the background subtraction for various background subtraction methods.

subtraction method	**Exclusive $\pi^+\pi^-$ cross-section [μb]**		
	elastic	**anti-elastic**	**overall**
opposite-sign, full region	$3.89 \pm 0.91^{(\mathrm{stat})}$	$7.66 \pm 4.89^{(\mathrm{stat})}$	$11.55 \pm 4.97^{(\mathrm{stat})}$
opposite-sign, outside signal	$3.91 \pm 0.91^{(\mathrm{stat})}$	$7.67 \pm 4.89^{(\mathrm{stat})}$	$11.58 \pm 4.97^{(\mathrm{stat})}$
same-sign, full region	$3.68 \pm 0.91^{(\mathrm{stat})}$	$7.45 \pm 4.89^{(\mathrm{stat})}$	$11.13 \pm 4.97^{(\mathrm{stat})}$
same-sign, outside signal	$3.63 \pm 0.91^{(\mathrm{stat})}$	$7.40 \pm 4.89^{(\mathrm{stat})}$	$11.02 \pm 4.97^{(\mathrm{stat})}$

[8] The exclusive pion pair events were removed from the central diffractive sample (Pythia8) on a particle level to keep only a background events.

The Table 24 summarises the results, before and after the background subtraction. The overall background fraction in data is about 12%; for the elastic configuration it is about 19% and for the anti-elastic configuration it is about 10%. The statistical error of the overall cross-section section is influenced by the event statistics of the anti-elastic configuration.

Table 24: Exclusive pion cross-section before and after the background subtraction.

	Exclusive $\pi^+\pi^-$ cross-section [μb]		
Background subtraction	**elastic configuration**	**anti-elastic configuration**	**overall**
before	$4.84 \pm 0.93^{(\text{stat})}$	$8.64 \pm 4.99^{(\text{stat})}$	$13.48 \pm 5.08^{(\text{stat})}$
after	$3.99 \pm 0.95^{(\text{stat})}$	$7.44 \pm 5.00^{(\text{stat})}$	$11.43 \pm 5.09^{(\text{stat})}$

10.5. Exclusive pion cross-section after ALFA reconstruction efficiency correction

The results presented above counted on the ALFA reconstruction efficiency based on the MC simulation. It is known that the ALFA reconstruction efficiency differs between the MC simulation and data. Therefore the correction factor on the ALFA reconstruction efficiency was calculated - as it is described in Sect. 8.2 - and applied on the result. The visible exclusive pion cross-section is now 14.41 ± 6.58(stat) and is summarized in Table 25.

Table 25: Exclusive pion cross-section before and after ALFA reconstruction efficiency correction.

	Exclusive $\pi^+\pi^-$ cross-section [μb]		
	elastic configuration	**anti-elastic configuration**	**overall**
before	$3.99 \pm 0.95^{(\text{stat})}$	$7.44 \pm 5.00^{(\text{stat})}$	$11.43 \pm 5.09^{(\text{stat})}$
after	$4.77 \pm 1.14^{(\text{stat})}$	$9.65 \pm 6.48^{(\text{stat})}$	$14.41 \pm 6.58^{(\text{stat})}$

The ALFA reconstruction efficiency correction was applied on each ALFA arm separately with appropriate weights. The weights were applied separately for the elastic and the anti-elastic configuration of the analysis. Each analysis configuration had two potential ALFA detector combinations - forming the arms 0 and 1 for the elastic configuration and the arms 2 and 3 for the anti-elastic configuration. Thus the value of the weight represents a ratio on the final results of a given arm of a given configuration.

The numbers are summarised in Table 26.

Table 26: ALFA reconstruction efficiency.

ALFA arm	**corr. fact.**	**weight**
0	1.187	16/27
1	1.204	11/27
2	1.298	2/3
3	1.295	1/3

11. Systematic uncertainties

The present analysis suffers from very low event statistics available in data (ATLAS run 191373). A very low statistics graduates in a very high statistical uncertainty which is about 46% for the exclusive pion cross-section of $\sigma^{\text{vis}}_{\pi^+\pi^-} = 14.41 \pm 6.58^{(\text{stat})}$ µb. So there is a good reason to say that dominant uncertainty comes from statistics.

Several key steps in this exclusive pion analysis are common with the ALFA elastic analysis related to the total cross-section of the proton-proton collisions [2], and are well described in the [28] including a very deep study of the systematic uncertainties. It was decided to follow some systematic uncertainties described in [28] and adopt them to the exclusive pion production, like the ones related to the ATLAS run 191373 and the ALFA detector properties.

The rest of the systematic uncertainties is described below in this section.

Some systematic uncertainties were calculated using Monte Carlo simulation and are included in Table 38 in Sect. 11.10.

11.1. Systematic uncertainty related to run properties

The exclusive pion analysis at 7 TeV is based on data taken by the ATLAS run 191373 in 2011. The integrated luminosity for the purpose of this study is $L_{\text{int}} = 78.72 \pm 0.13^{(\text{stat})} \pm 1.85^{(\text{syst})}$ µb^{-1}, see 7.1. The nominal energy of the initial beams was 3.5 TeV.

These two run related properties define the two systematic uncertainties studied in this analysis. The first systematic uncertainty is based on the precision of the luminosity measurement whereas the second systematic uncertainty is based on the precision of the initial beam energy measurement. Both uncertainties were estimated in the analysis of the total cross section measurement [2].

In the case of the systematic uncertainty study based on the luminosity measurement, the luminosity was varied about ±2.36% which is the relative uncertainty of the luminosity measurement. The nominal value of the luminosity with two edge values of luminosity were adopted in this calculation. The result is presented in the Table 27. It is seen that the effect of the luminosity measurement on the exclusive pion cross-section is ±0.34 µb. This uncertainty is measured directly on data sample.

Table 27: The effect of the precision of the luminosity measurement on the exclusive pion cross-section.

Data	**Luminosity [µb^{-1}]**		
	nominal 78.72	**down 76.87**	**up 80.57**
cross-section [µb]	14.41	14.75	14.07
uncertainty [µb]		0.34	0.34

The nominal energy of the initial beams was measured with a relative precision of ±0.1%, see [44]. The nominal energy is therefore changed by ±0.1%. The effect of this systematic uncertainty study is presented in Table 28. It is seen that the effect of the nominal beam energy measurement on the final cross-section

is quite low, only about ±0.02 µb. This uncertainty was applied to GenEx Monte Carlo simulation, as due to a very low statistics there is no visible effect in data.

Table 28: The effect of the precision of the nominal beam measurement on the exclusive pion cross-section.

GenEx	Beam energy [GeV]		
	nominal 3500.00	**down 3496.5**	**up 3503.5**
cross-section [µb]	13.72	13.75	13.71
uncertainty [µb]		0.02	0.02

11.2. Systematic uncertainty related to Inner Detector

A key role in the systematic uncertainty related to the ATLAS ID plays a dead material of the ID which is generally described in the ATLAS geometry database. The detector geometry and material description stored in that database contains a necessary amount of the dead material of the detector. It may happen that the amount of the dead material is not described well. Therefore an other set of the ATLAS detector geometries was created to study the effect.

The systematic uncertainty calculation was performed on the GenEx Monte Carlo simulation. The default ID geometry description is stored in the ATLAS off-line software databases under the geometry ATLAS_GEO_20_00_01 tag, see [45].

For the purpose of systematic uncertainty study there are three scenarios of the amount of the dead material in the ID which were used:

- +5% of the dead material in the whole ID (ATLAS_GEO_20_02_01 geometry tag)
- +10% of the dead material in the whole ID (ATLAS_GEO_20_03_01 geometry tag),
- +10% of the dead material in the Pixel detector only (ATLAS_GEO_20_17_01 geometry tag).

The analysis of a different amount of the dead material was performed with the same settings like in the analysis of a nominal geometry (with the geometry ATLAS_GEO_20_00_01 tag). This also means the usage of the same overall correction like for the nominal geometry. The other way is to calculate the overall correction for each dead material analysis separately. In both ways the results are the same.

A difference between the lowest and the highest value of the cross-section coming from the comparison of that four different ID geometries was chosen as the corresponding systematic uncertainty. The highest exclusive pion cross-section corresponds to the nominal ID geometry defined in ATLAS_GEO_20_00_01 tag whereas the the lowest cross-section corresponds to the ID geometry where the amount of the dead material in the whole ID is increased about 10%, as it is defined in ATLAS_GEO_20_03_01 tag. The systematic uncertainty of the dead material effect is 0.59 µb for the GenEx MC simulation. Recalculated to the data cross-section the systematic uncertainty of the dead material effect is determined to 0.61 µb. This systematic uncertainty is presented like the asymmetrical one in the negative direction. The Table 29 summarises the results of the dead material effect on the GenEx MC simulation cross-section.

Table 29: The effect of the amount of the dead material in the ID on the exclusive pion cross-section for the GenEx MC simulation.

GenEx	ID geometry tag			
	ATLAS_GEO 20_00_01	**ATLAS_GEO 20_02_01**	**ATLAS_GEO 20_03_01**	**ATLAS_GEO 20_17_01**
cross-section [μb]	13.72	13.45	13.14	13.39
uncertainty [μb]		-0.27	-0.59	-0.34

11.3. Systematic uncertainty related to Minimum Bias Trigger System

The MBTS selection condition based on the knowledge of the signal in the inner ring of the MBTS. This ring covers a different phase-space then the ID which is used to tag the pion pairs. Therefore one can assume almost no activity in the MBTS inner ring coming from the exclusive pion pair production. Due to imperfections, signal noise or another background activity, the MBTS inner cells can provide some signal. Based on the knowledge of the signal activity in that cells from the MC simulation, a condition on the MBTS activity is defined like $N_{\text{in}}^{\text{A}} + N_{\text{in}}^{\text{C}} < 2$, where N_{in}^{A} resp. N_{in}^{C} is a number of MBTS inner cells with a signal on the ATLAS side A resp. C. So this condition allows maximally one MBTS inner cell with the signal.

For the purpose of the systematic uncertainty study the threshold value of the condition above was changed by ±1 which means that in one case there is no signal allowed in the MBTS inner cells whereas in the second case the number of the inner cells with a signal is relaxed to maximally two.

The systematic uncertainty study was performed on data. For each MBTS condition a new set of overall correction and background estimation was performed and applied on the selected events. The additional background was suppressed from data and the cross-section was calculated. Then the MBTS systematic uncertainty is determined as a maximum difference between the default MBTS selection cut and its variation about ±1. The value of the uncertainty is 1.14 μb. The Table 30 summarises this uncertainty calculation.

Table 30: The effect of the number of MBTS inner cells with signal on the exclusive pion cross-section for data.

cut	**cross-section [μb]**	**uncertainty [μb]**
$N_{\text{in}^{\text{A}}} + N_{\text{in}}^{\text{C}} < 2$	14.41	
$N_{\text{in}^{\text{A}}} + N_{\text{in}}^{\text{C}} < 1$	15.55	1.14
$N_{\text{in}^{\text{A}}} + N_{\text{in}}^{\text{C}} < 3$	13.76	-0.65

11.4. ALFA reconstruction efficiency effect on the exclusive pion cross-section

It is known that the ALFA reconstruction efficiency based on MC simulation of the ALFA detectors does not agree well with the reconstruction efficiency derived by data driven techniques. We developed a selection technique described in Sect. 8.2.1 within which the events of MC and data should be selected with a very similar conditions.

The first part of the selection from Sect. 8.2.1 is dedicated to the selection efficiency which tells how big fraction of a signal is lost when the selection is applied. The systematic uncertainty of the selection efficiency is based on variation of its value about $\pm 1\sigma$. Such calculation is performed for each ALFA arm and then applied on the result of the exclusive pion cross-section. The systematic uncertainty was determined to 0.08 µb and summarized in Table 31.

Table 31: The effect of the event selection efficiency effect on the exclusive pion cross-section.

	nominal	$\mathbf{-1\sigma}$	$\mathbf{+1\sigma}$
cross-section [µb]	14.41	14.33	14.50
uncertainty [µb]		0.08	-0.09

The second part of the selection from Sect. 8.2.1 is dedicated to the ALFA reconstruction efficiency itself. The systematic uncertainty related to the ALFA reconstruction efficiency was calculated as an average value of the $\pm 1\sigma$ variation of the statistical uncertainty of each ALFA arm for both MC and data. Then the correction factor between MC and data was calculated and applied on the result of the exclusive pion cross-section. The uncertainty was determined to 0.004 µb and summarized in Table 32.

Table 32: The effect of ALFA reconstruction efficiency effect on the exclusive pion cross-section.

	nominal	$\mathbf{-1\sigma}$	$\mathbf{+1\sigma}$
cross-section [µb]	14.41	14.42	14.41
uncertainty [µb]		0.01	-0.00

The overall systematic uncertainty describing the ALFA reconstruction efficiency calculation is determined to 0.08 µb.

11.5. ALFA single-track selection effect on the exclusive pion cross-section

The exclusive pion analysis is based on ALFA single-track selection in full arm which should help to reduce the background. The selection allows to have maximally one reconstructed track in each ALFA detectors forming the full arm.

The single-track selection is described in Sect. 7.5 and its efficiency is a part of Sect. 8.2.1.

The systematic uncertainty related to the single-track selection was calculated as an average value of the $\pm 1\sigma$ variation of the statistical uncertainty of each ALFA arm for both MC and data. Then the correction

factor between MC and data was calculated and applied on the result of the exclusive pion cross-section. The uncertainty was determined to 0.02 µb. The Table 33 summarises this systematic uncertainty.

Table 33: The effect of ALFA single-track selection effect on the exclusive pion cross-section.

	nominal	-1σ	$+1\sigma$
cross-section [µb]	14.41	14.43	14.40
uncertainty [µb]		0.02	-0.02

11.6. ALFA kinematics reconstruction algorithms effect on the exclusive pion cross-section

The Lattice method algorithm is used as the default kinematics reconstruction algorithm in present analysis. We use the second algorithm called ALFA Reco to estimate the uncertainties. The results were compared on the level of the exclusive pion pair cross-section. A difference shows the impact of the proton kinematic reconstruction algorithms on the final cross-section which is about 1.14 µb. The Table 34 summarises this systematic uncertainty.

Table 34: The effect of ALFA kinematics reconstruction algorithms on the exclusive pion cross-section.

Data	**Lattice method**	**ALFA Reco method**
cross-section [µb]	14.41	13.27
uncertainty [µb]		1.14

11.7. Systematic uncertainty related to optics

The exclusive pion production analysis is based on data of the ATLAS run 191373 which was performed for the collision energy of 7 TeV and for the special (designed = nominal) high $\beta^{\star}$= 90 m optics. The so-called effective optics compensates the current-to-field calibration offset between Q1Q3 and Q2 quadrupole magnets. The effective optics was derived in the analysis of the elastic scattering [28].

An effect of the different optics applied on data analysis is studied and later presented as the systematic uncertainty related to the optics. Two data analysis were performed, one for the effective optics - the default analysis set-up - and one for the designed optics. The optics were changed only for the data. In the signal and background MC simulations the optics remained the same, the designed one. All the settings and the corrections remained also the same. Two results were obtained. The systematic uncertainty related to the optics setting is defined as the difference between the cross-section of the analysis using the effective optics and the cross-section of the analysis using the designed optics. The uncertainty was determined to be 0.08 µb, which shows that the impact of the optics is quite small on this exclusive pion analysis. The Table 35 summarises the uncertainty study.

Table 35: An impact of optics parameter settings on the exclusive pion cross-section.

	Optics	
	effective	**nominal**
cross-section [μb]	14.41	14.49
uncertainty [μb]		0.08

11.8. Systematic uncertainties related to background

The estimation of a background fraction of the exclusive pion pair analysis is based on the central diffractive processes simulated by the Pythia8, as described in Sect. 9. This source of the background is able to reasonably describe data outside the exclusive region as shown in Fig. 79 (Sect. 9) of the closure test as the effect of the background subtraction in data for various p_y/σ_{p_y} signal regions. It is used for the systematic uncertainty calculation. The closure test was performed only for the elastic configuration (due to insufficient statistics in the anti-elastic configuration) and its result was extrapolated to the overall configuration (it is assumed that the relative changes of the cross-section in the elastic configuration corresponds with the relative changes of the overall cross-section).

The systematic uncertainties related to background was calculated as an half value of a difference between the lowest and the highest cross-section value of a selected p_y/σ_{p_y} range (from 2.5 to 8). The half value of the difference between the minimal and the maximal value is 0.20 μb for the elastic configuration. This value extrapolated to the overall cross-section was determined to 0.70 μb. The Table 36 summarises the cross-section for the elastic configuration with minimal and maximal values highlighted.

Table 36: The exclusive pion pair cross-section of the elastic configuration for various p_y/σ_{p_y} signal regions.

p_y/σ_{p_y}	**2.5**	**3**	**3.5**	**4**	**4.5**	**5**	**5.5**	**6**	**6.5**	**7**	**7.5**	**8**
cross-section [μb]	3.98	**4.01**	3.99	3.71	3.65	3.73	3.81	3.81	3.76	3.76	3.62	**3.62**

11.9. Systematic uncertainty of overall correction due to used generator

The exclusive pion process is described by two independent models which are implemented in the the GenEx and DiMe generators. Both models are limited in their exclusive pion description. The basics of these two models are described in Sect. 4. This analysis uses the GenEx generator as the primary one. It means that all the corrections used in the analysis are based on the Monte Carlo simulation of the events generated by the GenEx generator.

The full analysis was completely repeated for the DiMe generator. The MC simulation of the DiMe generated events was performed and the correction calculation based on this simulation was calculated. Finally this correction was applied on the data to obtain the exclusive pion cross-section. Later the exclusive pion cross-section corrected by the correction based on DiMe MC simulation and the exclusive pion cross-section corrected by the correction based on GenEx MC simulation were compared to see

an effect of these two theoretical approaches on the exclusive pion cross-section calculated from data measurement. A value of this difference is about 1.42 µb and the Table 37 summarises the calculation.

Table 37: The effect of different models on the exclusive pion cross-section in data.

	Correction from	
Data	**GenEx**	**DiMe**
cross-section [µb]	14.41	13.09
uncertainty [µb]		1.32

11.10. Overall systematic uncertainty

Several systematic uncertainty studies were presented in previous sections. That systematic uncertainties were combined into the overall systematic uncertainty of the exclusive pion pair production analysis. The overall systematic uncertainty of the exclusive pion cross-section measurement was determined to $^{+1.5}_{-1.9}$(syst) ± 0.3(lumi) ± 1.3(model) µb. The Table 38 summarises the systematic uncertainties of the exclusive pion analysis.

Table 38: The summary of the exclusive pion cross-section systematic uncertainties.

	value [µb]	
uncertainty	**lower**	**upper**
Beam energy	-0.02	0.02
ID dead material	-0.61	—
veto on MBTS signal	-1.14	0.65
ALFA reconstruction efficiency	-0.08	0.08
ALFA kinematic reconstruction	-1.14	1.14
Optics	-0.08	0.08
Background	-0.70	0.70
Overall systematic uncertainty	-1.86	1.49
Luminosity	-0.34	0.34
Theoretical model	-1.32	1.32
Total	-2.31	2.02

12. Stability checks

This section contains additional studies devoted to the stability checks.

12.1. Stability check related to elliptical cut

The exclusive pion pair analysis cut flow contains one event selection related to the ALFA detector on which the stability check was performed. This event selection is defined as an elliptical cut of the correlation between the position of the reconstructed proton in the ALFA detector and its local angle, described in Sect. 7.7. The nominal value of this elliptical cut is set to 5.0σ.

The stability check calculation is performed for 2.5σ, 3.5σ and 5.0σ intervals. A dedicated correction was calculated for each interval, based on the GenEx MC simulation, and later applied on data. The background subtraction was also performed for each value of the interval. Due to the exclusive pion cross-section fluctuations visible in data - especially in the elastic configuration for the studied intervals from 2.5σ to 5.0σ. It was decided to take the maximal value between the neighbouring intervals (interval from 2.5σ to 3.5σ, or interval from 3.5σ to 5.0σ) as the uncertainty. Its value was determined to 0.26 µb. The main reason of the higher uncertainty is the low event statistics in data, especially in anti-elastic where is only few events together with the high trigger pre-scale. The Table 39 summarises this study.

Table 39: The effect of protons geometrical selection in ALFA detectors on the exclusive pion cross-section.

	sigma cut value		
Data	**3.5**	**2.5**	**5.0**
cross-section [µb]	14.41	14.68	14.15
uncertainty [µb]		0.27	0.26

12.2. Stability check related to momentum balance event selection

The analysis cut flow contains some event selection based on the momentum balance of the products. The momentum balance of the system was studied on the GenEx MC simulation. Its results serve to the determination of kinematic region. The momentum balance says that the system is balanced if the initial state momentum is equal to the momentum of the final state. The system momentum balance of P_x and P_y was only used in this exclusive pion analysis.

The nominal interval of the P_x and P_y event selection was set to 3.5σ, where σ comes from the fit of an appropriate distribution in GenEx MC simulation, for more details see 7.8.

The stability check related to the momentum balance was studied in the interval of $\pm 1\sigma$ around the nominal 3.5σ value. It was studied on data for both the P_x and P_y momentum separately. The effect on the cross-section is from 0.24 µb to 1.49 µb with an average uncertainty about 0.82 µb. The Table 40 summarises this study.

Table 40: The effect of P_x and P_y momentum balance event selection on the exclusive pion cross-section.

	sigma cut value		
Data	**3.5**	**2.5**	**4.5**
P_x: cross-section [μb]	14.41	14.10	14.95
P_x: uncertainty [μb]		-0.31	0.54
P_y: cross-section [μb]	14.41	14.17	15.90
P_y: uncertainty [μb]		-0.24	1.49

13. Results

The fiducial cross section of the exclusive pion pair production at centre-of-mass energy $\sqrt{s} = 7\,\text{TeV}$, together with its statistical and systematic errors, was determined.

There was no dedicated trigger for anti-elastic configuration and high scaling of L1_ALFA_ANY trigger led to the big statistical uncertainty. The fiducial cross-section for the elastic configuration is

$$\sigma^{\text{vis}}_{\pi^+\pi^-}(\text{elastic}) = 4.8 \pm 1.1(\text{stat})\,\mu\text{b}$$

whether for anti-elastic configuration it is

$$\sigma^{\text{vis}}_{\pi^+\pi^-}(\text{anti} - \text{elastic}) = 9.7 \pm 6.5(\text{stat})\,\mu\text{b}.$$

The ratio of the cross-section values for the elastic and the anti-elastic configuration is in data $1 : 2$ whereas the ratio predicted by GenEx is almost $1 : 1$ (see Table 42 in D.2).

The statistical uncertainty is the dominant source of the overall uncertainty. The result serves as the first estimate of the exclusive pion cross-section on the LHC scale energies.

The total fiducial cross section of the exclusive pion pair production at centre-of-mass energy $\sqrt{s} = 7\,\text{TeV}$ and the given analysis cut flow was determined to be

$$\sigma^{\text{vis}}_{\pi^+\pi^-} = 14.4 \pm 6.6(\text{stat})\,^{+1.5}_{-1.9}(\text{syst}) \pm 0.3(\text{lumi}) \pm 1.3(\text{model})\,\mu\text{b}.$$

The biggest contribution to systematic error comes from vetoing on the MBTS only, then from ALFA kinematic reconstruction algorithms, from the background and from Inner detector dead material description, viz Sect. 11.10.

There are few theoretical models describing the exclusive pion production and even less Monte Carlo generators based on existing theoretical studies Sect. 3. It was shown that the Monte Carlo generators are able to describe the exclusive pion process. Still there are mutual differences between the models and due to the limited statistics we were not able to find model limits nor to exclude any of them.

The obtained results is, within errors, compatible with predicted value 21 µb [7] obtained for a different distance ($\approx 4\,\text{mm}$) of ALFA detectors from the beam.

14. Summary

The work on the thesis and the thesis itself led to two main outputs:

1. the existence of the simulation and analysis frameworks with more than 20000 lines of code and with the ability to be used for any similar exclusive analysis at arbitrary energy in future (e.g. centre-of-mass energy $\sqrt{s} = 14\,\text{TeV}$, $\sqrt{s} = 1\,\text{TeV}$),
2. the determination of fiducial cross-section of the exclusive pion production $p + p \to p + p + \pi^+ + \pi^-$which has an ambitions to become the first published ATLAS diffractive analysis using the forward detectors.

The ongoing 8 TeV and 13 TeV analyses of the same process have (much) higher statistics of events and will allow more detailed analyses (especially 13 TeV one) as e.g. of the differential cross-section $\mathrm{d}\sigma/\mathrm{d}t$, still 7 TeV analysis leads to the process *observation* (3σ) in the elastic configuration.

Appendices

A. Monte Carlo Simulation

The Monte Carlo simulation set-up is included in this section.

Below one can see some parameters of the GenEx pion production.

```
eventGenerationStrategy = 2
tecm = 7000
TEventMaker2to4::y_min = -2.7
TEventMaker2to4::y_max = 2.7
sigma_tot = 102.722
B_elastic = 14
Beff = 4
Lambda2 = 1
cutType = 0
```

Below one can see an example of a job for HepMC to Athena collection conversion. Standalone transformation

```
import AthenaCommon.AtlasUnixGeneratorJob

from AthenaCommon.AppMgr import theApp
from AthenaCommon.AppMgr import ServiceMgr

from AthenaCommon.AlgSequence import AlgSequence
job=AlgSequence()
from ReadHepMCFromFile.ReadHepMCFromFileConf import HepMCReadFromFile
job += HepMCReadFromFile()

ServiceMgr.MessageSvc.OutputLevel               = INFO

theApp.EvtMax = 1000000

re = job.HepMCReadFromFile
re.AsciiFile= "events_7TeV_eta2.7_1Mevt.hepmc"

from AthenaPoolCnvSvc.WriteAthenaPool import AthenaPoolOutputStream
Stream1 = AthenaPoolOutputStream( "Stream1" )
Stream1.ItemList += [ "2101#*", "133273#*" ]
PoolSvc = ServiceMgr.PoolSvc
Stream1.OutputFile = "events_7TeV_eta2.7_1Mevt_GenEx_Truth.root"
```

PAthena transformation useful for GRID production

```
evgenConfig.description = "Exclusive pions via HepMC"
evgenConfig.keywords = ["QCD"  ,"pi+pi-", "exclusive"]
```

```
evgenConfig.minevents = 1000000
evgenConfig.contact = ["Petr Hamal <petr.hamal@cern.ch>"]
evgenConfig.inputfilecheck = 'Exclpipi_7TeV_eta2.7'
include("MC12JobOptions/HepMCReadFromFile_Common.py")
evgenConfig.tune = "none"
```

Pythia8_CD

```
Pythia8.Commands       += ["SoftQCD:centralDiffractive = on",
                           "Diffraction:PomFlux = 5"]
Pythia8.CollisionEnergy = 7000
```

Here is an example of a job for the simulation step. This step was perform in the Athena release 17.3.13.3 with updated `ALFA` packages.

```
AtlasG4_trf.py
  maxEvents=$evt
  physicsList='QGSP_BERT'
  inputEvgenFile=$in
  outputHitsFile=$out
  skipEvents=$skipEvt randomSeed=1234
  geometryVersion=ATLAS-GEO-20-00-01
  conditionsTag=OFLCOND-MC12-SIM-00
  preExec='from G4AtlasApps.SimFlags import
      simFlags;simFlags.MagneticField.set_On();
      simFlags.MagneticField.lock();
      jobproperties.Beam.energy.set_Value_and_Lock(3500*Units.GeV)'
  ALFAOn=True
  preInclude='../ForwardTransportSvcConfig.ALFA.py,../BeamEffects.py'
  postExec='conddb.addOverride(
      "<db>COOLOFL_FWD/OFLP200</db>/FWD/ALFA/position_calibration",
      "FWDALFAposition_r191373_v2" )'
  postInclude='RecJobTransforms/UseOracle.py'
```

And here is the example of the job merging the digitisation and the reconstruction steps. This step was performed in the Athena 17.3.12.12 release with updated `ALFA`, `ForwardDetectorsD3PDMaker` and `MinBiasD3PDMaker` packages.

```
DigiMReco_trf.py
  maxEvents=$evt
  inputHitsFile=$in
  outputRDOFile=$workBatchDir'/'$outRDO
  outputESDFile=$workBatchDir'/'$outESD
  outputNTUP_MINBIASFile=$workBatchDir'/'$outNTUP
  ALFAOn=True
  preInclude="../BeamEffectsReco.py"
  preExec_r2e='rec.Commissioning.set_Value_and_Lock(True);
      jobproperties.Beam.energy.set_Value_and_Lock(3500*Units.GeV);
      muonRecFlags.writeSDOs=True; from CaloRec.CaloCellFlags import
      jobproperties; jobproperties.CaloCellFlags.doLArCellEmMisCalib=False;
      rec.doAlfa.set_Value_and_Lock(True);
```

```
    rec.doForwardDet.set_Value_and_Lock(True); InDetFlags.doLowPt=True;
    InDetFlags.doSlimming=False;'
postExec_r2e='conddb.addOverride(
    "<db>COOLOFL_FWD/OFLP200</db>/FWD/ALFA/position_calibration",
    "FWDALFAposition_r191373_v2" )'
postInclude_r2e='RecJobTransforms/CalibrationHitsInESDConfig.py'
preExec_e2d='rec.doAlfa.set_Value_and_Lock(True);
    rec.doForwardDet.set_Value_and_Lock(True);'
RunNumber=999999
--ignoreerrors=ALL
autoConfiguration=everything
conditionsTag=OFLCOND-MC12-SIM-00
geometryVersion=ATLAS-GEO-20-00-01
DataRunNumber=-1
jobNumber=1
digiSeedOffset1=1
digiSeedOffset2=2
digiRndmSvc=AtDSFMTGenSvc
```

B. ALFA Alignment

ALFA alignment constants are stored in the COOL database under the tag `FWDALFAposition_r191373_v2` in the folder `/FWD/ALFA/position_calibration` of `COOLOFL_FWD/OFLP200` database and can be read by `AtlCoolConsole.py` utility which is a part of the ATLAS release.

```
-bash-4.1$ AtlCoolConsole.py "COOLOFL_FWD/OFLP200"
Connected to 'frontier://ATLF/();schema=ATLAS_COOLOFL_FWD;dbname=OFLP200'
>>> listtags /FWD/ALFA/position_calibration
>>> usetag FWDALFAposition_r191373_v2
>>> more /FWD/ALFA/position_calibration
```

C. Analysis scheme diagram

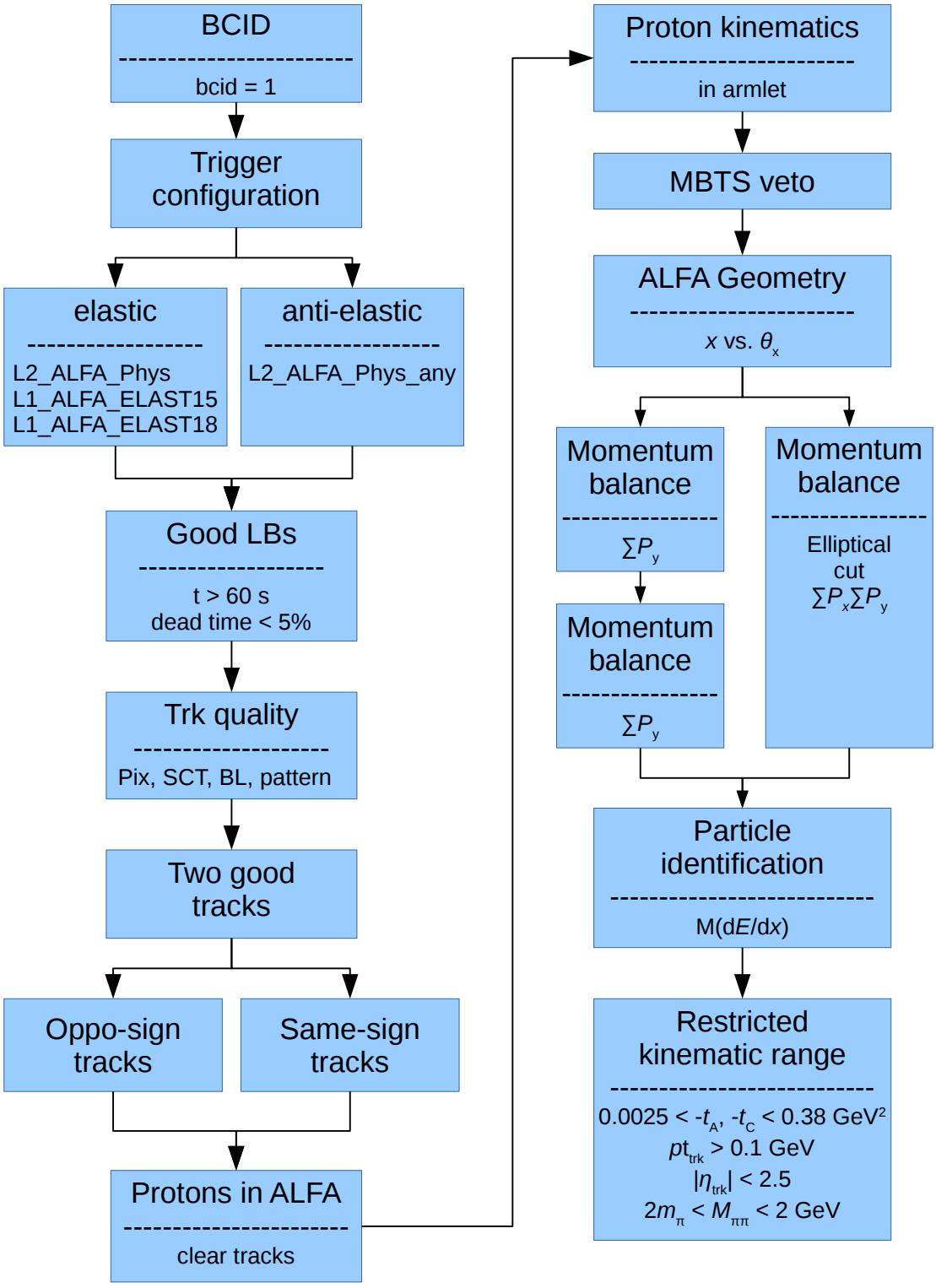

Figure 95: Analysis scheme diagram

D. Monte Carlo analysis

This section describes behaviour of the exclusive pion production on the Monte Carlo level. For the purpose of the MC study two different MC generators were used, GenEx and Pythia8.

First, the GenEx generator focuses directly on the exclusive processes (like $\pi^+\pi^-$ or K^+K^-). It generates only a continuum of that exclusive processes. For this study the exclusive $\pi^+\pi^-$ process was generated. The GenEx generator is described in Sect. 4.1.1.

Second, the Pythia8 generator with central diffraction processes was used. The aim to use this generator was to test the analysis cut flow imperfections and to estimate a background fraction of the exclusive pion production in data which would tell if the Pythia8 central diffraction is a main contributor of the background in data or not.

The Monte Carlo simulation with the Pythia8 central diffraction was studied in three cases:

- all generated events were processed,
- only the exclusive pion events on generated (particle) level were used for the analysis,
- only the non-exclusive pion events were studied.

The results of this case show the imperfection of the analysis cut flow and also could tells something about the background fraction in data. The Pythia8 generator is deeply described in Sect. 4.1.3.

It should be noticed and repeated that the exclusive pion analysis is performed for the two configurations, the elastic one and the anti-elastic one, so all the results in this section are divided into that two configurations. The configurations are based on both the ALFA triggers and ALFA arms selections, and are described in detail in Sects. 5.5 and 7.5.

D.1. GenEx Monte Carlo simulation after event basic selection

The GenEx Monte Carlo simulation is a signal simulation of the exclusive pion production, therefore no background contribution is included in this simulation.

The section is focused on the results after a basic event selection. From the cut flow described in Sect. 7 only two selections are applied, the ATLAS Inner detector track selection, described in Sect. 7.4, and the ALFA track selection, described in Sect. 7.5. The aim of this partial study is to look on the shape distributions to check whether the proton kinematic reconstruction described in Sect. 6.2 works properly. The main aim of this study is to tune up the kinematic cuts described in Sect. 7.8 which are used later in the analysis of the data. It is seen that the signal Monte Carlo plays an important role in the exclusive pion analysis.

It is important to mentioned that all the plots in this section are depicted for the analysis using Lattice method for the proton kinematics reconstruction as it is described in Sect. 6.2. If an other proton kinematics reconstruction algorithm is used it will be directly said.

It was mentioned that the analysis cut flow is tuned up using the results from the GenEx Monte Carlo simulation. The key cut flow tuning comes from the knowledge about the kinematics of the exclusive pion system. Therefore a first look goes on the first set of the control plots depicted on Figs. 96 and 97.

The histograms on that figures depict the distributions for the kinematic variables p_x and p_y for both the pion (Fig. 96) and the proton (Fig. 97) products. They show a good shape alignment, a good shape agreement between a positive (red distribution) and negative (blue distribution) pion and a good shape agreement between the proton on side A (red histogram) and on side C (blue histogram) from the IP.

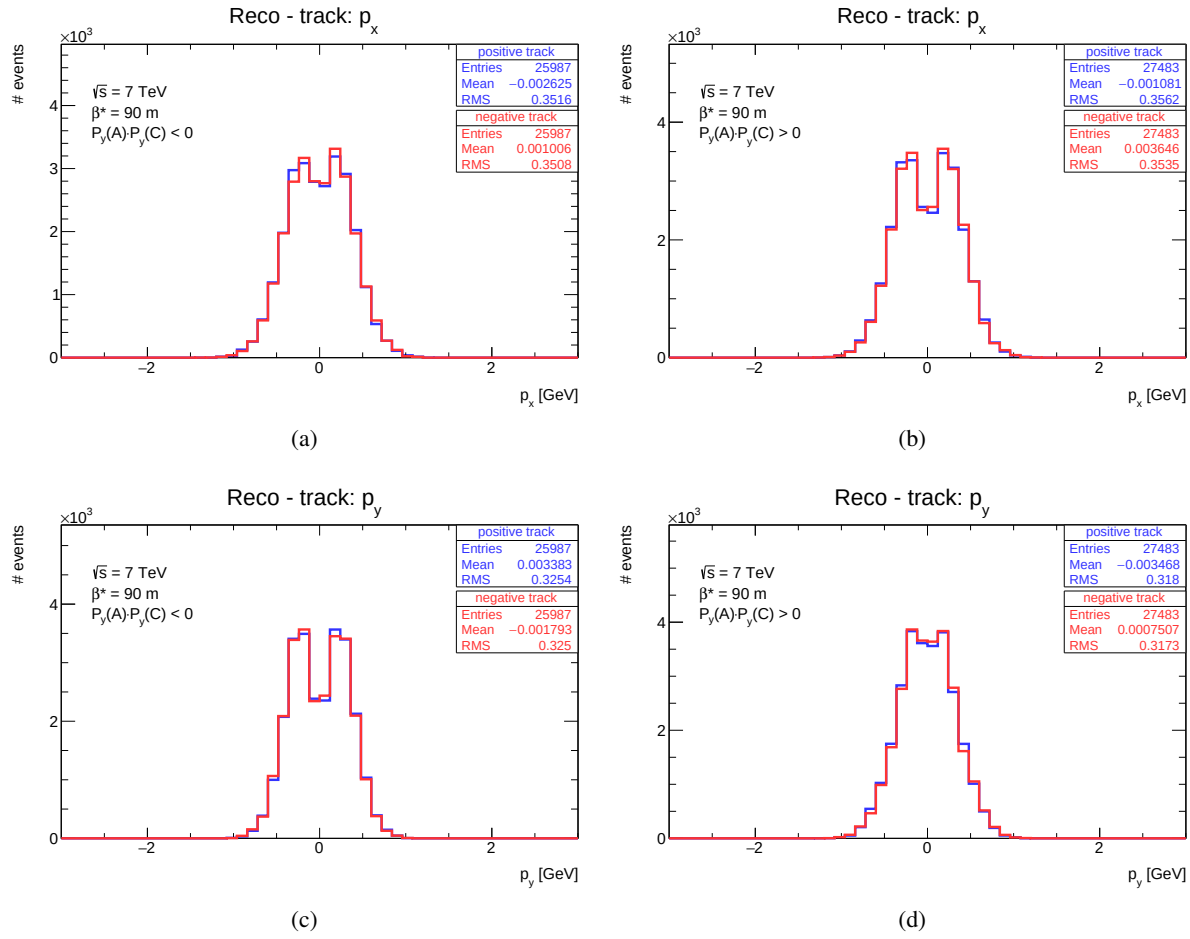

Figure 96: The reconstructed pion shape distribution for two different configurations, on (a) p_x and on (c) p_y the momentum components for the elastic configuration whereas on (b) p_x and on (d) p_y the momentum components for the anti-elastic configuration. The red histograms represent the positive pion whereas the blue histogram represent the negative pion.

The next set of the control plots is based on the summing up of the kinematics of the exclusive products. The momentum balance for the p_x and the p_y components is calculated and depicted on the Fig. 98. The exclusivity peak around the zero values is nicely seen. It says the system is balanced.

The distributions from the Fig. 98 are fit by a Gaussian function. A sigma fit is used to tune up the kinematic event selection described in Sect. 7.8. In default the 3.5 σ cut is used. This sigma fit is performed for the Lattice method of the proton kinematics reconstruction. in the case of the ALFA Reco proton kinematics reconstruction the results will slightly differ. Therefore at the beginning of each analysis one has to be sure that the interval of the kinematic events selection is correctly set up. In other case the results may be misrepresented.

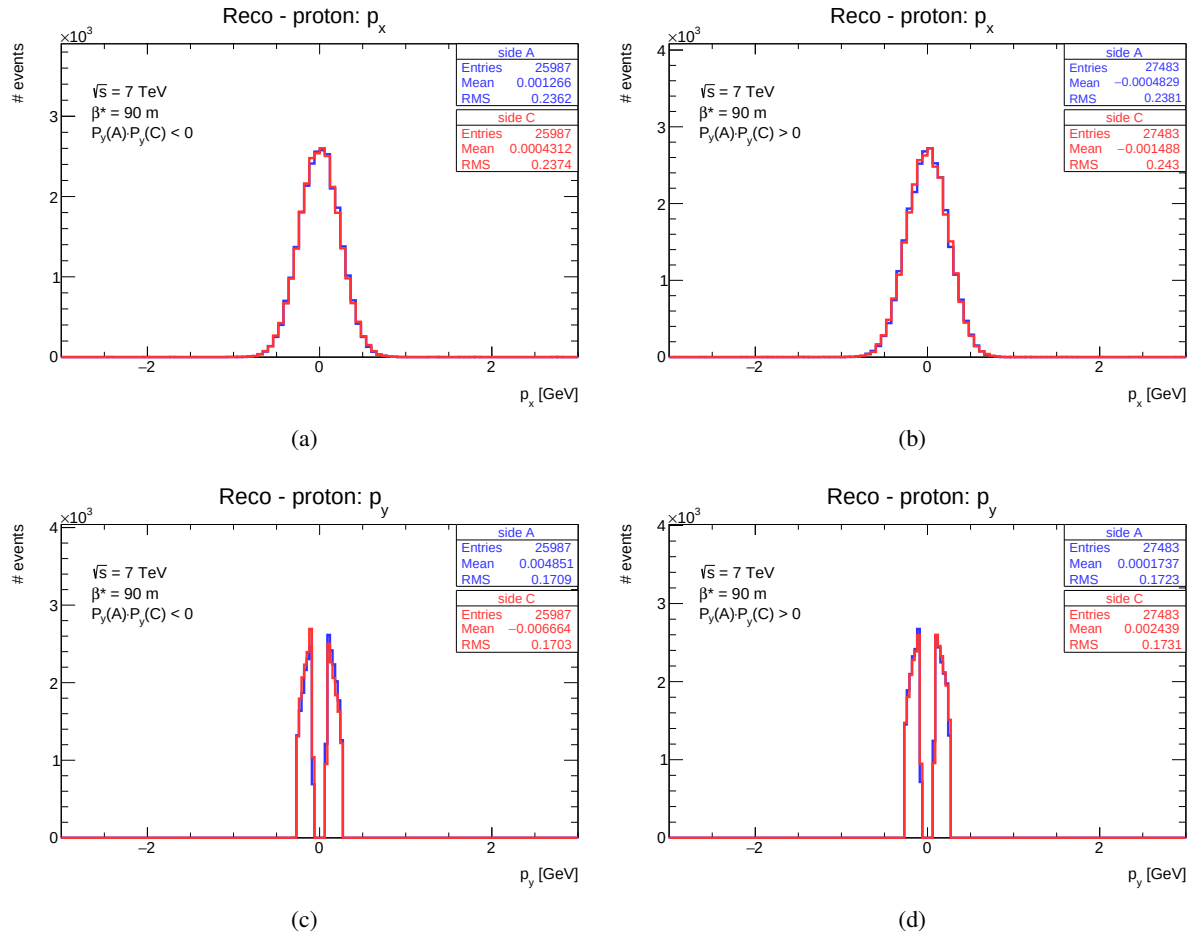

Figure 97: The reconstructed proton shape distribution for two configurations, on (a) p_x and (c) p_y the momentum components for the elastic configuration whereas on (b) p_x and on (d) p_y the momentum components for the anti-elastic configuration. The red histograms represent the proton on side A whereas the blue histogram represent the proton on side C of the ATLAS detector.

The Lattice method is the default method for the proton kinematics reconstruction used in the analysis. But let us to look also on the ALFA Reco method for the proton kinematics reconstruction to see if these two methods somehow differ. From the Sect. 6.2 it is known that the ALFA Reco method returns worse proton p_x resolution than the Lattice method. Therefore the fit resolution of the $\sum p_x$ distribution depicted on Fig. 99 is almost two times worse then for the Lattice method depicted on Fig. 98.

The $\sum p_x$ and the $\sum p_y$ fit results for both the ALFA Reco method and Lattice method of the proton kinematics reconstruction are summarised in Table 41. These results are used to define a range where the exclusive pion events are located. Only the two momentum balance components are used in this exclusive analysis due to the insufficient resolution in the proton kinematics reconstruction in the p_z and the E components as it is explained in Sect. 6.2.

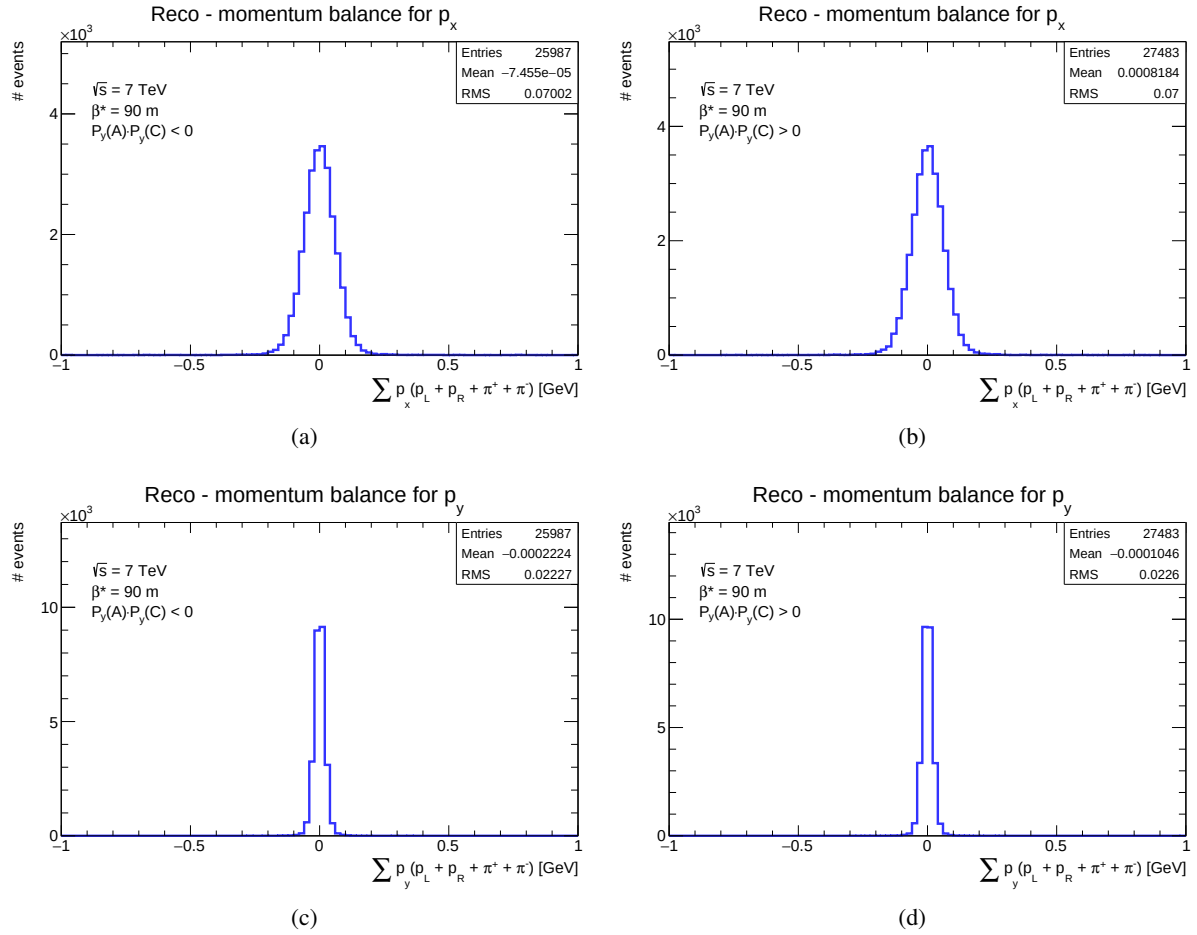

Figure 98: The system momentum balance for Lattice method algorithm proton kinematics reconstruction and the configurations, on (a) p_x and on (c) p_y the momentum components for the elastic configuration whereas on (b) p_x and on (d) p_y the momentum components for the anti-elastic configuration. The GenEx Monte Carlo simulation is used.

Table 41: The $\sum p_x$ and the $\sum p_y$ fit results for both the ALFA Reco and lattice methods of proton kinematics reconstruction.

	algorithm	
Momentum balance	**ALFA Reco σ [GeV]**	**Lattice method σ [GeV]**
$\sum p_x$	0.1407	0.0200
$\sum p_y$	0.0607	0.0204

The control plots describing the geometrical properties of the protons reconstructed in ALFA detectors were made too. The Fig. 100 depicts a map of proton hits in ALFA detectors for the elastic configuration whereas the Fig. 101 depict the proton hits map for the anti-elastic configuration. The shape of this spot is very close to the spot of the elastically scattered protons. This shows on the fact that the proton energy

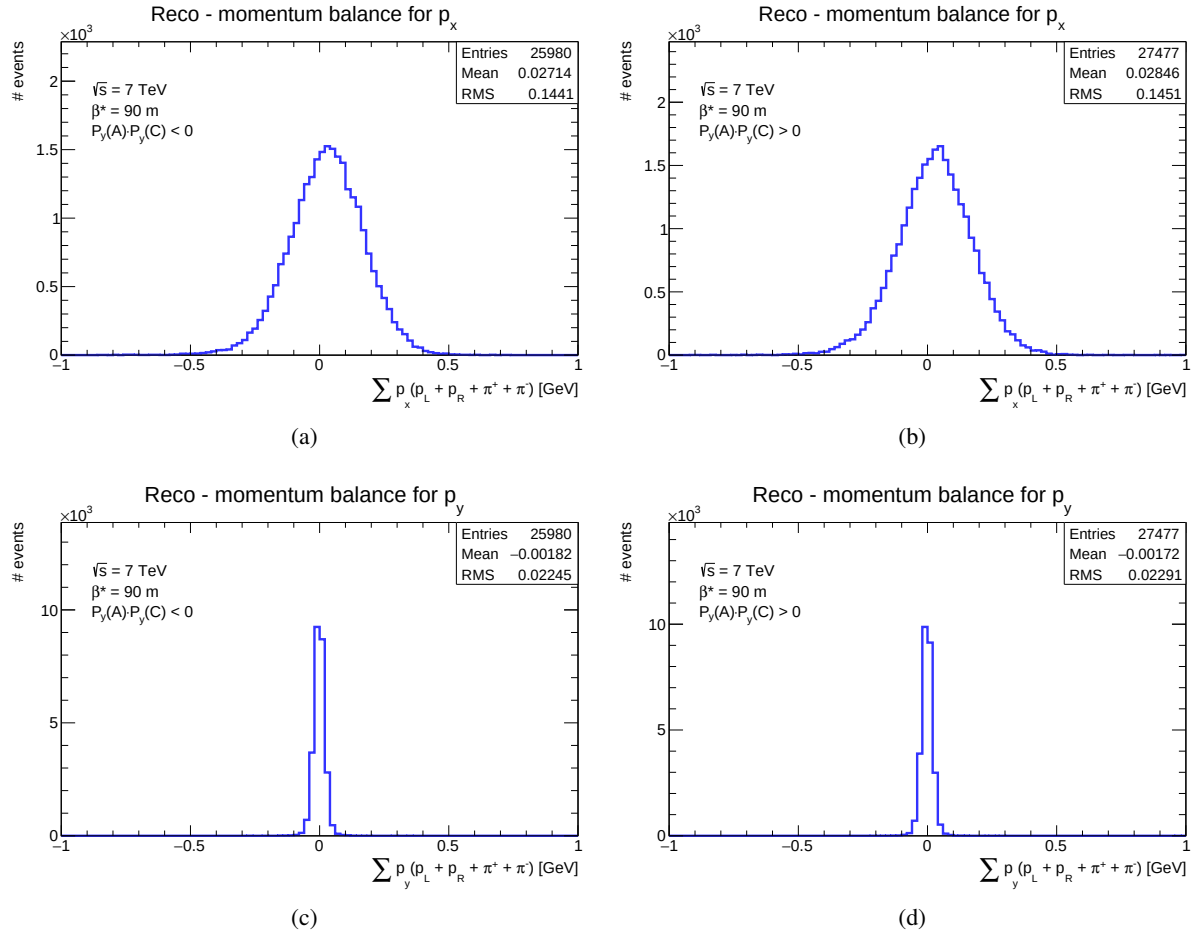

Figure 99: The system momentum balance for ALFA Reco algorithm proton kinematics reconstruction and the configurations, on (a) p_x and on (c) p_y the momentum components for the elastic configuration whereas on (b) p_x and on (d) p_y the momentum components for the anti-elastic configuration. The GenEx Monte Carlo simulation is used.

loss is very small in this exclusive pion production. It also means that the protons from the production behave as the elastic ones and therefore some techniques from the elastic analysis [28] would be adopted to this analysis.

Also the other distributions on Fig. 102 of the geometrical properties looks like from the analysis of the elastically scattered protons [28]. The Figs. 102a–102d depict a correlation between a proton local angle and its position in $x-$axis and the Figs. 102e–102h depict the same correlation but in $y-$axis. Also on these histograms the exclusive pion process looks like the elastic one. A difference can be find in the width and the length of the ellipses on the Figs. 102a–102d. They are slightly narrower and longer then in the study of the elastically scattered protons. That figures on Fig. 102 are depicted there for the elastic configuration whereas on the Fig. 103 they are depicted for the anti-elastic configuration. A difference between these two configuration is minimal in the case of the proton geometrical properties.

A quite good agreement of the shapes of the distributions on Figs. 102a–102h and on Figs. 103a–103h between this exclusive pion analysis and the study of the elastically scattered protons allows to take over

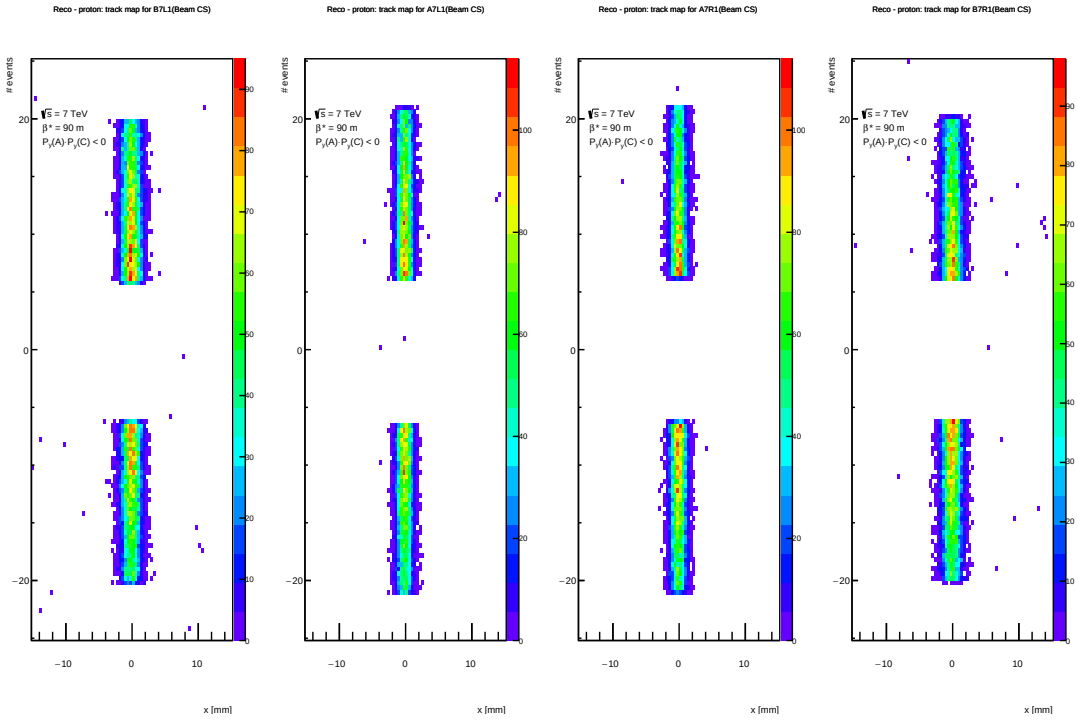

Figure 100: The hit map of proton hits in ALFA detectors for the elastic configuration.

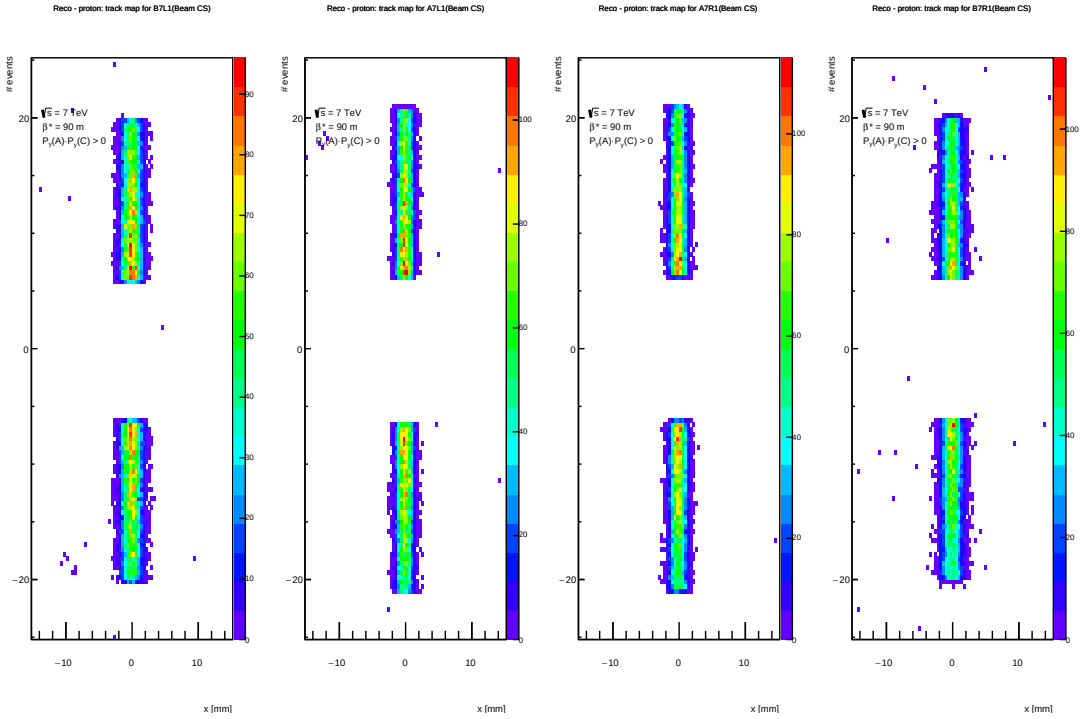

Figure 101: The hit map of proton hits in ALFA detectors for the anti-elastic configuration.

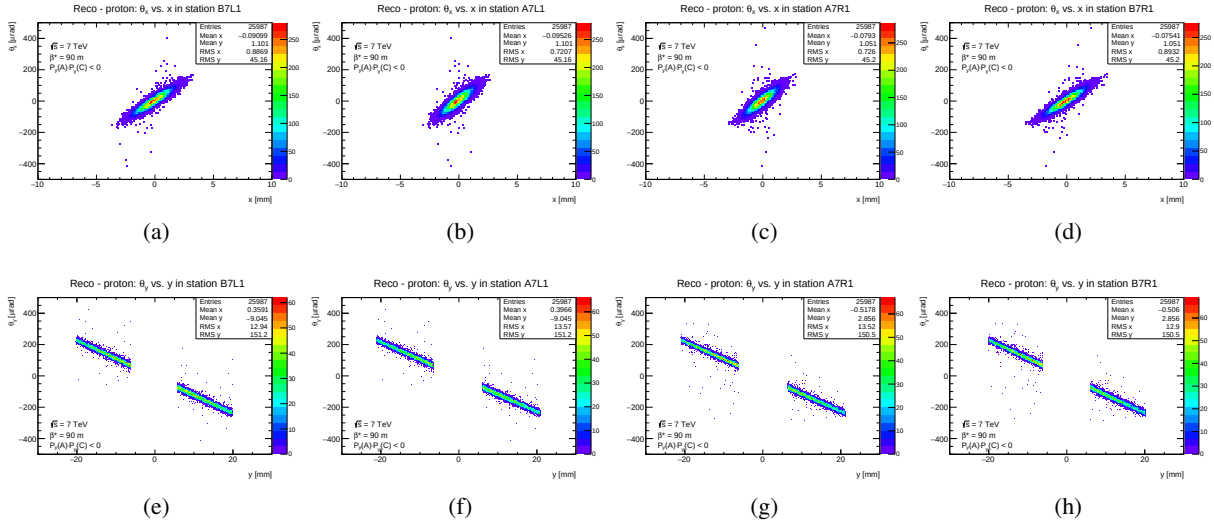

Figure 102: The hit maps of the protons reconstructed by the ALFA detectors in the elastic configuration, for the stations B7L1, A7L1, A7R1, B7R1 from left to right.

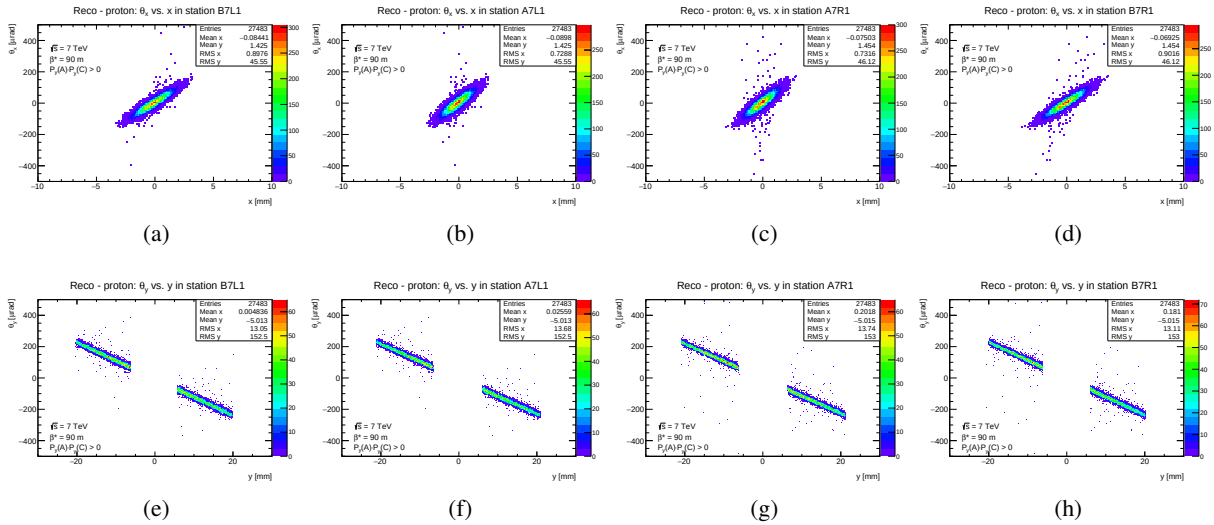

Figure 103: The hit maps of the protons reconstructed by the ALFA detectors in the anti-elastic configuration, for the stations B7L1, A7L1, A7R1, B7R1 from left to right.

some geometrical-based cuts from that elastic analysis. This is done mainly for ALFA geometrical cut (Sect. 7.7) which is based on the correlation of the proton local angle and its position.

Now back to pion tracks. In the case of the track reconstructed in the ATLAS Inner detector the distributions for the kinematic variables p_x and p_y were depicted on Fig. 96. One can make another set of the control distributions for that tracks. They are depicted on Figs. 104 and 105. These figures depict standard η_{trk} on Figs. 104a and 105a and ϕ_{trk} on Figs. 104b and 105b distributions. A good agreement between a positive (in a blue histogram) and a negative (in a red histogram) tracks is visible. The ϕ_{trk} distribution shows a flat shape whereas the η_{trk} shows that the reconstructed tracks prefer a central system[9].

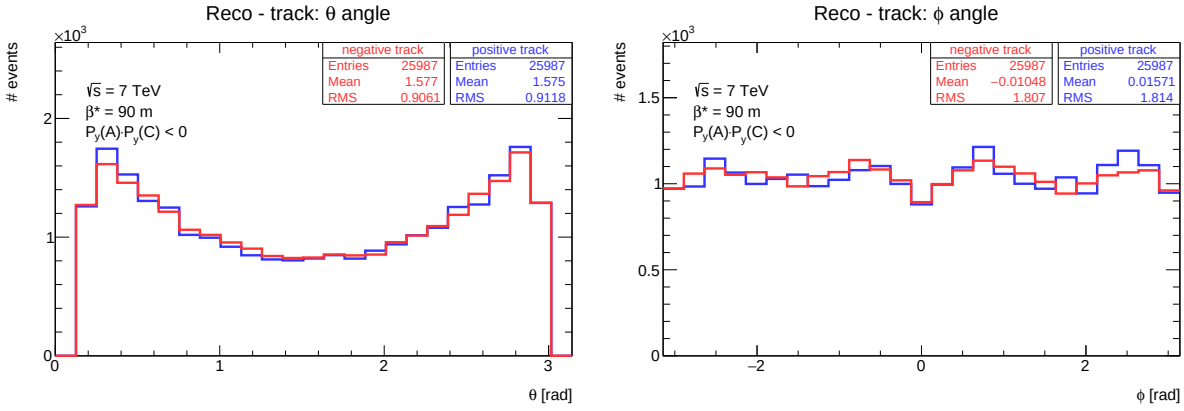

(a) (b)

Figure 104: The (a) η and the (b) ϕ distributions of the tracks reconstructed by the ATLAS Inner detector. The blue histograms represent the positive track whereas the blue histograms represent the negative track. The histograms are for the pion tracks from the elastic configuration of the analysis.

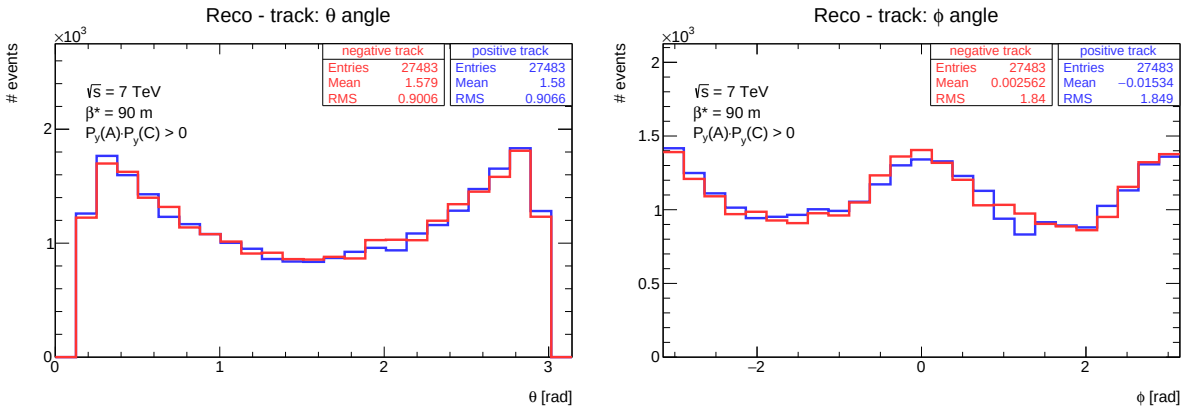

(a) (b)

Figure 105: The (a) η and the (b) ϕ distributions of the tracks reconstructed by the ATLAS Inner detector. The blue histograms represent the positive track whereas the blue histograms represent the negative track. The histograms are for the pion tracks from the anti-elastic configuration of the analysis.

The next set of the control plots show how well the tracks are reconstructed by the ATLAS Inner detector.

[9] The centrality of the tracks is expected due to a fact that the exclusive pion production belong to a central diffraction.

This set of plots focus on three distributions, the pt_{trk} distribution, the η_{trk} distribution and the ϕ_{trk} distribution. They compare the track distributions on the particle level with its distributions on the detector level for both the elastic and the anti-elastic configurations of the analysis. These distributions are depicted on Fig. 106 and they show that the distribution spread before and after the tracks reconstruction is small. The distributions are diagonal.

It is also useful to compare a distribution on the particle level (for the generated tracks - sometime known as a truth level) with a distribution on the detector level (for the reconstructed tracks - sometime known as a reconstructed level) to see the effects of the detector systems. The comparison is performed for the basic pions and protons distributions as well as for the pion pair distributions for both the elastic and the anti-elastic configuration. The distributions are not normalized. The total number of entries in the histogram if the same for both the detector level and the particle level distributions. Therefore it can be seen how well the distributions on detector level describe the distributions on particle level. Some differences are visible for the kinematic distributions p_{x} and p_{y} of the exclusive system. These differences are caused by the detectors resolution together with a combination of the exclusive products. Even if the basic distributions for protons and pions do not show a big differences between the detector level and the particle level, their combination into the system distribution is influenced quite well. All the distributions are depicted in Figs. 107 and 113.

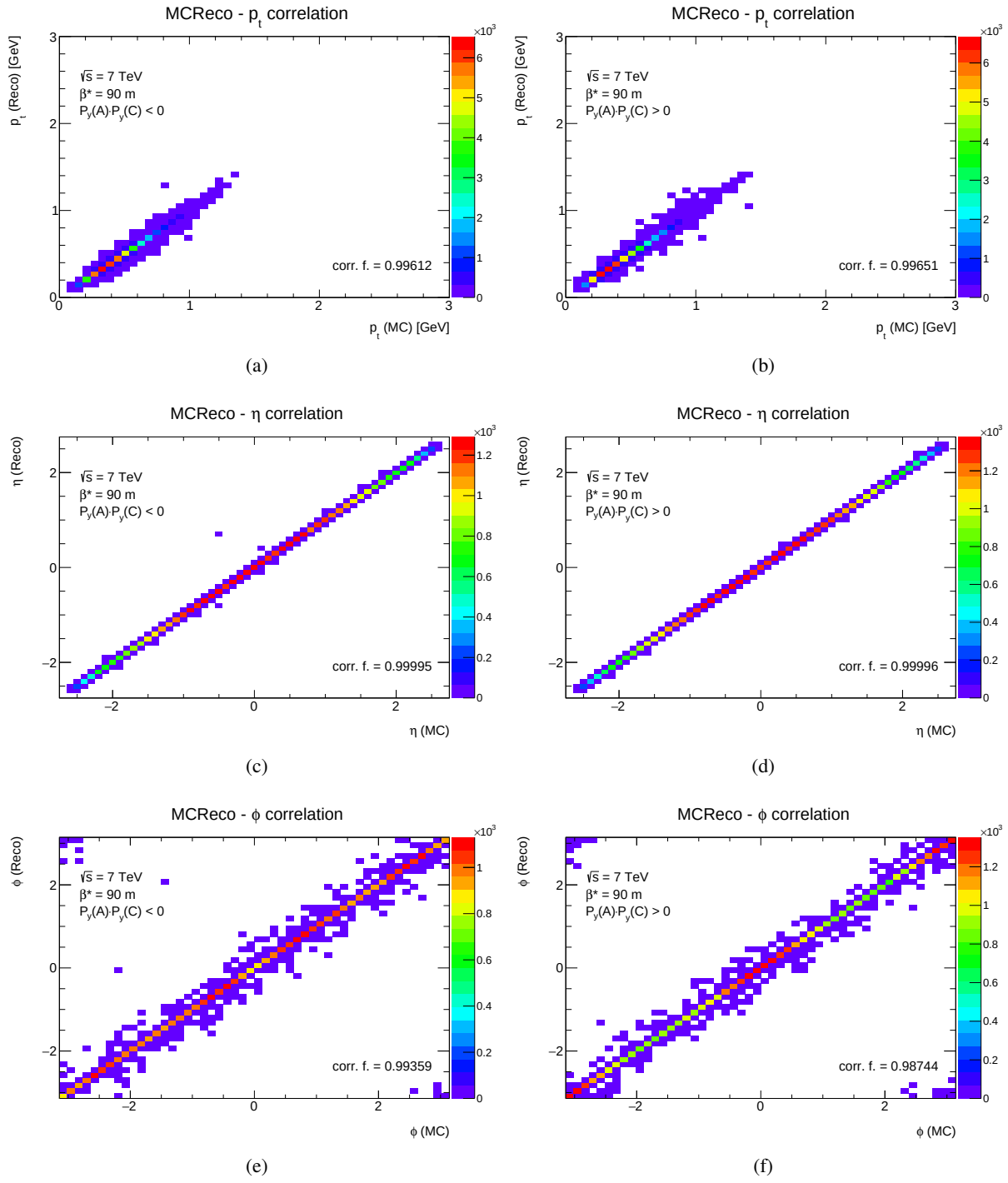

Figure 106: A set of control plots comparing a track on the particle level with a track on the detector level, on (a) and (b) for the pt_{trk} distribution, on (c) and (d) for the η_{trk} distribution and on (e) and (f) for the ϕ_{trk} distribution. The figures (a), (c) and (e) represent the analysis of the elastic configuration whereas the (b), (d) and (f) represent the analysis of the anti-elastic configuration. The figures are depicted after the ALFA track event selection.

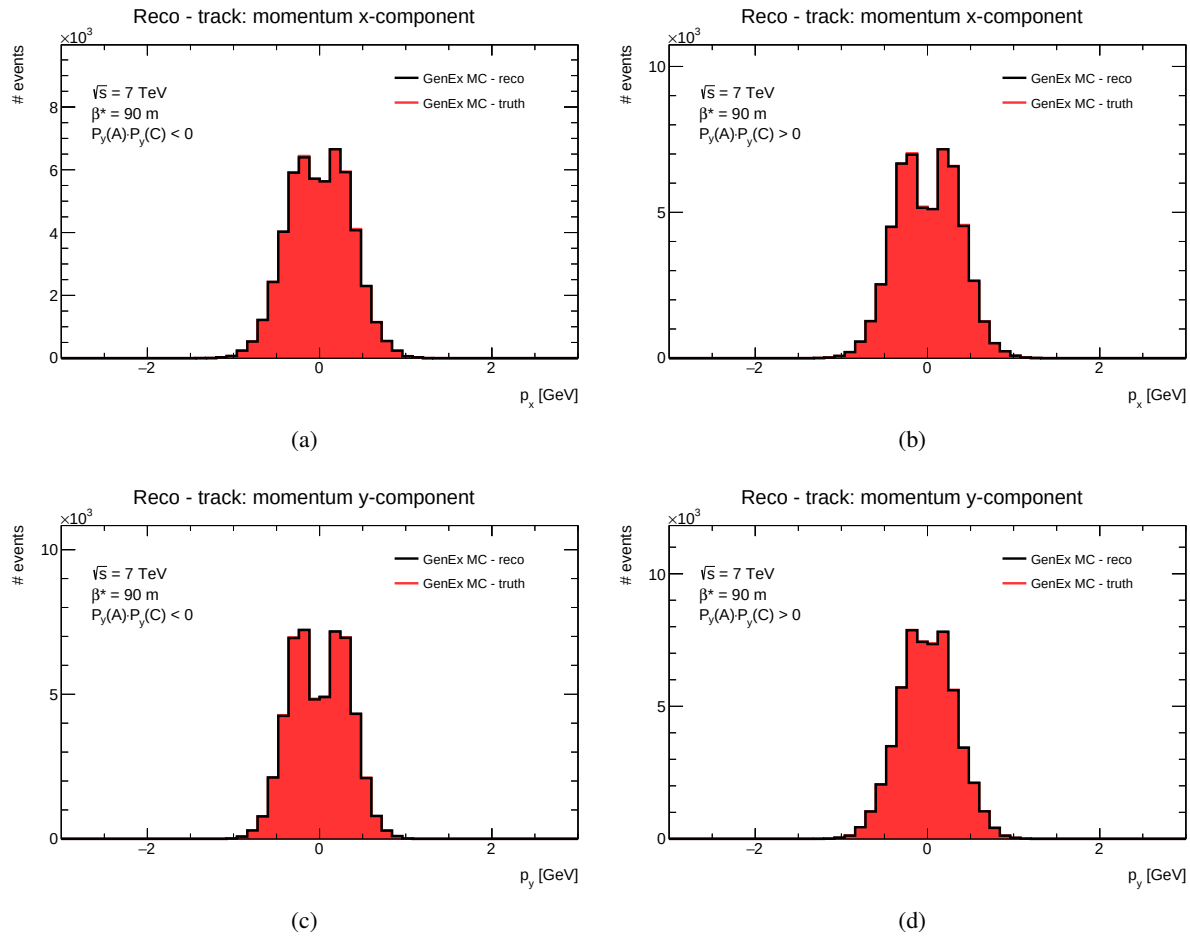

Figure 107: A comparison of the GenEx MC simulation distribution on the detector level (black histogram) with the particle level (red histogram) on (a, b) for the pion p_x, on (c, d) for the pion p_y for both the elastic configuration on (a, c) and the anti-elastic configuration on (b, d). The distributions are not normalized.

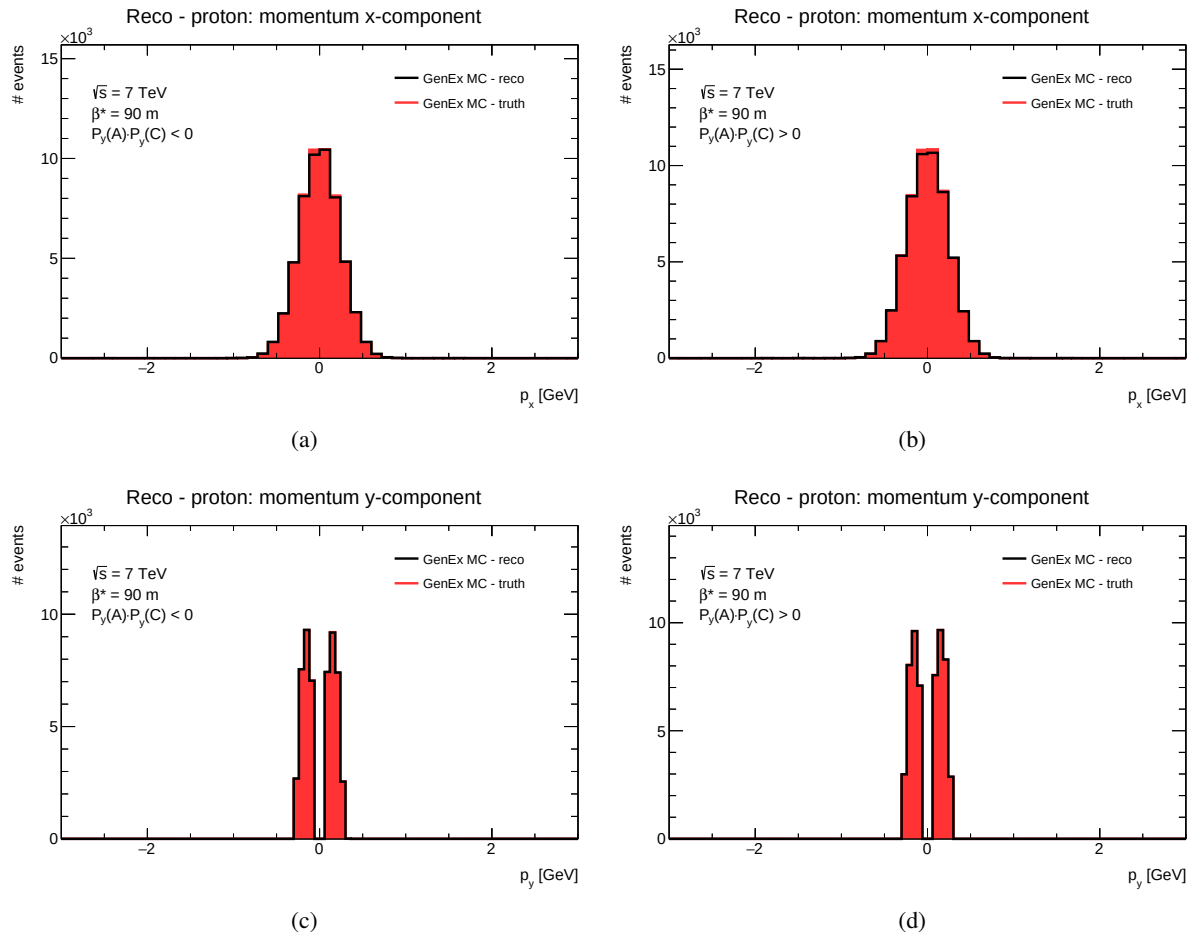

Figure 108: A comparison of the GenEx MC simulation distribution on the detector level (black histogram) with the particle level (red histogram) on (a, b) for the proton p_x, on (c, d) for the proton p_y for both the elastic configuration on (a, c) and the anti-elastic configuration on (b, d). The distributions are not normalized.

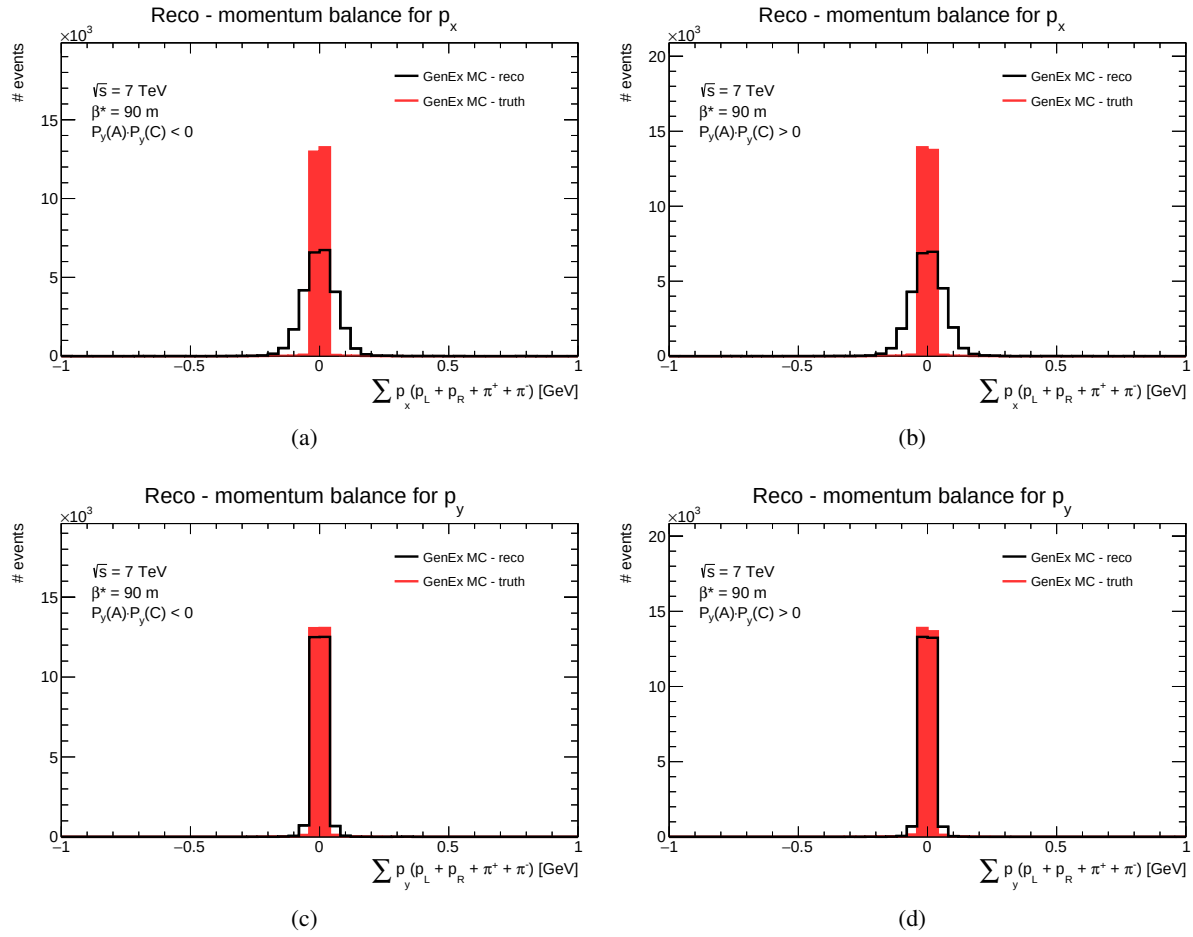

Figure 109: A comparison of the GenEx MC simulation distribution on the detector level (black histogram) with the particle level (red histogram) on (a, b) for the exclusive system p_x, on (c, d) for the exclusive system p_y for both the elastic configuration on (a, c) and the anti-elastic configuration on (b, d). The distributions are not normalized.

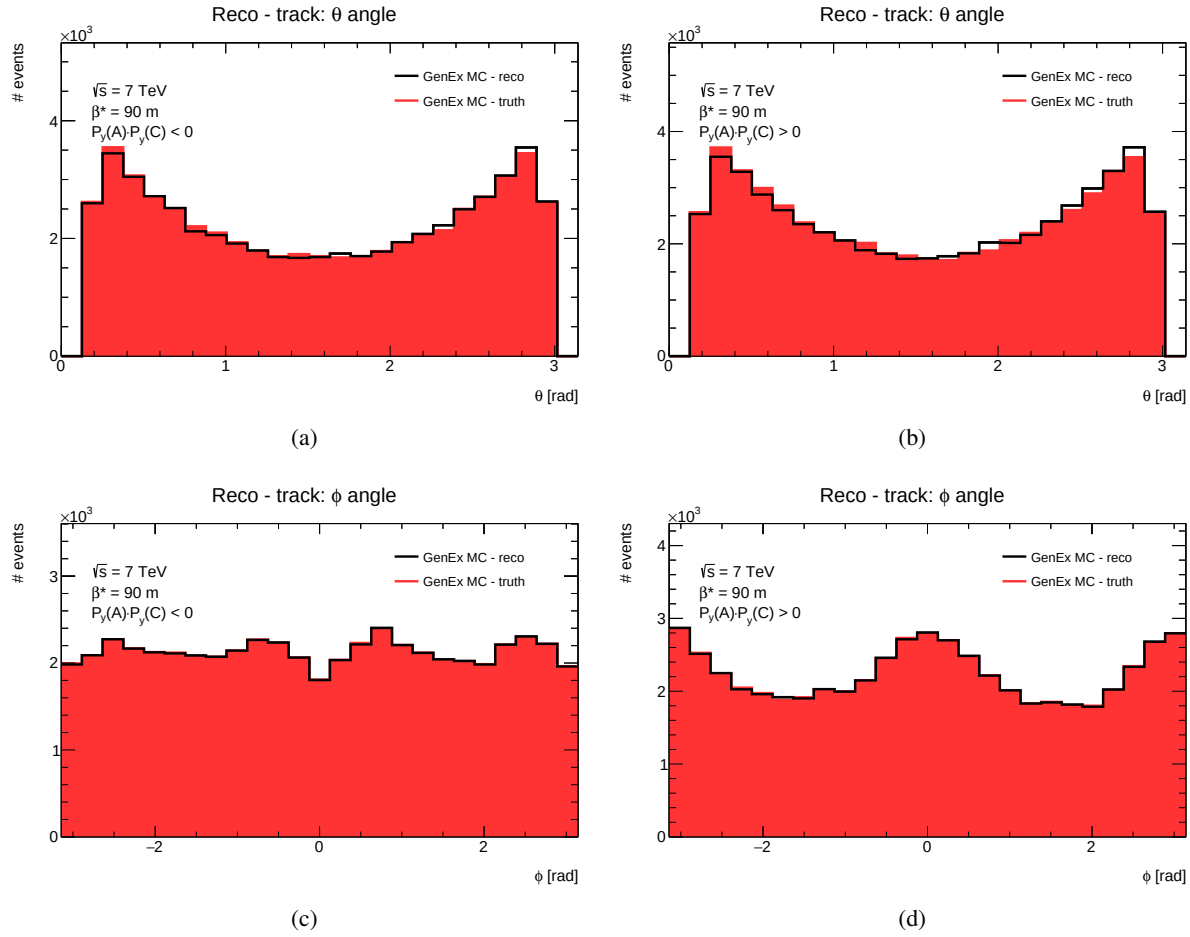

Figure 110: A comparison of the GenEx MC simulation distribution on the detector level (black histogram) with the particle level (red histogram) on (a, b) for the pion θ, on (c, d) for the pion ϕ for both the elastic configuration on (a, c) and the anti-elastic configuration on (b, d). The distributions are not normalized.

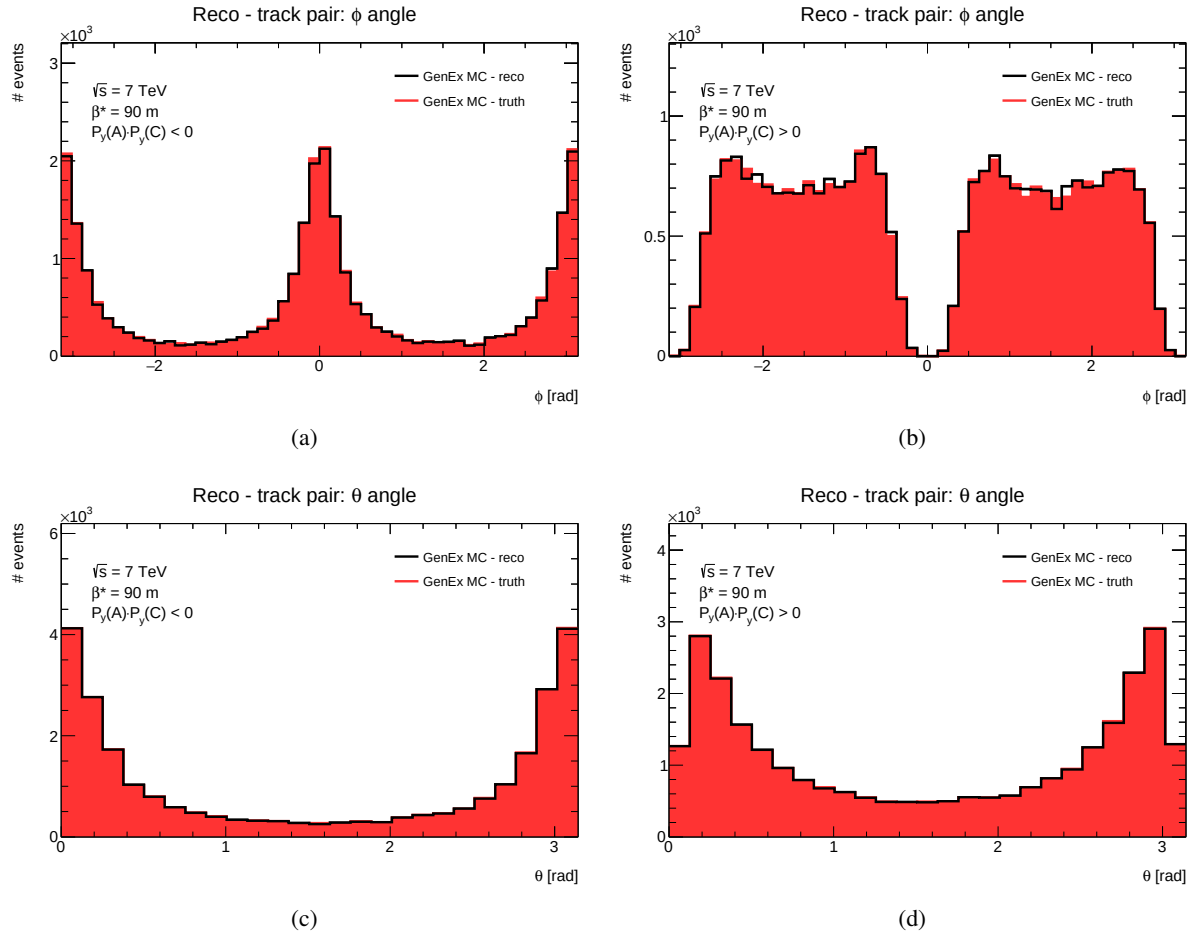

Figure 111: A comparison of the GenEx MC simulation distribution on the detector level (black histogram) with the particle level (red histogram) on (a, b) for the pion pair ϕ, on (c, d) for the pion pair θ for both the elastic configuration on (a, c) and the anti-elastic configuration on (b, d). The distributions are not normalized.

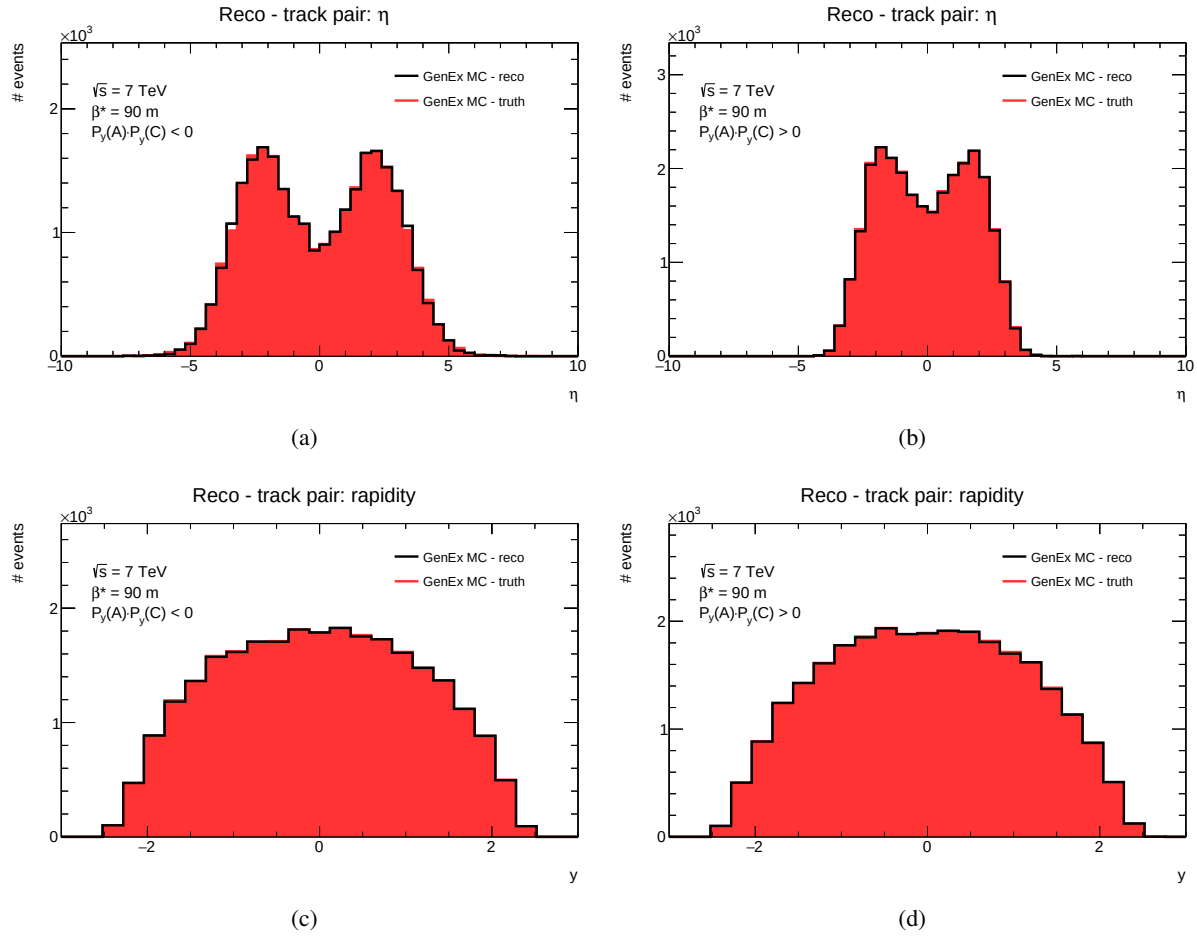

Figure 112: A comparison of the GenEx MC simulation distribution on the detector level (black histogram) with the particle level (red histogram) on (a, b) for the pion pair η, on (c, d) for the pion pair rapidity y for both the elastic configuration on (a, c) and the anti-elastic configuration on (b, d). The distributions are not normalized.

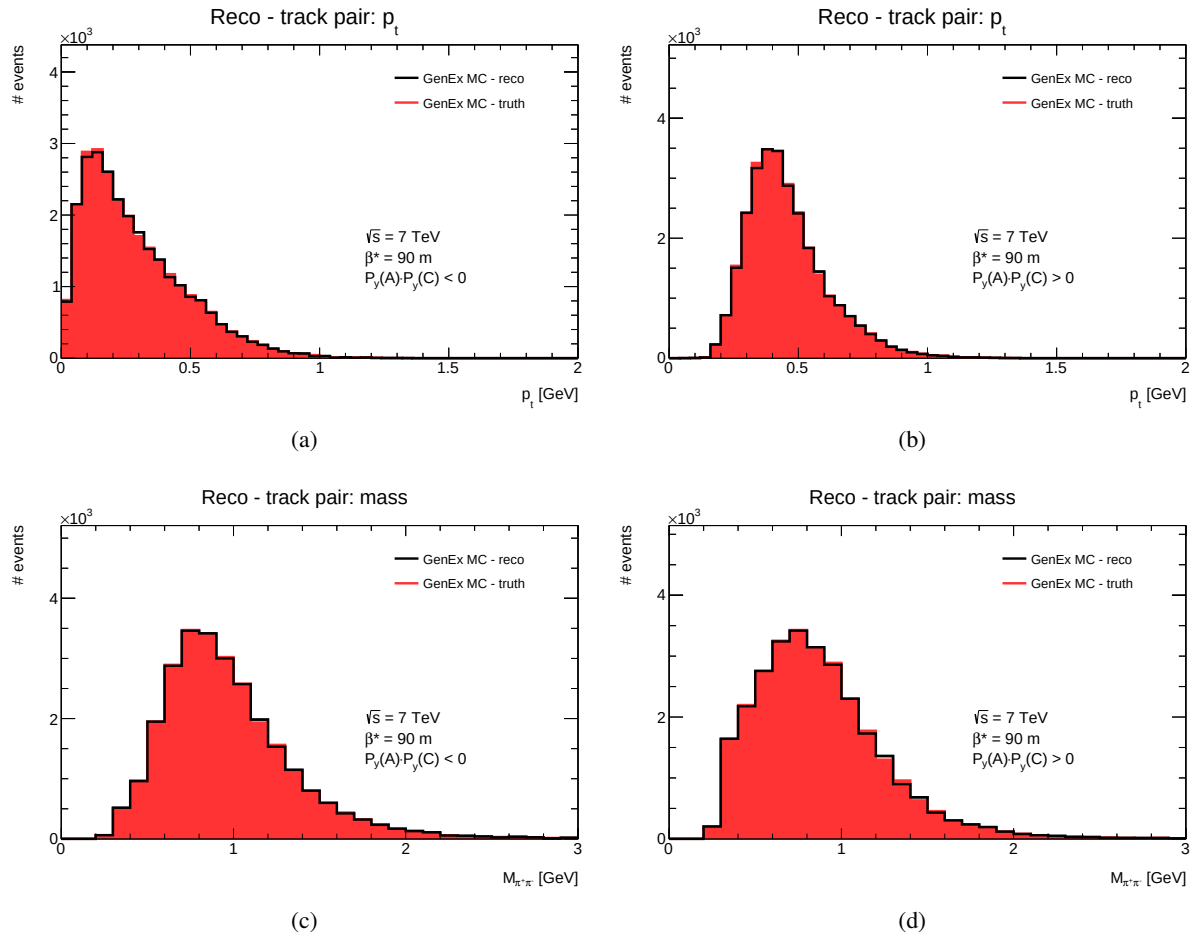

Figure 113: A comparison of the GenEx MC simulation distribution on the detector level (black histogram) with the particle level (red histogram) on (a, b) for the pion pair p_{t}, on (c, d) for the pion pair mass $M_{\pi^+\pi^-}$ for both the elastic configuration on (a, c) and the anti-elastic configuration on (b, d). The distributions are not normalized.

D.2. GenEx Monte Carlo simulation after analysis cut flow

This section describes the Monte Carlo simulation with GenEx generator after the whole cut flow which is described in Sect. 7. Again the analysis is done for the configurations, the elastic one and the anti-elastic one, which are in the case of the Monte Carlo simulation based on the ALFA detectors configuration. That two configurations are described in Sect. 7.5.

A first indicator how the analysis event selections work is the cut flow statistics. It is written in Table 42 and it describes the situation for the GenEx Monte Carlo simulation. The both ALFA Reco and Lattice methods are used as well as the both elastic and anti-elastic configurations. It is seen that a proton kinematic reconstruction resolution influence the two kinematic event selections $\sum p_x$ and $\sum p_y$. The fir results for that two distributions, the $\sum p_x$ and the $\sum p_y$ distribution, are written in Table 41. It is seen that the better kinematic resolution is obtained the less event after the cut flow survived. It is natural because the result of the kinematic resolution fit multiplied by $3.5\,\sigma$ is used as the exclusivity interval. All events outside the interval are removed from the analysis.

Table 42: The GenEx Monte Carlo simulation cut flow statistics for both proton kinematics reconstruction cases, the ALFA Reco method and the Lattice method. A difference is visible in the last two cuts where the fit results from Table 41 play a key role. The statistics for both the elastic and the anti-elastic configuration is included.

GenEx	configuration			
	elastic		anti-elastic	
	Lattice method	ALFA Reco method	Lattice method	ALFA Reco method
Initial number of events	1000000			
Inner detector selection	352781			
ALFA track selection	26563	26554	28047	26554
MBTS veto	26471	33387	26462	26462
ALFA geometry selection	26387	26389	27826	26386
Kinematic cut $\sum p_y$	26097	26100	27552	26087
Kinematic cut $\sum p_x$	25949	25994	27394	22294
Particle identification ($M_{dE/dx}$)	24787	24829	26234	21270
Kinematic region cut	23625	23597	25216	20333

Now let us move to a set of the distributions describing the events selected by the analysis cut flow. That distributions focus on the following pion pair kinematics, the azimuth angle $\phi_{\pi^+\pi^-}$, the polar angle $\theta_{\pi^+\pi^-}$, the pseudo-rapidity $\eta_{\pi^+\pi^-}$, the rapidity $y_{\pi^+\pi^-}$, the transverse momentum $pt_{\pi^+\pi^-}$ and the invariant mass $M_{\pi^+\pi^-}$. That distributions are depicted on Figs. 114–116 for the GenEx Monte Carlo simulation after the cut flow. They describe a behaviour of the di-pion system from the kinematic point of view. The GenEx generates only the pion continuum therefore no resonance impact should be seen in the distributions.

The $\phi_{\pi^+\pi^-}$ distribution of the exclusive pion system should be a flat distribution if no selection criterion is applied. But the Figs. 114a and 114b show a different shape of that distributions. This is caused by a proton tagging in the ALFA detectors, some $\phi_{\pi^+\pi^-}$ directions are preferred more then the other ones. The

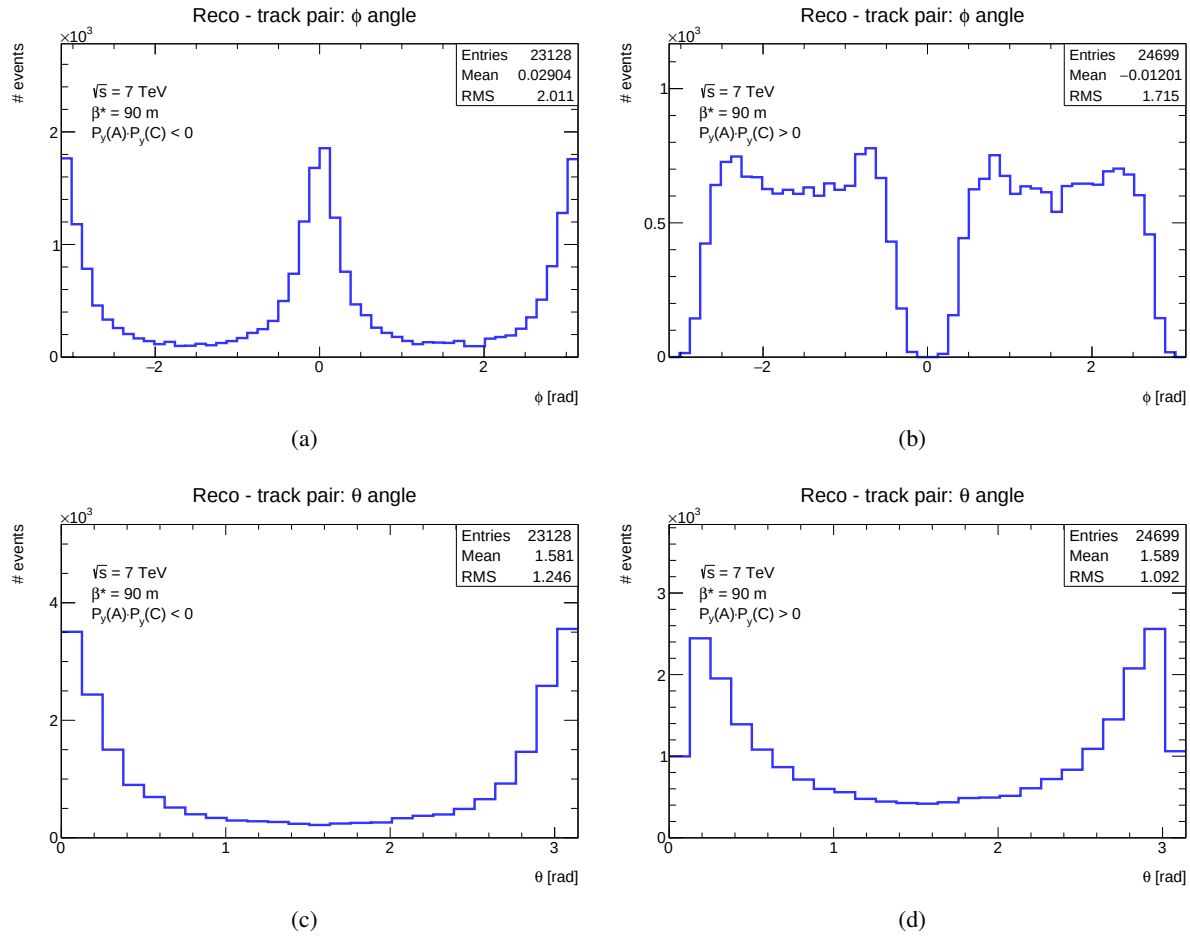

Figure 114: The azimuthal angle $\phi_{\pi^+\pi^-}$ and the polar angle $\theta_{\pi^+\pi^-}$ distributions of the exclusive pion system represented by the di-pion kinematics. On (a) and (c) for the elastic configuration whereas on (b) and (d) for the anti-elastic configuration.

same behaviour can be seen later in Sect. D.5 for the PYTHIA8 Monte Carlo simulation and in Sect. 10.1 for the data analysis.

The rapidity distributions on Figs. 115c and 115d show the centrality of the exclusive system. This centrality does not depend on the ALFA trigger or the ALFA detector configurations, elastic one or anti-elastic one.

It was mentioned in Sect. D.1 that the exclusive pion production looks like the elastic one on the side of the ALFA detectors. This fact could be supported by the distributions of the exclusive pion invariant mass which are depicted on Figs. 116c and 116d. It is seen that the most of the central system mass is within 2 GeV. This is a very low mass fraction which two protons keep in the central system after a collision. Therefore this process would be a kind of the background for the analysis of the elastically scattered protons. The low limit of the invariant mass of the exclusive central system is defined by the mass of the particles forming that central system, here the low limit is defined by the mass of two charged pions.

It was mentioned that the GENEX generates only the continuum of the exclusive pion production therefore

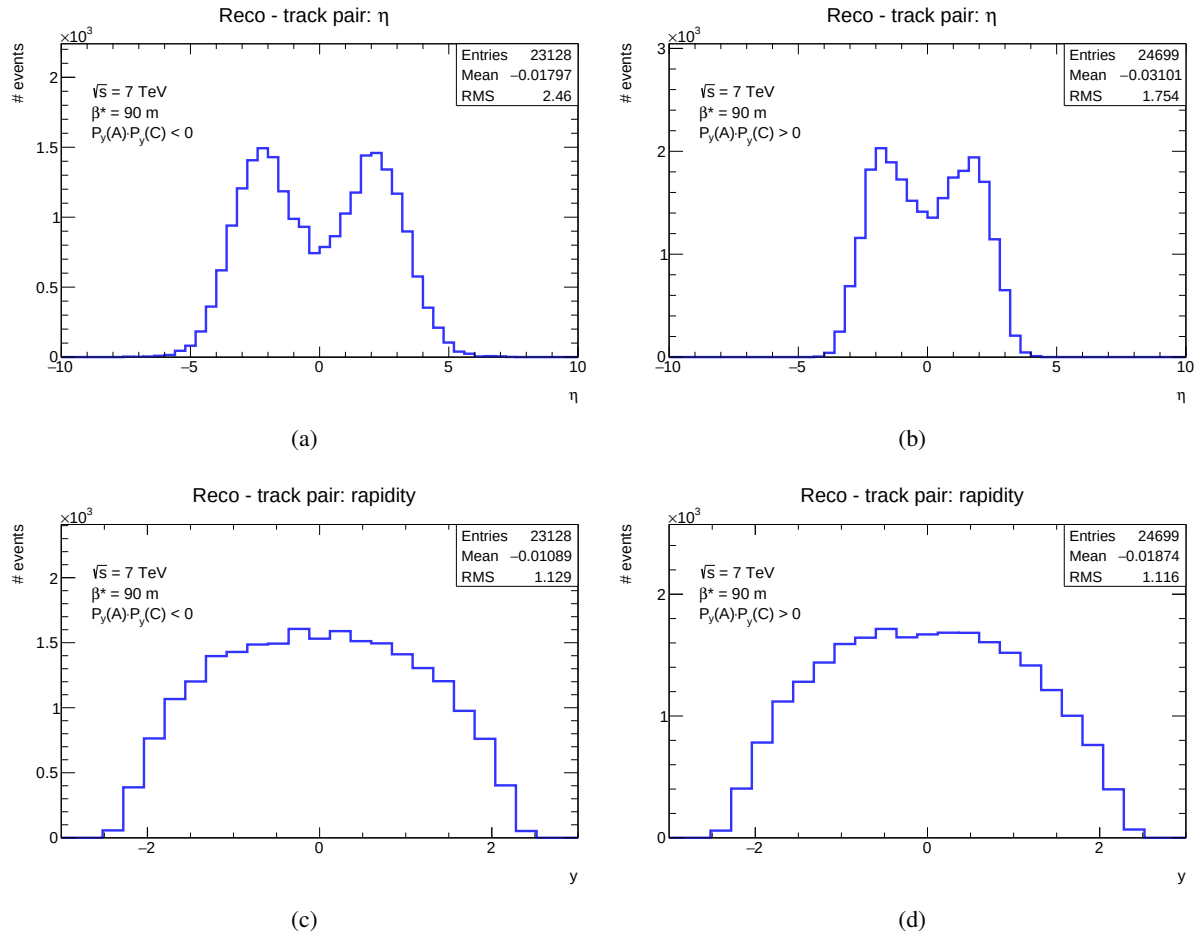

Figure 115: The pseudo-rapidity $\eta_{\pi^+\pi^-}$ and the rapidity $y_{\pi^+\pi^-}$ distributions of the exclusive pion system represented by the di-pion kinematics. On (a) and (c) for the elastic configuration whereas on (b) and (d) for the anti-elastic configuration.

no potential resonances are visible in the invariant mass distribution[10].

In the Monte Carlo simulation the identity of the particle reconstructed by the ATLAS Inner detector is known. The particle identification in data is more tricky. But there is some possibility which is based on the ionisation losses $\mathrm{d}E/\mathrm{d}x$ of the particle going among the Inner detector described by Bethe-Bloch formula. for the purpose of this analysis the information about $M_{\mathrm{d}E/\mathrm{d}x}$, which brings the particle mass and its ionisation losses together, is used. The $\mathrm{d}E/\mathrm{d}x$ measurement is described in detail in [43].

The particle identification is a part of the analysis event selection. In the case of the GenEx Monte Carlo simulation it makes no sense to use it because all the tracks reconstructed by the ATLAS Inner detector are the pion ones. But in data it plays a significant role in the event selection and background subtraction. The reason why this particle identification is studied in the MC simulation is simple. One has to know how many exclusive events from the signal are removed by this event selection to be able calculate an

[10] At present the exclusive pion process is not fully understand at the energies of LHC. There exists some model and generators of this exclusive production but all of them focus only on the exclusive pion continuum. There is no one which deals with a potential resonances like $f_2(1270)$

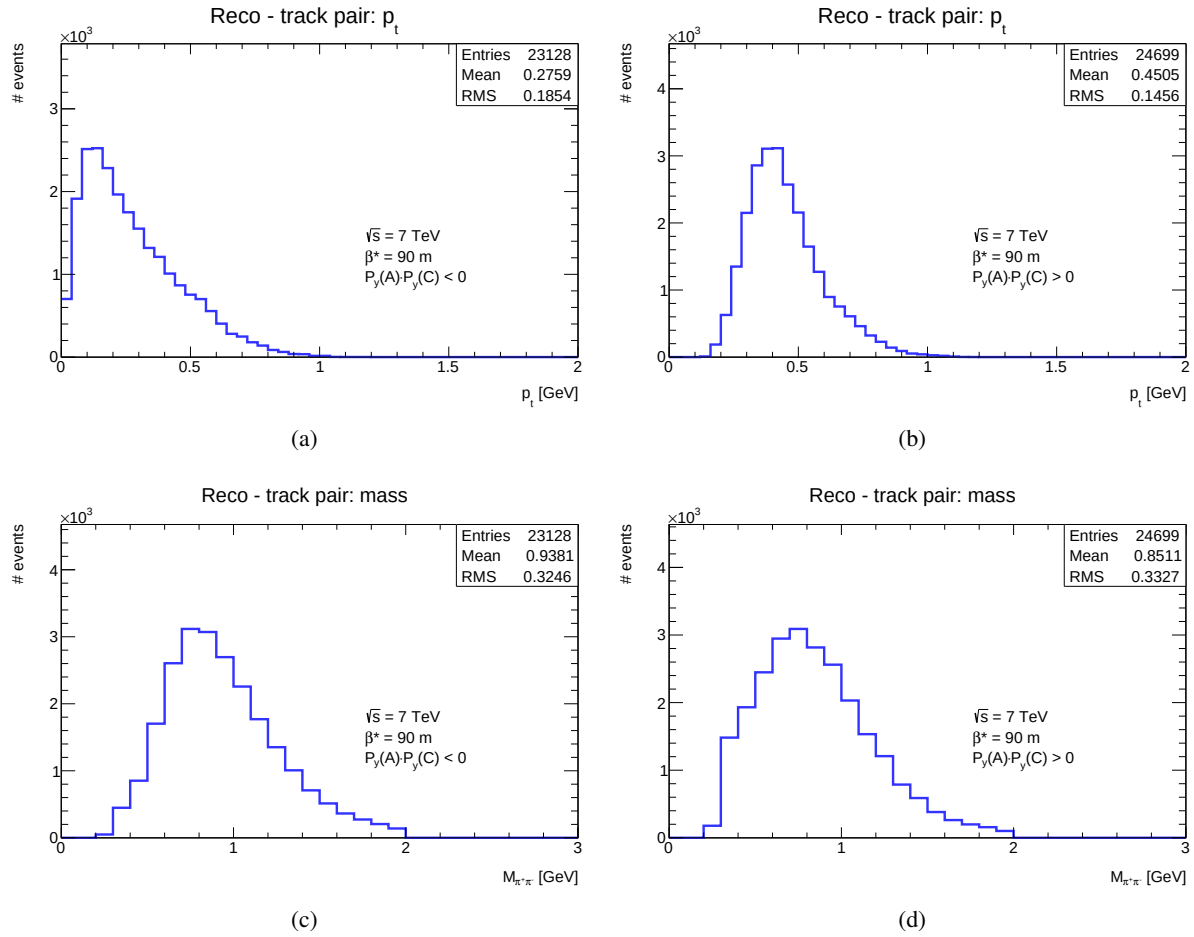

Figure 116: The transverse momentum $pt_{\pi^+\pi^-}$ and the invariant mass $\theta_{\pi^+\pi^-}$ distributions of the exclusive pion system represented by the di-pion kinematics. On (a) and (c) for the elastic configuration whereas on (b) and (d) for the anti-elastic configuration.

appropriate correction which is later used on data results to correct a signal loss there. Therefore some control plots for the particle identification were done also for the GenEx Monte Carlo simulation after the event selections. These plots are depicted on Fig. 117 which describes the situation for both the elastic and the anti-elastic configurations.

For the purpose of the exclusive pion production analysis the upper limit of the $M_{\mathrm{d}E/\mathrm{d}x}$ was set to 0.25 GeV, for more details please see Sect. 7.9. This is a safe limit to eliminate the particles like kaons or protons with higher masses then pion mass. On one side this is the safe limit, on the other side the $M_{\mathrm{d}E/\mathrm{d}x}$ reconstruction has a non zero imperfection thus a tiny amount of pions is removed too.

The Fig. 117 depicts a $M_{\mathrm{d}E/\mathrm{d}x}$ distribution after the cut flow, but before the last cut on $M_{\mathrm{d}E/\mathrm{d}x}$. It is seen that the main fraction of pions is situated below the threshold of 0.25 GeV. There is also some amount of pions above this threshold which is removed by the particle identification cut described in Sect. 7.9. This signal loss is included in the corrections, i.e. described in Sect. 8.

The Figs. 117a and 117b depict the $M_{\mathrm{d}E/\mathrm{d}x}$ distribution itself. The blue histogram is represented by the positive pions whereas the red histogram is represented by the negative pions. The distributions for both

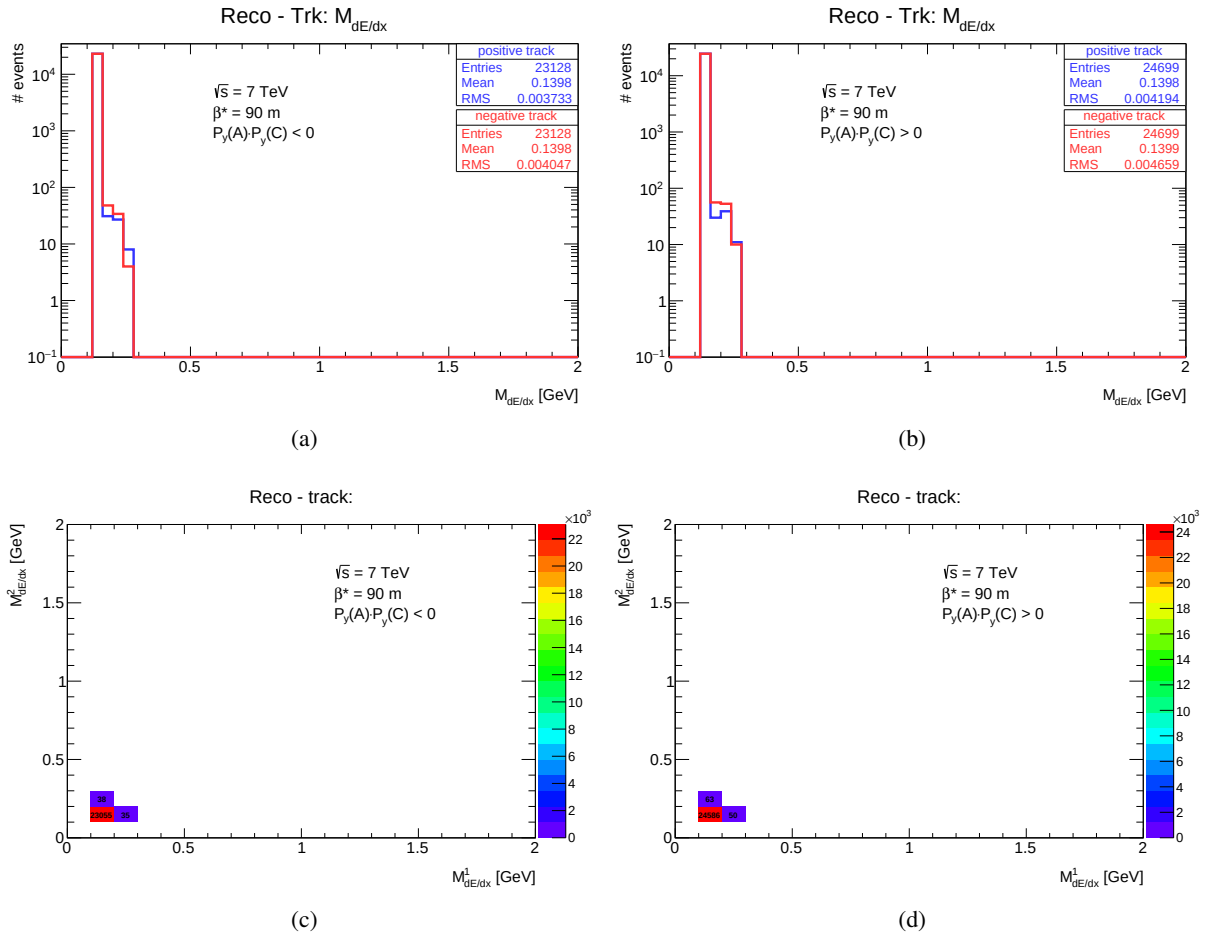

Figure 117: The distribution of the track mass $M_{\mathrm{dE/dx}}$ calculated from the track ionisation losses in the ATLAS Pixel detector on (a,b) and the correlation of the $M_{\mathrm{dE/dx}}$ between two charged tracks on (c, d) for both elatic configuration (a,c) and the anti-elastic configuration (b,d). The distributions are depicted after the analysis cut flow therefore a sharp cut around 0.25 GeV is visible.

the positive and the negative pions have a similar shape. The Figs. 117c and 117d depict the $M_{\mathrm{d}E/\mathrm{d}x}$ correlation between both pions creating the exclusive central system.

A comparison of the distribution on the particle level (for the generated tracks - sometime known as a truth level) with a distribution on the detector level (for the reconstructed tracks - sometime known as a reconstructed level) is also performed for the final events selection - after the analysis - to see the effects of the detector systems as well as the effects of the events selection. The comparison is performed for the basic pions and protons distributions as well as for the pion pair distributions for both the elastic and the anti-elastic configuration. The distributions are not normalized. The total number of entries in the histogram is the same for both the detector level and the particle level distributions. Therefore it can be seen how well the distributions on detector level describe the distributions on particle level. Some differences are visible for the kinematic distributions p_{x} and p_{y} of the exclusive system. These differences are caused by the detectors resolution together with a combination of the exclusive products. Even if the basic distributions for protons and pions do not show a big differences between the detector level and the particle level, their combination into the system distribution is influenced quite well. All the distributions

are depicted in Figs. 118 and 124.

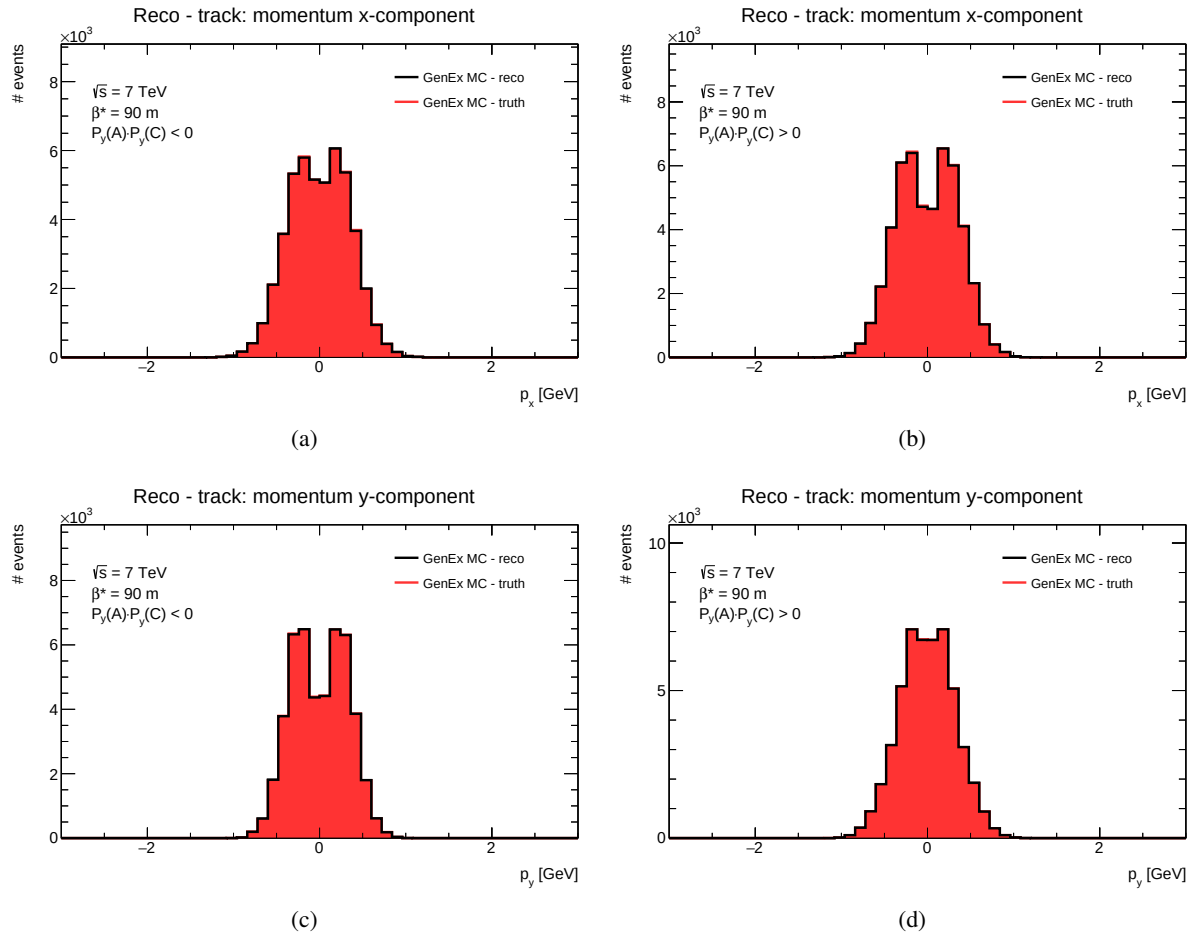

Figure 118: A comparison of the GenEx MC simulation distribution on the detector level (black histogram) with the particle level (red histogram) on (a, b) for the pion p_x, on (c, d) for the pion p_y for both the elastic configuration on (a, c) and the anti-elastic configuration on (b, d). The distributions are not normalized.

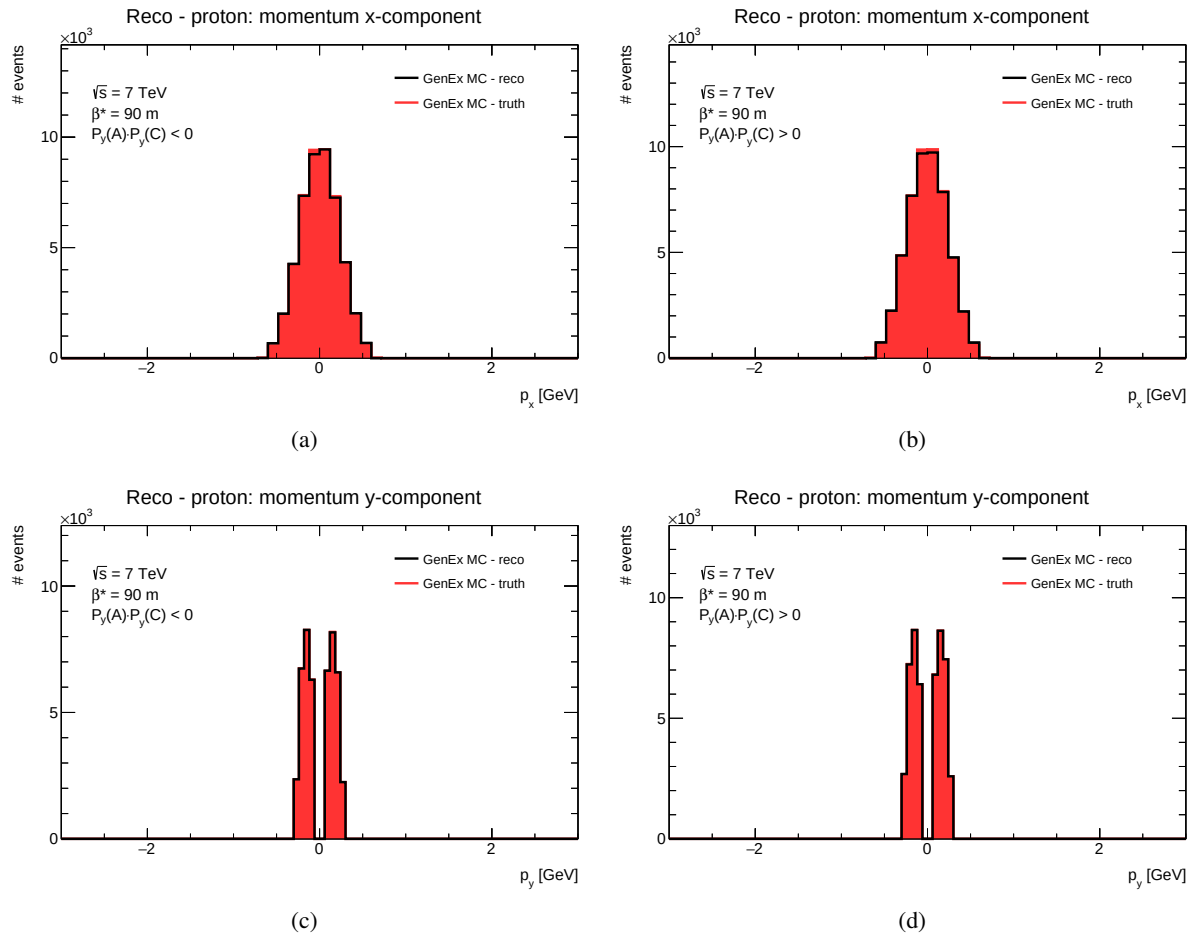

Figure 119: A comparison of the GenEx MC simulation distribution on the detector level (black histogram) with the particle level (red histogram) on (a, b) for the proton p_x, on (c, d) for the proton p_y for both the elastic configuration on (a, c) and the anti-elastic configuration on (b, d). The distributions are not normalized.

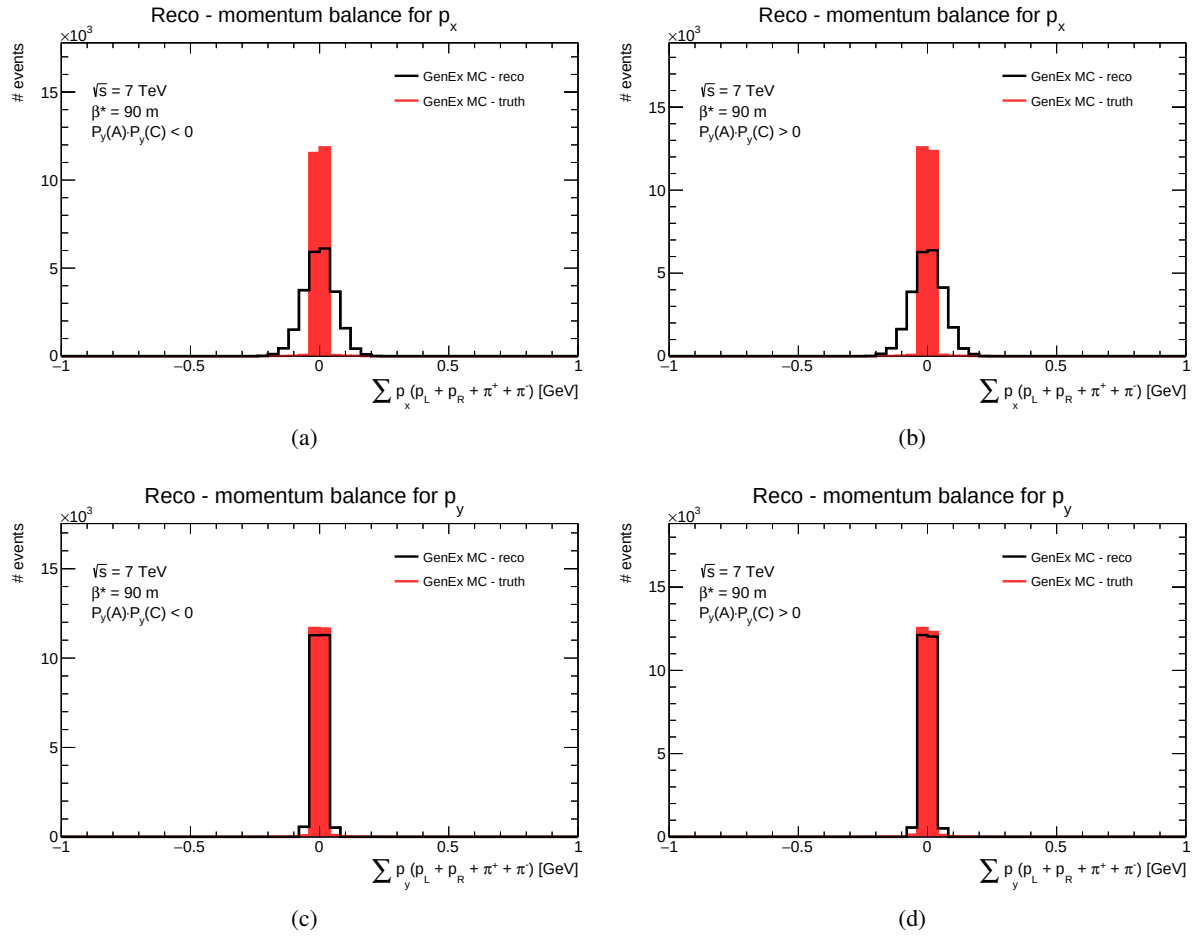

Figure 120: A comparison of the GenEx MC simulation distribution on the detector level (black histogram) with the particle level (red histogram) on (a, b) for the exclusive system p_x, on (c, d) for the exclusive system p_y for both the elastic configuration on (a, c) and the anti-elastic configuration on (b, d). The distributions are not normalized.

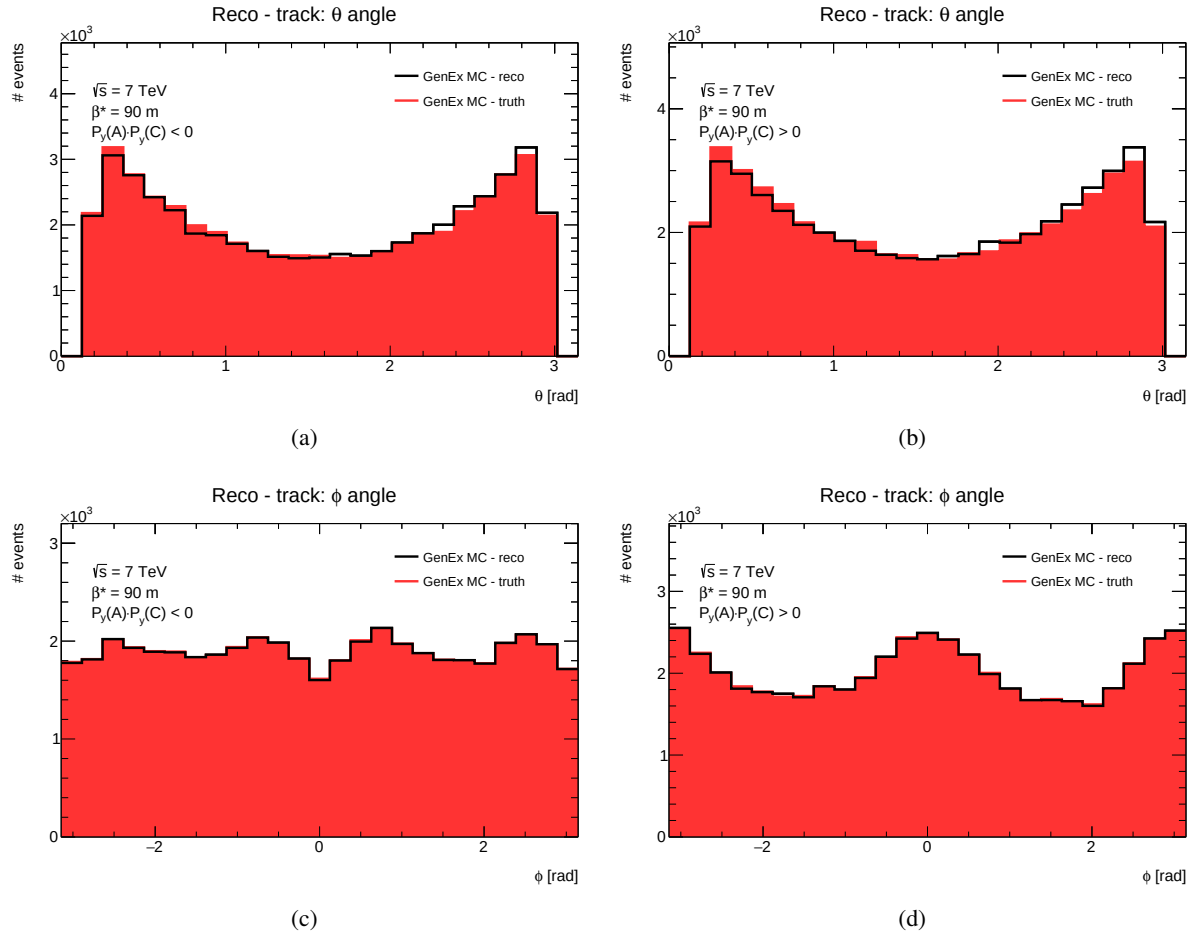

Figure 121: A comparison of the GenEx MC simulation distribution on the detector level (black histogram) with the particle level (red histogram) on (a, b) for the pion θ, on (c, d) for the pion ϕ for both the elastic configuration on (a, c) and the anti-elastic configuration on (b, d). The distributions are not normalized.

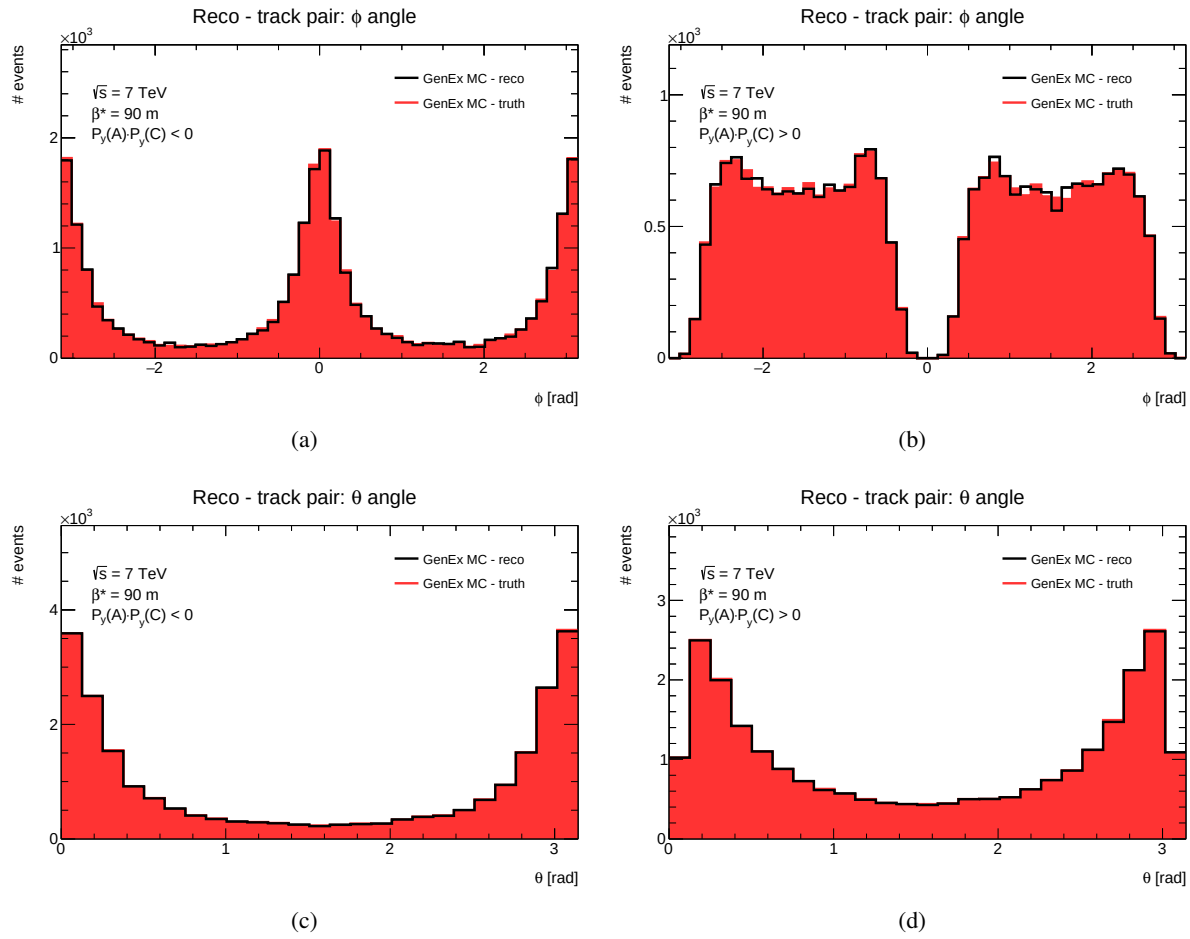

Figure 122: A comparison of the GenEx MC simulation distribution on the detector level (black histogram) with the particle level (red histogram) on (a, b) for the pion pair ϕ, on (c, d) for the pion pair θ for both the elastic configuration on (a, c) and the anti-elastic configuration on (b, d). The distributions are not normalized.

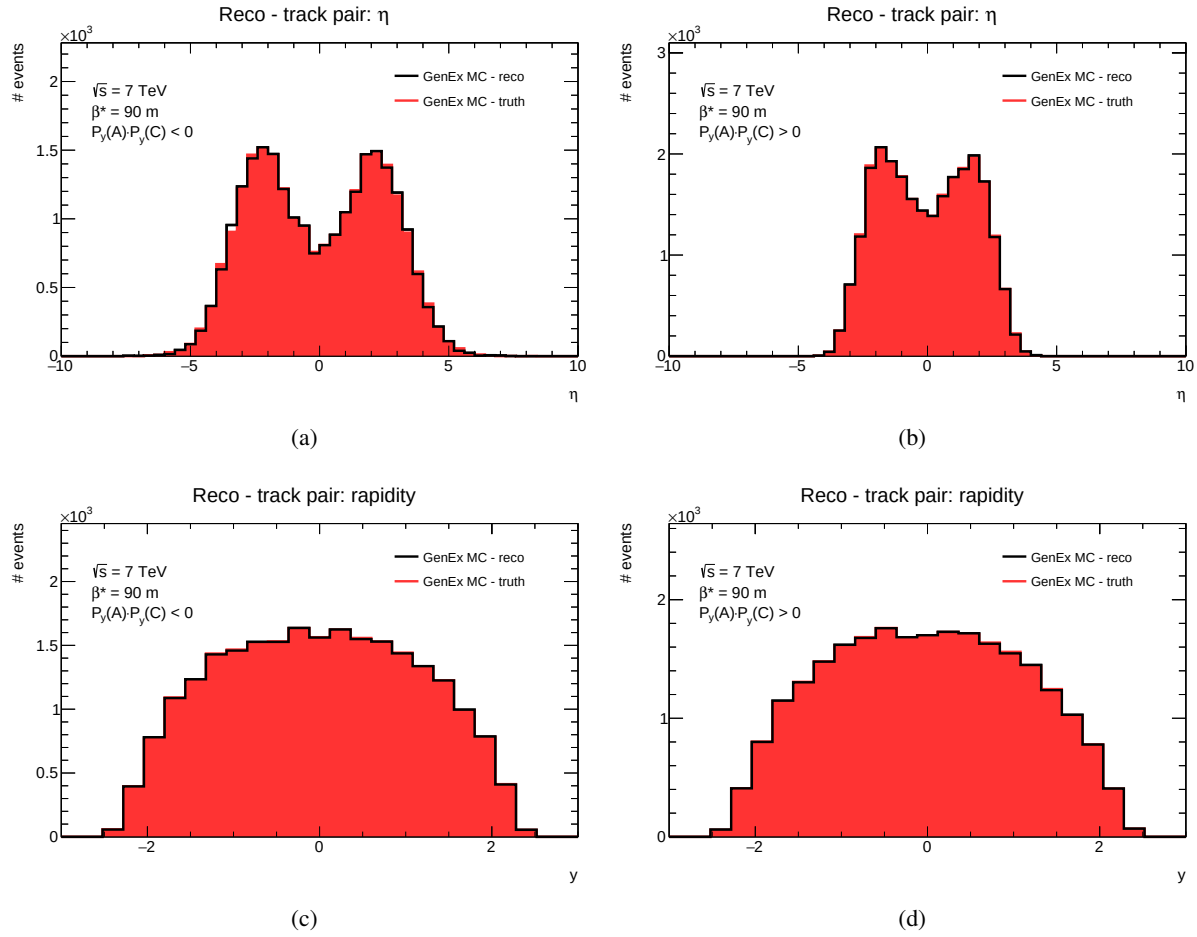

Figure 123: A comparison of the GenEx MC simulation distribution on the detector level (black histogram) with the particle level (red histogram) on (a, b) for the pion pair η, on (c, d) for the pion pair rapidity y for both the elastic configuration on (a, c) and the anti-elastic configuration on (b, d). The distributions are not normalized.

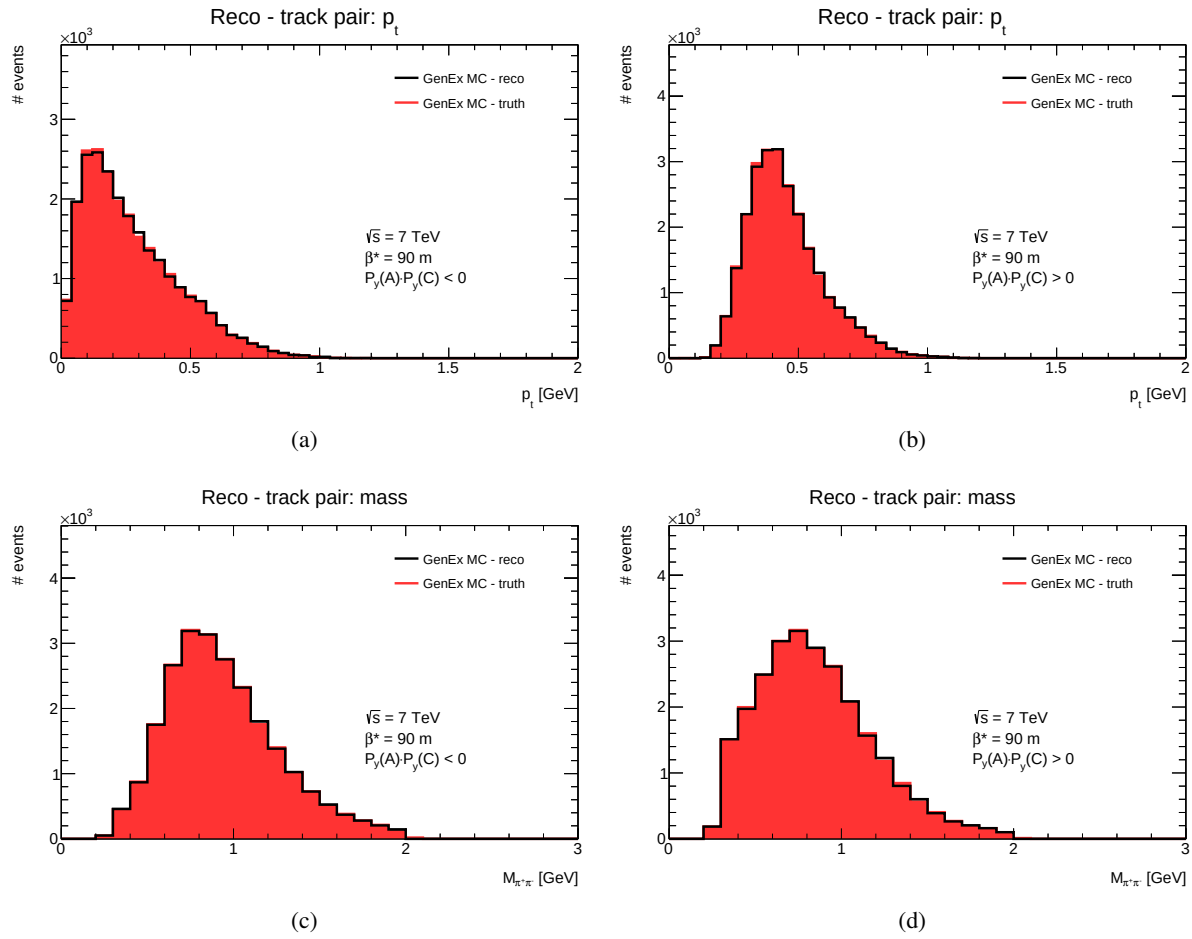

Figure 124: A comparison of the GenEx MC simulation distribution on the detector level (black histogram) with the particle level (red histogram) on (a, b) for the pion pair p_{t}, on (c, d) for the pion pair mass $M_{\pi^+\pi^-}$ for both the elastic configuration on (a, c) and the anti-elastic configuration on (b, d). The distributions are not normalized.

D.3. An effect of the analysis chain on GenEx distributions

The section summarizes an effect of the analysis chain used in the exclusive pion analysis. The results are presented by a set of the figures. Each figure depicts one distribution after each event selection. All the figures are performed on the MC simulation related to the GenEx generator which is a default exclusive pion generator of the exclusive pion analysis at 7 TeV. The figures show what event selection has the biggest impact on the statistics. The histograms of a selected distribution are very similar with the almost the same statistics expect the histograms related to the kinematics event selections where a decreasing of the event statistics is visible.

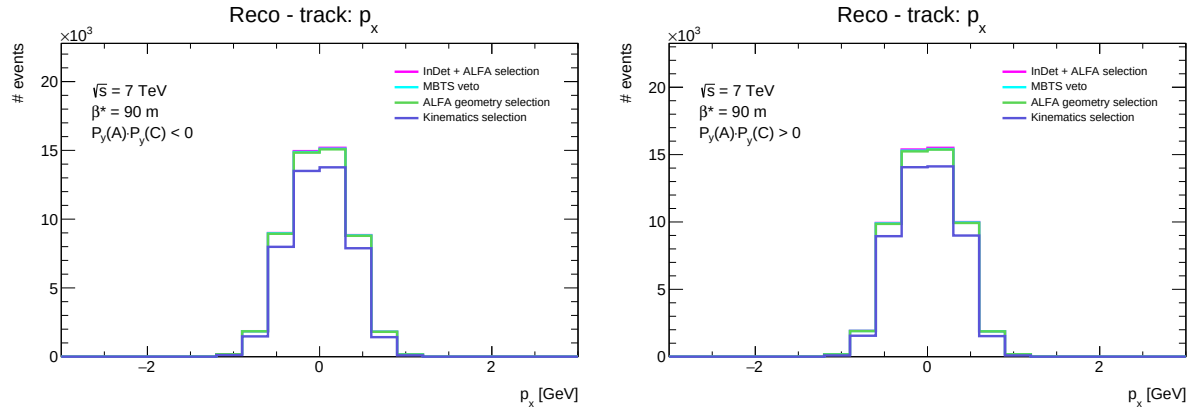

(a)

(b)

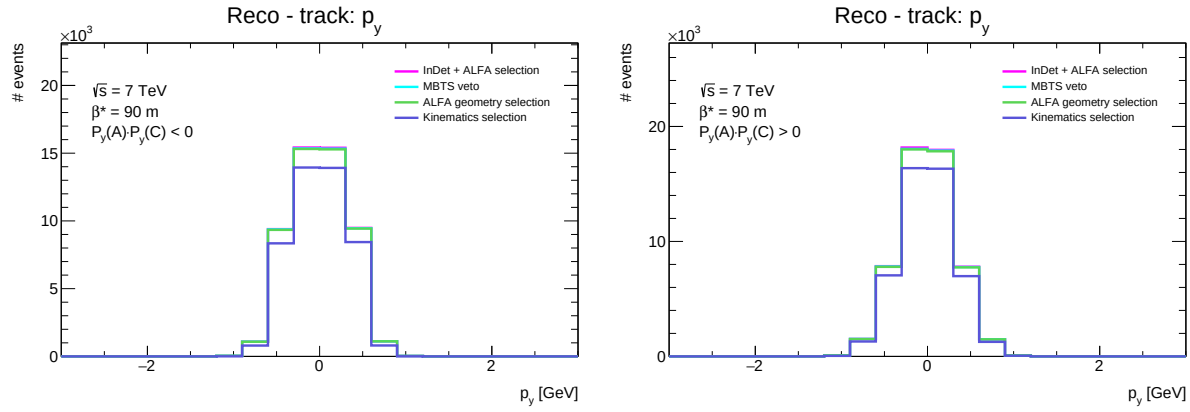

(c)

(d)

Figure 125: The p_x distribution (a,b) and the p_y distribution (c,d) of the track reconstructed in the Inner detector for various event selections, on (a,c) for the elastic configuration, on (b,d) for the anti-elastic configuration, performed on the GenEx MC simulation.

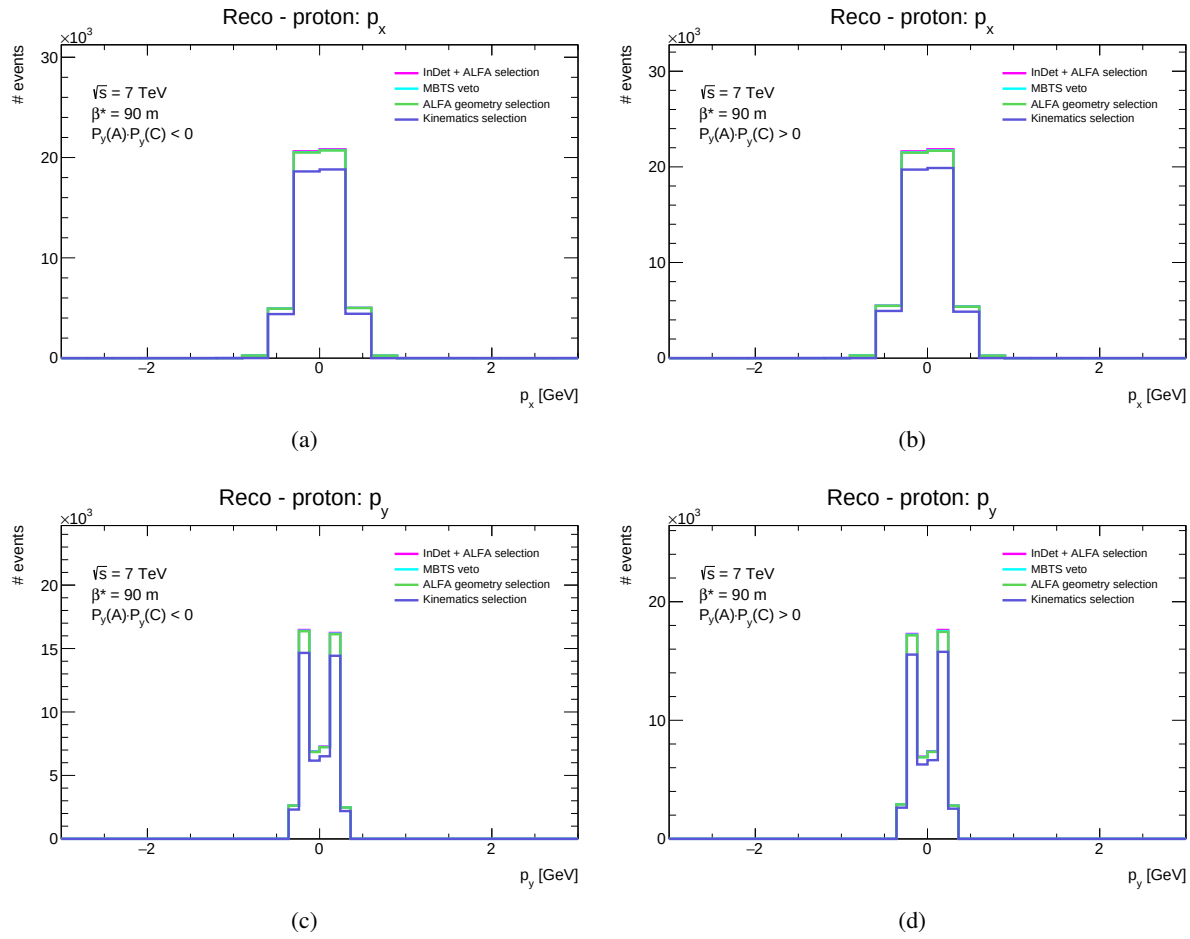

Figure 126: The p_x distribution (a,b) and the p_y distribution (c,d) of the proton reconstructed in the ALFA detector for various event selections, on (a,c) for the elastic configuration, on (b,d) for the anti-elastic configuration, performed on the GenEx MC simulation.

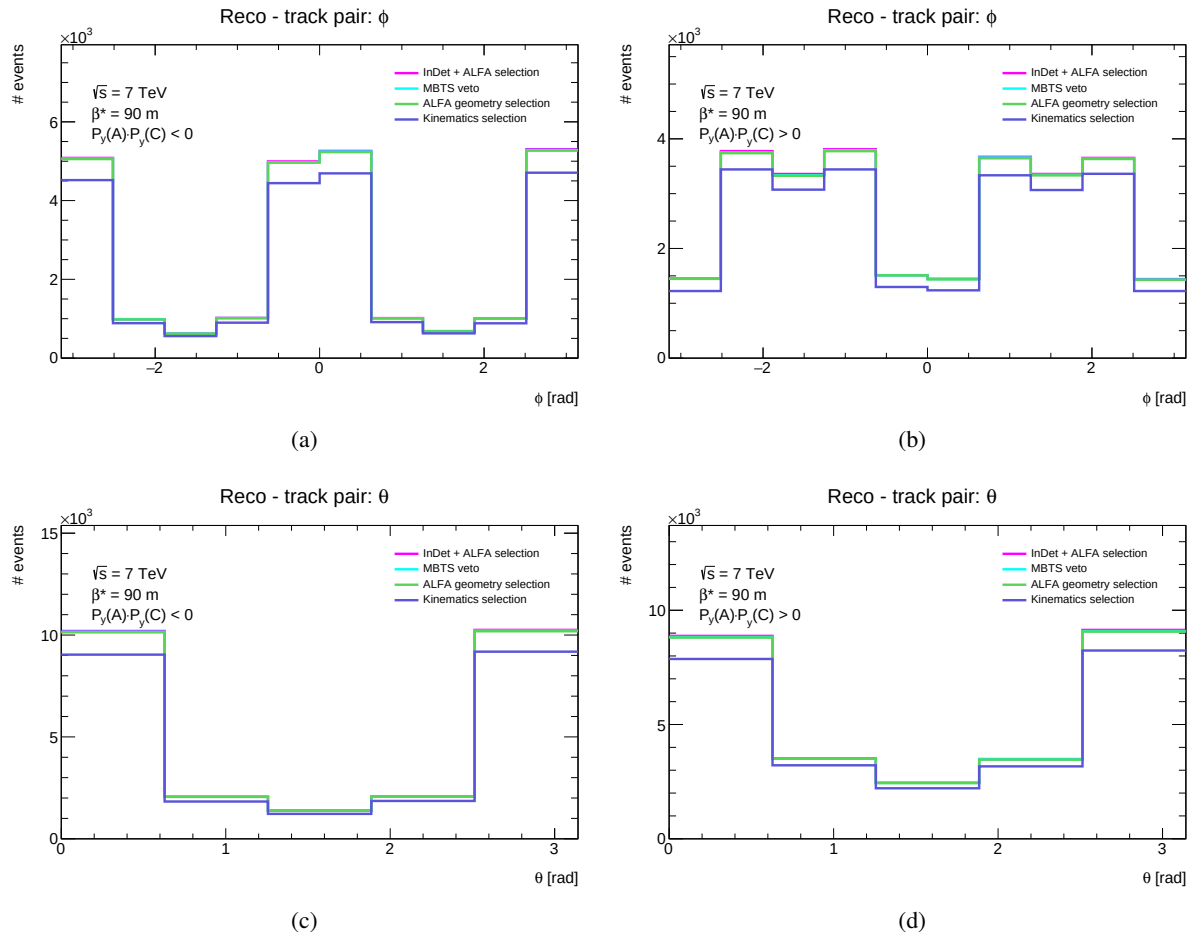

Figure 127: The pion pair ϕ distribution (a,b) and the θ distribution (c,d) for various event selections, on (a,c) for the elastic configuration, on (b,d) for the anti-elastic configuration, performed on the GenEx MC simulation.

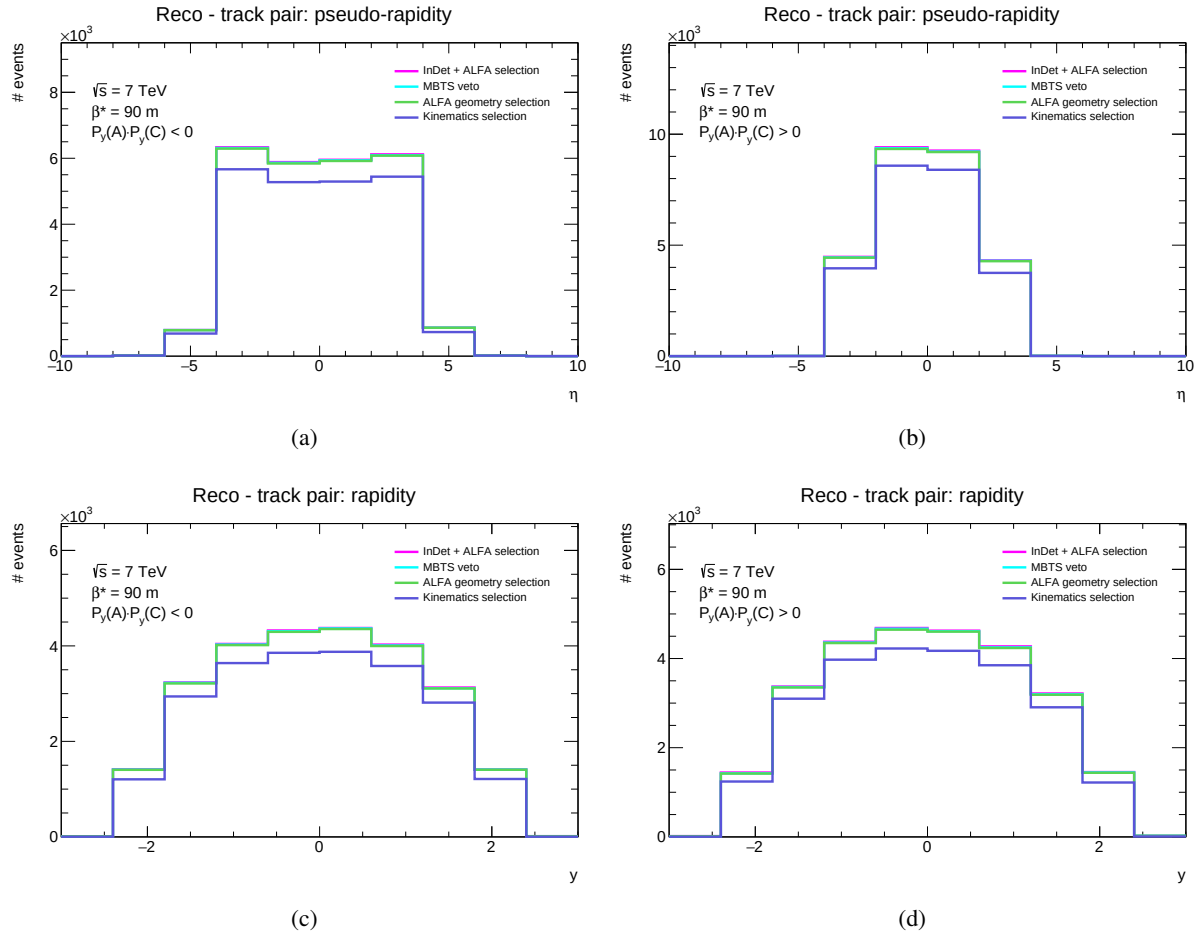

Figure 128: The pion pair pseudo-rapidity η distribution (a,b) and the rapidity distribution (c,d) for various event selections, on (a,c) for the elastic configuration, on (b,d) for the anti-elastic configuration, performed on the GenEx MC simulation.

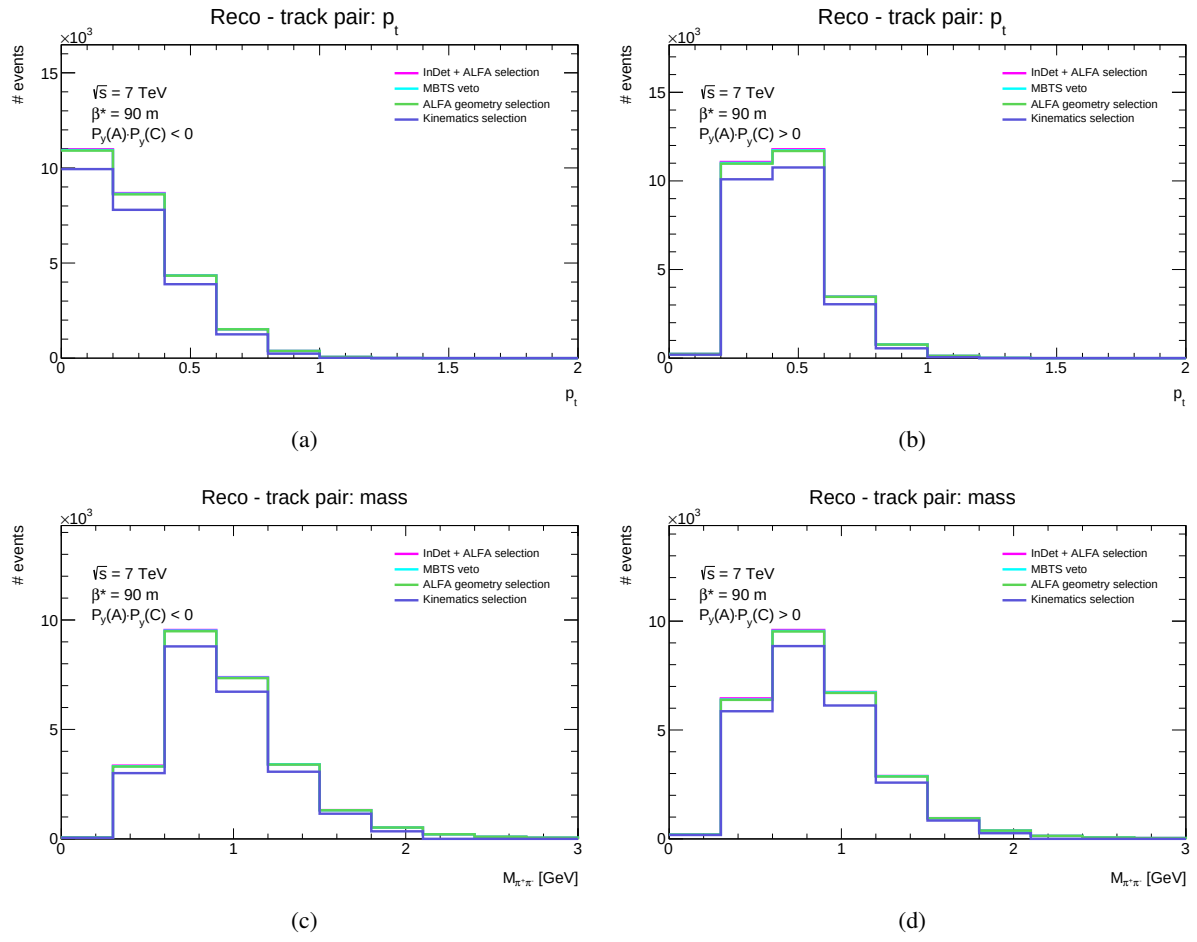

Figure 129: The pion pair pseudo-rapidity η distribution (a,b) and the rapidity distribution (c,d) for various event selections, on (a,c) for the elastic configuration, on (b,d) for the anti-elastic configuration, performed on the GenEx MC simulation.

D.4. GenEx and DiMe distribution comparison

The default MC signal simulation used in this exclusive pion analysis is performed on the events generated by the GenEx generator. Such simulation is used for the data analysis, all the event selections are based on that simulation, and thus the data analysis may be biased with the behaviour and the properties of the GenEx generator.

The exclusive pion production may be also generated with the DiMe generator. It generates the exclusive pion continuum as well as the GenEx generator. But there are some differences which may influence the results of the data analysis. A set of control plots was performed to see differences between GenEx and DiMe generator for a various distributions. They are depicted on Figs. 130 and 134. A difference between these two generators is visible on presented figures. The biggest differences are visible for the pion pair invariant mass where the DiMe generator prefers higher central system mass then the GenEx generator.

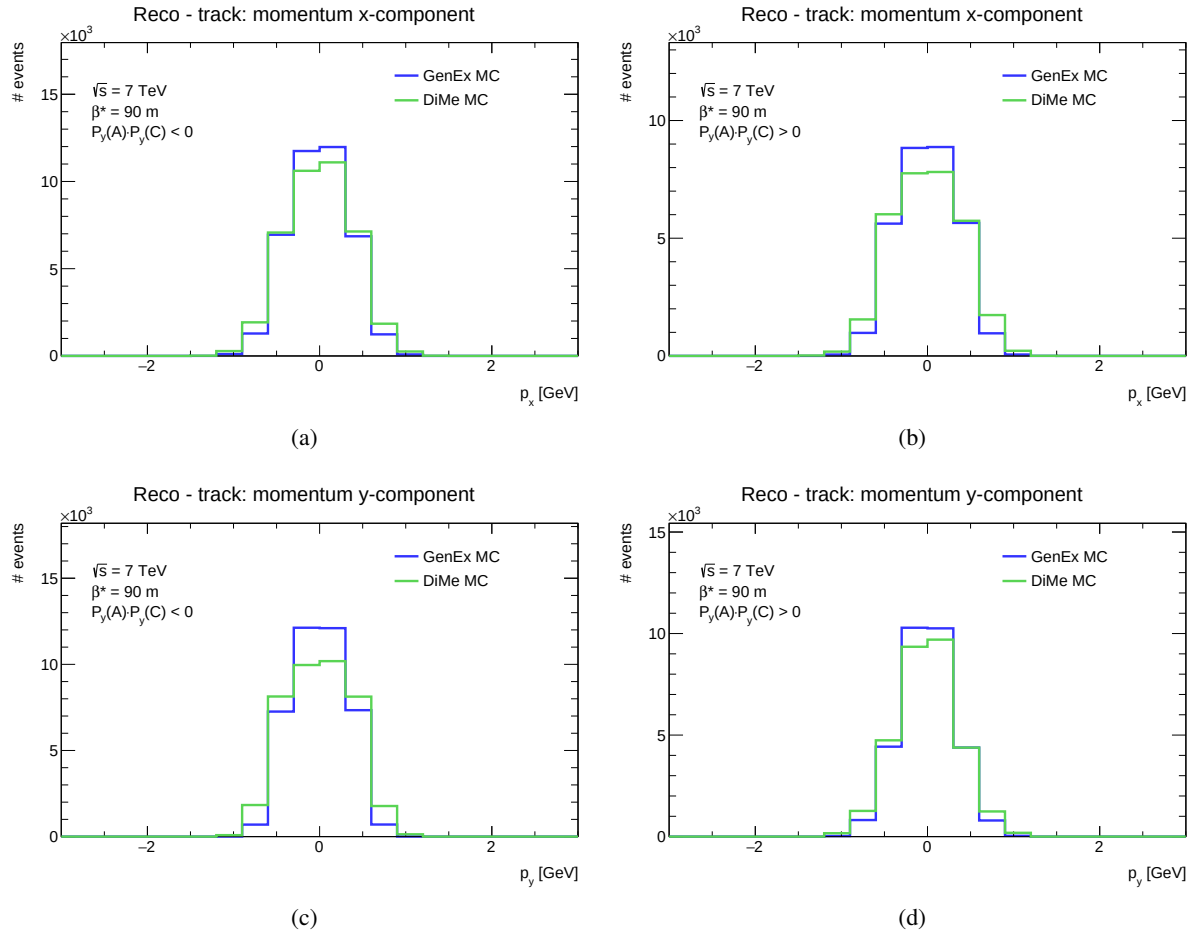

Figure 130: The p_x distribution (a,b) and the p_y distribution (c,d) of the track reconstructed in the Inner detector for the GenEx MC simulation (blue histogram) and for the DiMe MC simulation (green histogram), on (a,c) for the elastic configuration, on (b,d) for the anti-elastic configuration.

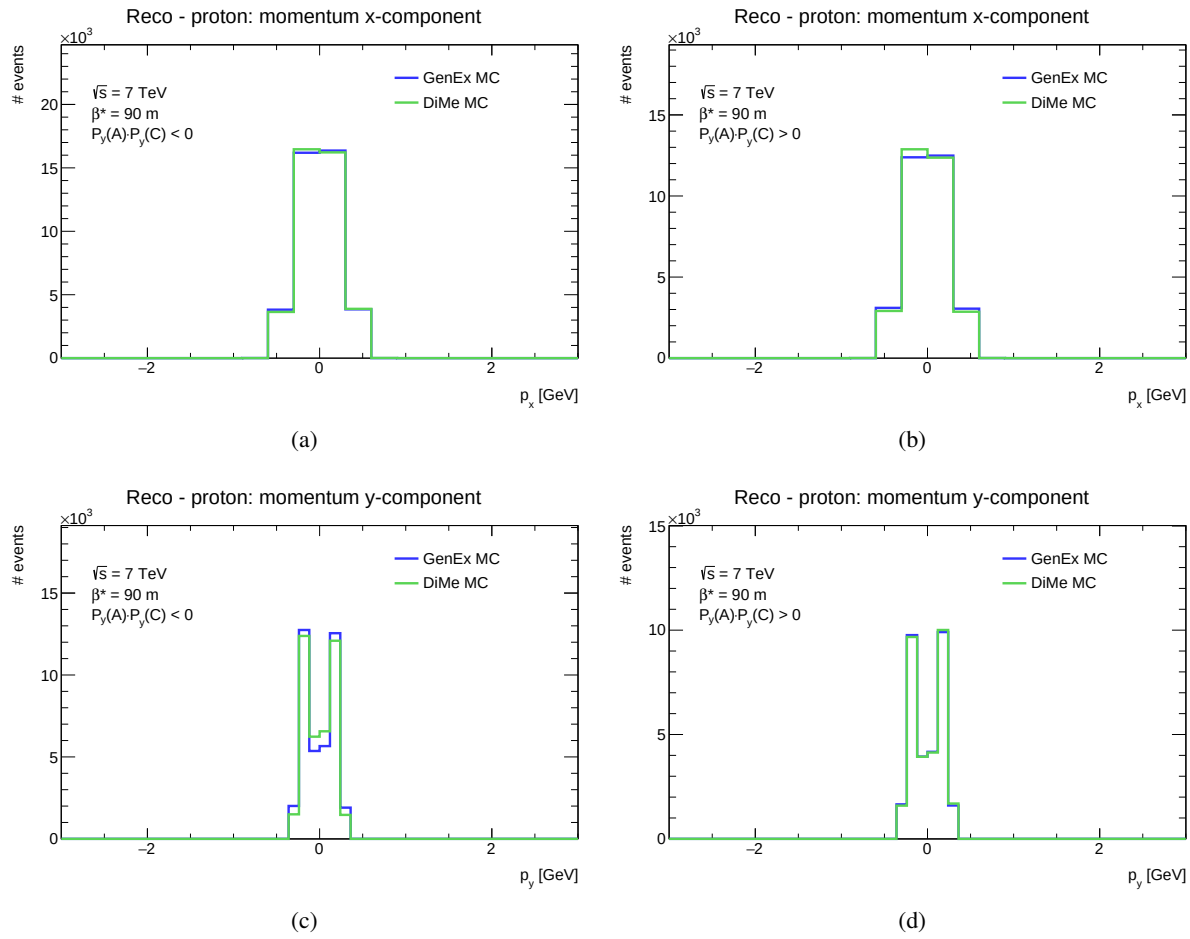

Figure 131: The p_x distribution (a,b) and the p_y distribution (c,d) of the proton reconstructed in the ALFA detector for the GenEx MC simulation (blue histogram) and for the DiMe MC simulation (green histogram), on (a,c) for the elastic configuration, on (b,d) for the anti-elastic configuration.

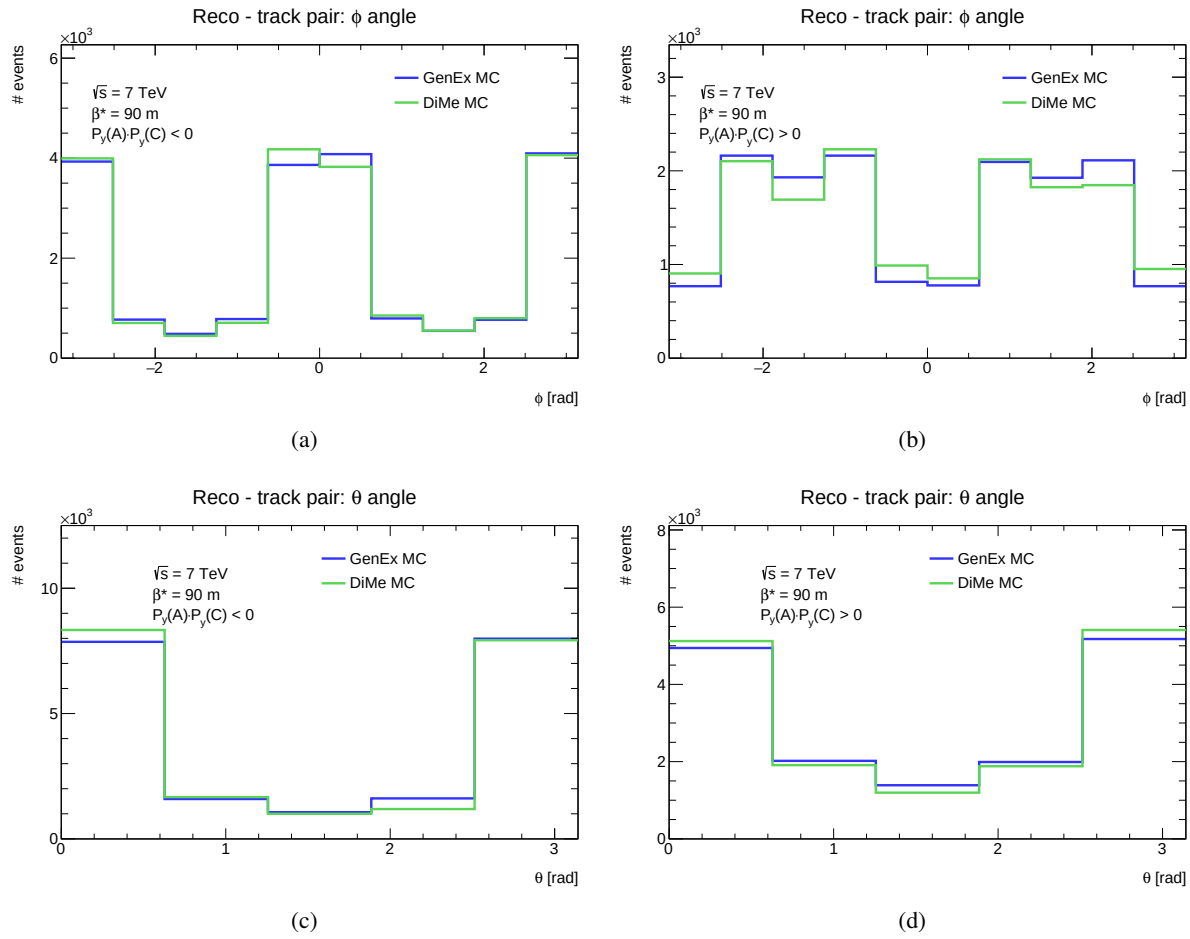

Figure 132: The pion pair ϕ distribution (a,b) and the θ distribution (c,d) for the GenEx MC simulation (blue histogram) and for the DiMe MC simulation (green histogram), on (a,c) for the elastic configuration, on (b,d) for the anti-elastic configuration.

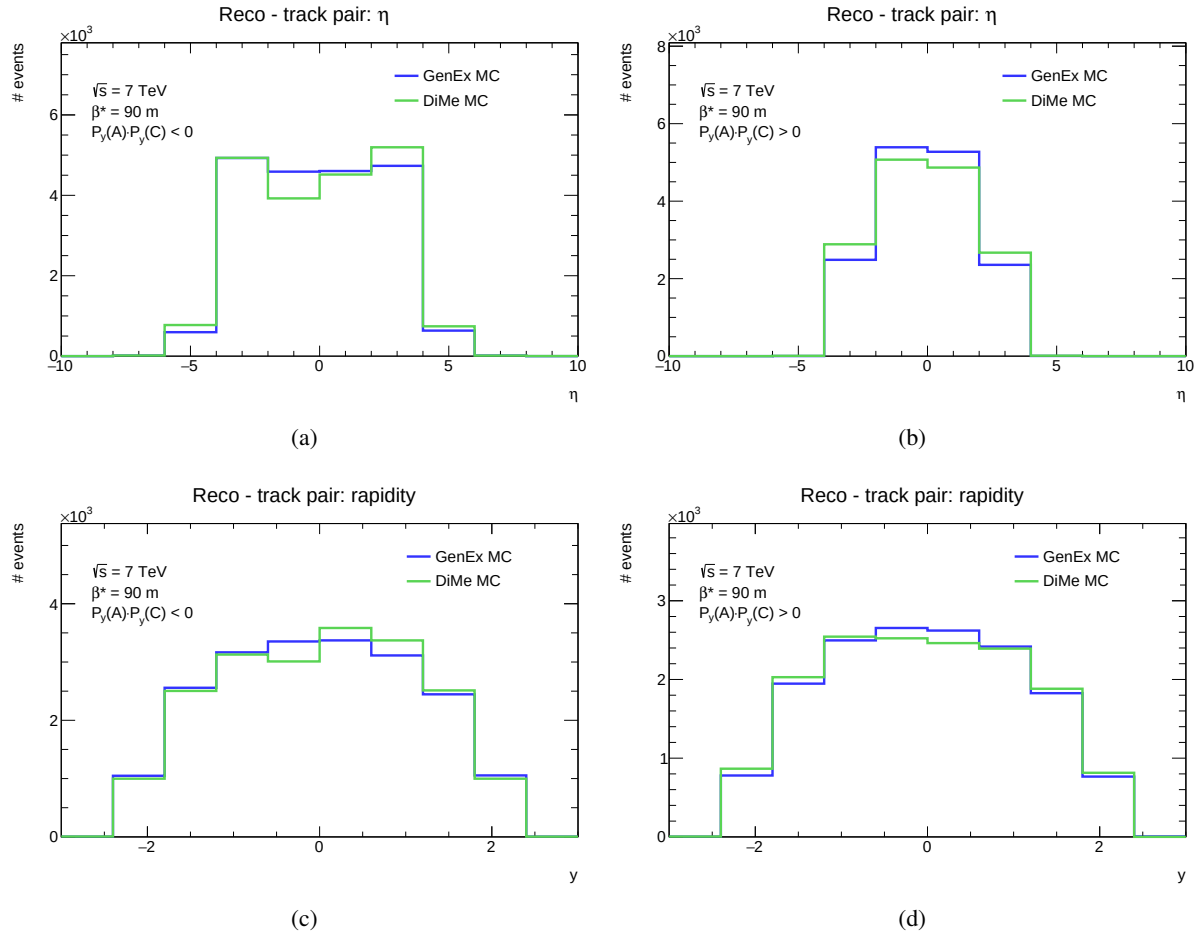

Figure 133: The pion pair pseudo-rapidity η distribution (a,b) and the rapidity distribution (c,d) for the GenEx MC simulation (blue histogram) and for the DiMe MC simulation (green histogram), on (a,c) for the elastic configuration, on (b,d) for the anti-elastic configuration.

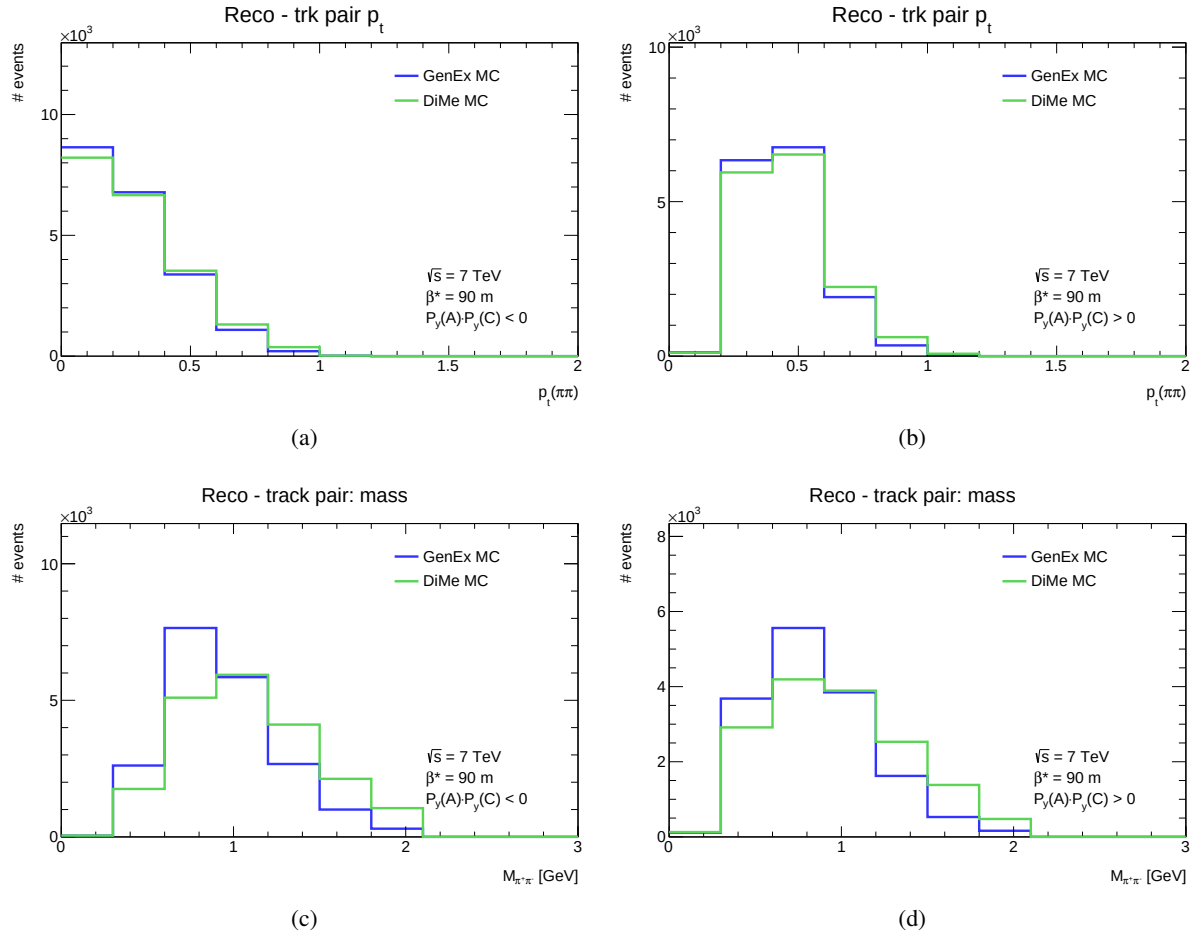

Figure 134: The pion pair transverse momentum p_t distribution (a,b) and the invariant mass M distribution (c,d) for the GenEx MC simulation (blue histogram) and for the DiMe MC simulation (green histogram), on (a,c) for the elastic configuration, on (b,d) for the anti-elastic configuration.

D.5. PYTHIA8 Monte Carlo simulation

A diffractive part of the PYTHIA8 generator includes also a central diffraction processes (a.k.a Double Pomeron Exchange). The model of the central diffraction is able to generate the processes with a central system mass above 1 GeV, see Fig. 11 in Sect. 4.1.3. It is shown in the Sect. D.2 that the significant part of the exclusive pion production lies below 1 GeV limit of the central system mass. Therefore it could seem to be not correct to use this generator for the exclusive pion production study. But in principle PYTHIA8 Monte Carlo simulation can be used to show the imperfections of a developed analysis cut flow and to processed the background study of the central exclusive production.

The PYTHIA8 Monte Carlo simulation simulation with the diffractive process would be studied for three cases, the PYTHIA8 central diffraction with all generated events, the PYTHIA8 central diffraction including only the exclusive pion events on a particle level and the PYTHIA8 central diffraction including only the non-exclusive pion events on the particle level. Regarding to the fact that the PYTHIA8 Monte Carlo simulation is used for the background estimation in this analysis, the main is focused on the PYTHIA8 central diffraction including only the non-exclusive pion events on the particle level. In this sample there are no exclusive events and therefore the events which pass the analysis cut flow represent the background fraction for the exclusive pion production. How the PYTHIA8 central diffraction is used for the background fraction estimation is described in Sect. 9 dedicated to the background study.

The statistics of the PYTHIA8 Monte Carlo simulation of the central diffraction process with the non-exclusive pion events on the particle level is discussed in this section. The Table 43 summarises the statistics. An effect of both ALFA kinematics reconstruction algorithms on the number of the events which passed the analysis cut flow is visible mainly in the momentum balance selection. As it was shown in Table 41 in Sect. D.1, the proton momentum balance p_x is reconstructed by the ALFA Reco method almost two times worse then by the Lattice method. This has an impact on the number of events after the analysis cut flow. But this effect is common for both the background and the exclusive events. Therefore it is not possible to make a conclusion on that number of background events and say what ALFA kinematic reconstruction algorithm is better for the exclusive pion production analysis. This is a topic of the systematic uncertainty discussed in Sect. 11.

Table 43: The PYTHIA8 Monte Carlo simulation cut flow statistics for both proton kinematics reconstruction cases, the ALFA Reco method and the Lattice method. The table covers PYTHIA8 central diffraction simulation with the events containing the non-exclusive pion production on the particle level.

GENEX	configuration			
	elastic		anti-elastic	
	Lattice method	ALFA Reco method	Lattice method	ALFA Reco method
Total events	3789000			
Inner detector selection	230149			
ALFA track selection	13925	13920	13017	13017
MBTS veto	6759	6758	6661	6661
ALFA geometry selection	6612	6616	6540	6531
Kinematic cut $\sum p_y$	1096	1122	995	1013
Kinematic cut $\sum p_x$	494	903	466	789
Particle identification ($M_{dE/dx}$)	422	799	386	689
Kinematic region cut	371	715	334	619

E. ALFA detector multiplicity

The Figs. 135 and 138 represent the ALFA detector multiplicity for various ALFA detector combinations. They compare data (the blue histogram) with the GENEX MC simulation (the red histogram).

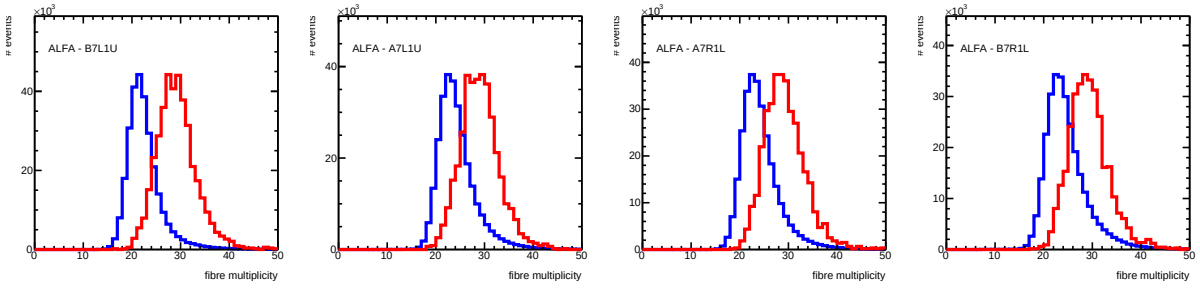

Figure 135: The fibre multiplicity of the elastic arm with B7L1U, A7L1U, A7R1L and B7R1L detectors.

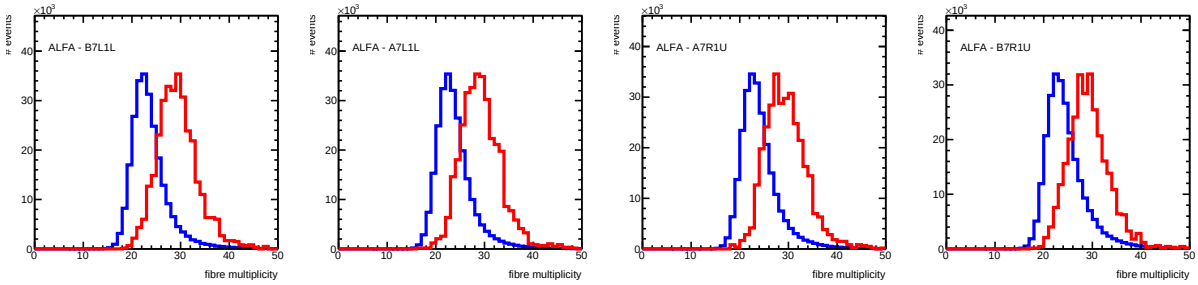

Figure 136: The fibre multiplicity of the elastic arm with B7L1L, A7L1L, A7R1U and B7R1U detectors.

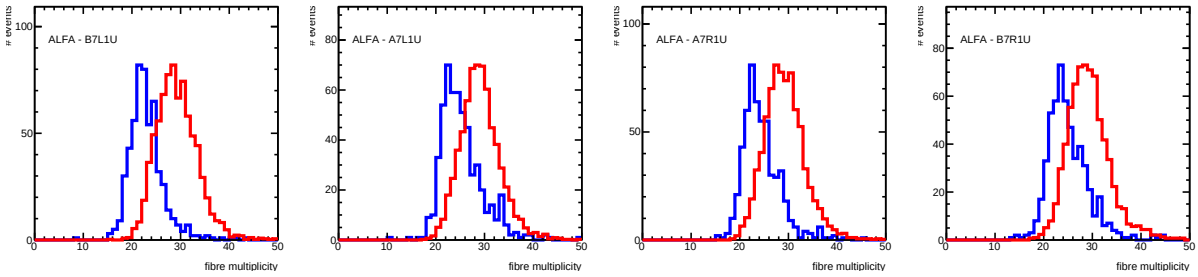

Figure 137: The fibre multiplicity of the anti-elastic arm with B7L1U, A7L1U, A7R1U and B7R1U detectors.

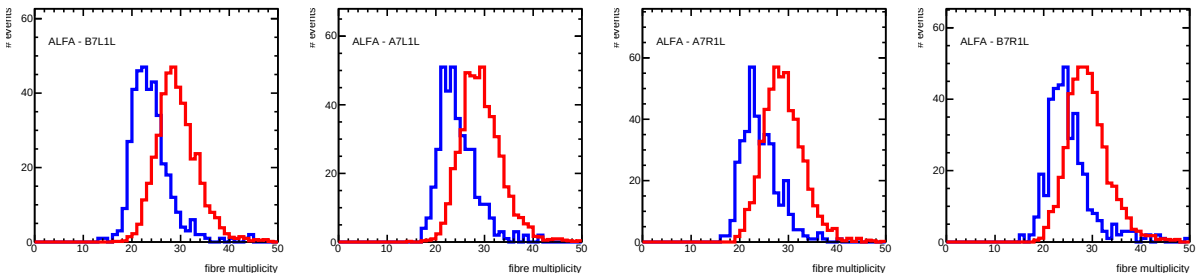

Figure 138: The fibre multiplicity of the elastic arm with B7L1L, A7L1L, A7R1L and B7R1L detectors.

References

[1] S. A. Khalek et al., *The ALFA Roman Pot detectors of ATLAS*,
Journal of Instrumentation **11**.11 (2016) P11013,
URL: http://stacks.iop.org/1748-0221/11/i=11/a=P11013.

[2] G. Aad et al., *Measurement of the total cross section from elastic scattering in pp collisions at $\sqrt{s}$ = 7 TeV with the ATLAS detector*, Nucl.Phys. **B889** (2014) 486–548,
arXiv: 1408.5778 [hep-ex].

[3] S. Agostinelli et al., *Geant4—a simulation toolkit*,
Nuclear Instruments and Methods in Physics Research Section A: Accelerators, Spectrometers, Detectors and Associated Equipment **506**.3 (2003) 250–303, ISSN: 0168-9002,
URL: http://www.sciencedirect.com/science/article/pii/S0168900203013688.

[4] ATLAS Collaboration, *The Athena Framework*, 2016,
URL: https://twiki.cern.ch/twiki/bin/view/AtlasComputing/AthenaFramework
(visited on 21/06/2016).

[5] R. Brun and F. Rademakers, *{ROOT} — An object oriented data analysis framework*,
Nuclear Instruments and Methods in Physics Research Section A: Accelerators, Spectrometers, Detectors and Associated Equipment **389**.1–2 (1997) 81 –86, New Computing Techniques in Physics Research V, ISSN: 0168-9002.

[6] M. Aaboud et al., *Measurement of the total cross section from elastic scattering in pp collisions at $\sqrt{s}$ = 8 TeV with the ATLAS detector*, Physics Letters B **761** (2016) 158–178,
arXiv: 1607.06605 [hep-ex].

[7] R. Staszewski et al., *Exclusive $\pi^+\pi^-$ Production at the LHC with Forward Proton Tagging*,
Acta Phys.Polon. **B42** (2011) 1861–1870, arXiv: 1104.3568 [hep-ex].

[8] O. C. Jacob and L. S. Kisslinger, *Applicability of Asymptotic QCD for Exclusive Processes*,
Phys. Rev. Lett. **56** (1986) 225.

[9] P. Lebiedowicz, O. Nachtmann and A. Szczurek,
Central exclusive diffractive production of $\pi^+\pi^-$ continuum, scalar and tensor resonances in pp and $p\bar{p}$ scattering within tensor pomeron approach, Phys. Rev. **D93**.5 (2016) 054015,
arXiv: 1601.04537 [hep-ph].

[10] P. Lebiedowicz, *Exclusive reactions with light mesons: From low to high energies*, thesis, The Henryk Niewodniczanski Institute of Nuclear Physics, Polish Academy of Sciences (2014).

[11] P. Lebiedowicz and A. Szczurek, *Exclusive $pp \to pp\pi^+\pi^-$ reaction: From the threshold to LHC*,
Phys.Rev. **D81** (2010) 036003, arXiv: 0912.0190 [hep-ph].

[12] L. A. Harland-Lang, V. A. Khoze and M. G. Ryskin,
Modelling exclusive meson pair production at hadron colliders, Eur. Phys. J. **C74** (2014) 2848,
arXiv: 1312.4553 [hep-ph].

[13] M. G. Albrow, T. D. Coughlin and J. R. Forshaw,
Central Exclusive Particle Production at High Energy Hadron Colliders,
Prog. Part. Nucl. Phys. **65** (2010) 149–184, arXiv: 1006.1289 [hep-ph].

[14] R. Kycia et al.,
GenEx: A simple generator structure for exclusive processes in high energy collisions (2014), arXiv: 1411.6035 [hep-ph].

[15] P. Soding, *On the Apparent shift of the rho meson mass in photoproduction*, Phys. Lett. **19** (1966) 702–704.

[16] C. Ewerz, M. Maniatis and O. Nachtmann,
A Model for Soft High-Energy Scattering: Tensor Pomeron and Vector Odderon, Annals Phys. **342** (2014) 31–77, arXiv: 1309.3478 [hep-ph].

[17] ATLAS Collaboration, *The ATLAS job transforms*, 2016,
URL: https://twiki.cern.ch/twiki/bin/view/AtlasComputing/JobTransform (visited on 21/06/2016).

[18] ATLAS Collaboration, *Documentation for the D3PDMaker Project*, 2016,
URL: https://twiki.cern.ch/twiki/bin/view/AtlasProtected/D3PDMaker (visited on 21/06/2016).

[19] S. Campana, T. Wenaus et al., *The Atlas Computing*, 2016,
URL: https://twiki.cern.ch/twiki/bin/view/AtlasComputing/AtlasComputing (visited on 21/06/2016).

[20] G. Stewart, W. Lampl et al., *The Software Tutorial*, 2016, URL:
https://twiki.cern.ch/twiki/bin/viewauth/AtlasComputing/SoftwareTutorial (visited on 21/06/2016).

[21] S. Lloyd et al., *The ATLAS Computing Workbook*, 2016,
URL: https://twiki.cern.ch/twiki/bin/view/AtlasComputing/WorkBook (visited on 21/06/2016).

[22] S. Lloyd et al., *The ATLAS Software Development Workbook*, 2016, URL: https://twiki.cern.ch/twiki/bin/view/AtlasComputing/SoftwareDevelopmentWorkBook (visited on 21/06/2016).

[23] T. Sjöstrand et al., *An Introduction to PYTHIA 8.2*, Comput.Phys.Commun. **191** (2015) 159–177, arXiv: 1410.3012 [hep-ph].

[24] J. Monk and A. Pilkington, *ExHuME 1.3: A Monte Carlo event generator for exclusive diffraction*, Computer Physics Communications **175**.3 (2006) 232 –239, ISSN: 0010-4655.

[25] P. Lebiedowicz, O. Nachtmann and A. Szczurek,
Exclusive diffractive production of $\pi^+\pi^-\pi^+\pi^-$ via the intermediate $\sigma\sigma$ and $\rho\rho$ states in proton-proton collisions within tensor pomeron approach (2016), arXiv: 1606.05126 [hep-ph].

[26] M. Dobbs et al., 'HepMC 2: a C++ Event Record for Monte Carlo Generators', 2010,
URL: http://hepmc.web.cern.ch/hepmc/releases/HepMC2_user_manual.pdf.

[27] S Cavalier et al., *90 m OPTICS COMMISSIONNING*, CERN-ATS-2011-133 (2011) 3 p,
URL: http://cds.cern.ch/record/1382027.

[28] S Cavalier et al., 'Measurement of the total cross section in pp collisons at sqrt(s) = 7 TeV from elastic scattering with the ATLAS detector', tech. rep. ATL-COM-PHYS-2013-1357, CERN, 2013, URL: https://cds.cern.ch/record/1602297.

[29] A. Collaboration, *ATLAS DCS - Beam position monitoring*, 2011,
URL: https://atlas-dcs.cern.ch/index.php?datestring=2011-10-20-16-55&page=LHC_INS::INS_BPM (visited on 30/03/2017).

[30] ATLAS Collaboration, *Minimum Bias D3PD Documentation*, 2016, URL: https://twiki.cern.ch/twiki/bin/view/AtlasProtected/MinBiasD3PDDocu (visited on 21/06/2016).

[31] ATLAS Collaboration, *ALFA d3pd Maker and ntuple content*, 2016, URL: https://twiki.cern.ch/twiki/bin/view/Atlas/ALFAd3pdMaker (visited on 21/06/2016).

[32] *ATLAS inner detector: Technical design report. Vol. 1* (1997).

[33] G. Aad et al., *The ATLAS Inner Detector commissioning and calibration*, Eur.Phys.J. **C70** (2010) 787–821, arXiv: 1004.5293 [physics.ins-det].

[34] E. Feng and J. E. Pilcher, 'Triggering ATLAS with Minimum Bias Trigger Scintillators', tech. rep. ATL-TILECAL-INT-2007-004. ATL-COM-TILECAL-2007-013, CERN, 2007, URL: https://cds.cern.ch/record/1034461.

[35] L Nozka, *ALFA_Geometry Package - Description and User Manual*, 2010, URL: https://twiki.cern.ch/twiki/pub/Atlas/AlfaSoftware/SRD_ALFAGeometryPackage.pdf (visited on 30/03/2017).

[36] S. Jakobsen et al., 'Commissioning of the Absolute Luminosity For ATLAS detector at the LHC', Presented 31 Jan 2014, PhD thesis: Bohr Inst., 2013, URL: https://cds.cern.ch/record/1637195.

[37] J. Stelzer and T. Bold, *Trigger configuration for the ATLAS run 191373*, 2016, URL: https://atlas-trigconf.cern.ch/listruns/?runs=191373 (visited on 21/06/2016).

[38] M. Medici and S. Jakobsen, 'Trigger efficiency for the ALFA detector in 2011', tech. rep. ATL-COM-LUM-2013-006, CERN, 2013, URL: https://cds.cern.ch/record/1519629.

[39] T Cornelissen et al., 'Concepts, Design and Implementation of the ATLAS New Tracking (NEWT)', tech. rep. ATL-SOFT-PUB-2007-007. ATL-COM-SOFT-2007-002, CERN, 2007, URL: https://cds.cern.ch/record/1020106.

[40] S. S. Mortensen, 'Kinematic reconstruction of diffractive processes with tagged protons in the ALFA detector at sqrt(s) = 8 TeV', MA thesis: University of Copenhagen, 2013, URL: http://discoverycenter.nbi.ku.dk/teaching/thesis_page/Stark-Thesis.pdf.

[41] H Burkhardt and S Cavalier, *Intermediate 90m Optics for ATLAS-ALFA* (2011), URL: http://cds.cern.ch/record/1345332.

[42] S van der Meer, 'Calibration of the effective beam height in the ISR', tech. rep. CERN-ISR-PO-68-31. ISR-PO-68-31, CERN, 1968, URL: http://cds.cern.ch/record/296752.

[43] 'dE/dx measurement in the ATLAS Pixel Detector and its use for particle identification', tech. rep. ATLAS-CONF-2011-016, CERN, 2011, URL: http://cds.cern.ch/record/1336519.

[44] J Wenninger, 'Energy Calibration of the LHC Beams at 4 TeV', tech. rep. CERN-ATS-2013-040, CERN, 2013, URL: https://cds.cern.ch/record/1546734.

[45] ATLAS Collaboration, *Top level tags in the ATLAS Geometry Database*, 2016, URL: https://twiki.cern.ch/twiki/bin/view/AtlasComputing/AtlasGeomDBTagsOld (visited on 01/07/2016).

List of Figures

List of Tables

PALACKÝ UNIVERSITY IN OLOMOUC

FACULTY OF SCIENCE

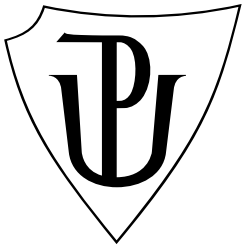

SUMMARY OF THE PH.D. THESIS

Mgr. Petr Hamal

Modelling and Simulation in High Energy Physics

Joint Laboratory of Optics of Palacký University and the Institute of the Czech Academy of Sciences

Supervisor of the doctoral thesis:	Mgr. Tomáš Sýkora Ph.D.
Study programme:	Physics
Specialization:	Applied physics

Olomouc 2017

UNIVERZITA PALACKÉHO V OLOMOUCI

PŘÍRODOVĚDECKÁ FAKULTA

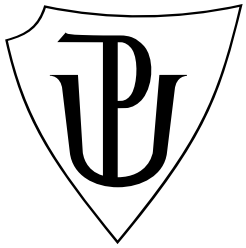

AUTOREFERÁT DIZERTAČNÍ PRÁCE

Mgr. Petr Hamal

Modelování a simulace ve fyzice vysokých energií

Společná laboratoř optiky Univerzity Palackého v Olomouci a Fyzikálního ústavu Akademie věd ČR

Školitel: Mgr. Tomáš Sýkora Ph.D.

Studijní program: Fyzika

Studijní obor: Aplikovaná fyzika

Olomouc 2017

I declare that I carried out this doctoral thesis independently under supervision of Mgr. Tomáš Sýkora, Ph.D., and only with the cited sources, literature and other professional sources.

In Olomouc, 3rd July 2017 .....

Ph.D. candidate: **Mgr. Petr Hamal**

Supervisor: **Mgr. Tomáš Sýkora, Ph.D.**
Institute of Particle and Nuclear Physics
Faculty of Mathematics and Physics
Charles University

Reviewers: **prof. RNDr. Miroslav Mašláň, CSc.**
Department of Experimental Physics
Faculty of Science
Palacky University

RNDr. Petr Trávníček, Ph.D.
Department of Astroparticle Physics
Division of Elementary Particle Physics
Institute of the Czech Academy of Science

Oral defence will take place on 30th August 2017 at Joint Laboratory of Optics of Palacký University and the Institute of the Czech Academy of Sciences, room n. 248, 17. listopadu 50a, 772 46 Olomouc.

The Ph.D. thesis is available in the library at Faculty of Science at Palacký University.

Abstrakt: Cílem předložené disertační práce je prezentovat schopnost autora aplikovat získané znalosti z oblasti modelování a simulace ve fyzice vysokých energií na příkladu fyzikální analýzy využívající experimentálně naměřených dat a následné porovnání získaných výsledků s teorií studovaného procesu. Práce je zaměřena na exluzivní proces produkce pionového páru $p + p \rightarrow p + p + \pi^+ + \pi^-$ v proton-protonových srážkách o těžišťové energii $\sqrt{s} = 7\,\text{TeV}$ měřeného experimentem ATLAS na urychlovači LHC v CERNu. Tento proces je nejprve studován po teoretické stránce s využitím výsledků simulací uvedeného procesu. Celý softwarový rámec je pak následně aplikován i na experimentální data za účelem určení viditelného účinného průřezu exkluzivní produkce. Ke studiu procesu a jeho analýze jsou využity standardní softwarové nástroje z oblasti fyziky vysokých energií a analýzy dat jako jsou GEANT4, knihovny a nástroje ROOT, příslušné generátory studované produkce (GENEX, DIME) a softwarový rámec Athena standardně využívaný experimentem ATLAS.

Klíčová slova: Athena, ATLAS, CERN, difrakční fyzika, dopředné detektory, exkluzivní produkce, simulace, modelování, GENEX, DIME, ROOT, analýza

Abstract: The aim of this doctoral thesis is to present author's ability to apply the gained knowledge of modelling and simulation in high energy physics to the physical analysis of a given process using experimental data followed by a comparison of given results with a corresponding theory. The thesis is focused on the exclusive pion production $p+p \rightarrow p+p+\pi^+ +\pi^-$ in proton-proton collisions measured by ATLAS experiment at centre-of-mass energy $\sqrt{s} = 7\,\text{TeV}$. First of all this production is studied on a theoretical level using the results of the appropriate simulations. The obtained results are later applied on experimental data to estimate the cross-section of a given production. A common software tools are used to study the exclusive pion production, namely GEANT4, ROOT framework, generators of the given production like GENEX and DIME or the common tools used by ATLAS experiment known as Athena framework.

Keywords: Athena, ATLAS, CERN, diffractive physics, exclusive production, forward detectors, simulation, modelling, GENEX, DIME, ROOT, analysis

Contents

1 Preface

The main aim of the thesis "Modelling and Simulation in High Energy Physics" is to present author's ability to apply his knowledge of modelling and simulations in the analysis of the exclusive pion production data obtained by ATLAS (**A** **T**oroidal **L**HC **A**pparatu**S**) collaboration during proton-proton collisions at the LHC at centre-of-mass energy $\sqrt{s} = 7\,\text{TeV}$.

Gained knowledge of modelling and simulation came thanks to author's work for ALFA (**A**bsolute **L**uminosity **F**or **A**TLAS) community of the ATLAS in CERN (**C**onseil **E**uropéen pour la **R**echerche **N**ucléaire). The ALFA community which stands behind the detector of the same name - the ALFA detector [1][1] - gave the author an excellent opportunity to become its essential member and to fulfil oneself in the area of the modelling and simulation. The author worked with common tools and frameworks used in ATLAS collaboration including the GEANT4 framework [3] (serving for a simulation on a particle interaction with a mass), the Athena framework [4] (the main simulation, reconstruction and analysis framework of ATLAS collaboration) and ROOT Data Analysis Framework [5] (providing functionality for data analysis).

The author joint the ALFA community to work on the topics of the modelling and simulations which are essential for an understanding of the correct behaviour of the ALFA detectors. At the beginning the author contributed to the development of various software tools needed for simulations of the ALFA detectors within the ATLAS official framework - Athena. These steps included a development of the software tools used for a digitization, for a reconstruction and for a data preparation. This part of author's work made an unquestionable contribution not only to the ALFA community but also to the whole ATLAS collaboration. Author gave a plenary talk about the use of GUI for Athena developers.

Beside the modelling and simulation studies the author contributed to ALFA community by the analysis of data collected during several testing campaigns in CERN. The author contributed also to the ALFA community from his position as the Data Preparation convener (2012-2014).

The author contributed to two analysis of the total cross-section measurement in ATLAS using the ALFA detectors, [2] and [6].

Still, the exclusive pion production measured by ATLAS at centre-of-mass energy $\sqrt{s} = 7\,\text{TeV}$ makes a principal topic of the author's doctoral thesis on which he presents the knowledge and the skills achieved during his doctoral study.

The exclusive pion production analysis goes behind the ALFA detector itself. It combines the knowledge of two detector systems of the ATLAS collaboration, the Inner detector as a part of the central ATLAS detector and the ALFA detector system as the part of the forward region of the ATLAS. This is also the first time when such analysis is done by ATLAS.

The introductory section Sect. 2 provides a physics motivation for a study of the exclusive pion production $p + p \to p + p + \pi^+ + \pi^-$ and is followed by the Sect. 3 describing the basic mechanisms of the exclusive pion production. The Monte Carlo (MC) simulation section (Sect. 4) focusses on MC generators able to describe the studied process.

The next part of the thesis is devoted to the exclusive pion production analysis itself. The experimental set-up is described in Sect. 5, the particle kinematic reconstruction, data taking and the chain of the selection criteria are described in Sects. 6 and 7. Following Sects. 8 and 9 are devoted to the overall corrections and the background estimation which are important for a correct interpretation of the analysis results. The results of

[1] The main purpose is to determine the total cross-section of proton-proton collisions (i.e. [2])

the data analysis are described in Sect. 10 and are followed by a study of systematic uncertainty in Sect. 11. The summary of the results and the thesis itself are given in Sects. 12 and 13.

2 Introduction

The significant amount of proton-proton collisions at the LHC is either elastic ($\approx 20\%$) or diffractive ($\approx 20\%$ of the remaining in-elastics collisions, i.e. approximately 16%). In many of these collisions the transferred momentum is too small to make the perturbative QCD applicable, and instead of the QCD the alternative, Regge, theory has to be used. Naturally, if we believe in a universality of the QCD, there should be a "bridge" (mapping) between the Regge theory and the QCD and e.g. pomeron, the basic object in soft diffraction description, can be, in some kinematic region and in a good approximation, considered as a color-singlet state of two gluons.

The simplest process with the exchange of a pomeron is proton-proton (pp) elastic scattering. As the simplest example of a (inelastic) diffractive process can be considered the exclusive production of pion pairs $p + p \rightarrow p + p + \pi^+ + \pi^-$, in which pomeron-pomeron fusion (double pomeron exchange) can be tested, together with relevant corrections (proton-proton and pion-pion re-scattering).

Another, and probably very attractive, reason to study exclusive pion production is a search for glueballs - strongly interacting states with no valence quarks, which existence was predicted more than 40 years ago. Nevertheless, despite of some evidence based on the analysis of observed scalar meson decay modes, to which processes via pomeron fusion represent background, their existence was not established.

Finally, there is another potential motivation for measurement of exclusive pion production, as it can be used, at least theoretically, as an alternative for a forward detector position alignment and accelerator optics cross-check.

Data analysed in the present thesis were taken during the special low luminosity LHC runs (with the dedicated $\beta^\star = 90\,\text{m}$ accelerator optics) at centre-of-mass energy $\sqrt{s} = 7\,\text{TeV}$ in Autumn 2011. The main aim is to estimate the cross-section of exclusive pion pair production in pp collisions.

Pion pairs were detected by the ATLAS inner detector whereas the outgoing protons were measured by ALFA detector situated on both sides of ATLAS forward region $\approx 240\,\text{m}$ from the ATLAS Interaction Point (IP).

The use of ALFA detectors makes this study different from any existing measurement done at higher (TeV) energies till now as outgoing protons were directly detected and a contamination of the measurement by proton remnants (if only the rapidity gap technique is used) is minimized.

The estimated visible $\pi^+\pi^-$ cross section measured by ALFA was estimated in work [7] to 21 µb, under conditions that ALFA is 4 mm from the beam, the minimal pion energy is 100 MeV and the minimal energy deposited in the calorimeter is 4 GeV.

The analysis profits from the previous analysis *Measurement of the total cross section from elastic scattering in pp collisions at $\sqrt{s}$ =7 TeV with the ATLAS detector* [2] which was performed on the same dataset, with the same data taking conditions and the ALFA detector settings.

3 Pion pair production - theory

The exclusive production of a pion pair in pp collisions is one of the simplest processes intermediated by the strong interaction. Correspondingly, there is a long history of models describing the process including a discussion about applicability of the perturbative QCD, see e.g. [8].

The plot in Fig. 1 of reconstructed scattered protons Mandelstam variable t

$$t \approx {p_0}^2(1-\xi)\theta^2\,, \tag{1}$$

where θ is an angle between ATLAS z-axis and outgoing proton momentum 3-vector, ξ is a proton momentum loss during the interaction shows that the transferred momenta (from protons to central systems out of which pion pairs are created) are below 1 GeV.[2] This means that this part of the production mechanism cannot be described by the perturbative QCD. Instead Regge description is used.

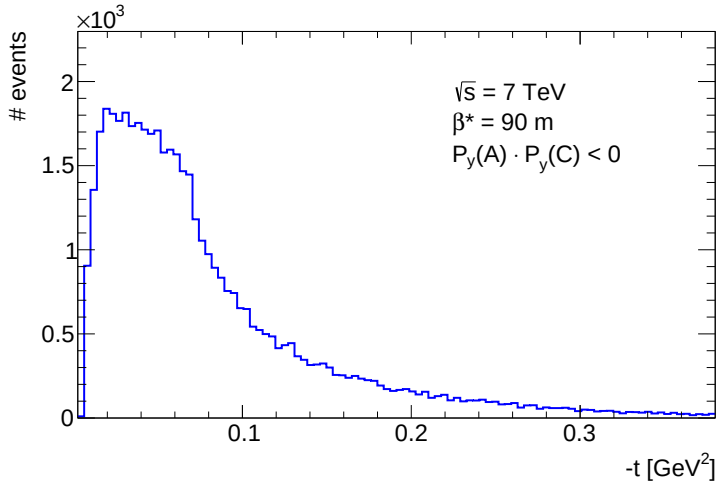

Figure 1: Outgoing proton t distribution in MC signal simulation (GenEx).

There are several recent works ([9–13] and references therein) summarizing the state of art leading to two existing signal generators, GenEx [14] and DiMe [12], used in the present analysis. The models are relatively similar, but not identical, and provide different predictions. Each of the models uses several parameters which are not fixed by the underlying theory.

In what follows a general description of the exclusive pion pair production is briefly given and it is explained from where free parameters of models origin.

The exclusive production of $\pi^+\pi^-$ pair in pp collisions can be described by the generic diagram in Fig. 2.

Internal zigzag lines in Fig. 2 denote exchanges of objects O_1 and O_2, not necessarily of the same type, but having all hadronic charges equal to zero; $O_i \in \gamma, \mathbb{P}, \mathbb{O}, \mathbb{R}$, where γ stands for photon, $\mathbb{P}$ for pomeron, $\mathbb{O}$ for oderon, and $\mathbb{R}$ represents a set or reggeons: $f_{2\mathbb{R}}$, $a_{2\mathbb{R}}$, $\omega_{\mathbb{R}}$ and $\rho_{\mathbb{R}}$. In case when both pions are measured (i.e. they do not form a bound state), the C-parities of O_1 and O_2 have to be the same to get for pion system value equal to 1.

In the first approximation a pion pair creation via diagrams in Figs. 3a and 3b can be described.

[2] Not full story! It has to be shown that the same restriction is valid for t in $O_iO_j \to \pi^+\pi-$ process. But since the energy entering into this process is already restricted, the condition $t < 1\,\mathrm{GeV}^2$ is automatically satisfied.

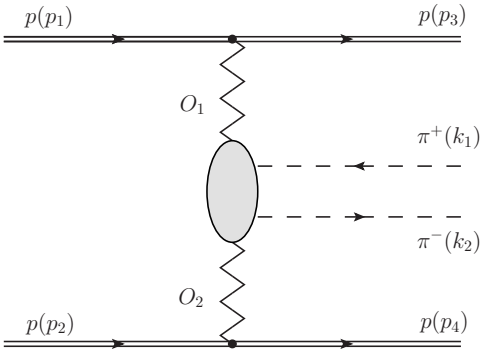

Figure 2: Generic diagram describing exclusive pion pair production in pp collisions.

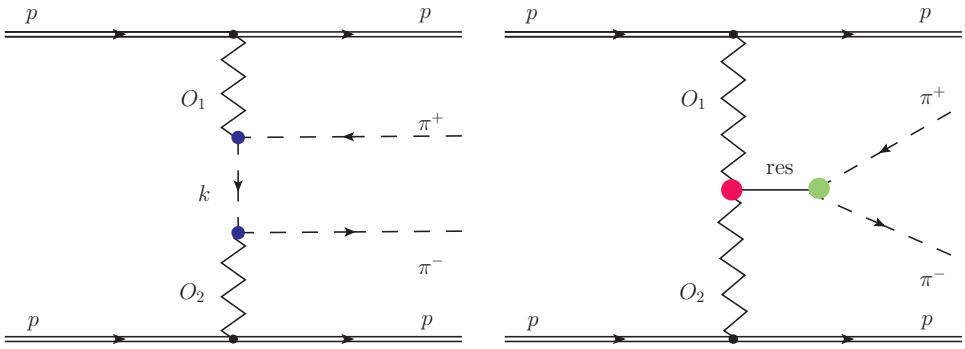

Figure 3: Schematic plot of central exclusive pion pair production in proton-proton collisions mediated by objects O_1 & O_2 and via (a) the internal meson propagator or (b) a resonance `res`.

The abbreviation `res` stands for any (energetically) possible resonant state.

The full amplitude $\mathcal{M}$ for processes in Fig. 3a - so called continuum part - sets contributions from different components of isospin:

$$|\mathcal{M}|^2 = |\mathcal{M}_{I=0}|^2 + |\mathcal{M}_{I=1}|^2 + |\mathcal{M}_{I=2}|^2, \tag{2}$$

but since the following inequalities [10]

$$|\mathcal{M}_{I=0}|^2 \gg |\mathcal{M}_{I=1}|^2 \gg |\mathcal{M}_{I=2}|^2, \tag{3}$$

only the first term $M_{I=0}$ can be considered. The $I = 0$ component dominance was discussed also in [12].

There are several contributions to the $M_{I=0}$ component which have to be taken in account, namely $\mathbb{P}$-$\mathbb{P}$, $\mathbb{P}$-$f_{2\mathbb{R}}$, $\mathbb{P}$-γ, $f_{2\mathbb{R}}$-γ and $f_{2\mathbb{R}} - f_{2\mathbb{R}}$ [9, 10] - meanwhile the other contributions can be neglected.

There is the second set of contributing diagrams, Fig. 3b, where a pion pair originates from a resonance decay.

Finally, the interference terms between all amplitudes have to be taken in account. The relevance of the effect of interference was documented on the shift of the position of the peak ρ resonance [15].

To calculate amplitudes of above mentioned diagrams vertex functions/form-factors (i.e. $p - O_i - p$, $\pi^+ - O_i - \pi^-$, $O_i - \texttt{res} - O_j$) have to be known/estimated [16].

3.1 Pion form factor and pion propagator reggeization

The pion form-factor is normalized on-shell, its value can be established from the reaction $p\pi \to p\pi$. There are several parametrization of off-shell pion form-factor, see eg. [10] (Eqs. 2.32, 2.29-31), [12] (Eqs. 4-5). For the mass of the central system $M_{\pi^+\pi^-}$ up to 1.5 GeV or $p_T(\pi)$ up to 1 GeV the difference between these parametrization is rather small although the final effect on the cross section is still of the order of hundreds percent [12] (Fig. 4). As the examples of off-shell form-factor parametrization following forms can taken [12]:

$$F_M^{\rm exp}(t) = \exp\left(b_{\rm exp} t'\right) \tag{4}$$

$$F_M^{\rm or}(t) = \exp\left(-b_{\rm or}\sqrt{-t' + a_{\rm or}^2} + a_{\rm or} b_{\rm or}\right) \tag{5}$$

$$F_M^{\rm pow}(t) = \frac{1}{1 - t'/b_{\rm pow}} \tag{6}$$

where $t' = t - M^2$. It is clear that at the limit $t \to M^2$ the form-factors become equal to unity.

At the higher energies s, the standard pion propagator standing for an exchange of a pion of mass M, may be replaced by a full family of objects [10] (eq. 2.32):

$$\frac{1}{t - {m^2}_M} \to \beta_M(s)\frac{1}{t - {m^2}_M} + \beta_R(s)\mathcal{P}^{M^*}(t, s) \tag{7}$$

where

$$\mathcal{P}^{M^*}(t) = \frac{\pi\alpha'_{M^*}}{2\Gamma(\alpha_{M^*}(t)) + 1}\frac{1 + \exp(-i\pi\alpha_{M^*}(t))}{\sin\pi\alpha_{M^*}(t)}\left(\frac{s}{s_0}\right)^{\alpha_{M^*}} \tag{8}$$

is the reggeized propagator [10] (p. 144-145), Γ stands for Euler gamma function, the scale s_0 is selected to be 1 GeV^2 and α_{M^*} is the Regge trajectory with the slope $\alpha'_{M*} = \alpha'_\pi = 0.7\,\text{GeV}^{-2}$.

The functions $\beta_M(s)$ and $\beta_M(R)$ are introduced to interpolate between the meson and Regge exchange:

$$\beta_M(s) = \exp\left(-\left(s - 4m_{M*}^2\right)/\Lambda_{\rm off}^2\right), \quad \beta_R(s) = 1 - \beta_M(s) \tag{9}$$

and $\Lambda_{\rm off}$ is a free parameter of the model.

There are other possibilities to reggeize propagator (an option in DiMe, by default it is switched off)

$$\frac{1}{t - {m^2}_M} \to \frac{1}{t - {m^2}_M}\left(\frac{s}{s_0}\right)^{\alpha_{M^*}(t)}, \tag{10}$$

where $\alpha_M(t) = \alpha_M(t) + \alpha'_M t$ is the Regge trajectory of the meson M, or

$$\frac{1}{t - {m^2}_M} \to \frac{1}{t - {m^2}_M}\exp(\alpha_M(t)\,|y_{M_3} - y_{M_4}|), \tag{11}$$

where y_{M_3} and y_{M_4} are rapidities of produced pions.

Clearly, at the present there is no other enough strong argument restricting the form of the pion off-shell form-factor or/and propagator.

3.2 Survival factor

The full picture of the exclusive pion pair production is more complicated as the diagrams containing protons pp re-scattering (Fig. 4a), $\pi\pi$ re-scattering (Fig. 4b) and also re-scattering of pion(s) with proton (Fig. 4c) have to taken into account.

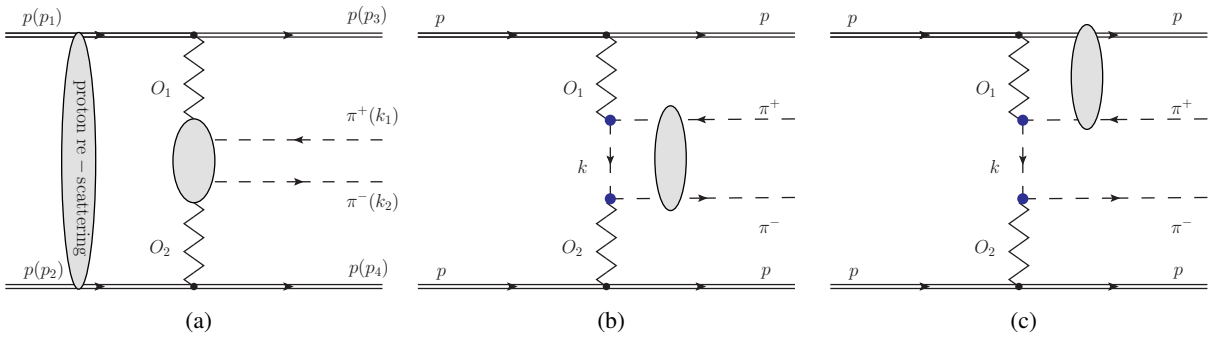

Figure 4: Schematic plot of a central exclusive pion pair production in proton-proton collisions, with (a) proton re-scattering, (b) pion re-scattering and (c) meson-proton re-scattering.

Naturally, the same type of contributions can be expected also in a pion pair production via a resonance decay (Fig. 5).

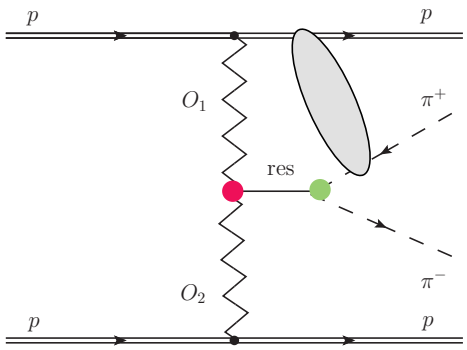

Figure 5: Schematic plot of a central exclusive pion pair production in proton-proton collisions with meson re-scattering and a pion pair production via a resonance decay.

3.3 Theory versus models

The effect of a proton-proton re-scattering (survival factor) is not implemented into the GenEx, the survival factor (= 0.22) was (independently on the interaction kinematics) introduced into the analysis by hand after the communication with GenEx authors. On the other hand DiMe has implemented a survival factor with the choice for 4 models describing it, including the Poisson suppression factor [12] originating from the requirement that no other particles may be produced in $\mathbb{PP} \to \pi\pi$ sub-process. For the process description, DiMe considers only contributions from $\mathbb{P}/\mathbb{RP}/\mathbb{R}$ as relevant ones.

Neither of the models has implemented contributions in which a pion pair originates from a resonance decay. As for off-shell form-factor, both models offer free parameters - Λ_{off} in case of GenEx, three sets of

parameters for Eqs. 4 and 6.

The same Λ_{off} parameter enters into the reggeization of the pion propagator in case of GenEx whether DiMe parametrization is based on the Regge trajectory in Eqs. 10 and 11. In general, in case of small t it is not easy to distinguish GenEx and DiMe generators, the differences come with higher t value or higher statistics.

4 Monte Carlo Simulation

Three different generators able to generate the exclusive pion production, together with the procedure how to generate and simulate such events, are described together with a description of the tools used in the Monte Carlo simulations. The main tool used in the simulations is the ATLAS offline software Athena [4]. The full simulation chain implemented in Athena consists of four steps: the event generation, the Geant4 simulation, the digitization and the reconstruction step. A production of each step is controlled by the transformation jobs [17] which are a part of the ATLAS offline software. A result of the Monte Carlo simulation is stored in a file of ROOT [5] format called D3PD provided by the D3PD maker [18].

More about the ATLAS software computing can be found in [19–22].

4.1 Generators

The three generators are used for the Monte Carlo simulations in the present analysis of the exclusive pion production, the GenEx generator [14], the di-meson (DiMe) generator [12] and the Pythia8 generator [23] with a production of central diffraction processes switched on. None of the generators used in this analysis has been tuned for exclusive pion production at LHC energies.

The **GenEx** [14] is a Monte Carlo event generator designed for the exclusive processes in proton-proton collisions focused on the exclusive production of meson pairs, $pp \to pM^+M^-p$, like $\pi^+\,\pi^-$ or $K^+\,K^-$. It is able to produce unweighted events within a relativistic phase space.

The GenEx, unlike other generators (e.g. Exhume [24] or Pythia8 [23]) does not use parton structure functions of the colliding protons but rather Regge description. This makes it suitable for modelling of soft processes. Thus it is possible to generate events with masses of a central system below 1 GeV.

Only a non-resonant production - continuum - is implemented in the GenEx generator version used in this analysis. Because of the absence of an implementation of the absorption correction in the model it was decided to implement it additionally on the cross-section result of the GenEx simulation. The value of the absorption correction factor was set to 0.22, see Sect. 3.3.

The **DiMe** [12] is a Monte Carlo event generator designed for the di-meson processes in proton-proton collisions, like the exclusive pion production. The DiMe generator implements only a non-resonant production. It means that the DiMe generates the exclusive pion continuum without any resonant contribution. The several models of the absorption corrections are implemented in DiMe.

The **Pythia8** generator [23] is a set of tools for a generation of events in high energy collisions. It is mainly based on a parton level structure of the hadron-hadron collisions. The Pythia8 generator contains a wide range of processes including soft-QCD processes like the central diffraction (a.k.a. Double Pomeron Exchange - DPE). The model describing the central diffraction processes is limited with a minimum central-system-mass of 1 GeV. Unfortunately the most of the exclusive pion-pair-system-mass value is below this limit and thus the Pythia8 is used only for the background studies of this exclusive process.

4.2 Simulation set-up

The exclusive pion production is studied on the data from the ATLAS run 191373 and the Monte Carlo simulation is set-up according to this run. Proton beams are collided with a centre-of-mass energy at 7 TeV and transported with a nominal optics of a special high $\beta^\star$optics of 90 m [25]. The beam parameters are the same as in the analysis of the elastic scattering [26].

5 Experimental set-up

5.1 ATLAS Inner Detector

The ATLAS Inner detector (ID) [27] (Fig. 6) is the closest detector to the interaction point (IP) and contains three subsystems providing high-precision track reconstruction: the silicon pixel detector (innermost), the silicon microstrip detector, and the transition radiation tracker (outermost), which also helps to discriminate electrons from hadrons. The ID covers a range of pseudorapidity $|\eta| < 2.5$. It is surrounded by the superconducting solenoid, which produces the 2 T axial field within the ID.

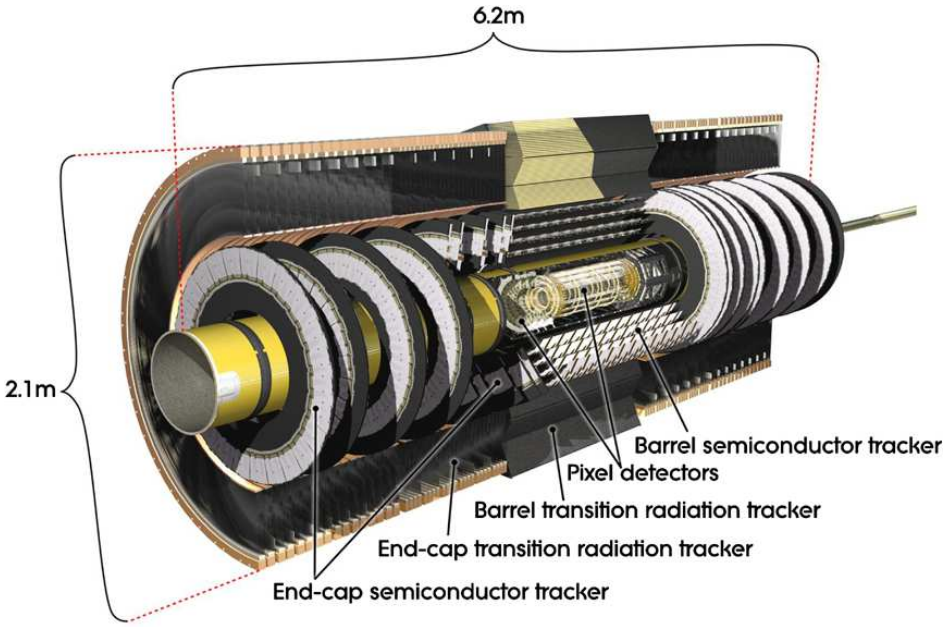

Figure 6: Cut-away image of the ATLAS Inner detector [28].

5.2 Minimum Bias Trigger Scintillators

The Minimum Bias Trigger Scintillators (MBTS) is one of the ATLAS Detector sub-components. It is placed ±3.6 m far from the ATLAS IP (on both ATLAS sides, A and C). It consists of 16 cells in two rings, the outer one and the inner one (Fig. 7). MBTS has the full ϕ space coverage in a transverse plane. The pseudo-rapidity acceptance of the outer ring is $2.08 < |\eta| < 2.78$, whereas the pseudo-rapidity acceptance the inner ring is $2.78 < |\eta| < 3.75$.

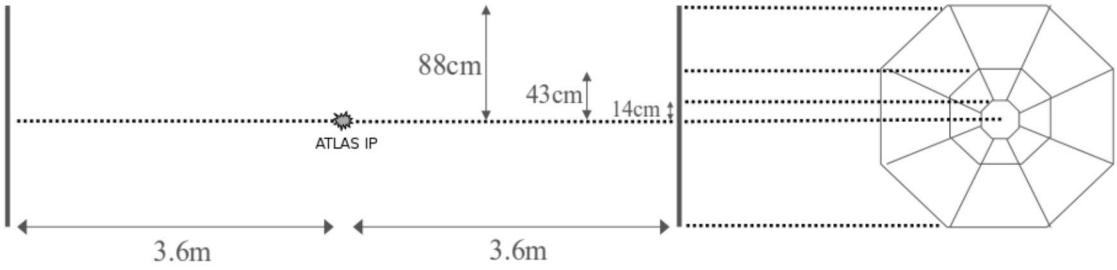

Figure 7: Minimum Bias Trigger Scintillators [29].

5.3 ALFA Detectors

The ALFA - **A**bsolute **L**uminosity **F**or **A**TLAS [1] - is a system of eight tracking detectors placed in so-called Roman Pots Fig. 8a vertically movable in four stations (Fig. 8b) which are located in the outgoing beam lines of the ATLAS forward region ±240 m from the ATLAS IP. The active part of ALFA, depicted in Fig. 8b, consists of a nearly edge-less scintillating fibres used for its two sub-components, the Main Detector (MD) and the Overlap Detector (OD). This system allows to detect the protons scattered under a very small angle outgoing from the IP.

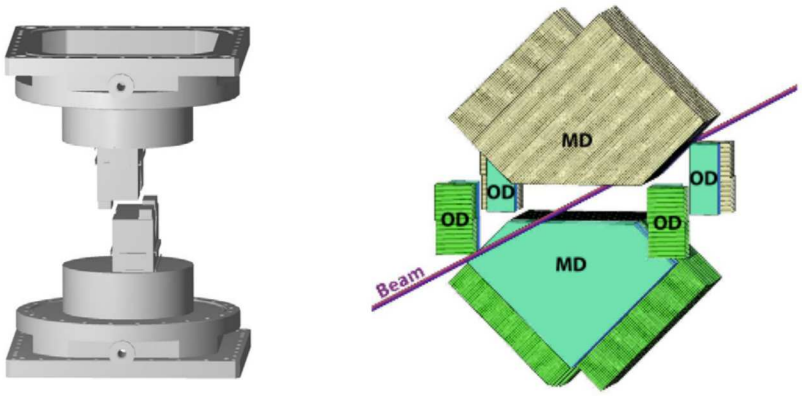

(a) (b)

Figure 8: A schematic view (a) of the main and the overlap detectors in two Roman pots of the station [2] and (b) of two Roman Pots in the ALFA station [2].

The schematic view of the ALFA set-up in the LHC tunnel in Fig. 9 shows ALFA positions with respect to the ATLAS detector, the quadrupoles (Q1-Q7) and the dipoles (D1, D2) magnets.

5.4 Beam parameters and optics

The data were taken during the special ATLAS low luminosity run 191373 in Autumn 2011 using the special high $\beta^\star$ = 90 m optics. In the ALFA elastic scattering analysis [2] the optics parameters were tuned to re-calibrate the magnet strength of Q1Q3 and the small residual crossing angle is compensate by a machine compensation system. The new set of optics parameters was found and called as the effective optics. it should be compared with the so-called nominal optics which was originally designed for runs with a special high $\beta^\star$ = 90 m optics. The nominal optics is used in Monte Carlo simulation and it is a part of the ATLAS offline software and each Athena framework [4] releases.

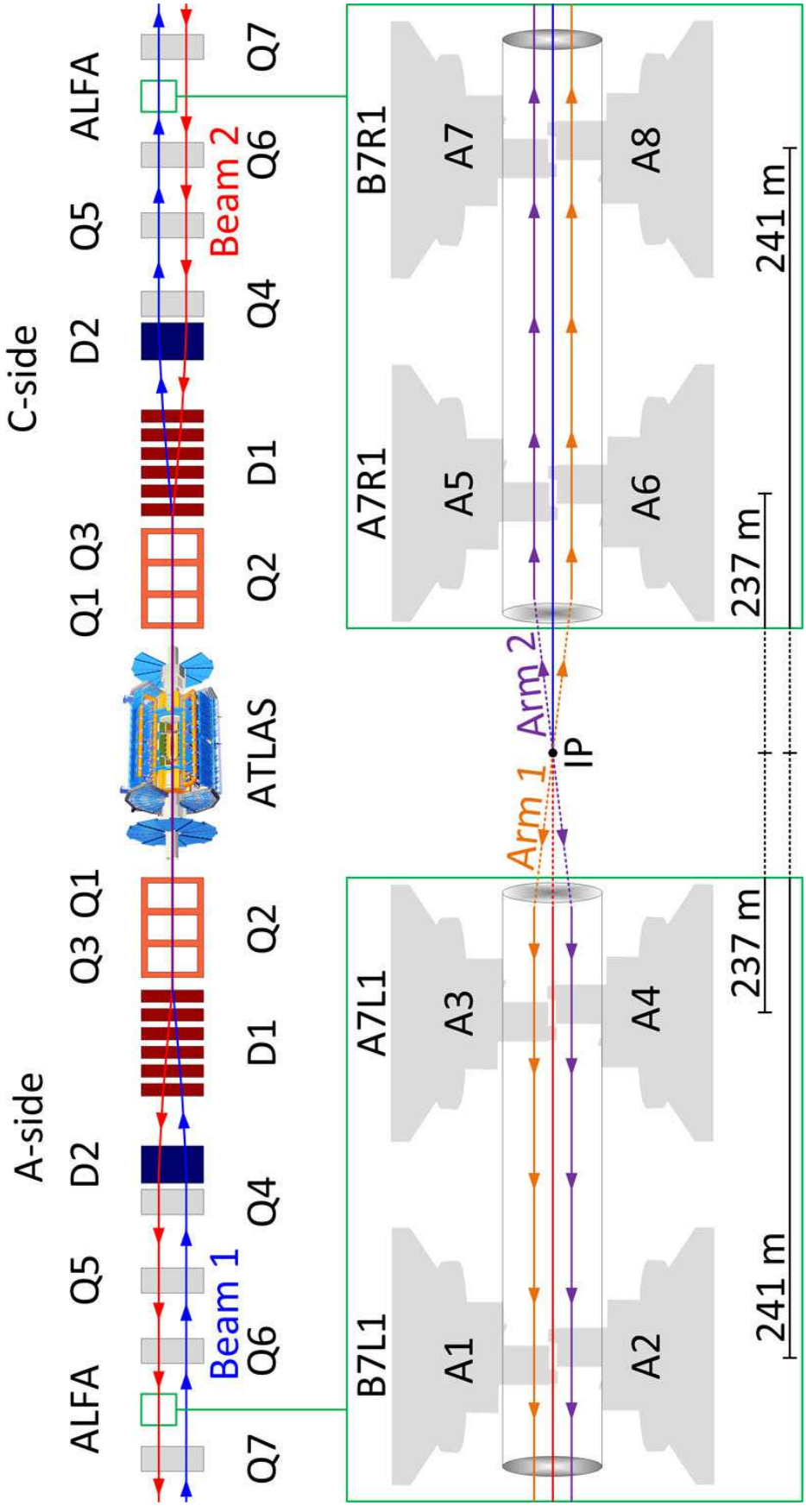

Figure 9: Schematic view of the ALFA set-up defining the naming and numbering conventions.

5.5 Trigger conditions

The ATLAS run 191373 was dedicated run mainly for the measurement of the elastically scattered protons. Therefore the trigger settings were not the most ideal for the measurement of the exclusive pion production. The ATLAS trigger system consists of the two trigger levels, depicted in Fig. 10, the hardware triggering (L1) [30] and software triggering (HLT) [31].

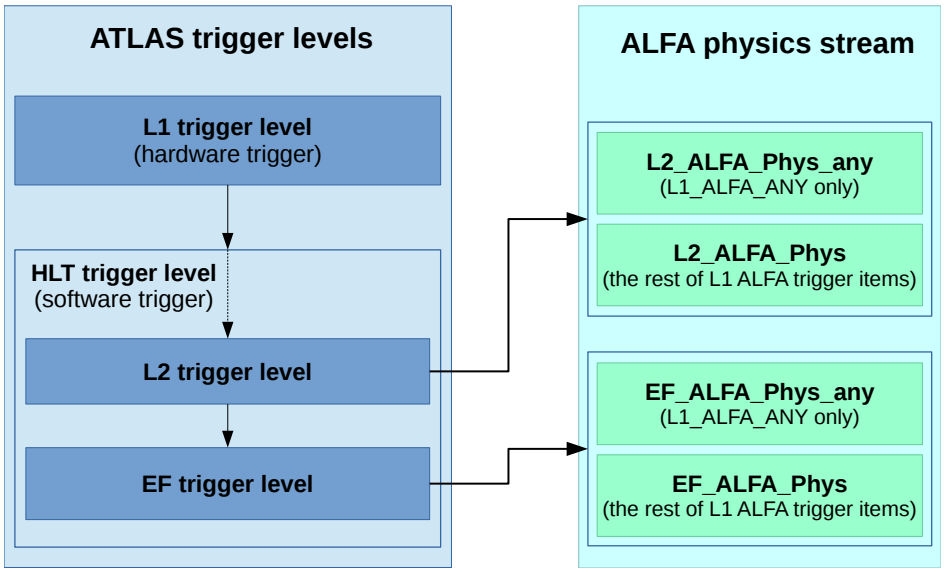

Figure 10: ALFA trigger level scheme.

The exclusive pion analysis is split into two configurations, the **elastic** one and the **anti-elastic** one, based on the used triggers. The elastic configuration is based on *L2_ALFA_Phys* HLT trigger chain, whereas the anti-elastic configuration is based on *L2_ALFA_Phys_any* HLT trigger chain. The efficiency of the ALFA triggers is more than 99%, more precisely studied in [32].

6 Particle kinematic reconstruction

In the exclusive production kinematic parameters of two pions and two protons have to be reconstructed. The pion kinematics is provided by the Inner detector whereas the kinematics of the protons is reconstructed by the ALFA detector system.

6.1 Inner detector kinematic reconstruction

The Inner Detector (ID) is a detector system able to reconstruct a particle trajectory as well as its complete set of kinematics [33]. In the case of the exclusive pion production the ID reconstructs the pion kinematics with $\approx$10 MeV precision in both, p_x and p_y. The pion kinematics resolution for the GenEx Monte Carlo simulation of the exclusive pion production is shown in Fig. 11, where the red distribution corresponds to the negatively charged pions whereas the blue distribution corresponds to the positively charged pions.

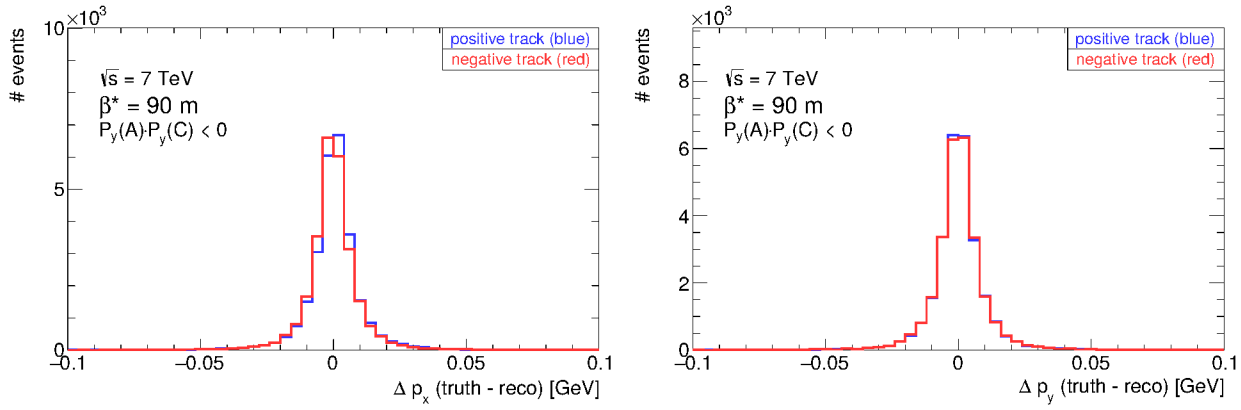

(a) (b)

Figure 11: The pion track kinematic reconstruction resolution (as a difference between the particle and detector level) for p_x in (a) and p_y in (b) reconstructed by the Inner detector in the MC simulation. The red distribution is for negative pions whereas the blue distribution is for positive pions.

6.2 ALFA kinematic reconstruction

The ALFA detector is a tracking detector, see Sect. 5.3, which is not able to directly reconstruct proton kinematics. Therefore dedicated reconstruction algorithms were developed. Two of them are presented, the ALFA Reco algorithm [34] and the Lattice method algorithm [26].

The **ALFA Reco** is an algorithm based on a parametrization of the reverse mapping: $x, y, x', y' \rightarrow \Theta^*, \varphi^*, \xi$, where $*$ denotes proton's kinematics at the IP. It requires a knowledge of the reconstructed diffractive proton position in two consequent ALFA detectors (see Fig. 12) and of the beam spot position in the IP.

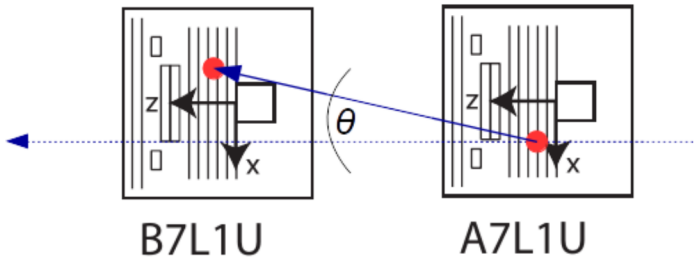

Figure 12: The local angle θ between two consequent ALFA detectors, here between B7L1U and A7L1U. The local angle is defined in both x and y coordinate.

The **Lattice method** is an algorithm based on the knowledge of elastic protons transport equations from the ATLAS IP to the ALFA detectors and on the knowledge of the optics settings during the data taking. This method was used for the studies where the protons energy loss is zero-like in the analysis of the elastically scattered protons [26]. But it can be shown - and in fact this analysis shows it - that the proton energy loss in the current analysis is very small and that such diffractive protons detected by the ALFA detector can be treated as elastic-like. The proton trajectory equation for the transport of the elastically scattered protons can

be described as

$$\begin{pmatrix} u^\star \\ u^{\star\prime} \end{pmatrix} = \begin{pmatrix} T_{11}T_{12} \\ T_{21}T_{22} \end{pmatrix} \begin{pmatrix} u(s) \\ u'(s) \end{pmatrix}, \tag{12}$$

where $u(s)$ represents the x (or y) position of a proton in the beam coordinate system at a given position s, whereas the $u'(s)$ represents the θ angle in a given position of s, and $T = M^{-1}$ is the inverse of transport matrix M described by the elements

$$\begin{aligned} M_{11} &= \sqrt{\frac{\beta}{\beta^\star}}(\cos\Psi + \alpha^\star \sin\Psi), & M_{12} &= \sqrt{\beta\beta^\star}(\sin\Psi), \\ M_{21} &= \frac{(\alpha^\star - \alpha)\cos\Psi - (1 - \alpha\alpha^\star)\sin\Psi}{\sqrt{\beta\beta^\star}}, & M_{22} &= \sqrt{\frac{\beta^\star}{\beta}}(\cos\Psi - \alpha\sin\Psi)\,. \end{aligned} \tag{13}$$

β resp. $\beta^\star$ is the optical function in a given position s resp. in the interaction point ($s = 0\,\mathrm{m}$) and α is proportional to the β derivative. From a knowledge of the reconstructed proton position ($u(s)$) in ALFA detector and its local angle ($u'(s)$) the proton position and its angle in the ATLAS IP using [26] can be established as

$$u^\star = T_{11} \cdot u + T_{12} \cdot u', \quad u^{\star\prime} = T_{21} \cdot u + T_{22} \cdot u'\,. \tag{14}$$

7 Data taking and event selection

This section describes the events selection used in the exclusive pion pair production analysis. A cut flow of event selection was developed to select a signal from either LHC data or Monte Carlo (MC) simulation and it is based on event-by-event selection which is split into several modules. All modules are common both for data and Monte Carlo simulation except the pre-selection module (covering proton's bunch selection and trigger selection) used only for data.

The cut flow (see Fig. 13) covers the track selection in both ATLAS Inner detector (trk quality, two good tracks, oppo-sign tracks) and the ALFA detectors (protons in ALFA, proton kinematics), the vetoing on the signal from the Minimum Bias Trigger Scintillators (MBTS veto), the background suppression based on the geometrical properties of the tracks reconstructed in ALFA detectors (ALFA Geometry), the cut on the kinematics of the exclusive system based on a momentum balance conservation law (Momentum balance), the selection of Inner detector tracks which identified as pions (Particle identification) and a selection of the kinematic region in which the analysis is done (Restricted kinematic range).

The data for the ATLAS Run 191373 were taken in the period of Oct 20 2011 12:58:42 - 17:14:21 during the special high $\beta^\star = 90\,\mathrm{m}$ (the LHC fill 2232). The collisions at IP1 were obtained for the RF bucket 1 (BCID 1) for both beams. The ATLAS run was filled with one nominal bunch of the intensity $7 \cdot 10^{10}$ protons and 12 pilot bunches of the intensity $1 \cdot 10^{10}$ protons as well as of one unpaired bunch of the intensity $7 \cdot 10^{10}$ protons.

The important parameter for each data analysis is the knowledge of the luminosity. The principles of the luminosity measurement are described in the ATLAS total cross-section measurement [2]. The exclusive

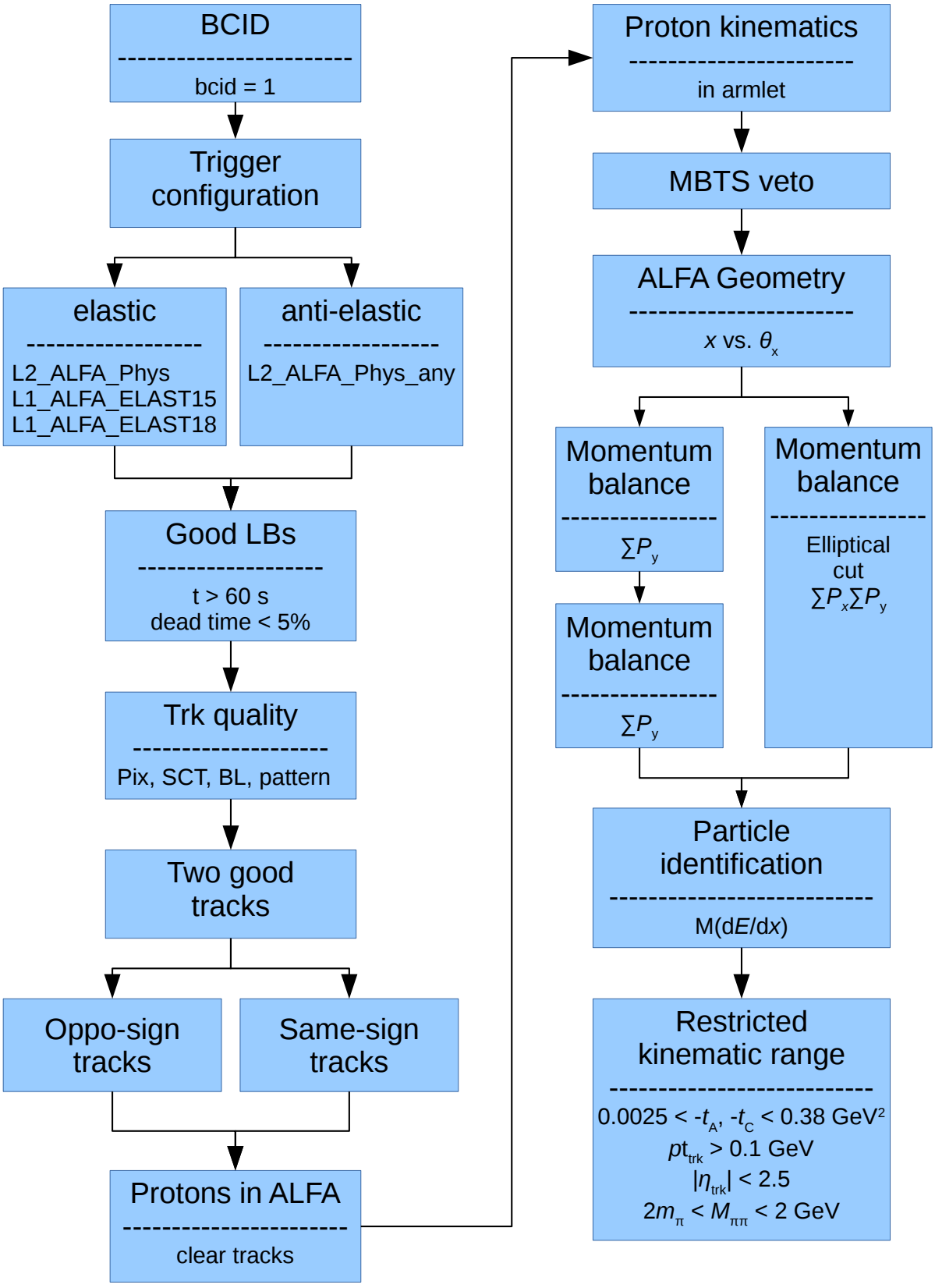

Figure 13: Analysis scheme diagram

pion production analysis inherits the luminosity results from the [2] due to the same data of the ATLAS run 191373 with the same sets of the good luminosity blocks as in the [2]. The luminosity was determined from the LHC beam parameters using van der Meer scans [35]. The final result of the integrated luminosity for the ATLAS run 191373 including the statistical and the systematic errors is

$$L_{\text{int}}^{\text{run}} = 79.68 \pm 0.13^{(\text{stat})} \pm 1.87^{(\text{syst})}\ \mu\text{b}^{-1}. \tag{15}$$

The MBTS veto selection is designed to suppress the non-exclusive pion events using the information from the Minimum Bias Trigger system, described in Sect. 5.2. The effect of this selection is shown in Fig. 14 where the background suppression is visible not only in tails of the $\sum p_y$ distribution but also within the signal peak around zero. The signal peak is well identifiable (Fig. 14b) in the data distribution and the MC background simulation.

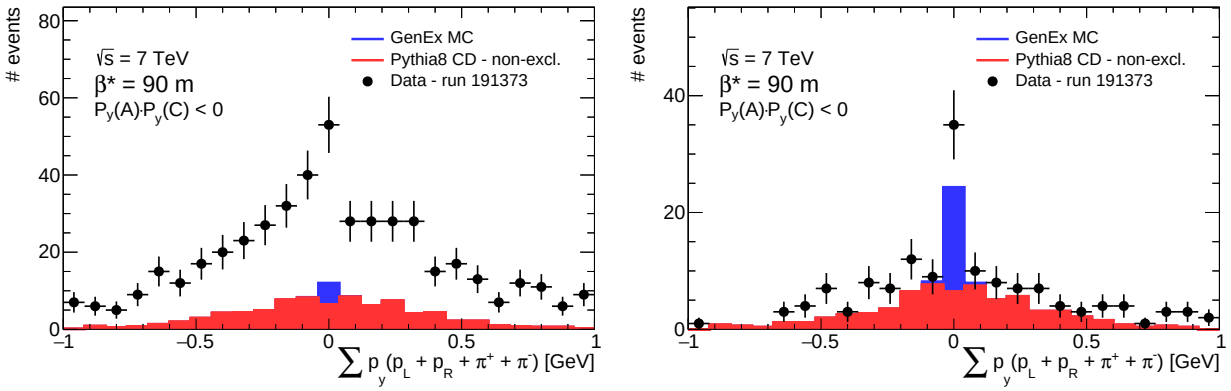

Figure 14: The $\sum p_y$ of the exclusive pion production final state products (a) before and (b) after the MBTS veto is applied. The data are represented by the black points whereas the Monte Carlo simulations are represented by the blue histogram for the GenEx simulation and by the red histogram for the Pythia8 central diffraction containing only the non-exclusive events. The MC histograms are stacked.

The kinematic event selection is based on the system momentum balance which allows us to select the exclusive events. It would be ideal to use the full information about the system momentum balance. But as it was mentioned in Sect. 6 the proton kinematic reconstruction precision of the proton energy - together with its p_z - is insufficient for the purpose of our analysis. Only the p_x and p_y momentum components can be safely used. This also means that after the kinematic event selection our sample can still contain non exclusive events. Following two equations describe the momentum balance of the exclusive system for p_x and p_y momentum components

$$p_x(\text{p}_A^{\text{in}}) + p_x(\text{p}_C^{\text{in}}) = p_x(\text{p}_A^{\text{out}}) + p_x(\text{p}_C^{\text{out}}) + p_x(\pi^+) + p_x(\pi^-), \tag{16}$$

$$p_y(\text{p}_A^{\text{in}}) + p_y(\text{p}_C^{\text{in}}) = p_y(\text{p}_A^{\text{out}}) + p_y(\text{p}_C^{\text{out}}) + p_y(\pi^+) + p_y(\pi^-), \tag{17}$$

where p_A^{in} and p_C^{in} are two protons incoming into the interaction and p_A^{out}, p_C^{out}, π^+ and π^- are two protons and two pions outgoing from the interaction.

It is assumed that the main fraction of the reconstructed tracks in the ID consists of the pions. But particles like kaons or protons would be also present in the reconstructed tracks which then can contribute to the

background of considered process and should be removed. A technique based on the knowledge of the particles ionization losses when passing through the ATLAS Pixel detector - which is a part of the ATLAS Inner detector - is able to (probabilistically) identify the particles. The Pixel detector is able to measure the average specific energy loss $\mathrm{d}E/\mathrm{d}x$ for the charged particles coming from proton-proton interactions at high energies [36]. The charged particle ionization loss $\mathrm{d}E/\mathrm{d}x$ is described by the Bethe-Bloch function, in simplified way $\mathrm{d}E/\mathrm{d}x \approx \beta\gamma$. This energy loss can be combined with the particle momentum, $p = mc\beta\gamma$. Then the particle is identified by calculating of its mass from a measurement of its momentum and its energy loss. The whole procedure is fully described in [36].

8 Acceptance and unfolding

The acceptance and unfolding corrections play an important role on the road to the final results, as they influences the result of a measurement: the geometrical acceptance of the detector systems, reconstruction efficiencies of used reconstruction algorithms, trigger pre-scales used during the data taking, the restriction of kinematic region wherein the process is studied, the particle identification efficiency for a particle determination or the distributions shape corrections.

This section describes needed corrections and their effects on the exclusive pion production analysis. Due to the low statistics in data it was decided to calculate only one overall correction (single-bin correction) representing/covering all corrections mentioned above. The final number of the exclusive events - after the background subtraction - is corrected by this overall correction and the cross-section is obtained.

The exclusive pion analysis is divided into two configurations: the elastic and the anti-elastic ones. The overall corrections are calculated for both configurations, independently.

All correction calculations were made using the GenEx Monte Carlo simulation (i.e. only signal). Both the particle and the detector levels[3] of the simulation and the analysis were performed for the same fiducial volume (restricted kinematic region in Fig. 13). The number of events that passed two levels is calculated. Then the overall correction factor is expressed as a ratio between the number of events $N^{\text{passed}}_{\text{detector\_level}}$ passed the analysis on the detector level and the number of events $N^{\text{passed}}_{\text{partical\_level}}$ passed the fiducial volume selection on the particle level,

$$f_{\text{corr}} = \frac{N^{\text{passed}}_{\text{detector\_level}}}{N^{\text{passed}}_{\text{partical\_level}}}. \tag{18}$$

The variable f_{corr} represents the overall correction which corrects the data final event selection to the cross-section value; the luminosity value is not a part of the overall correction. The Table 1 summarizes the values of f_{corr} for various case studies like the elastic/anti-elastic configurations, LatticeMethod/ALFAReco methods of the proton kinematics reconstruction or the GenEx/DiMe MC simulations.

[3] By the particle level in the Monte Carlo simulation the truth particle level is meant. By the detector level in the Monte Carlo simulation the reconstructed particle level is meant, and an information about a particle after the reconstruction is used.

Table 1: The overall correction values for several studies including elastic/anti-elastic configuration, different proton kinematic reconstruction algorithms or different MC signal simulations.

	GenEx				DiMe	
	elastic		anti-elastic		elastic	anti-elastic
	Lattice	ALFA Reco	Lattice	ALFA Reco	Lattice	Lattice
overall correction	0.0724611	0.0723752	0.0674902	0.0674795	0.0962788	0.0950474

9 Background

The background in data has several components. To remove background first the condition on MBTS (Sect. 7) is applied and removes a significant amount of the background. In case of the exclusive $\pi^+\pi^-$ production it is assumed that remaining fraction of the background comes from the central diffraction processes. One of the reasons supporting this expectation is that the exclusive pion production is studied on a special low-μ run ($\mu = 0.035$), so almost no pile-up is expected and coincidences of SD + beam halo, or SD + SD or beam halo + beam halo can be safely neglected.

The Pythia8 simulation with processes of the central diffraction is used to estimate the level of background and its subtraction. Although the Pythia8 central diffraction does not fully describe the exclusive $\pi^+\pi^-$ production fiducial volume due to the lower threshold of a generated central mass in Pythia8 which is 1 GeV. So the main fraction of the exclusive $\pi^+\pi^-$ production can lie under this threshold. Nevertheless, it is still possible to estimate the background fraction. The exclusive pion pair events were removed from the Pythia8 MC simulation on particle level[4] and thus only the central diffraction events are used in the background subtraction. A number of events N_{bckg} which passed the analysis chain are counted as the background events. This number is later used to be subtracted from the number of the events N_{data} which passed the analysis chain for data. After the background events subtraction defined by Eq. 19 the rest of the events N_{sig} from the data is counted as the exclusive events. Finally the overall correction is applied on the signal events to calculate the cross-section of the exclusive pion production:

$$N_{\text{sig}} = N_{\text{data}} - N_{\text{bckg}}. \tag{19}$$

Still, the situation is more complex. A normalisation of MC sample to data has to be made. There are two ways of the background normalisation, using opposite-sign or same-sign events. The ideal behind is simple: let us consider several kind of processes, $p + p \to p + p + \pi^+ + \pi^-$, $p + p \to p + p + \pi^+ + \pi^- + \pi^+ + \pi^-$ which can be studied using the same-sign events and $p + p \to p + p + \pi^+ + \pi^- + \pi^0$ which contributes into opposite-sign events. Independently on considered process the background normalisation can be performed also in a different system momentum space, outside the expected system-momentum signal region (the signal region is removed) and within the whole system-momentum region. In total four methods for normalization of MC to data are considered. The normalisation process is performed before the $\sum p_y$ kinematic selection (but after the condition on MBTS, particle identification and fiducial volume selection).

It was found out that all methods return comparable results of the background subtraction which shows Fig. 15. The same figure also shows that the process of background subtraction is reasonably stable among

[4] The removing of the events on particle level means to remove MC truth (or generated) events from the sample before any sample analysis

various system-momentum signal regions (with a default signal region defined by $3.5\,\sigma(\sum p_y)$) and thus it can be assumed that this background suppression method fully describe the background in data.

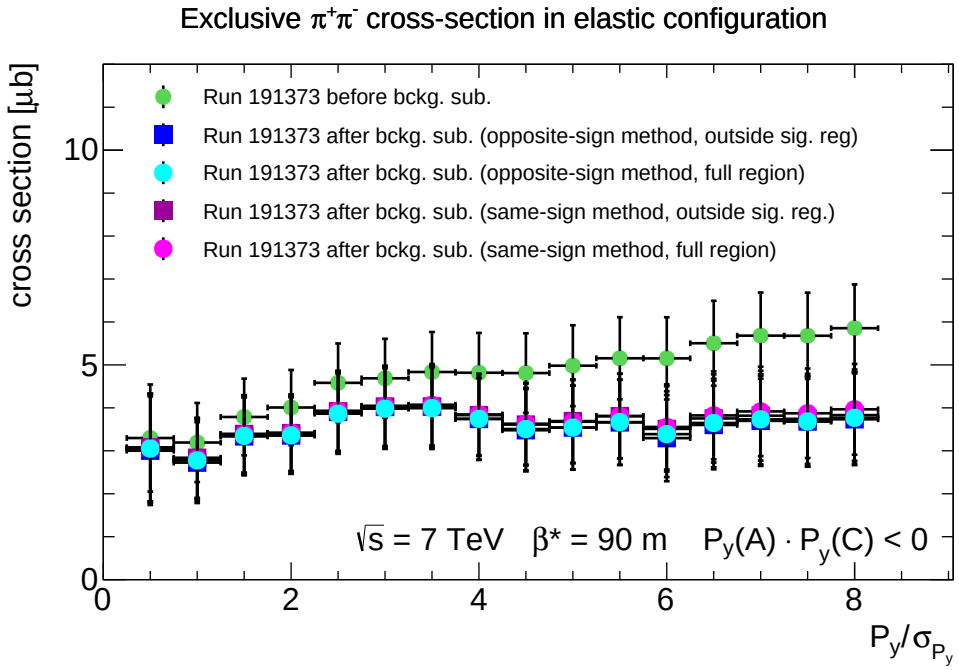

Figure 15: A background subtraction evolution as the function of p_y/σ_{p_y} ratio signal region for the elastic configuration of data and the PYTHIA8 CD non-exclusive sample. The blue graph represents data before background subtraction. The last three graphs represent the data after background subtraction, in cyan graph for a background normalisation using same-sign events in full region, in green graph for a background normalisation using same-sign events outside the signal region and in magenta graph for a background normalisation using opposite-sign events outside the signal region.

10 Data analysis

The effect of pre-selection steps on the number of events are summarized in Table 2 and covers both the elastic and the anti-elastic configurations.

Table 2: The data cut flow statistics for both the elastic and the anti-elastic configurations.

Run 191373	**Number of events**	
	Elastic configuration	**Anti-elastic configuration**
Total number of events	6620953	
BCID	1898901	
Trigger pre-selection	1155523	413096
Good lumi-blocks	1106855	397683

The rest of data cut flow (from Sect. 7) is summarised in Table 3 which includes statistics for both the ALFA Reco and Lattice method proton kinematics reconstruction (Sect. 6.2). It also compares the two

configurations, the elastic and the anti-elastic one. Only few events survived the chain, for the elastic configuration there are 27 events whereas for the anti-elastic configuration are only 3 events when lattice method was used. The big statistical error is expected due to the low statistics. The analysis is split into two configurations, as for the anti-elastic configuration the trigger pre-scale is 15 (quite high) in comparison with the trigger pre-scale of the elastic configuration equal to 1.

Table 3: The data cut flow statistics for both proton kinematic reconstruction cases, the ALFA Reco method and the Lattice method.

GenEx	configuration			
	elastic		anti-elastic	
	Lattice method	**ALFA Reco method**	**Lattice method**	**ALFA Reco method**
Data Quality & Trigger pre-selection	1106855		397683	
ID selection	1505		1099	
ALFA track selection	485	484	11	11
MBTS veto	138	137	5	5
ALFA geometry selection	112	112	5	5
Kinematic cut $\sum p_y$	42	42	3	3
Kinematic cut $\sum p_x$	34	39	3	3
Particle identification ($M_{dE/dx}$)	31	36	3	3
Kinematic region cut	27	31	3	3

10.1 Shape distribution comparison

The aim of this section is to show an agreement between the basic distributions made of the data and the Monte Carlo simulations. The overall correction which is described in Sect. 8 and is used to correct the final result is based on this agreement. In case of big differences and without their clear understanding the overall correction calculation would not be used.

An example of control distributions is shown in Fig. 16. These distributions are filled by the events collected before the kinematics event selection to avoid a bias by the artificial cuts. They compare the tracks and protons kinematics of p_x and p_y reconstructed by the ATLAS ID and ALFA detectors and within the statistical errors in data the shape distributions are comparable between data (represented by black points) and the GenEx MC simulation (represented by a blue histogram).

10.2 Exclusive pion momentum balance distributions

The shape of the momentum balance of the exclusive pion system is considered here. Only the x and y components of the products momentum are used due to the insufficient proton kinematic reconstruction of proton p_z and the E four-momentum components. Due to the low statistics in the case of the anti-elastic configuration, only the distributions for the elastic configuration of the analysis are considered.

The $\sum p_x$ and $\sum p_y$ distributions are shown in Fig. 17. The black points represent the data whereas the blue histogram represents the GenEx MS simulation and the red histogram represents the Pythia8 MC

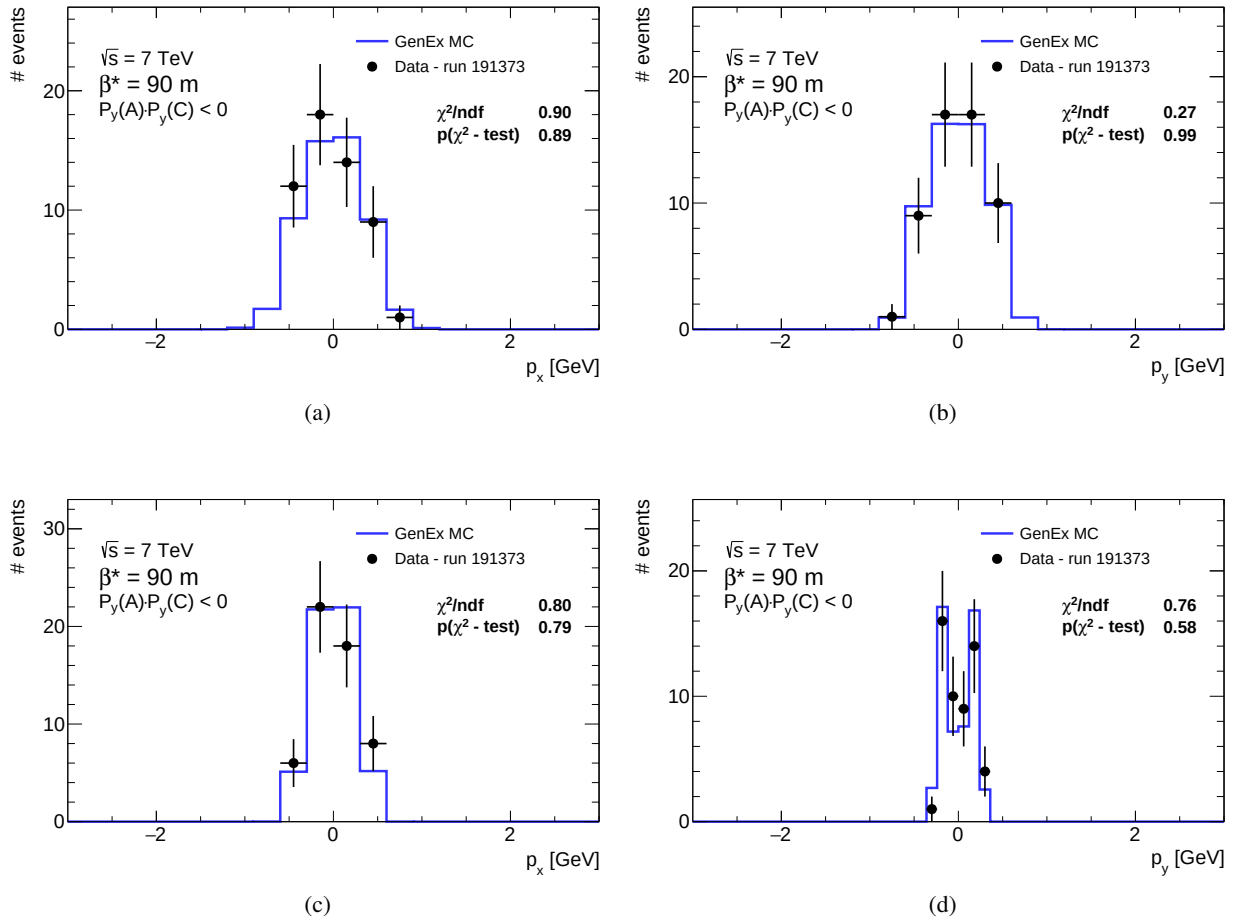

Figure 16: Distributions of (a) p_x and (b) p_y momentum components of the track reconstructed in the ATLAS ID and of (c) p_x and (d) p_y components of the proton reconstructed in the ALFA detectors. Both the data and the GenEx Monte Carlo simulations are drawn.

simulation. The distributions contain events before the kinematics selections on $\sum p_y$ and $\sum p_x$ to see their full ranges. In case of the GenEx MC simulation (only signal) a clear peak around the zero value is well visible, showing that the system is balanced and the signal region defined. In the case of data the peak is accompanied tails on both sides outside the signal region. It assumed that the tails in data outside the signal region contain only the non-exclusive events. To understand the tails in data one can look on the Pythia8 Monte Carlo simulation of the central diffraction processes which are a dominant background processes for the exclusive pion production. A comparison of the data with the Pythia8 Monte Carlo simulation shows a quite good agreement of the distributions shape (especially in $\sum p_y$ case) in both the central peak and the tails. This agreement is used also in the background subtraction process.

10.3 Exclusive pion cross-section distributions

In this section the distributions after analysis cut flow - but before the background subtraction are presented. Only the distributions for the analysis of the elastic configuration are discussed. The Fig. 18a shows the central system transverse momentum $p_{t_{\pi^+\pi^-}}$ distribution whereas the Fig. 18b describes the central system

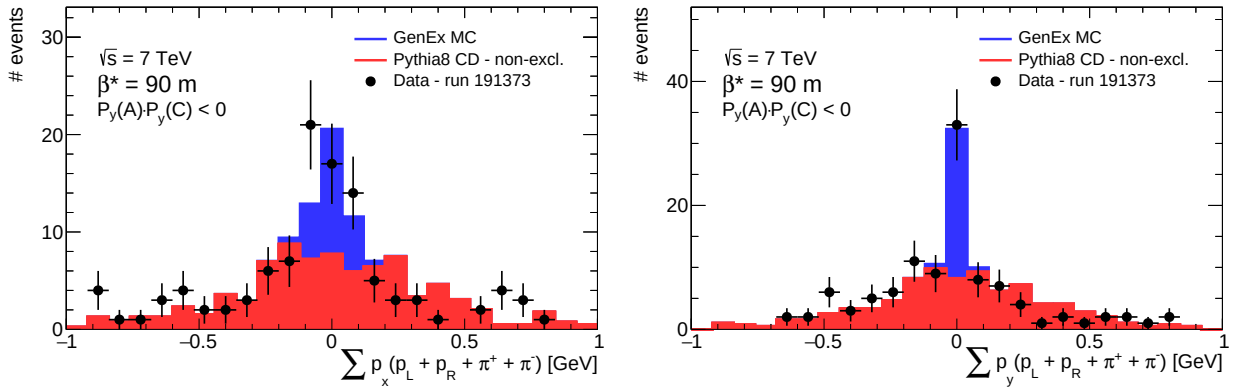

(a) (b)

Figure 17: The momentum balance distributions for the p_x and p_x components of the exclusive central system. The blue histograms represent the GenEx MC simulation, the red histograms represent the Pythia8 central diffraction MC simulation and the black distribution shows data. The event selection before the momentum balance cut is applied.

invariant mass $M_{\pi^+\pi^-}$ distribution of the exclusive pion production as an example here. Comparing the data with the Monte Carlo simulation no good agreement of $p_{t_{\pi^+\pi^-}}$ values is achieved yet, but the data evince lower statistics. On the other hand the $M_{\pi^+\pi^-}$ distribution does not indicate almost any differences between the data and the Monte Carlo simulation.

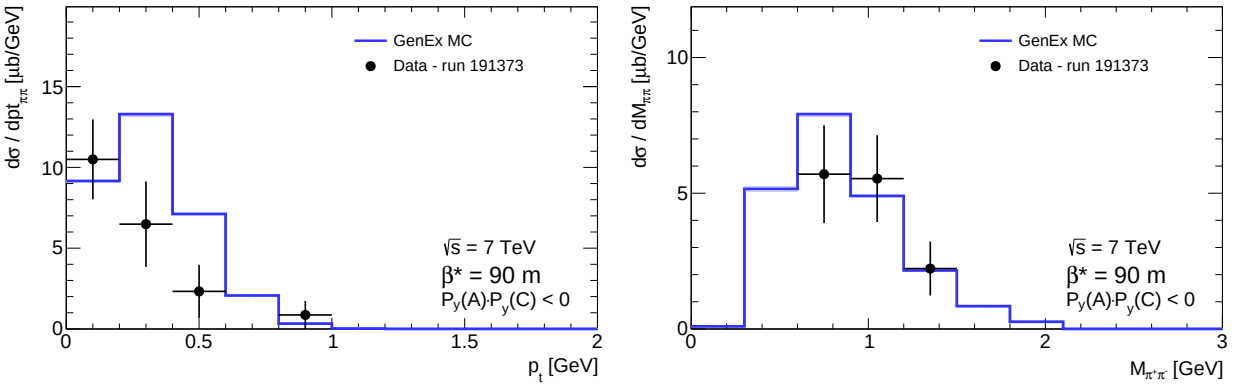

(a) (b)

Figure 18: A differential cross-section distribution as the function of (a) the central system transverse momentum $pt_{\pi^+\pi^-}$ and (b) the central system invariant mass $M_{\pi^+\pi^-}$. The data are represented by the black points whereas the GenEx MC simulation is represented by the blue histogram.

The cross-section for the elastic configuration was calculated for each distribution of the differential cross-section and the results are summarised in Table 4. The results are compared with the cross-section calculated using the overall (single-bin) correction which is a default correction method in this exclusive pion analysis. Quite big fluctuations between the cross-sections calculated integration of the differential cross-sections is visible. Differences can be caused by low data statistics followed with by event fluctuations. The effect of the fluctuation can be suppressed with the cross-section calculation using the overall correction. This is also the reason why the overall correction is used as the default method for exclusive pion cross-section

calculation. Note that the calculation based of the differential cross-section is performed only for the elastic configuration where the statistics allow to do such calculation (although very limited). In the case of the anti-elastic configuration (of a very low statistics) the only way is to calculate the integrated cross-section using the overall corrections.

Table 4: The integrated exclusive pion cross-section at centre-of-mass energy $\sqrt{s} = 7$ TeV calculated in two ways, using overall calculation and integrating the differential cross-section. Before background subtraction.

	Elastic configuration					
cross-section	single bin calculation	$\phi_{\pi^+\pi^-}$	$\eta_{\pi^+\pi^-}$	$y_{\pi^+\pi^-}$	$pt_{\pi^+\pi^-}$	$M_{\pi^+\pi^-}$
σ [μb]	4.73 ± 0.91	5.59 ± 1.21	4.45 ± 0.87	4.82 ± 0.94	4.04 ± 0.81	4.04 ± 0.78

10.4 Exclusive pion cross-section after background subtraction

The basic assumption used in the present analysis is that the main source of the background in the exclusive pion production comes from the central diffractive processes. Pythia8 with the central diffraction (Pythia8 CD) was used for the background estimation. The background subtraction process is described in Sect. 9 where it is shown that the central diffractive processes without the exclusive pion pair production[5] in Pythia8 reasonably describe the shape outside the signal region in data as well as the amount of the background for various p_y/σ_{p_y} intervals. The Table 5 summarises the results, before and after the background subtraction. The overall background fraction in data is about 15%; for the elastic configuration it is about 18% and for the anti-elastic configuration it is about 13%. The statistical error of the overall cross-section section is influenced by the event statistics of the anti-elastic configuration.

Table 5: Exclusive pion cross-section before and after the background subtraction.

	Exclusive $\pi^+\pi^-$ cross-section [μb]		
Background subtraction	**elastic configuration**	**anti-elastic configuration**	**overall**
before	$4.84 \pm 0.93^{(\mathrm{stat})}$	$8.64 \pm 4.99^{(\mathrm{stat})}$	$13.48 \pm 5.08^{(\mathrm{stat})}$
after	$3.99 \pm 0.95^{(\mathrm{stat})}$	$7.44 \pm 5.00^{(\mathrm{stat})}$	$11.43 \pm 5.09^{(\mathrm{stat})}$

10.5 Exclusive pion cross-section after ALFA reconstruction efficiency correction

The results presented above counted on the ALFA reconstruction efficiency based on the MC simulation. It is known that the ALFA reconstruction efficiency differs between the MC simulation and data. Therefore the correction factor on the ALFA reconstruction efficiency was calculated and applied on the result. The visible exclusive pion cross-section is now 14.41 ± 6.58(stat) and is summarized in Table 6.

[5] The exclusive pion pair events were removed from the central diffractive sample (Pythia8) on a particle level to keep only a background events.

Table 6: Exclusive pion cross-section before and after ALFA reconstruction efficiency correction.

	Exclusive $\pi^+\pi^-$ cross-section [μb]		
	elastic configuration	**anti-elastic configuration**	**overall**
before	$3.99 \pm 0.95^{(\text{stat})}$	$7.44 \pm 5.00^{(\text{stat})}$	$11.43 \pm 5.09^{(\text{stat})}$
after	$4.77 \pm 1.14^{(\text{stat})}$	$9.65 \pm 6.48^{(\text{stat})}$	$14.41 \pm 6.58^{(\text{stat})}$

11 Systematic uncertainties

The present analysis suffers from very low event statistics available in data (ATLAS run 191373). A very low statistics graduates in a very high statistical uncertainty and there is a good reason to say that dominant uncertainty of the measurement comes from statistics. Despite of it a study of the systematic uncertainty was performed.

The systematic uncertainty was studied as an effect of a beam energy uncertainty, an amount of a dead material in the Inner detector, a vetoing on MBTS signal, ALFA particle reconstruction efficiency, the effect of various ALFA kinematic reconstruction, different description of accelerator optics, background subtraction, a precision of the luminosity measurement and the effect of various theoretical models. The Table 7 summarises the systematic uncertainties of the exclusive pion analysis. The overall systematic uncertainty of the exclusive pion cross-section measurement was determined to $^{+1.5}_{-1.9}(\text{syst}) \pm 0.3(\text{lumi}) \pm 1.3(\text{model})$ μb.

Table 7: The summary of the exclusive pion cross-section systematic uncertainties.

	value [μb]	
uncertainty	**lower**	**upper**
Beam energy	-0.02	0.02
ID dead material	-0.61	—
veto on MBTS signal	-1.14	0.65
ALFA reconstruction efficiency	-0.08	0.08
ALFA kinematic reconstruction	-1.14	1.14
Optics	-0.08	0.08
Background	-0.70	0.70
Overall systematic uncertainty	-1.86	1.49
Luminosity	-0.34	0.34
Theoretical model	-1.32	1.32
Total	-2.31	2.02

12 Results

The fiducial cross section of the exclusive pion pair production at centre-of-mass energy $\sqrt{s} = 7\,\text{TeV}$, together with its statistical and systematic errors, was determined.

There was no dedicated trigger for anti-elastic configuration and high scaling of L1_ALFA_ANY trigger led to the big statistical uncertainty. The fiducial cross-section for the elastic configuration is

$$\sigma^{\text{vis}}_{\pi^+\pi^-}(\text{elastic}) = 4.8 \pm 1.1(\text{stat})\,\mu\text{b}$$

whether for anti-elastic configuration it is

$$\sigma^{\text{vis}}_{\pi^+\pi^-}(\text{anti}-\text{elastic}) = 9.7 \pm 6.5(\text{stat})\,\mu\text{b}.$$

The ratio of the cross-section values for the elastic and the anti-elastic configuration is in data $1:2$ whereas the ratio predicted by GenEx is almost $1:1$ (which results from GenEx MC simulation).

The statistical uncertainty is the dominant source of the overall uncertainty. The result serves as the first estimate of the exclusive pion cross-section on the LHC scale energies.

The total fiducial cross section of the exclusive pion pair production at centre-of-mass energy $\sqrt{s} = 7\,\text{TeV}$ and the given analysis cut flow was determined to be

$$\sigma^{\text{vis}}_{\pi^+\pi^-} = 14.4 \pm 6.6(\text{stat})\,^{+1.5}_{-1.9}(\text{syst}) \pm 0.3(\text{lumi}) \pm 1.3(\text{model})\,\mu\text{b}.$$

The biggest contribution to systematic error comes from vetoing on the MBTS only, then from ALFA kinematic reconstruction algorithms, from the background and from Inner detector dead material description, see Sect. 11.

There are few theoretical models describing the exclusive pion production and even less Monte Carlo generators based on existing theoretical studies Sect. 3. It was shown that the Monte Carlo generators are able to describe the exclusive pion process. Still there are mutual differences between the models and due to the limited statistics neither model limits nor any model can be excluded.

The obtained result is, within errors, compatible with predicted value 21 µb [7] obtained for a different distance ($\approx 4\,\text{mm}$) of ALFA detectors from the beam.

13 Summary

The work on the thesis and the thesis itself led to two main outputs:

1. the existence of the simulation and analysis frameworks with more than 20000 lines of code and with the ability to be used for any similar exclusive analysis at arbitrary energy in future (e.g. centre-of-mass energy $\sqrt{s} = 14\,\text{TeV}$, $\sqrt{s} = 1\,\text{TeV}$),
2. the determination of fiducial cross-section of the exclusive pion production $p+p \to p+p+\pi^+ +\pi^-$ which has an ambitions to become the first published ATLAS diffractive analysis using the forward detectors.

The ongoing 8 TeV and 13 TeV analyses of the same process have (much) higher statistics of events and will allow more detailed analyses (especially 13 TeV one) as e.g. of the differential cross-section $\mathrm{d}\sigma/\mathrm{d}t$, still 7 TeV analysis leads to the process *observation* (3σ) in the elastic configuration.

List of author's publications

The first author:

- P. Hamal, T. Sýkora, *Simulace detektoru ALFA*, Jemná mechanika a optika, 2017, 62 (4), pp. 119-122.
- P. Hamal, T. Sýkora, *Exclusive pion production measured by ATLAS at* $\sqrt{s} = 7\,\text{TeV}$, under internal ATLAS Collaboration review, will be published as ATLAS Collaboration publication.

Author's relevant ATLAS Collaboration publications. The author has been a member of the collaboration since 13th of January 2011.

- G. Aad et al., *Measurement of the total cross section from elastic scattering in pp collisions at* $\sqrt{s} = 7\,\text{TeV}$ *with the ATLAS detector*, Nucl.Phys. B889 (2014) 486–548, arXiv: 1408.5778 [hep-ex]
- M. Aaboud et al., *Measurement of the total cross section from elastic scattering in pp collisions at* $\sqrt{s} = 8\,\text{TeV}$ *with the ATLAS detector*, Physics Letters B 761 (2016) 158–178, arXiv: 1607.06605 [hep-ex]

Co-author:

- S. Abdel Khalek, B. Allongue, F. Anghinolfi, P. Barrillon, G. Blanchot, S. Blin-Bondil, A. Braem, L. Chytka, P. Conde Muíño, M. Düren, P. Fassnacht, S. Franz, L. Gurriana, P. Grafström, M. Heller, M. Haguenauer, W. Hain, P. Hamal, K. Hiller, W. Iwanski, S. Jakobsen, C. Joram, U. Kötz, K. Korcyl, K. Kreutzfeldt, T. Lohse, A. Maio, M.J.P. Maneira, A. Mapelli, D. Notz, L. Nozka, A. Palma, D. Petschull, X. Pons, P. Puzo, S. Ravat, T. Schneider, L. Seabra, T. Sykora, R. Staszewski, H. Stenzel, M. Trzebinski, S. Valkar, M. Viti, V. Vorobel, A. Wemans, *The ALFA Roman Pot detectors of ATLAS*, Journal of Instrumentation 11.11 (2016) P11013
- L. Nozka, A. Brandt, M. Rijssenbeek, T. Sykora, T. Hoffman, J. Griffiths, J. Steffens, P.Hamal, L. Chytka, M. Hrabovsky, *Design of Cherenkov bars for the optical part of the time-of-flight detector in Geant4*. Optics Express, 2014, NOV 17 2014, Vol. 22, Issue 23, pp. 28984-28996. ISSN: 1094-4087. DOI: 10.1364/OE.22.028984.
- L. Nožka, L. Adamczyk, G. Avoni, A. Brandt, P. Buglewicz, E. Cavallaro, G. Chiodini, L. Chytka, K. Ciesla, P. M. Davis, M. Dyndal, S. Grinstein, P. Hamal, M. Hrabovský, K. Janas, K. Jiráková, M. Kocian, T. Komárek, K. Korcyl, J. Lange, D. Mandát, V. Michálek, I. Lopez Paz, D. Northacker, M. Rijssenbeek, L. Seabra, P. Schovánek, R. Staszewski, P. Swierska, T. Sýkora, *Construction of the optical part of a time-of-flight detector prototype for the AFP detector*. Opt Express, 2016, Vol. 24, No. 24, pp. 27951-1-27951-10. ISSN 1094-4087, doi:10.1364/OE.24.027951

References

[1] S. A. Khalek et al., *The ALFA Roman Pot detectors of ATLAS*,
Journal of Instrumentation **11**.11 (2016) P11013,
URL: http://stacks.iop.org/1748-0221/11/i=11/a=P11013.

[2] G. Aad et al., *Measurement of the total cross section from elastic scattering in pp collisions at* $\sqrt{s} = 7$ *TeV with the ATLAS detector*, Nucl.Phys. **B889** (2014) 486–548, arXiv: 1408.5778 [hep-ex].

[3] S. Agostinelli et al., *Geant4—a simulation toolkit*,
Nuclear Instruments and Methods in Physics Research Section A: Accelerators, Spectrometers, Detectors and Associated Equipment **506**.3 (2003) 250–303, ISSN: 0168-9002,
URL: http://www.sciencedirect.com/science/article/pii/S0168900203013688.

[4] ATLAS Collaboration, *The Athena Framework*, 2016,
URL: https://twiki.cern.ch/twiki/bin/view/AtlasComputing/AthenaFramework
(visited on 21/06/2016).

[5] R. Brun and F. Rademakers, *{ROOT} — An object oriented data analysis framework*, Nuclear Instruments and Methods in Physics Research Section A: Accelerators, Spectrometers, Detectors and Associated Equipment **389**.1–2 (1997) 81 –86, New Computing Techniques in Physics Research V, ISSN: 0168-9002.

[6] M. Aaboud et al., *Measurement of the total cross section from elastic scattering in pp collisions at* $\sqrt{s} = 8$ *TeV with the ATLAS detector*, Physics Letters B **761** (2016) 158–178,
arXiv: 1607.06605 [hep-ex].

[7] R. Staszewski et al., *Exclusive* $\pi^+\pi^-$ *Production at the LHC with Forward Proton Tagging*,
Acta Phys.Polon. **B42** (2011) 1861–1870, arXiv: 1104.3568 [hep-ex].

[8] O. C. Jacob and L. S. Kisslinger, *Applicability of Asymptotic QCD for Exclusive Processes*,
Phys. Rev. Lett. **56** (1986) 225.

[9] P. Lebiedowicz, O. Nachtmann and A. Szczurek, *Central exclusive diffractive production of* $\pi^+\pi^-$ *continuum, scalar and tensor resonances in pp and* $p\bar{p}$ *scattering within tensor pomeron approach*, Phys. Rev. **D93**.5 (2016) 054015, arXiv: 1601.04537 [hep-ph].

[10] P. Lebiedowicz, *Exclusive reactions with light mesons: From low to high energies*, thesis, The Henryk Niewodniczanski Institute of Nuclear Physics, Polish Academy of Sciences (2014).

[11] P. Lebiedowicz and A. Szczurek, *Exclusive* $pp \to pp\pi^+\pi^-$ *reaction: From the threshold to LHC*, Phys.Rev. **D81** (2010) 036003, arXiv: 0912.0190 [hep-ph].

[12] L. A. Harland-Lang, V. A. Khoze and M. G. Ryskin,
Modelling exclusive meson pair production at hadron colliders, Eur. Phys. J. **C74** (2014) 2848,
arXiv: 1312.4553 [hep-ph].

[13] M. G. Albrow, T. D. Coughlin and J. R. Forshaw,
Central Exclusive Particle Production at High Energy Hadron Colliders,
Prog. Part. Nucl. Phys. **65** (2010) 149–184, arXiv: 1006.1289 [hep-ph].

[14] R. Kycia et al., *GenEx: A simple generator structure for exclusive processes in high energy collisions* (2014), arXiv: 1411.6035 [hep-ph].

[15] P. Soding, *On the Apparent shift of the rho meson mass in photoproduction*,
Phys. Lett. **19** (1966) 702–704.

[16] C. Ewerz, M. Maniatis and O. Nachtmann,
A Model for Soft High-Energy Scattering: Tensor Pomeron and Vector Odderon,
Annals Phys. **342** (2014) 31–77, arXiv: 1309.3478 [hep-ph].

[17] ATLAS Collaboration, *The ATLAS job transforms*, 2016,
URL: https://twiki.cern.ch/twiki/bin/view/AtlasComputing/JobTransform (visited on 21/06/2016).

[18] ATLAS Collaboration, *Documentation for the D3PDMaker Project*, 2016,
URL: https://twiki.cern.ch/twiki/bin/view/AtlasProtected/D3PDMaker (visited on 21/06/2016).

[19] S. Campana, T. Wenaus et al., *The Atlas Computing*, 2016,
URL: https://twiki.cern.ch/twiki/bin/view/AtlasComputing/AtlasComputing (visited on 21/06/2016).

[20] G. Stewart, W. Lampl et al., *The Software Tutorial*, 2016,
URL: https://twiki.cern.ch/twiki/bin/viewauth/AtlasComputing/SoftwareTutorial (visited on 21/06/2016).

[21] S. Lloyd et al., *The ATLAS Computing Workbook*, 2016,
URL: https://twiki.cern.ch/twiki/bin/view/AtlasComputing/WorkBook (visited on 21/06/2016).

[22] S. Lloyd et al., *The ATLAS Software Development Workbook*, 2016, URL: https://twiki.cern.ch/twiki/bin/view/AtlasComputing/SoftwareDevelopmentWorkBook (visited on 21/06/2016).

[23] T. Sjöstrand et al., *An Introduction to PYTHIA 8.2*, Comput.Phys.Commun. **191** (2015) 159–177, arXiv: 1410.3012 [hep-ph].

[24] J. Monk and A. Pilkington, *ExHuME 1.3: A Monte Carlo event generator for exclusive diffraction*, Computer Physics Communications **175**.3 (2006) 232 –239, ISSN: 0010-4655.

[25] S Cavalier et al., *90 m OPTICS COMMISSIONNING*, CERN-ATS-2011-133 (2011) 3 p,
URL: http://cds.cern.ch/record/1382027.

[26] S Cavalier et al., 'Measurement of the total cross section in pp collisons at sqrt(s) = 7 TeV from elastic scattering with the ATLAS detector', tech. rep. ATL-COM-PHYS-2013-1357, CERN, 2013,
URL: https://cds.cern.ch/record/1602297.

[27] *ATLAS inner detector: Technical design report. Vol. 1* (1997).

[28] G. Aad et al., *The ATLAS Inner Detector commissioning and calibration*,
Eur.Phys.J. **C70** (2010) 787–821, arXiv: 1004.5293 [physics.ins-det].

[29] E. Feng and J. E. Pilcher, 'Triggering ATLAS with Minimum Bias Trigger Scintillators',
tech. rep. ATL-TILECAL-INT-2007-004. ATL-COM-TILECAL-2007-013, CERN, 2007,
URL: https://cds.cern.ch/record/1034461.

[30] *ATLAS level-1 trigger: Technical Design Report*, Technical Design Report ATLAS,
Geneva: CERN, 1998, URL: https://cds.cern.ch/record/381429.

[31] P. Jenni et al., *ATLAS high-level trigger, data-acquisition and controls: Technical Design Report*,
Technical Design Report ATLAS, Geneva: CERN, 2003,
URL: https://cds.cern.ch/record/616089.

[32] M. Medici and S. Jakobsen, 'Trigger efficiency for the ALFA detector in 2011', tech. rep. ATL-COM-LUM-2013-006, CERN, 2013, URL: https://cds.cern.ch/record/1519629.

[33] T Cornelissen et al., 'Concepts, Design and Implementation of the ATLAS New Tracking (NEWT)', tech. rep. ATL-SOFT-PUB-2007-007. ATL-COM-SOFT-2007-002, CERN, 2007, URL: https://cds.cern.ch/record/1020106.

[34] S. S. Mortensen, 'Kinematic reconstruction of diffractive processes with tagged protons in the ALFA detector at sqrt(s) = 8 TeV', MA thesis: University of Copenhagen, 2013, URL: http://discoverycenter.nbi.ku.dk/teaching/thesis_page/Stark-Thesis.pdf.

[35] S van der Meer, 'Calibration of the effective beam height in the ISR', tech. rep. CERN-ISR-PO-68-31. ISR-PO-68-31, CERN, 1968, URL: http://cds.cern.ch/record/296752.

[36] 'dE/dx measurement in the ATLAS Pixel Detector and its use for particle identification', tech. rep. ATLAS-CONF-2011-016, CERN, 2011, URL: http://cds.cern.ch/record/1336519.